Aus dem Medizinischen Zentrum für Innere Medizin

des Universitätsklinikums Gießen und Marburg GmbH, Standort Gießen

Medizinische Klinik und Poliklinik II, Abteilung für Infektiologie

Leiterin: Prof. Dr. S. Herold, PhD

Antibakterielle Eigenschaften von organspezifischen Makrophagen

Kumulative Habilitationsschrift

zur Erlangung der Venia Legendi

des Fachbereichs Medizin

der Justus-Liebig-Universität Gießen

vorgelegt von Dr. med. univ. Ulrich Matt, PhD

Gießen 2021

Inhaltsverzeichnis

1. Einleitung

Bakterielle Infektionen stellen auch nach der Entdeckung von Antibiotika eine große medizinische Herausforderung dar. Der durch die Antwort des Immunsystems bedingte Gewebeschaden kann lokal (z.B. Lungenschaden bei Pneumonie) oder systemisch (Sepsis mit Multiorgandysfunktion) vital bedrohend sein. Zudem bergen die zunehmenden antibiotischen Resistenzen die Gefahr der Entstehung einer zumindest partiellen „post-antibiotischen Ära“, die die moderne Medizin als Gesamtes gefährden. Auch nach Jahrzehnten klinischer und Grundlagenforschung ist es noch nicht gelungen, diesen Gewebeschaden medikamentös therapeutisch zu verringern. Am Entzündungsgeschehen wesentlich beteiligte Zellen sind organspezifische Makrophagen. Sie sind sogenannte Wächterzellen des jeweiligen Gewebes, und als solche entscheidende Regulatoren der Homöostase, als auch von Entzündungsantworten in ihrem jeweiligen Organ. Durch ihre antibakteriellen Eigenschaften tragen sie auch wesentlich zur Abwehr von Bakterien lokal und auch teils systemisch (z.B. Kupffer Zellen) bei. Neuere Forschungsarbeiten haben gezeigt, dass Organe während der Embryonalzeit durch Makrophagen besiedelt werden, und diese postnatal großteils lokal proliferieren. Dies und die unterschiedlichen Anforderungen und Bedingungen in ihren Organen (z.B. Beteiligung an der Reizleitung im Herzen, steriles Peritoneum versus zur Umwelt exponierte Gas-Austauschfläche in der Lunge) deuten auf eine große Verbundenheit mit dem jeweiligen Gewebe hin, und unterstreicht die heterogenen Funktionen und Eigenschaften von organspezifischen Makrophagen. Diese gewebsspezifischen Unterschiede könnten die Grundlage für neue gezielte therapeutische Angriffspunkte sein.

In der vorliegenden Arbeit wurden organspezifische Makrophagen während klinisch relevanten Entzündungen der Lunge und des Peritoneums, sowie in einer Infektion von Makrophagen mit *Mycobacterium tuberculosis in vitro* und *in vivo* auf ihre antibakteriellen Eigenschaften untersucht. Dabei konnten Mechanismen entschlüsselt werden, die die Grundlage für weitere Studien, und für mögliche therapeutische Angriffspunkte liefern, um Makrophagen gezielt während Inflammationen therapeutisch beeinflussen zu können.

1.1 Makrophagen – Funktion und Herkunft

Makrophagen finden sich im gesamten Körper, und sind bekannt für ihre antibakteriellen Eigenschaften. Ihr Entdecker Eli Metchnikoff postulierte Ende des 19. Jahrhunderts, dass „Phagozyten“ essentiell in der Erhaltung der Homöostase sind, indem sie fremde Eindringlinge und eigene Schadstoffe beseitigen, und damit die Organstruktur erhalten [1]. Die Entdeckung von Pathogen Recognition Receptors (PRRs) wie Toll-like Rezeptoren (TLRs), die es Zellen des Immunsystems ermöglichen, gezielt konservierte Strukturen von Pathogenen zu erkennen, als auch die neueren Erkenntnisse über die Ontogenese von Makrophagen, haben sie erneut in das wissenschaftliche Rampenlicht gerückt. Forschungen der letzten 10 bis 20 Jahre haben die Annahme von Metchnikoff, dass Makrophagen vielfältige Funktionen haben, bestätigt. So spielen Makrophagen nicht nur in der Einleitung und Resolution von Entzündungen, sondern auch in der Organogenese, in der Restoration von Gewebeschaden, der Angiogenese, im Metabolismus lokal als auch systemisch, sowie in der Tumorabwehr eine entscheidende Rolle. Diese Entwicklung könnte dazu führen, neue Therapieansätze in Infektionskrankheiten, Tumorerkrankungen, aber auch chronischen Entzündungen wie Autoimmunkrankheiten, oder Arteriosklerose zu finden.

1.1.1 Ontogenese, Organspezifität und Polarisierung

Dass Makrophagen je nach Organ verschiedene Aufgaben zu erfüllen haben, und dadurch andere Eigenschaften aufweisen müssen, ist seit längerem bekannt. So nehmen zum Beispiel alveoläre Makrophagen (AM) Surfactant, der von pulmonalen Epithelzellen produziert wird, auf. Osteoklasten sind wesentlich am Umbau des Knochens beteiligt, indem sie Knochengewebe abbauen. Eine erbliche Unterfunktion der Osteoklasten, genannt Osteopetrosis, geht mit schweren Entwicklungsstörungen einher [2]. Nierenmakrophagen beseitigen Immunkomplexe aus der Zirkulation [3], oder Makrophagen der roten Pulpa in der Milz verdauen Erythrozyten, und haben so eine wichtige Funktion in der Eisenhomöostase [4]. Kardiale Makrophagen begünstigen die Reizüberleitung von Vorhof in die Kammer [5], und schützen vor Arrythmien [6]. Pathologien, wie ein Mangel an granulocyte-macrophage colony-stimulating factor (GM-CSF), der zu einem Fehlen von AM führt, bedingt die alveoläre

Proteinose, die mit einer Entwicklungsstörung, Lungendysfunktionen, und gehäuften Lungeninfektionen einhergeht [7].

Über Jahrzehnte ging man davon aus, das Makrophagen durch Monozyten ersetzt werden. Der Begriff „mononukleäres Phagozytensystem“ beschrieb die Annahme, das Monozyten und Makrophagen den gleichen Ursprung haben [8]. Gestärkt wurde dieses Konzept durch die Beobachtung, dass nach Bestrahlung organspezifische Makrophagen und dendritische Zellen durch infiltrierende Monozyten aus der Blutstrombahn ersetzt werden können [9, 10]. Beginnend mit der Beobachtung, dass Makrophagen unabhängig von Knochenmarksvorläuferzellen entstehen und proliferieren können [11], entwickelte sich das gegenwärtige Modell: Makrophagen entstehen aus embryonalen Stammzellen („erythromyeloid progenitors“ EMPs), die im Dottersack gebildet werden, und dann auch die fötale Leber kolonisieren, sowie aus einer zweiten Welle von fötalen Monozyten, und aus hämatopoetischen Zellen (Abb. 1) [12]. Es wurde gezeigt, dass Makrophagen, je nach Organ komplett unabhängig vom Knochenmark, wie im Fall von Mikroglia, bis zu nahezu komplett durch Monozyten aus der Blutstrombahn, wie bei intestinalen Makrophagen, ersetzt werden können (vgl. Abb. 1). Subpopulationen im gleichen Organ können aber auch eine andere Ontogenese aufweisen. So wurde für Mikroglia gezeigt, dass sogenannte „border-associated“ Makrophagen, die sich in den Meningen und im Plexus choroideus befinden, einen anderen Ursprung haben als Mikroglia, und im Laufe des Lebens durch Monozyten ersetzt werden [13]. Ebenso werden nicht alle Darm-Makrophagen durch Monozyten ersetzt, sondern eine Population von intestinalen Makrophagen stammt von fötalen Vorläuferzellen ab, und proliferiert selbst [14]. Nicht geklärt ist bis dato, ob es bestimmte Stammzellen unter den organspezifischen Makrophagen gibt, oder ob alle Makrophagen sich „vor Ort“ vermehren können. In der Leber, der Niere, der Epidermis, oder der Lunge erhalten sich Makrophagen vorwiegend unabhängig, während es im Myokard, oder dem Pankreas zu einem langsamen Ersatz durch Monozyten kommt (Abb. 1). Aber auch in Organen, in denen sich Makrophagen selbst erhalten können, kann es zu einem Ersatz durch rekrutierte Monozyten kommen. Dies kommt dann zum Tragen, wenn durch Inflammation die Gewebsnische freigemacht wurde, also Makrophagen depletiert wurden [15].

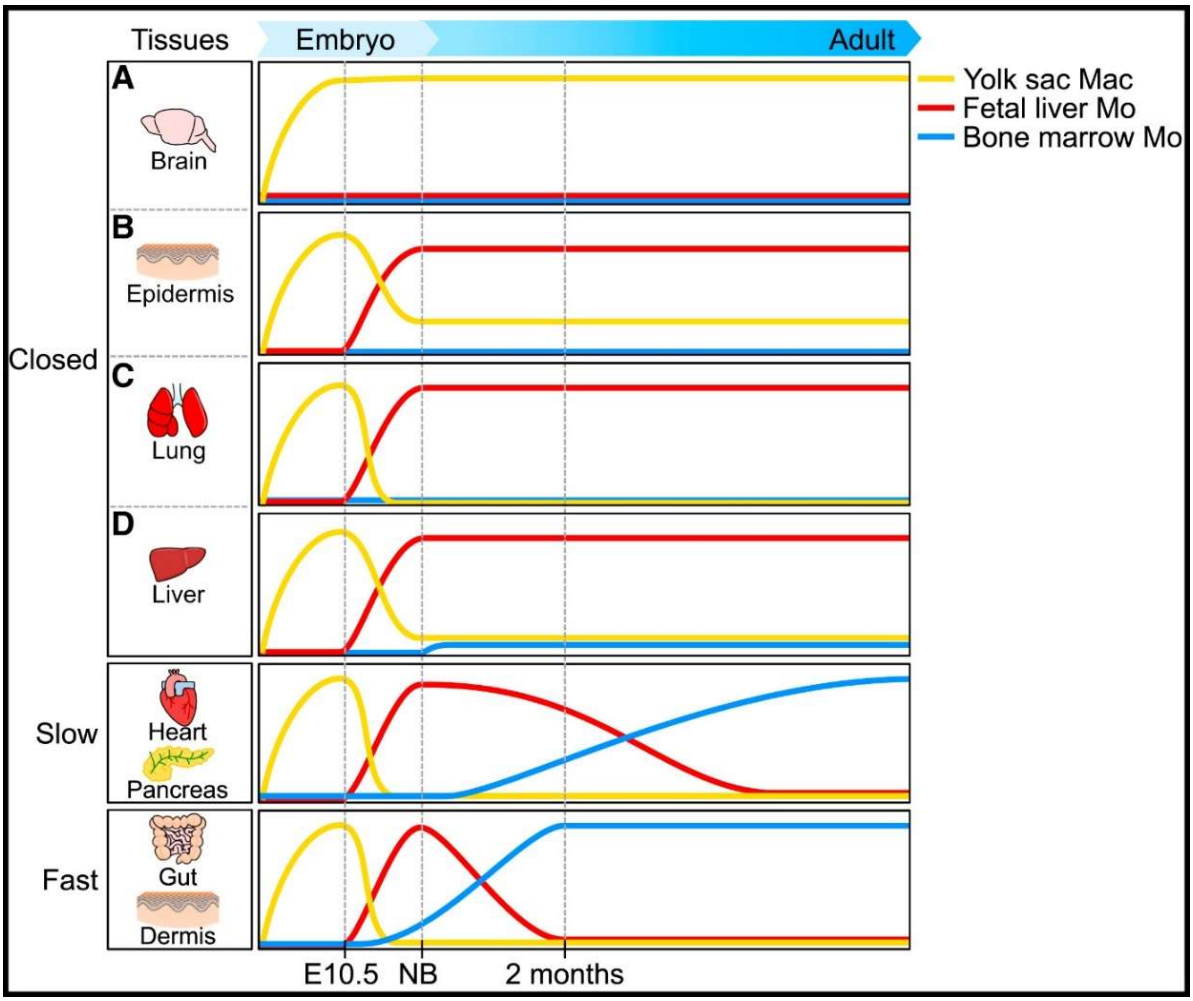

Abbildung 1: Schematische Darstellung der Organbesiedlung durch Makrophagen. Im Großteil der Organe erhalten sich Makrophagen gewebsspezifisch, ohne der Rekrutierung von Monozyten. In Gelb: „yolk sac macrophages“, in Rot „fetal liver monocytes“, und in blau „bone marrow monocytes“; adaptiert von Ginhoux & Guillams [16], mit Erlaubnis.

Organspezifische Makrophagen weisen gewebsspezifische transkriptionelle und epigenetische Programme auf, die durch Stimuli des Gewebes bedingt werden [17, 18]. Somit können rekrutierte, aus dem Knochenmark stammende Monozyten, sich den Gegebenheiten des jeweiligen Organs anpassen, und gleiche epigenetische Veränderungen wie Alveolarmakrophagen aufweisen [17]. Passend hierzu wurde gezeigt, dass AM fötaler und postnataler Herkunft transkriptionell nahezu ident sind, aber auch funktionell (Phagozytose, Efferozytose, Zytokinsekretion) gleiche Eigenschaften aufweisen [19]. Diese Beobachtungen wurden jedoch im steady-state gemacht. Inwiefern diese genetischen und funktionellen Gemeinsamkeiten auch während einer Entzündung auftreten, ist weitgehend unbekannt.

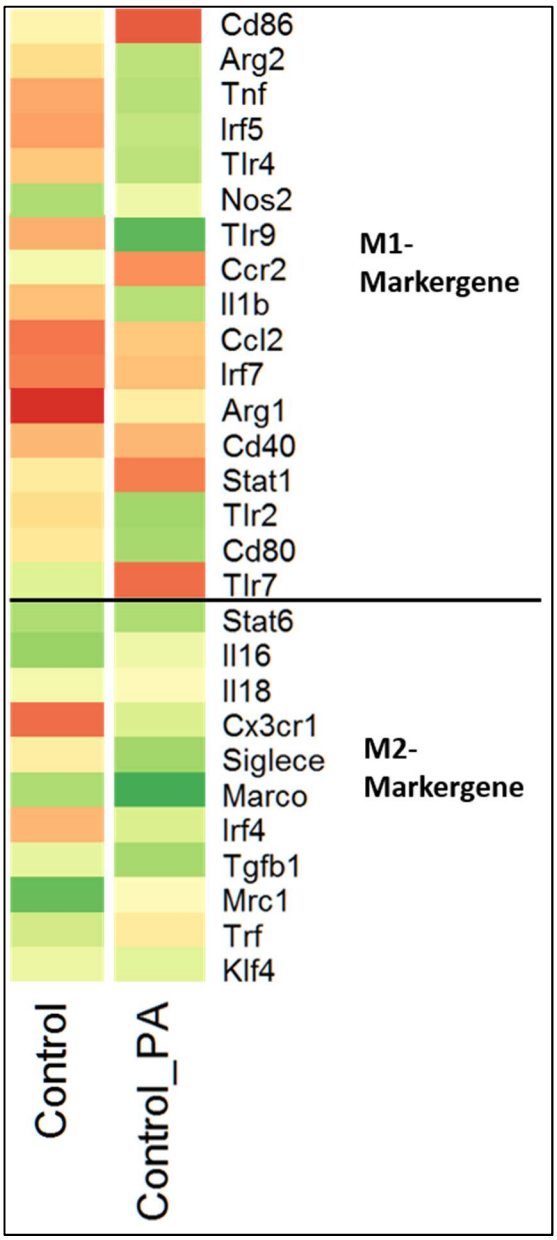

Wie eingangs erwähnt, bedingte das Konzept des mononukleären Phagozytensystems, dass KM als prototypisch für alle Makrophagen angesehen wurden. Bei KM führt *in vitro* eine Stimulation mit IFN-γ/LPS zu sogenannten „M1“ oder klassisch aktivierten Makrophagen, und eine Stimulation mit IL-4 zu sogenannten „M2“ oder alternativ aktivierten Makrophagen. M1-Makrophagen sind pro-inflammatorisch und weisen höhere antimikrobielle Eigenschaften auf [20], während M2-Makrophagen anti-inflammatorisch sind, und sich durch regenerative Eigenschaften auszeichnen [21]. Auch diese extremen Polarisierungszustände sind nicht irreversibel [22], und zeigen die hohe Plastizität von Makrophagen. Am Entzündungsgeschehen selbst gibt es jedoch eine Vielzahl von Stimuli, welche zeitgleich pro- und anti-inflammatorisch sein können [23].

Abbildung 2: Polarisierung von AM nach Infektion mit *P. aeruginosa in vivo*. C57BL/6 Mäuse wurden intranasal mit 1*10E4 Kolonie-bildenden Einheiten *P. aeruginosa* infiziert, 4 Stunden später wurde eine broncho-alveolärer Lavage (BAL) durchgeführt, aus dieser mittels Durchflusszytometrie die residenten AM isoliert. Diese wurden einer Transkriptomanalyse unterzogen. Gezeigt sind klassische „M1“ (oben), und „M2“-Marker (unten), und deren Expression abweichend vom Mittelwert. N=4 pro Gruppe (unpublizierte Daten).

Zudem bestehen in den jeweiligen Organen gewebsspezifische Signale. Da aber ein Großteil der Studien mit Knochenmarks (KM) durchgeführt wurde, ist die Polarisierung gewebsspezifischer Makrophagen im Laufe von Entzündungen großteils unbekannt [24, 25]. Wir fanden in eigenen Untersuchungen, dass residente AM nicht - wie KM nach LPS-Stimulation – nach *in vivo* Infektion mit dem gramnegativen Bakterium *Pseudomonas aeruginosa* (*P. aeruginosa*) M1-assoziierte Markergene hoch- und M2-assoziierte Markergene hinunterregulieren (Abb. 2). Daraus ergibt sich klar die Notwendigkeit, funktionale Eigenschaften gewebsspezifischer Makrophagen in

Homöostase und Entzündung zu studieren, um sich diese diagnostisch und therapeutisch nutzbar machen zu können.

1.1.2 Antibakterielle Eigenschaften von Makrophagen

Makrophagen besitzen die Fähigkeit, größere Partikel (> 0,5µm) wie Bakterien aufzunehmen (Phagozytose), und intrazellulär abzutöten. Dies dient nicht nur dem Beseitigen von Pathogenen, sondern auch der Einleitung einer adaptiven Immunantwort durch Präsentation von Antigenen. Die Erkennung der Mikroorganismen erfolgt entweder direkt über „pathogen associated molecular patterns“ (PAMPs), oder indirekt über Opsonine, wie Antikörper oder Komplement, die dann über Rezeptoren an Makrophagen (z.B. Fcγ-Rezeptoren für Antikörper, oder Komplementrezeptoren) erkannt werden [26]. Danach erfolgt die Aufnahme über strukturelle Veränderungen des Aktin-Zytoskeletts, und die Bakterien werden in das Phagosom eingeschlossen. Dieses maturiert, indem es Hydrolasen akquiriert und im Verlauf durch die Aktivität von Proton-Pumpen der pH abnimmt, dann wird es mit Proteasen und lysosomal-associated membrane proteins (LAMPs) angereichert [27]. Schließlich fusioniert das Phagosom mit dem Lysosom zum Phagolysosom. Durch ein saures Milieu (ph bis zu 4.5), Sauerstoffradikale und hydrolytische Enzyme ist es in der Lage Pathogene abzutöten. Sauerstoffradikale werden direkt oder indirekt durch NOX2 gebildet. Patienten mit chronischer Granulomatose haben einen Defekt in einem der 4 Komponenten dieser NADPH-Oxidase, und weisen eine erhöhte Infektanfälligkeit auf [28]. NOX2 oxidiert NADPH, und es entsteht $O2^-$, welches ins Phagosom sezerniert wird. Über das Enzym Superoxid-Dismutase kann dann H_2O_2, und in weiterer Folge auch Hydroxylradikale oder mittels Myeloperoxidase unter anderem HOCl gebildet werden [29]. Andere wichtige Sauerstoffradikale („reactive oxygen species“ - ROS) sind mitochondriale ROS (mROS), die an mehreren Stellen in der Atmungskette entstehen können [30], und die in Makrophagen bedeutend in der Infektabwehr sind [31-33]. Des weiteren wird vor allem durch NOS2 Stickoxid, und dadurch reaktive Stickstoffspezies (RNS) gebildet. NOS2 ist eines der Gene, das in M1-Makrophagen besonders hochreguliert ist. ROS und RNS reagieren mit Lipiden, Proteinen und Nukleinsäuren der Mikroben, und dadurch können diese irreparabel geschädigt werden [29].

Zusätzlich besitzen Makrophagen antimikrobielle Peptide, die das Wachstum von Pathogenen behindern können. Deren Wirkmechanismen sind vielfältig, so entzieht zum Beispiel Lactoferrin den Mikroorganismen Eisen; Defensine oder Kathelizidine wirken direkt toxisch, indem sie zu einer Permeablisierung der Zellmembran der Pathogene führen [34].

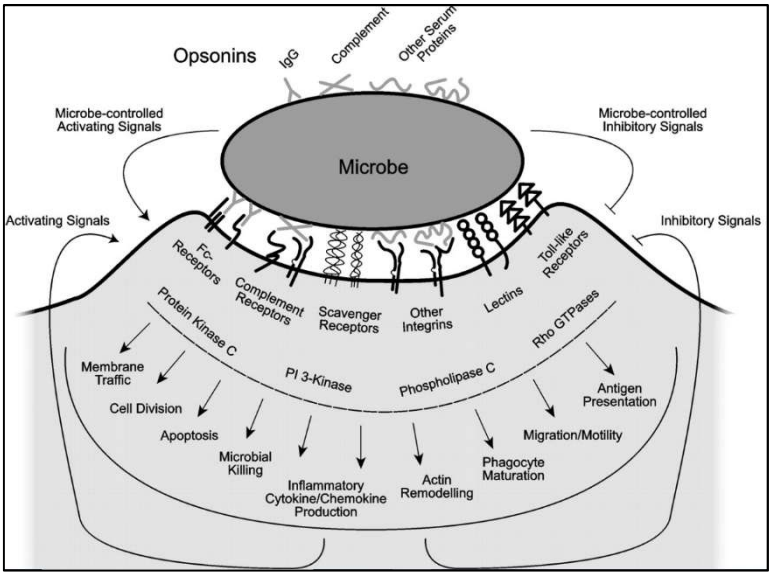

Abbildung 3: Erkennung und Phagozytose von Mikroben durch Rezeptoren und Opsonine. Inhibitorische und aktivierende Signale induzieren intrazelluläre Signalwege. Viele Pathogene modulieren diese Signalwege. Adaptiert von [26], mit Erlaubnis.

Eine Vielzahl von Pathogenen haben Gegenmechanismen entwickelt, um der Zerstörung zu entgehen. Ein paar wenige wie *Listeria monocytogenes*, *Coxiella burnetii* oder Legionellen haben sich an das intrazelluläre Milieu angepasst, und können in Makrophagen überleben. Ebenso *Mycobacterium tuberculosis* (*M. tuberculosis*), das die Maturierung des Phagolysosoms verhindert, und somit in Makrophagen überleben, und sich vermehren kann [35]. Durch die Aktivierung von Makrophagen durch IFN-γ, gebildet von T-Lymphozyten, kann die Bildung des Phagolysysoms induziert, und somit die Mykobakterien abgetötet werden. Die Bedeutung von IFN-γ wird unterstrichen durch die erhöhte Anfälligkeit für Infekte mit Mykobakterien in Personen mit angeborenen Defekten in INF-γ assoziierten Signalwegen [36]. Die antibakteriellen Fähigkeiten organspezifischer Makrophagen sind wenig untersucht, da die meisten Daten aus KM stammen. Die unterschiedlichen Anforderungen der verschiedenen Organe (z.B. steriles Peritoneum versus mit Kommensalen besiedelte Atemwege und Darm), sowie die teils unterschiedliche Prädilektion von bestimmten Bakterien für einzelne Organe (z.B. Legionellen und Pneumokokken für die Lunge) verlangen jedoch eine differenzierte Betrachtung der Interaktion von unterschiedlichen organspezifischen Makrophagen mit den verschiedenen Bakterien.

1.2 Alveoläre Makrophagen

AM stellen 90-95% des zellulären Gehalts des alveolären Raums in Homöostase dar [37]. AM befinden sich zu 95% in den Alveolen, und zu 5% in den Atemwegen [38]. Sie sind langlebige Zellen, die von fötalen Vorläuferzellen stammen, und eigenständig proliferieren können [39, 40]. Wie in Abb. 1 dargestellt stammen sie initial von “yolk sac macrophages” (Dottersackmakrophagen), und werden dann von fötalen Monozyten ersetzt [16]. Während Infektionen oder Entzündungen werden sie je nach Ausmaß der Elimination teils durch im Blut zirkulierende Monozyten ersetzt. Der Begriff „niche competition“ entstand, in dem (in der Lunge) gezeigt wurde, dass embryonale Vorläuferzellen (Dottersackmakrophagen, fötale Monozyten), und Monozyten aus dem postnatalen Knochenmark bei Freiwerden der Nische, diese besetzen können, und zu funktionsfähigen AM differenzieren, und sich reproduzieren können [13]. Interessanterweise trifft das, in der Lunge, nicht für Peritoneal-, Intestinal-, oder Lebermakrophagen (LM) zu. Dies deutet auf ein Priming durch das Gewebe hin, welches nicht voll reversibel zu sein scheint. Für die Differenzierung und Proliferation brauchen AM den granulocyte-macrophage-colony stimulating factor (GM-CSF), welcher über GM-CSF-Rezeptor den Transkriptionsfaktor PPAR-γ induziert [15, 41]. Zudem wurde gezeigt, dass das Zytokin transforming growth factor- β (TGF-β) autokrin in AM ebenso über PPAR-γ essentiell für die Proliferation und Differenzierung von AM ist [42]. AM sind hohen Sauerstoffkonzentrationen, exogenen Partikeln, sowie kommensalen und pathogenen Bakterien ausgesetzt. Dementsprechend exprimieren sie in hohem Ausmaß PRRs (z.B. “scavenger”- und Toll-like-Rezeptoren), die eine große Bandbreite an Erregern und Partikeln erkennen können [40]. Während der Homöostase bedingen anti-inflammatorische Zytokine wie Interleukin-10, TGF-β, Surfactant-Proteine, die Interaktion mit Epithelzellen über CD200/CD200R oder connexin 43 basierende gap junctions, dass AM in einem ruhigen, immuntoleranten Zustand verbleiben [43, 44] (Abb. 3). AM können aber durch die Expression diverser PRRs eine starke pro-inflammatorische Antwort einleiten, die zu einer Aktivierung der Epithelzellen und Rekrutierung von Leukozyten führt [45]. Kleinere Mengen an Pathogenen können von AM, auch mit Hilfe von Migration in andere Alveolen, kontrolliert werden [46]. Im Gegenzug sind AM auch wichtig in der Auflösung der Entzündung, indem sie apoptotische Zellen beseitigen (Efferozytose) (eigene unpublizierte Daten), und die Wiederherstellung der Gewebeintegrität fördern [47].

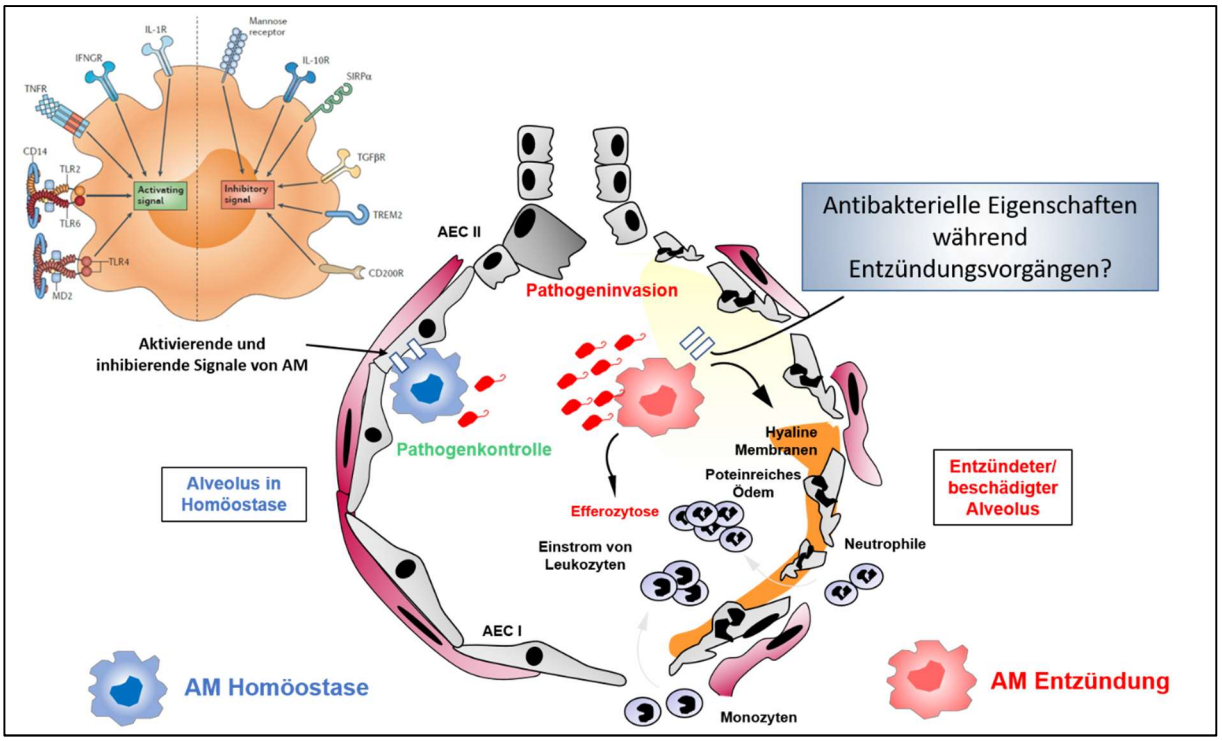

Abbildung 3: AM verändern ihren Aktivierungszustand, um Entzündungen zu steuern (pro- bis anti-inflammatorisch). Während der Resolution der Entzündung müssen apoptotische Zellen, Zelldebris und das Ödem beseitigt werden. Im Verlauf der Entzündung ändern sich die antibakterielle Eigenschaften von AM. Abbildung links oben: aktivierende und inhibierende Signale von AM, adaptiert von [48], mit Erlaubnis.

In dieser Phase haben AM meist verminderte antibakterielle Fähigkeiten, und bakterielle Pneumonien können leichter entstehen. So konnten Medeiros et al. zeigen, dass Efferozytose die antimikrobiellen Eigenschaften von AM einschränkt, und zu einer erhöhten Anfälligkeit für bakterielle Infektionen führt [49]. Nach einer Influenza-Infektion ist der scavenger Rezeptor MARCO durch IFN-γ vermindert exprimiert, wodurch *Streptococcus pneumoniae* (*S. pneumoniae*) weniger gut aufgenommen werden kann, und dadurch Pneumonien leichter entstehen können [50].

Nach einer milden Influenzavirus-Pneumonie kommt es zu einer eingeschränkten Bildung von reaktiven Sauerstoffmolekülen über NADPH. Dies führt zu einer verminderten Beseitigung von *Staphylococcus aureus* (*S. aureus*) [51]. Eine milde Influenza-Infektion führt auch zu einer reduzierten Migrationsfähigkeit der AM, und dadurch zu einer beeinträchtigten Pathogen-Kontrolle [46]. Auch nach Influenza oder bakterieller Pneumonie zeigen AM eine verminderte Produktion von pro-inflammatorischen Zytokinen, sowie eine eingeschränkte Antigenpräsentation, wodurch es über mehrere Wochen zu einer erhöhten Anfälligkeit für bakterielle Infektionen kommt [52, 53]. Nach selbstlimitierender *Escherichia coli* (*E. coli*) oder Influenza-Pneumonie bewirken Signale in der Gewebenische, dass AM über mehrere

Monate einen Phagozytosedefekt aufweisen [54]. Bei einer starken Influenza-Pneumonie kommt es jedoch zur Apoptose der AM, und in der Folge zu einem Einstrom von Monozyten. Diese weisen vorübergehend verbesserte antimikrobielle Eigenschaften auf [55]. Im Gegensatz hierzu kommt es nach Adenovirus-Infektion zur Bildung von sogenannten „Memory AM“, die über eine Rekrutierung von Neutrophilen zu einer verbesserten Bakterienabwehr über bis zu 16 Wochen beitragen [56]. Somit wurde auch in AM eine „trained immunity“, also ein Gedächtnis oder Prägung durch vorangegangene Entzündungen, nachgewiesen. Es ist also davon auszugehen, dass durchgemachte Entzündungen die Funktion von AM nachhaltig beeinflussen können. Zusammenfassend zeigen diese Daten, dass AM während oder nach Entzündungen, je nach Ontogenese und Infektionsmodell, verschiedene Aktivierungszustände annehmen, die mit unterschiedlichen antibakteriellen Eigenschaften einhergehen.

1.3 Peritoneale Makrophagen

Peritoneale Makrophagen (PM) sind die residenten Makrophagen des Peritoneums. Basierend auf Oberflächenmarkern, Morphologie und Funktion können sie in zwei verschiedene Gruppen unterteilt werden: „large“ PM (LPM) exprimieren viel („high“) F4/80 und CD11b, und wenig bis kein MHC-II (IA^b), und stellen in der Homöostase in etwa 90% der PM dar [57]. „Small“ PM (SPM) haben wenig („low“) F4/80 und CD11b, und viel MHC-II an ihrer Oberfläche (Abb. 4). LPM entsprechen morphologisch den klassischen Makrophagen und haben prominente Vakuolen und viel Zytoplasma, wohingegen – vor allem in Kultur – SPM mehr dendritischen Zellen ähneln [58]. LPM stammen wahrscheinlich von Dottersack-Vorläuferzellen ab, und erneuern sich unabhängig der Myelopoiese in „steady-state“ Bedingungen selbst. SPM hingegen haben wahrscheinlich eine kurze Lebensdauer und stammen von Monozyten ab [59]. Wobei neuere Daten zeigen, dass LPM-Vorläuferzellen in Mäusen ab dem Alter von 4 Monaten von Knochenmarksvorläuferzellen (mit SPM-Profil) ersetzt werden [60]. Passend hierzu wurde nach Bestrahlung und Knochenmarkstransplantation gezeigt, dass sowohl SPM, als auch LPM überwiegend vom Spender stammen [61].

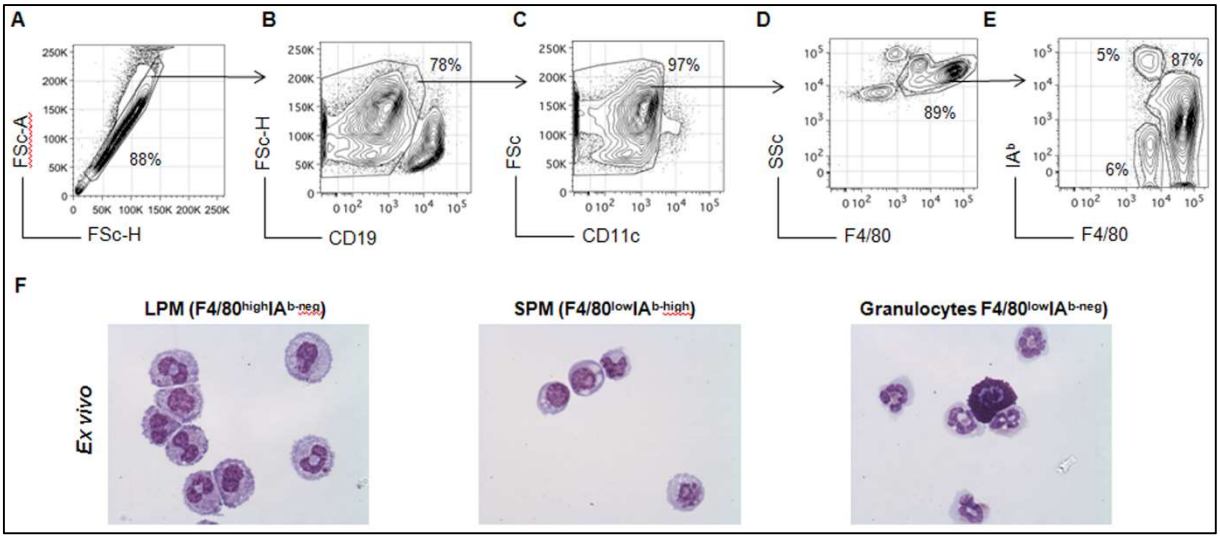

Abbildung 4: **LPM und SPM: 2 verschiedene Makrophagen-Subtypen von PM.** Peritoneallavage von C57BL/6 Mäusen wurde mit Antikörpern für F4/80, CD19, CD11c und IA^b markiert und mittels Durchflusszytometrie analysiert. Doublets und (**A**), $CD19^{high}$ (**B**) und $CD11c^{high}$ (**C**) wurden exkludiert. F4/80 und IA^b (**D**+**E**) Expression definierte drei Gruppen: LPM ($F4/80^{high}IA^{b\text{-}neg}$), SPM ($F4/80^{low}IA^{b\text{-}high}$) und Granulozyten ($F4/80^{low}$ $IA^{b\text{-}neg}$). Sortierte Zellen wurden auf Zytospins mit Hämatoxylin & Eosin gefärbt (**F**), Vergrößerung x40. Adaptiert von [58] mit Erlaubnis.

Während Entzündungen durch Thioglykolat, oder LPS kommt es zu einem Monozyteneinstrom und einer Zunahme von SPM über die Zeit [57, 61], wobei LPM ins Omentum wandern, und im Verlauf wieder ins Peritoneum zurückkehren [57, 58, 61-63]. LPM können nach steriler Peritonitis mit Thioglykolat aber auch aus Monozyten

generiert werden [64]. LPM vermehren sich *in situ* abhängig vom Transkriptionsfaktor GATA6 [63], der von der Retinsäure induziert wird [61]. Zudem kontrolliert GATA6 den „class switch“ zu IgA in peritonealen B-1 Zellen [61]. B-1 Zellen stellen den Großteil der Zellen in der peritonealen Lavage, und ca. 40-70% der peritonealen B-Zellen dar; LPM und SPM hingegen 30-35% der Zellen in der peritonealen Lavage in Homöostase [65]. B1-Zellen produzieren den Großteil der natürlichen IgM-Antikörper, so auch Antikörper gegen Phosphorylcholine oder oxidiertes Phosphorylcholine, Phosphatidylcholine und oxidierte Lipide [66]. Im Menschen wurden $CD14^{high}CD16^{high}$ als Äquivalent von LPM beschrieben [67]. Eine andere Arbeit konnte zeigen, dass humane LPM $CD206^{pos}$ sind, und dieses auch sezernieren können [68]. Funktionell weisen sowohl LPM als auch SPM Phagozytose-Aktivität auf, wobei für SPM eine bessere Aufnahme von *E. coli* und Zymosan gezeigt wurde [57]. Beide produzieren nach LPS Gabe NO *in vivo* [57]. Zu erwähnen ist, dass in LPM *in vitro* nach LPS Stimulation weniger NO induziert wird [57], wobei Unterschiede in den Mauslinien existieren [69]. PM (ohne Unterscheidung zwischen SPM und LPM) produzieren mROS über Glutaminolyse induzierte oxidative Phosphorylierung am Komplex II der Atmungskette [70]. Die auf diese Weise gebildeten mROS sind entscheidend für die antimikrobiellen Eigenschaften der PM [70]. Neben organspezifischen Funktionen von PM konnten Wang und Kubes zeigen, dass in akutem Leberschaden LPM über das Mesothel in die Leber wandern, und dort wichtige regenerative Funktionen haben [71]. Die gleiche Gruppe entdeckte, dass früh während einer Bakteriämie mit *S. aureus*, Kupffer Zellen ins Peritoneum wandern, und dabei LPM infizieren [72]. Eine reduzierte Anzahl von LPM verminderte eine weitere Dissemination in die Nieren, und intraperitoneale aber nicht intravenöse Vancomycin-Gabe verhinderte diese Dissemination.

Zusammenfassend sind PM aufgrund ihrer Zugänglichkeit neben KM die meiststudierten Makrophagen. Neue Erkenntnisse über ihren Ursprung, die Klassifizierung und die Funktion von PM rücken diese Daten in ein neues Licht. Welche antibakteriellen Eigenschaften von PM bzw. deren Subtypen in diversen Infektionen entscheidend sind, ist weitgehend unklar. Ob PM neben der beschriebenen Migration in die Leber [71], und der aktiven Dissemination von *S. aureus* [72], auch in bakteriellen Infektionen in viszeralen Organen oder gar während einer Bakteriämie eine Rolle spielen, muss erst untersucht werden.

1.4 Kupffer Zellen

Kupffer Zellen (KPC) sind residente Lebermakrophagen, die für die Homöostase des Organs, aber auch des Körpers wichtig sind. KPC finden sich in den Lebersinusoiden, wo Blut der Portalvenen aber auch der Leberarterien sich mischt, und ca. 30% des gesamten Blutvolumens durchströmt [73]. Sie stellen 35% der nichtparenchymatösen Zellen der Leber dar, und ca. 80-90% aller Makrophagen im Körper. KPC stammen von fötalen Vorläuferzellen ab, und können sich in Homöostase selbst regenerieren (Abb. 1)[74]. Neben KPC wurden kürzlich noch Leberkapselmakrophagen als residente Makrophagen der Leber beschrieben [75]. Diese weisen zwar makrophagentypische Oberflächenmarker wie CD64 und F4/80, aber auch dendritische Zellmarker wie MHCII und CD11c auf [76]. Ebenso wurden Subpopulationen von KPC beschrieben [77], jedoch bleibt deren funktionelle Bedeutung noch unklar. Ähnlich wie in der Lunge können Inflammationen zu einer Rekrutierung von Monozyten führen, die zu KPC differenzieren [78, 79]. Darüber hinaus wurde gezeigt, dass PM nach thermalem Schaden in die Leber rekrutiert werden; wird dies blockiert, kommt es zu einer Verzögerung der Wundheilung [71]. KPC spielen eine zentrale Rolle im Eisenstoffwechsel, indem sie beschädigte Erythrozyten, und Hämoglobin-haltige Komplexe oder Vesikel aus dem Blut beseitigen [80]. Im Bedarfsfall werden Monozyten in die Leber rekrutiert, um den KPC in der Beseitigung von Erythrozyten zu assistieren [81]. KPC sind ebenso wichtig in der Beseitigung von aktivierten und apoptotischen Neutrophilen. Wird deren Phagozytose blockiert, kommt es zur Akkumulation von Neutrophilen in der Milz und in den Lungen [82].

Die Leber ist für den Metabolismus (Glukoneogenese, Lipidstoffwechsel) zentral, und KPC scheinen eine wichtige Rolle in der Entstehung der nichtalkoholischen Fettleber im Rahmen einer metabolischen Dysregulation zu spielen [83, 84]. Aber KPC können die Fibroseentstehung nicht nur begünstigen, sondern durch den Abbau extrazelllulärer Matrix diese auch verhindern [85]. Daher stellen KPC auch ein attraktives „drug target“ in der Fibrose dar.

Die antibakteriellen Eigenschaften von Lebermakrophagen sind auch während der Homöostase wichtig, da sie das Blut der Portalvenen von Bakterien säubern [86]. Experimentell wurde gezeigt, dass sie auch während einer Bakteriämie wichtig in der Abwehr der Pathogene sind, und diese auch rasch ohne Komplementbindung über Scavenger-Rezeptoren und Komplementrezeptoren (durch Bindung an

Lipoteichonsäure) unter Flussbedingungen aufnehmen können [87, 88]. Eine langsamere Aufnahme ist nach Komplement- oder Thrombozytenbindung beschrieben [89, 90]. Die erhöhte Infektanfälligkeit bei Leberschäden könnte zum Teil auf die Beeinträchtigung der antibakteriellen Eigenschaften der KPC zurückzuführen sein [91]. Unklar ist bislang der Einfluss von Entzündungen in der Leber oder in anderen Organen auf antibakterielle Eigenschaften von KPC.

1.5 Pneumonie

Auch nach Einführung von Antibiotika gehören bakterielle Pneumonien zu den 10 häufigsten Todesursachen, und stellen die häufigste Todesursache aller Infektionskrankheiten dar [92]. Pneumonien werden vor allem durch Bakterien, und/oder Viren verursacht. Eine Pneumonie entsteht bei eingeschränkter Immunantwort, wie nach Aspirationspneumonitis oder nach Influenza, bei Inhalation eines großen Inokulums oder eines speziell pathogenen Erregers. Abwehrmechanismen der oberen und unteren Atemwege inkludieren Anatomie (Nasopharynx, Bronchienabzweigung), Mechanik (Husten), das Epithel (mukoziliäre Clearance, Schleim- und Surfactantproduktion, antibakterielle Peptide), sowie das Immunsystem (zelluläres angeborenes und adaptives Immunsystem, sowie humoral durch Antikörper und Komplement) [93]. In den Alveolen gibt es keine mukoziliäre Clearance, aber AM, die als Wächterzellen als erste Kontakt mit Pathogenen haben, können diese beseitigen, und andere Immunzellen aktivieren bzw. rekrutieren. Neben den alveolären gibt es die interstitiellen Makrophagen, die vermutlich durch Monozyten regeneriert werden [94], und vermutlich eine höhere Kapazität zur Antigen-Präsentation als AM aufweisen, aber deren Rolle allgemein und in der Infektabwehr noch relativ unklar ist [95]. Dendritische Zellen residieren im Epithel der Atemwege (Trachea bis Alveolen), an Lungengefäßen und an der viszeralen Pleura, und spielen eine wichtige Rolle bei der Einleitung der Immunantwort durch ihre Antigen-präsentierenden und chemotaktischen Eigenschaften [96]. Antigen-präsentierende Zellen wie Makrophagen und dendritische Zellen können lokale Lymphozyten, oder Lymphozyten in den drainierenden Lymphknoten, und somit das adaptive Immunsystem aktivieren. Die ersten rekrutierten Immunzellen sind neutrophile Granulozyten, denen eine wichtige Rolle in der Beseitigung von Bakterien zukommt. Kommt es zu einer Verminderung des Immunsystems zum Beispiel durch Noxen (Rauchen, Alkohol), immunsuppressive Therapie oder vorangehende Entzündungen

(vgl. Kapitel „Alveolarmakrophagen“ und „Aspirationspneumonitis“), ist das Risiko für eine bakterielle Pneumonie erhöht.

Klinisch geht eine Lungenentzündung in der Regel mit respiratorischen Symptomen, wie Husten, bei schweren Verläufen mit Atemnot begleitet von Allgemeinsymptomen wie Fieber und Abgeschlagenheit einher. Aufgrund der großen Variabilität der klinischen Symptomatik ist die klinische Diagnose einer Pneumonie mit Unsicherheit behaftet [97]. Jedoch konnte gezeigt werden, dass bei normalen Vitalparametern (wie Herz-, und Atemfrequenz, oder Körpertemperatur) eine Pneumonie mit hoher Sicherheit ausgeschlossen werden kann [98, 99]. Die Diagnose sichern kann ein konventionelles Röntgen-Bild des Thorax mit Nachweis eines Infiltrats. Der fehlende Nachweis kann eine Lungenentzündung aber nicht sicher ausschließen. Im Gegenzug müssen auch bei Nachweis eines Infiltrats nicht-infektiöse Ursachen in Betracht gezogen werden (z.B. Autoimmunerkrankungen). Die Therapie ist bei klassischen bakteriellen Erregern (nicht Mykobakterien) oft empirisch, und schließt häufige Erreger mit ein. Einer der häufigsten und wichtigsten bakteriellen Pathogene der ambulant erworbenen Pneumonie ist *S. pneumoniae* (Pneumokokken), schwere nosokomial erworbene Pneumonie werden häufig durch *Pseudomonas aeruginosa* (*P. aeruginosa*) verursacht. Während Pneumokokken weitgehend auf die meisten Antibiotika empfindlich sind, zeichnet sich *P. aeruginosa* durch eine schnelle und breite antibiotische Resistenzentwicklung aus. Aufgrund der Pathogenität beider Bakterien und der Ausbildung von Resistenzen vor allem bei nosokomialen Erregern wie *P. aeruginosa* sind zusätzliche Therapieoptionen wünschenswert. Weitere wichtige Erreger einer ambulant erworbenen bakteriellen Pneumonie sind *Haemophilus influenzae*, Legionellen, oder Mykoplasmen. Weitere häufige Erreger einer nosokomialen Pneumonie sind gramnegative Erreger wie Klebsiellen, Enterobacter, Proteus oder Serratia. Weniger akute Verläufe bedingt eine pulmonale Tuberkulose, die bei entsprechender Anamnese (Kontakt mit Tuberkulosepatienten, Reiseanamnese/Herkunftsland), oder einem entsprechenden Risiko (HIV-Infektion, Immunsuppression) immer als Differentialdiagnose in Betracht gezogen werden sollte. Die Pathophysiologien die einer Pneumonie zugrunde liegt variieren, und sind erregerabhängig sehr verschieden.

1.6 Aspiratonspneumonitis

Aspiration von Mageninhalt resultiert in steriler Pneumonitis oder Mendelson Syndrom, und kommt in Patienten mit eingeschränktem Bewusstsein durch zum Beispiel Allgemeinanästhesie, Intoxikation oder Schlaganfall bedingt durch eingeschränkte Reflexe und einen verminderten Epiglottis-Verschluss vor [100]. Aber auch nur im Schlaf kann der verminderte Epiglottis-Verschluss Aspirationen begünstigen [101]. In einer prospektiven Studie wurde zumindest eine Aspiration in 88,9% aller intubierten Patienten festgestellt [102]. Abhängig von der Menge des Aspirats und dem pH des Mageninhaltes, kann es zu einem akuten Lungenschaden bis zu einem ARDS (acute respiratory distress syndrome) kommen [103]. Wichtig zu erwähnen ist, dass die Aspiration von Mageninhalt der stärkste unabhängige Risikofaktor für eine bakterielle beatmungsassoziierte Pneumonie ist [102, 104, 105]. Zudem haben Patienten mit ARDS ein höheres Risiko bakterielle Superinfektionen zu erleiden als intubierte Patienten ohne ARDS [106, 107]. Auch gastroösophagealer Reflux kann das Entstehen einer Pneumonie begünstigen [108, 109]. Zusammenfassend erhöhen also die Aspirationspneumonie, als auch ein ARDS das Risiko für eine bakterielle Pneumonie. In experimentellen Arbeiten konnte unter anderem auch in der vorliegenden Arbeit gezeigt werden, dass eine bakterielle Superinfektion nach Säureaspiration zu einem starken unkontrollierten Bakterienwachstum führt [110, 111]. In der klinischen Praxis ist eine antibiotische Therapie nach Aspiration initial nicht empfohlen [100], da dies zu erhöhtem antibiotischem Druck ohne klinischen Benefit führt [112]. Sollte der Patient sich jedoch klinisch verschlechtern, zum Beispiel Fieber oder Tachypnoe entwickeln, ist eine antibiotische Therapie zu empfehlen. Diese Entwicklung weist auf eine bakterielle Superinfektion hin, die bis ca. 48 Stunden nach dem Aspirationsereignis am häufigsten ist, und klinisch selten eindeutig von einer sterilen „reinen“ Aspiration zu unterscheiden ist [100] (eigene unpublizierte Daten). Die Mechanismen dieses unkontrollierten Wachstums sind sicher multifaktoriell, und durch eine Vielzahl lokaler Faktoren bedingt [93]. Welche Faktoren aber maßgeblich nach Säureaspiration die Anfälligkeit für bakterielle Infektionen erklärt, ist bisher weitgehend unbekannt. AM spielen jedenfalls eine wichtige Rolle in der Beseitigung geringer Mengen von Bakterien, die in die unteren Atemwege gelangen.

1.7 Peritonitis

Die infektiöse Peritonitis ist definiert als eine Entzündungsreaktion hervorgerufen durch Mikroorganismen im sonst sterilen Peritoneum (Bauchfell). Das Peritoneum besteht aus einer Epithelschicht (Mesothel), und erstreckt sich von der Unterseite des Zwerchfells bis zum Beckenboden. Innerhalb des Peritoneums liegt der Großteil des Magen-Darm-Trakts (Magen, Jejunum, Ileum, Caecum, Appendix, Colon transversum und sigmoideum, distales Rektum, Leber, Gallenblase, Pankreasschwanz und Milz; bei Frauen zudem der Eierstock und die Eileiter). Eine Peritonitis kann entweder primär, ohne Perforation oder vorbestehender gastrointestinaler Infektion, oder sekundär nach Infektionen/Perforationen der angrenzenden Organe wie zum Beispiel perforierter Sigmadivertikulitis, Appendizitis oder bei Anastomoseninsuffizienz nach Darmoperationen oder gynäkologischen oder urologischen Operationen, vorkommen. Bestätigt wird die Diagnose durch eine erhöhte Zahl an neutrophilen Granulozyten (>250/µl) in der peritonealen Lavage, und/oder einem entsprechenden Erregernachweis. Die auslösenden Erreger sind meist Enterobakterien, am häufigsten *E. coli* [113]. Diese Infektionen sind meist polymikrobiell, zumindest experimentell wurde jedoch *E. coli* als relevantester Erreger polymikrobieller Peritonitiden nach Darmperforation beschrieben [114]. Die tertiäre Peritonitis wird definiert als eine erneute Infektion nach behandelter sekundärer Peritonitis mit nosokomialen Erregern wie koagulase-negativen Staphylokokken, Enterokokken, *P. aeruginosa*, oder Candida [115]. Gesondert betrachtet werden können Peritonitiden bei liegendem Dialysekatheter, da hier vor allem Hautkeime eine Rolle spielen. Während bei sekundärer und tertiärer Peritonitis meist eine klare Ursache (vorliegende Infektion/Penetration) vorliegt, führen bei der primären Peritonitis andere Ursachen zu einer Infektion der sonst sterilen Bauchhöhle. Im klinischen Alltag kommt die primäre Peritonitis am häufigsten bei Patienten mit Leberzirrhose vor. Hier spielen mehrere Faktoren, die die Immunabwehr beeinträchtigen, eine Rolle: bei Vorliegen von Aszites kommt es zu einer Verdünnung von Antikörpern oder Komplement [116, 117]; auch wurden zelluläre Defekte der Bakterienabwehr bei Zirrhose beschrieben [118, 119], sowie soluble Faktoren, die die Immunabwehr von PMs beeinträchtigen [120]. In primärer bakterieller Peritonitis in Patienten mit Zirrhose wurde, analog zu Tierversuchen (s. „Peritoneale Makrophagen“), ein Verlust von LPMs zu Beginn der Infektion beschrieben [68]. PM kommt wahrscheinlich in der Erkennung und Beseitigung von Erregern als „first line of defense“, als auch im weiteren Verlauf der

Infektion eine zentrale Bedeutung zu. Beeinträchtigungen der antibakteriellen Abwehr von PM zu verstehen ist daher wichtig, um mögliche neue Diagnose- oder Therapieansätze entwickeln zu können.

2. Ergebnisse und Diskussion

2.1. Die Entzündung der Säureaspiration vermindert antibakterielle Eigenschaften von alveolären Makrophagen (Anlage A)

American Journal of Respiratory and Critical Care Medicine, 2009, 180(12):1208-17

Eine erhöhte Anfälligkeit für eine bakterielle Superinfektion ist für eine Vielzahl von Lungenschäden beschrieben. Jedoch gibt es nur eine beschränkte Anzahl von Daten, die antimikrobielle Eigenschaften von AM während einer Inflammation charakterisieren. Durch ihre zentrale Rolle nicht nur in der Initiierung, sondern auch Terminierung einer Entzündung, ist davon auszugehen, dass deren anti-inflammatorische Polarisierung während der Resolutionsphase einer Entzündung beschränkte antibakterielle Eigenschaften bedingt. Wie bereits erwähnt, ist die Aspiration von Säure der stärkste unabhängige Risikofaktor für die Entwicklung einer bakteriellen Pneumonie bei beatmeten Patienten [102]. *P. aeruginosa* ist einer der wichtigsten Erreger der nosokomialen Pneumonie [121]. Zudem weist *P. aeruginosa* eine hohe Pathogenität auf, und kann schnell Resistenzen gegenüber Antibiotika entwickeln [122]. Wir konnten in der vorliegenden Arbeit zeigen, dass eine Superinfektion mit *P. aeruginosa* nach Säureaspiration zu einer massiv erhöhten Bakterienlast in der Lunge, und einer höheren Mortalität führt. *Ex vivo* wiesen AM während der Resolution einer Entzündung, gekennzeichnet durch fast normalisierte Zytokinparameter, starkem Rückgang von Neutrophilen im alveolären Raum, sowie einer starken Expression von IRAK-M, einem Gegenspieler der TLR-Signalwege, eine reduzierte Fähigkeit auf, *P. aeruginosa* zu phagozytieren. In diesem Zusammenhang testeten wir das Peptid $B\beta_{15\text{-}42}$, welches bis dahin in anderen Organen durch Hemmung der Leukozytendiapedese, und eine Reduktion der Ödembildung anti-inflammatorische Eigenschaften aufwies [123, 124]. Wir konnten diese Ergebnisse auf die Lunge erweitern, und zeigen, dass das Peptid sowohl nach LPS- als auch Säure-Applikation intratracheal den Neutrophileneinstrom, als auch die Ödembildung, und im Trend die Oxidierung von Phospholipiden, vermindert. Durch Verabreichung des Peptids während der Säureaspiration kam es dadurch zu einer stark verminderten Entzündung, und in Folge konnten die antibakteriellen Eigenschaften von AM *ex vivo* erhalten, als auch die Bakterienlast und die Mortalität in der Superinfektion *in vivo* normalisiert werden. Dieser therapeutische Nutzen von $B\beta_{15\text{-}42}$ bestand jedoch nur bei einer sehr frühen Gabe nach Aspiration (bis 2 Stunden später).

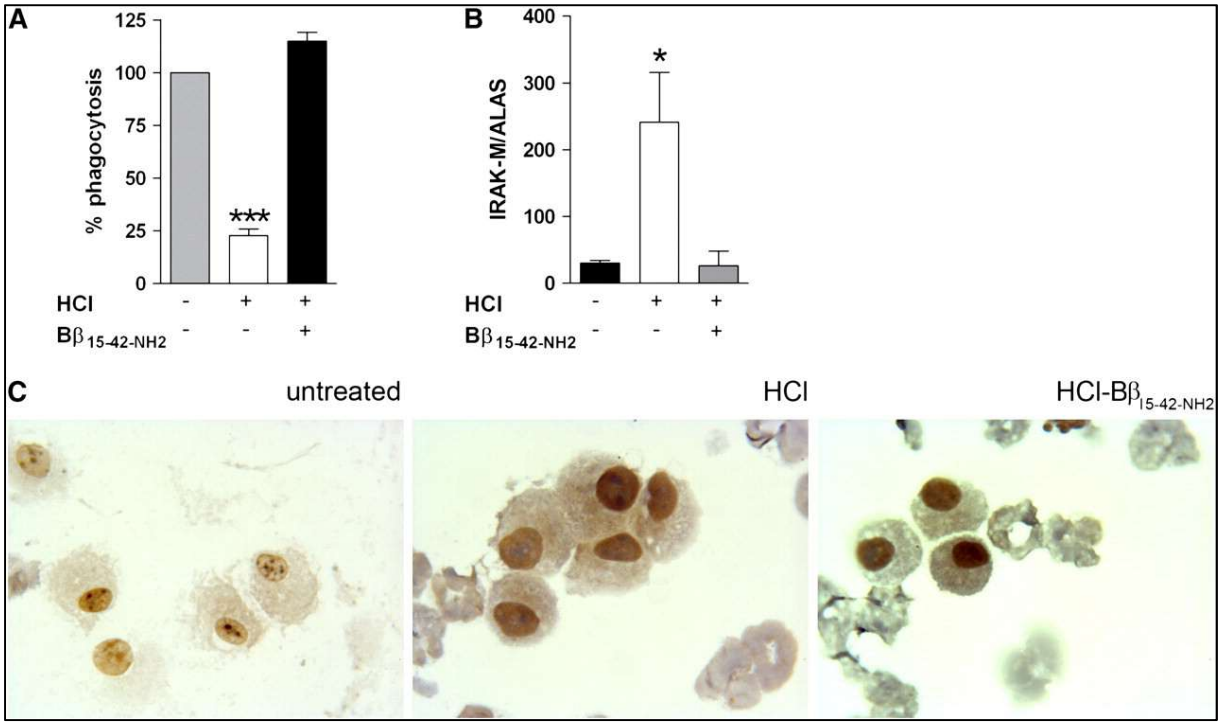

Abbildung 5: **Säureaspiration vermindert die Phagozytosefähigkeit von AM während der Resolutionsphase der Entzündung.** 24 Stunden nach Gabe von 50µl 0,9% NaCl oder 0,1N HCl intratracheal (mit/ohne intraperitonealer Injektion von Bβ15-42 zum Zeitpunkt 0, 1h und 6h nach Aspiration), wurden AM ex vivo auf deren Fähigkeit untersucht *P. aeruginosa* aufzunehmen (**A**). Die unter den gleichen Versuchsbedingungen gewonnenen AM wurden auf IRAK-M Expression transkriptionell (**B**), oder auf Proteinebene mittels Immunhistochemie (**C**) untersucht. *P < 0.05; *** P < 0.001 versus Kontrolle (sham). Adaptiert nach [110], mit Erlaubnis.

Wie erwähnt sind bakterielle Superinfektionen nach Aspiration vor allem bei beatmeten Patienten sehr häufig. Bei diesen Patienten kommt es oftmals zu einer Kolonisation der Atemwege mit meist gramnegativen Bakterien (*P. aeruginosa*, *A. baumannii* oder *Klebsiella pneumoniae*). AM befinden sich in den Alveolen und den Atemwegen, und können geringere Mengen dieser Bakterien auch in benachbarten Alveolen in Schach halten [46]. Unsere Arbeit zeigt, dass Entzündungen, wie hier eine Pneumonitis induziert durch Säure, den Aktivitätszustand von AM verändert, und deren antibakterielle Eigenschaften reduziert. Wird die Entzündung abgeschwächt, wie durch das Peptid $B\beta_{15\text{-}42}$, bleiben die antibakteriellen Eigenschaften, trotz Gabe von Säure, erhalten. Wir fanden keinen direkten Einfluss des Peptids $B\beta_{15\text{-}42}$ auf antibakterielle Eigenschaften von AM (unpublizierte Daten). Man kann davon ausgehen, dass diese Polarisierung andere Funktionen, wie zum Beispiel die Geweberegeneration, begünstigt. So konnten wir in Folgearbeiten zeigen, dass AM zu dem Zeitpunkt, an dem sie verminderte antibakterielle Eigenschaften aufweisen, apoptotische Neutrophile besser aufnehmen können, und die Geweberegeneration fördern

(unpublizierte Daten). Mechanistisch dürfte dies auf einen veränderten Metabolismus zurückzuführen sein. Eine kürzlich erschienene Arbeit fand ebenso einen Phagozytosedefekt von AM nach *E. coli* oder Influenza Pneumonie, welcher bis 6 Monate nach der Infektion fortbestand [54]. Interessanterweise waren hierfür Signale in der Gewebenische verantwortlich, sodass transplantierte AM unbehandelter Mäuse in der geschädigten Lunge ebenso eine Einschränkung der Phagozytose aufwiesen. Zeitlich fanden wir eine komplette Erholung der antimikrobiellen Eigenschaften 8 Tage nach der Aspiration (unpublizierte Daten).

Zusammenfassend konnten wir in der vorliegenden Arbeit zeigen, dass antibakterielle Eigenschaften von AM während der Resolutionsphase einer Aspirationspneumonitis vermindert sind, und eine Pneumonie mit *P. aeruginosa* begünstigen. Der Aktivitätszustand von AM ist somit in der Kontrolle von Bakterien entscheidend. Die Identifizierung von funktionellen Eigenschaften von AM, die sich im Laufe der Resolution einer Lungenentzündung ändern, sowie die Entschlüsselung der jeweiligen Mechanismen können einen Therapieansatz für diverse Entzündungszustände bzw. Infektionen liefern.

2.2 Myeloisches PTEN fördert die Entzündung, und vermindert antibakterielle Eigenschaften während einer Pneumokokken-Pneumonie (Anlage B)

Journal of Immunology, 2010, 185(1):468-76

Der bekannte Tumor-Suppressor PTEN (phosphatase and tensin homolog deleted on chromosome 10) ist eine Phosphatase, die die enzymatische Aktivität von Phosphoinositid-3-Kinase (PI3K) antagonisiert. PI3K ist wichtig in zentralen zellulären Abläufen, wie in der Zellproliferation, aber auch in Effektorfunktionen von Leukozyten (Neutrophile, Monozyten, sowie Lymphozyten) wie der Chemotaxis, der Phagozytose oder der Phagosom-Reifung [125]. So konnte zum Beispiel in Neutrophilen gezeigt werden, dass PTEN deren Superoxid-Produktion und Transmigration antagonisiert [126]. Die antibakterielle Rolle von PTEN in organspezifischen Makrophagen war bislang nicht bekannt. In der vorliegenden Arbeit untersuchten wir diese in myeloiden Zellen (Neutrophile, Monozyten, Makrophagen) während der Pneumokokkenpneumonie. Hierfür verwendeten wir zellspezifische PTEN-KO Mäuse, die kein PTEN in Zellen aufweisen, die Lysozym M (LysM) exprimieren. Dies sind Makrophagen, Monozyten, Neutrophile und einige dendritische Zellen [127]. In diesen KO-Zellen ist PI3K konstitutiv aktiv, und dies resultierte in Akt- und GSK3β-Phosphorylierung, Signalwege die „downstream“ der PI3K sind. Mäuse mit diesem Defekt (LysM-Cre/PTEN$^{flox/flox}$, in der Folge kurz PTEN^{MC-KO} - myeloid-cell KO - genannt), überlebten eine Pneumokokkenpneumonie besser, und wiesen eine geringere Morbidität als Wildtyp-Mäuse auf. In zellbasierten Analysen fanden wir, dass AM von PTEN^{MC-KO} Mäusen nach Stimulation mit *S. pneumoniae* weniger TNF-α, und – im Gegensatz zu KM – weniger Stickstoff-Radikale bildeten, jedoch überraschenderweise die Bakterien besser phagozytieren und abtöten konnten (Abb. 6). *In vivo* fanden sich zu einem frühen Zeitpunkt (6 Stunden nach Infektion) bei PTEN^{MC-KO} Mäusen in der Lunge weniger TNF-α und keratinocyte-derived chemokine (KC), jedoch mehr IL-10. Überraschenderweise war die Neutrophilenmigration in diesen Tieren vermindert, und die Bakterienlast aber in beiden Gruppen gleich. 48 Stunden nach Infektion bestätigten sich diese Befunde, jedoch war die Bakterienlast in der BAL erhöht. Schließlich fand sich in den PTEN^{MC-KO} Mäusen 65 Stunden nach Infektion bei geringerem Lungenschaden eine gleiche Bakterienlast wie in den Wildtyp-Mäusen.

Da mehrere Arbeiten, im Gegensatz zu unseren Resultaten, einen erhöhten Neutrophileneinstrom bei erhöhter PI3K Aktivität zeigten, so zum Beispiel in *E. coli* Peritonitis [126], verabreichten wir Mäusen *S. pneumoniae* intraperitoneal. In diesen Versuchen konnten wir den erhöhten Neutrophileneinstrom in $PTEN^{MC\text{-}KO}$ Tieren auch mit einem grampositiven Erreger peritoneal bestätigen. Zudem sezernierten PM dieser Tiere *in vitro* höhere Mengen an KC.

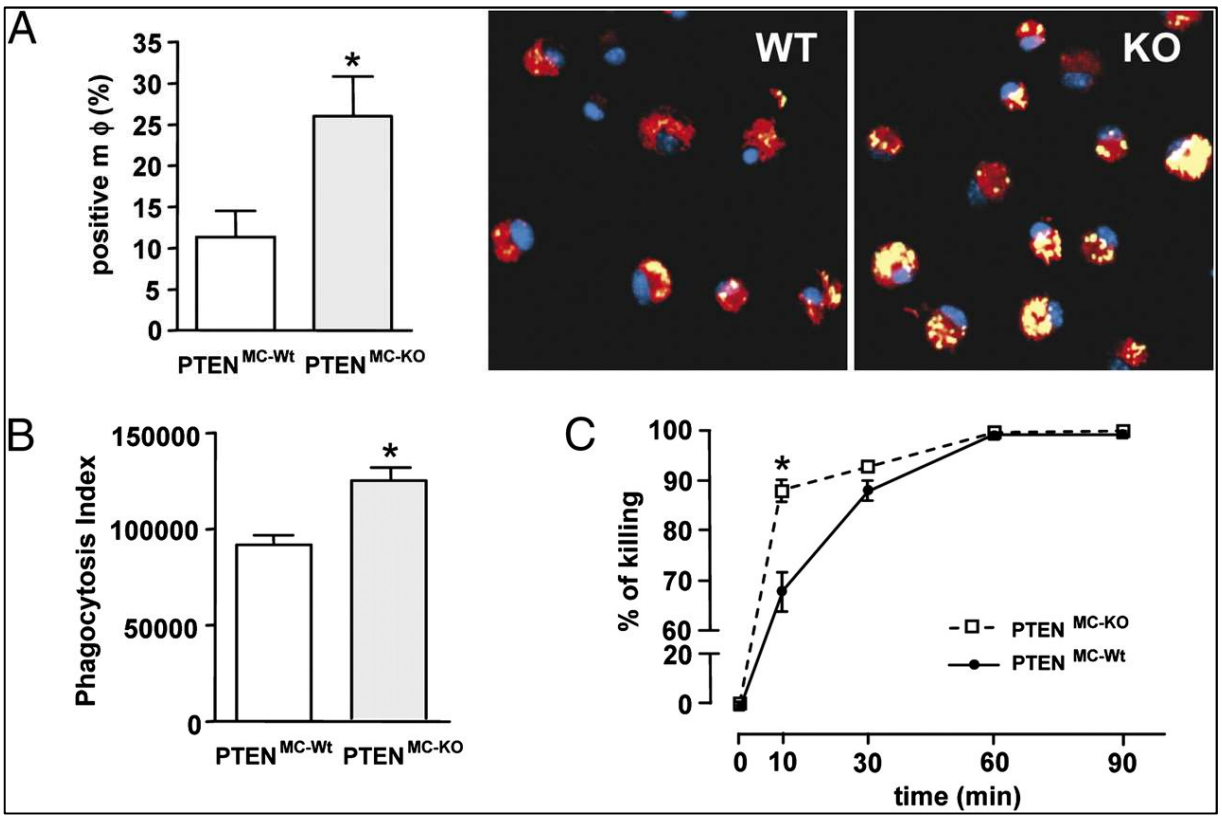

Abbildung 6: **PTEN vermindert antimikrobielle Eigenschaften von AM.** AM von $PTEN^{MC\text{-}KO}$ Mäusen und WT-Kontrollen ($PTEN^{MC\text{-}Wt}$) wurden mittels BAL gewonnen, und *ex vivo* auf deren Fähigkeit mit einem Farbstoff (FITC) markierte *S. pneumoniae* nach 30 Minuten zu phagozytieren, untersucht, und mikroskopisch (**A**) oder mittels FACS (**B**) quantifiziert. (**A**) rechts: der Zellkern wurde mittels DAPI (blau), FITC-markierte (grün) aufgenommene Bakterien (gelb) wurden durch Kolokalisation mit Lysosomen (rot) identifiziert. Abtöten von intrazellulären *S. pneumoniae* wurde über die Zeit analysiert (**C**). Daten sind als Mittelwert +/- Standardfehler gezeigt. *P < 0.05 $PTEN^{MC\text{-}Wt}$ versus $PTEN^{MC\text{-}KO}$. Adaptiert nach [128], mit Erlaubnis.

PI3K ist involviert in eine Vielzahl von zellulären Prozessen. In Zusammenhang mit Entzündungen wurden sowohl pro- als auch anti-inflammatorische Eigenschaften der Kinase gezeigt [129-131]. PI3K-Antagonisten von teils komplementären Klassen oder Isoformen wurden zur Behandlung von Autoimmunkrankheiten entwickelt [129]. PTEN-Defizienz in Makrophagen resultierte jedoch in bisherigen Studien durchweg in einer anti-inflammatorischen Polarisierung [128, 132, 133]. Hiervon ausgenommen ist

eine Arbeit in Zusammenhang mit zystischer Fibrose, die eine erhöhte entzündliche Aktivität in KM fand [134]. In einem Modell der Pneumokokken-Pneumonie wurde gezeigt, dass die γ–Untereinheit (p110γ) von PI3K, nicht für den Neutrophilen-, jedoch für den Monozyteneinstrom wichtig ist, und insgesamt, dass die Hemmung oder der knock out sich nachteilig auf den Verlauf einer Pneumokokkenpneumonie auswirkt [63]. Antibakterielle Eigenschaften von Makrophagen wurden in dieser Arbeit nicht adressiert.

In der vorliegenden Studie fanden wir erhöhte antibakterielle Eigenschaften (Phagozytose und intrazelluläres Abtöten) von Pneumokokken durch AM von $PTEN^{MC-KO}$ Mäusen. Interessant ist, dass PTEN-Defizienz in AM zu einer verminderten Zytokinproduktion, aber gleichzeitig zu erhöhten antibakteriellen Eigenschaften führt. Andere Arbeiten zeigten einen M2-Phänotyp in PTEN-KO Makrophagen im Knochenmark [135] oder in KPC [136], wobei antibakterielle Eigenschaften nicht untersucht wurden. In AM ohne PTEN fanden wir eine verminderte Produktion von Stickstoffradikalen, passend zu einem „M2-ähnlichen“ Phänotyp. Die Ursache für das verbesserte Abtöten widerspricht diesem Ergebnis, und bleibt somit unklar. Teilweise passend zu unseren Ergebnissen zeigten Riquelme und Mitarbeiter, dass in Patienten mit zystischer Fibrose der CFTR (cystic fibrosis transmembrane conductance regulator)-Defekt zu verminderter PTEN-Aktivität führt. Eine Korrektur des CFTR-Defektes erhöhte die PTEN-Aktivität, und führte zu verbessertem Abtöten von *P. aeruginosa* in einem Tiermodell, korrigierte aber auch eine starke Entzündung in murinen KM und humanen Monozyten [134]. Die antientzündlichen Eigenschaften von PTEN in dieser Studie verhielten sich hier somit gleich zu unserer Arbeit, aber die antimikrobiellen Eigenschaften waren in Anwesenheit bzw. Erhöhung von PTEN verbessert. Zellspezifische Experimente mit AM und *P. aeruginosa* wurden in dieser Arbeit leider nicht durchgeführt. Die verbesserte Bakterienabwehr ist somit wahrscheinlich auf eine Verbesserung der Grundkrankheit zurückzuführen.

Ein sehr unerwartetes Ergebnis unserer Arbeit war die konsistent geringere Neutrophilenmigration während einer Pneumonie. Ursächlich hierfür könnten die erhöhten antibakteriellen Eigenschaften der AM sein, so dass in weiterer Folge weniger Neutrophile rekrutiert werden. Dagegen spricht aber, dass die Neutrophilenzahl auch dann erniedrigt war, als die Bakterienlast in PTEN-defizienten Mäusen erhöht war. Eine andere Erklärung könnte die verminderte Produktion von TNF-α sein, die dann zu einer verminderten Produktion von KC zu frühen und späten

Zeitpunkten führt. Möglicherweise ist, wie für *E. coli* gezeigt [137], auch die Phagozytose von Pneumokokken durch Neutrophile die kein PTEN exprimieren erhöht, sodass weniger Neutrophile rekrutiert werden müssen. Ein anderer entscheidender Faktor, der zur besseren Bakterienkontrolle beiträgt, könnte die konstitutiv erhöhte Anzahl von AM in PTEN-KO Mäusen sein (unpublizierte Daten) [137].

Subramanian et al. demonstrierten zuvor, dass der KO von PTEN die Transmigration von Neutrophilen in *in vitro* Versuchen, als auch während *E. coli*-induzierter und steriler Peritonitis (induziert durch Thioglykolat) klar erhöht. Wir konnten diese Ergebnisse mit Thioglykolat bestätigen, und fanden auch eine erhöhte Neutrophilenmigration in einer Pneumokokken-Peritonitis. Im Gegensatz dazu führt eine *E. coli* Pneumonie ebenso zu einer erhöhten Neutrophilenmigration in PTEN-defizienten Mäusen [137]. Diese klar organ- und pathogenspezifischen Unterschiede machen einmal mehr deutlich wie wichtig Untersuchungen der ortsansässigen Makrophagen bzw. unterschiedlicher Infektionsmodelle sind, und allgemeine Aussagen ohne vorhergehende Untersuchungen unzulässig sind.

Zusammenfassend konnten wir zeigen, dass der KO von PTEN in myeloischen Zellen protektiv während einer Pneumokokkenpneumonie ist. Ursächlich hierfür dürften die erhöhten antibakteriellen Eigenschaften von AM zusammen mit anti-inflammatorischen Eigenschaften sein, die einen geringeren Lungenschaden bedingten.

2.3 Entzündungen erhöhen die Expression der Efflux-Pumpe BCRP-1 auf Makrophagen – Einfluss auf die intrazelluläre Beseitigung von *Mycobacterium tuberculosis* (Anlage C)

International Journal of Antimicrobial Agents, 2017, 50(1):55-62

Tuberkulose verursacht ungefähr 1,5 Millionen Todesfälle pro Jahr, und Patienten, die mit resistenten Stämmen infiziert sind, weisen häufiger Therapieversagen auf [138]. Die Aktivierung von Makrophagen, speziell durch IFN-γ, während einer Tuberkulose-Infektion trägt entscheidend zur Kontrolle der Mykobakterien bei [139, 140]. Makrophagen stellen zudem eine mögliche Niche, in denen Mykobakterien medikamentöse Therapien überleben können, dar [141, 142]. Ungleiche Verteilung der Medikamente in den verschiedenen Kompartimenten (intrazellulär und extrazellulär) könnte zur Entwicklung von Resistenzen, und der Persistenz von Mykobakterien beitragen. Efflux-Pumpen sind auf Zell- oder endosomalen Membranen lokalisiert und befördern fremde (xenobiotische) oder eigene Substanzen (z.B. Gallensäuren) aus der Zelle. So konnte gezeigt werden, dass Efflux-Pumpen während einer onkologischen Chemotherapie hochexprimiert werden können, und zum verminderten Therapieansprechen durch reduzierte intrazelluläre Konzentrationen beitragen können [143]. Im Gegensatz zu Efflux-Pumpen, die auf Bakterien oder Mykobakterien exprimiert sind [144], gibt es wenig Daten zu solchen auf Makrophagen. Ob Efflux-Pumpen auf Makrophagen die intrazelluläre Niche beeinflussen, bzw. im Rahmen einer Entzündung moduliert werden, und dadurch antimykobakterielle Eigenschaften beeinflussen, ist bisher weitgehend unbekannt.

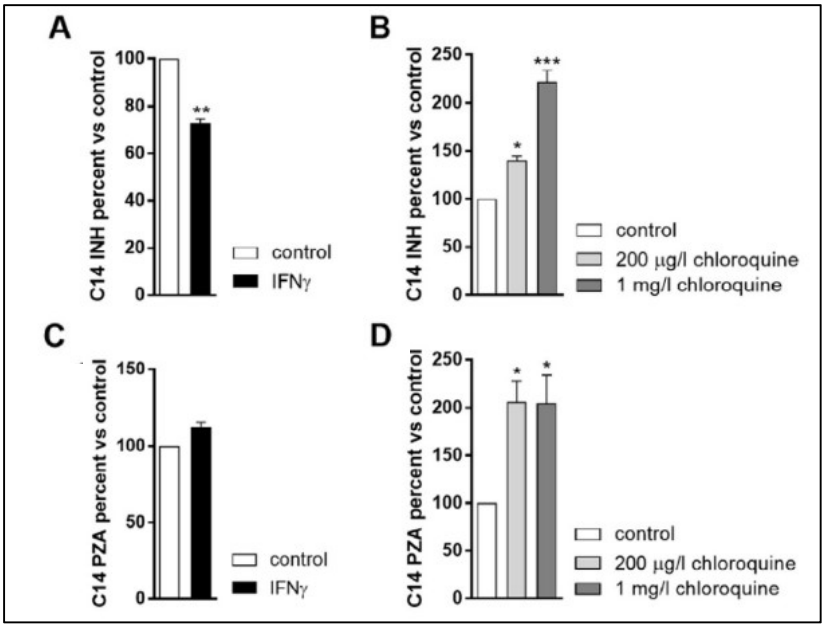

Abbildung 7: Einfluss einer Entzündung und von Chloroquin (CQ) auf intrazelluläre INH und PZA-Konzentrationen. THP-1 Makrophagen wurden mit 50 ng/ml IFN-γ über die Nacht stimuliert. Im Anschluss wurde unmarkiertes und radioaktiv markiertes INH (14C) oder PZA (14C) für 30 Minuten hinzugegeben, gewaschen, und im Anschluss wurde die Radioaktivität per flüssiger Szintillation gemessen (**A**, **C**). In den anderen Experimenten wurde nach

Inkubation mit INH oder PZA die Zellen mit Chloroquin (**B**, **D**) für 30 Minuten inkubiert. Daten (A-D) sind als Mittelwert +/- Standardfehler gezeigt. *P < 0.05; **P < 0.01; ***P < 0.001 versus Kontrolle. Adaptiert nach [145], mit Erlaubnis.

Wir haben in der vorliegenden Arbeit gefunden, dass Isoniazid (INH) und Pyrazinamid (PZA) Substrate der Efflux-Pumpe „breast cancer resistance protein-1“ (BCRP-1) sind, welche auf humanen Makrophagen, und murinen AM (unpublizierte Daten) *in vitro* und im Tuberkulose-Granulom *in vivo* exprimiert ist. Interferon-γ (IFN-γ) erhöhte die Expression von BCRP-1, und führte zeitgleich zu einer verminderten intrazellulären Konzentration von INH, nicht aber von PZA (Abb. 7). Zudem konnte gezeigt werden, dass das bekannte Antimalaria-Medikament Chloroquin BCRP-1 blockiert, was wiederum zu einer erhöhten intrazellulären Konzentration von INH und PZA (Abb. 7), aber auch zu einem verbesserten Abtöten von Mykobakterien in den Makrophagen führte. Ebenso bewirkte ein BCRP-1 Inhibitor in Kombination mit INH, jedoch nicht alleine, eine verbesserte intrazelluläre Clearance von *M. tuberculosis*. Die tuberkulostatische Wirkung und intrazelluläre Konzentration von PZA konnte durch Chloroquin ebenso erhöht werden, jedoch blieben die intrazellulären PZA Konzentrationen sowohl durch IFN-γ, als auch einen BCRP-1 Inhibitor unbeeinflusst. Dies könnte daran liegen, dass Substrate und Inhibitoren von Efflux-Pumpen polyspezifisch sind [122], und Chloroquin somit eventuell mehrere Efflux-Pumpen hemmt. Chloroquin oder der BCRP-1 Inhibitor konnten weiters nicht für sich alleine, und auch nicht in Kombination mit INH oder PZA das Wachstum extrazellulärer Mykobakterien beeinflussen. Somit ist nicht von einer direkten antimykobakteriellen Wirkung von Chloroquin oder dem BCRP-1 Inhibitor auszugehen.

Obwohl die Erstlinenmedikamente INH, Rifampicin, Ethambutol und PZA bereits seit Jahrzehnten in Verwendung sind, weiss man relativ wenig über deren Pharmakokinetik und -dynamik [120]. Das liegt vor allem an der Komplexität einer Tuberkulose-Erkrankung, da Mykobakterien intra- und extrazellulär in verschiedenen Kompartimenten zu finden sind, die sich über Monate bis Jahre etablieren können. Für einen Therapieerfolg, und um Resistenzen zu vermeiden, muss die tuberkulostatische Therapie 6 Monate eingenommen werden, und stellt daher eine medizinische und logistische Herausforderung dar. Verkürzte Therapieregime konnten bislang nicht erfolgreich eingesetzt werden [121]. Unsere Ergebnisse zeigen, dass die intrazelluläre Konzentration von zumindest INH durch eine Entzündung, in diesem Fall imitiert durch das im Kontext mit Mykobakterien-Infektionen relevante IFN-γ, verändert werden kann.

Unabhängig vom Kontext der Mykobakterien und antibiotischen Therapie konnten wir auch zeigen, dass BCRP-1 durch IFN-γ, aber auch LPS (unpublizierte Daten) alleine hochreguliert wird. Eine erhöhte Expression der Efflux-Pumpe P-glycoprotein (P-gp) wurde auch nach Stimulation mit IFN-γ in humanen Makrophagen beobachtet [123]. Bislang wurde gezeigt, dass P-gp antivirale Eigenschaften zumindest gegen behüllte Viren wie HIV oder Influenza aufweist [124]. Welche pathophysiologische Bedeutung die Induktion von P-gp oder BCRP-1 in Makrophagen während bakteriellen Infektionen haben könnte, ist unseres Wissens bislang unbekannt. Der BCRP-1 Inhibitor zeigte alleine keinen Einfluss auf das Abtöten intrazellulärer Mykobakterien. Auch konnten wir keine Effekte auf die Sekretion diverser Zytokine nach Stimulation mit grampositiven und gramnegativen Bakterien beobachten (unpublizierte Daten). Um die Rolle von Efflux-Pumpen auf Makrophagen während bakteriellen Infektionen zu verstehen, wäre es interessant Knockout Mäuse diverser Efflux-Pumpen in entsprechenden Infektionsmodellen zu studieren. Arbeiten zu diesem Thema liegen bislang nicht vor.

Zusammenfassend konnte in der vorgelegten Arbeit gezeigt werden, dass die wichtigen Erstlinienmedikamente PZA und INH über BCRP-1 aus Makrophagen gepumpt werden, die Expression und Funktion von BCRP-1 durch IFN-γ erhöht wird, und Chloroquin durch eine Hemmung der Efflux-Pumpe das intrazelluläre Abtöten von *M. tuberculosis* in Kombination mit den Tuberkulostatika unterstützt.

Allgemein erweitern unsere Daten die komplexe Pharmakodynamik von Tuberkulostatika, und zeigen eine mögliche Therapie zur Eradikation von intrazellulären Persistern in Makrophagen, und damit eine mögliche Therapieverkürzung bei Behandlung der latenten oder aktiven Tuberkulose auf. Die pathophysiologische Funktion einer erhöhten Expression von Effluxpumpen während bakteriellen Infektionen, wie hier erstmals mit BCRP-1 gezeigt, ist bislang unerforscht.

2.4 Oxidierte Phospholipide inhibieren die Phagozytose in peritonealen Makrophagen über WAVE-1 (Anlage D)

Journal of Clinical Investigation, 2013, 123(7):3014–3024

Peritonitis ist eine häufige Ursache von Sepsis, und *E. coli* ist ein wichtiger, wenn nicht der wichtigste Erreger dieser Infektion. Oxidierte Phospholipide (OxPL) kommen in „low density lipoproteins“ (LDL) oder in der Zellmembran vor, und können im Rahmen von Entzündungen enzymatisch (über 12/15-Lipoxygenase) oder nicht-enzymatisch durch Sauerstoffradikale, die zum Beispiel von neutrophilen Granulozyten am Entzündungsort gebildet wurden, generiert werden [146]. OxPL selbst modulieren das Entzündungsgeschehen, so zum Beispiel in der Arteriosklerose [147]. Daher nahm man lange an, dass sie vor allem pro-inflammatorische Eigenschaften besitzen. Im Gegensatz hierzu fanden Bochkov et al., dass OxPL die Erkennung von LPS über den TLR-4-Komplex verhindern, und dadurch in einem Modell der LPS-Peritonitis protektive anti-inflammatorische Eigenschaften aufwiesen [148]. In einer Folgestudie fanden wir, dass die intraperitoneale Gabe von OxPL, verglichen zu nichtoxidierten Phospholipiden, in einem Peritonitis-Modell mit *E. coli* das Überleben verminderte [149]. Gegen unsere Erwartungen war die Zytokinproduktion nicht vermindert, jedoch die Phagozytose von PM *E. coli* eingeschränkt. In der hier vorgelegten Studie konnten wir nicht nur den Mechanismus dieser Inhibition in PM, sondern weitere wichtige pathophysiologische Erkenntnisse gewinnen. So fanden wir unter anderem, dass OxPL während einer *E. coli* Peritonitis in Mengen gebildet werden, die die antibakteriellen Eigenschaften von PM beeinträchtigen. Mechanistisch gelang uns der Nachweis, dass OxPL über eine durch die Proteinkinase A (PKA) vermittelte Aktivierung eine Aktinpolymerisation in PM verursachen. PKA weist eine Vielzahl von Eigenschaften auf, und deren Aktivität wird zeitlich und örtlich durch sogenannte „PKA-anchoring proteins“ (AKAPs) bestimmt [150]. Von diesen AKAPs sind drei beschrieben, die an das Aktin-Zytoskelett gebunden sind. Von diesen konnten wir das AKAP WAVE-1 als relevantes Protein ermitteln, das die Wirkung von OxPL vermittelt. Verminderung oder KO von WAVE-1 in PM führte zu einer uneingeschränkten Phagozytose von *E. coli*, und reversierte den Phänotyp erhöhter Mortalität in der *E. coli* Peritonitis *in vivo*. Zwar sahen wir einen Trend zu geringerer Bakterienlast in WAVE-1 KO Mäusen, jedoch zeigte sich, obwohl per se in der *E. coli* Peritonitis OxPL

gebildet werden (Abb. 8A), kein verbessertes Überleben dieser Tiere in unserem Modell.

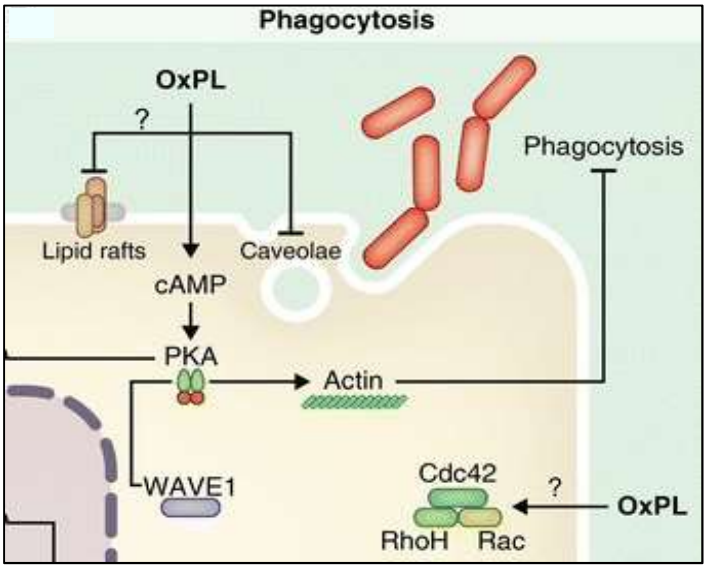

Abbildung 8: Schematische Darstellung der Wirkung von OxPL auf das Zytoskelett in PM, adaptiert aus Matt el al. [151], mit Erlaubnis.

Dies konnten wir auf natürlich vorkommende Antikörper zurückführen, die OxPL, genauer oxidiertes Phosphatidylcholin (OxPC), binden. Solche Antikörper sind für OxPC beschrieben, und deren Titerhöhe korreliert mit der Progression der Arteriosklerose [152]. OxPL konnten wir auch in Peritoneal-Lavage (PL) von Patienten mit chronischer Bauchfelldialyse feststellen. Doch erst nach Elimination von Antikörpern hemmte die PL dieser Patienten die Phagozytose in PM in Abhängigkeit von WAVE-1. RAG-1-knock out-Mäuse besitzen keine reifen T- und B-Zellen, und daher keine Antikörper. Die PL von Mäusen ohne LDL-Rezeptor und ohne RAG-1, die mit einer „high fat diet" gefüttert wurden, hemmten ebenso die Phagozytose in PM. Dies konnte durch einen AKAP-Inhibitor reversiert werden.

Die Vielzahl der entzündungsmodulatorischen Eigenschaften von OxPL belegen, dass nicht nur Proteine, sondern auch Lipide das Entzündungsgeschehen beeinflussen können. Die Wirkung von OxPL auf das Entzündungsgeschehen ist pleiotrop und abhängig vom untersuchten Zelltyp, den Lipiden, und der Konzentration der OxPL [146, 153]. So fokussieren sich die meisten, wie auch unsere Arbeiten, auf oxidiertes Phosphatidylcholin (OxPC), welches selbst wieder verschiedene Lipide umfasst [154]. Eigenschaften anderer OxPL wie oxidiertes Phosphatidylethanolamin, -serin, -glycerol, -inositol, - oder Phosphatitidsäure auf Makrophagen wurden ebenso beschrieben [155]. Der Großteil der Studien wurde mit sterilen Entzündungsmodellen durchgeführt. Im Zusammenhang mit Infektionskrankheiten gibt es – im Verhältnis zu anderen Inflammationen – bislang eine limitierte Anzahl an Publikationen [151]. Unsere Daten zeigen, dass OxPL im Rahmen einer *E. coli* Peritonitis gebildet werden, aber auch in Patienten unter Bauchfelldialyse, oder in Mäusen ohne LDL-Rezeptor unter Vielfettdiät („high-fat diet") im Peritoneum vorzufinden sind. Es ist anzunehmen,

dass ein entzündlicher Prozess, bzw. eine fehlende oder eingeschränkte Clearance derselben - wie experimentell in RAG-1-KO-Mäusen gezeigt – die Makrophagen in ihren antibakteriellen Eigenschaften hemmen können. OxPL sind in diesem Setting als danger associated molecular patterns (DAMPs) anzusehen, die durch natürlich vorkommende Antikörper beseitigt werden. Eine zu starke Konzentration von OxPL ist also nicht wünschenswert. Welchen Zweck ein Herunterregulieren der Phagozytose hat, ist jedoch unklar. Es könnte auf eine anti-inflammatorische Polarisation der PM zurückzuführen sein, die durch eine zu starke Entzündung, abgebildet durch eine hohe Freisetzung von Sauerstoffradikalen, getriggert wurde. Welche funktionellen Eigenschaften von PM durch OxPL im Gegenzug begünstigt werden ist aber bislang unklar.

Kadl et al. konnten zeigen, dass in KM OxPL zu einer Polarisierung in Abhängigkeit des Redox-sensitiven Transkriptionsfaktors Nrf2 führte [156]. Diese zeichneten sich durch eine verminderte Fähigkeit der Phagozytose (apoptotische Zellen, beads), Hochregulation von anti-oxidativen „response elements“ (ARE) und eine gewisse pro-inflammatorische Antwort aus. Makrophagen mit einem ähnlichen Polarisationsprofil fanden sich in arteriosklerotischen Läsionen in Mäusen. Im Gegensatz hierzu fand eine andere Gruppe, dass Makrophagen aus arteriosklerotischen Läsionen heterogen im Sinne der M1 oder M2-Polarisation sind, und es nicht klar ist, welcher Makrophagentyp (PM oder KM) sich besser als Modellzelle für arteriosklerotische Studien eignet [157]. Wir sahen, dass KM nach Behandlung mit OxPL ebenso eine eingeschränkte Phagozytose von Bakterien aufwiesen, jedoch auch nach Stimulation mit Bakterien (gramnegativ und –positiv) mit einer verminderten Zytokinantwort reagierten (unpublizierte Daten). Dies mag durch den Antagonismus über TLR-4 teilweise erklärbar sein. Jedoch zeigte die Vorstimulation denselben Effekt (unpublizierte Daten), und dies deutet somit auf eine anti-inflammatorische Polarisation der Makrophagen hin. Stimulation von Makrophagen mit OxPL zeigte jedoch auch wiederholt pro-inflammatorische Wirkungen, wie in Arteriosklerose oder Diabetes [155], und führte *in vivo* zur Rekrutierung von Monozyten [158]. Kürzlich konnte in KM gezeigt werden, dass OxPL eine Steigerung der oxidativen Phosphorylierung über Glutamin bewirken, und dadurch pro-inflammatorisch wirken [159]. In diesen Untersuchungen wurde meist „nur“ die Wirkung der OxPL isoliert im jeweiligen Modell untersucht, und der Makrophagentyp waren meist KM. Während Infektionen *in vivo* sind jedoch eine Vielzahl von Stimuli („environmental cues“) über die Zeit in

verschiedenen Konzentrationen anwesend. Es zeigt sich also erneut, dass der untersuchte Makrophagentyp (KM versus PM), also der Gewebekontext, aber auch das Entzündungsmodell entscheidend sind. Zudem wurde eine veränderte Komposition der PM in Bezug auf LPM und SPM im Entzündungsverlauf mehrfach beschrieben (siehe „1.3 Peritoneale Makrophagen“ und „1.7 Peritonitis“). Unsere Studie unterschied nicht zwischen LPM und SPM. Eventuell zeigen sich hier Unterschiede in der Antwort auf OxPL, wobei in unseren Arbeiten der Phänotyp (egal ob *ex vivo* nach Knochenmarks-Transplantation oder während der Infektion) sehr stabil war, und wir somit keine Unterschiede zwischen den Makrophagentypen erwarten würden.

Zusammenfassend konnte in der Arbeit gezeigt werden, dass OxPL in einer Peritonitis in funktionell relevanter Menge gebildet werden, und die Phagozytose in PM durch eine WAVE-1 abhängige Alteration des Zytoskeletts hemmen. *In vivo* wird dieser Mechanismus durch natürlich vorkommende Antikörper zumindest partiell gehemmt. In welchen Infektionsgeschehen OxPL vor- oder nachteilhaft *in vivo* sind, muss sich erst zeigen, da, wie bereits erwähnt, die überwiegende Anzahl der Studien in sterilen Entzündungen durchgeführt wurde. Klinisch relevante Situationen in denen OxPL sich nachteilig auf das Infektionsgeschehen auswirken müssten identifiziert werden, und könnten einen Therapieeinsatz zur verbesserten Bakterienclearance ermöglichen.

2.5 Aspirationspneumonitis vermindert die Fähigkeit von Lebermakrophagen Bakterien abzutöten (Anlage E)

American Journal of Respiratory Cell and Molecular Biology, 2021, 64(5):641-643

ARDS kann nicht nur durch direkten, sondern auch durch indirekten Lungenschaden entstehen. So kann zum Beispiel eine Peritonitis oder Pankreatitis ein ARDS auslösen. Umgekehrt wurde gezeigt, dass ein ARDS Entzündungsvorgänge in mehreren Organen verursachen kann [160, 161]. Auch für die Säureaspiration wurde experimentell ein Entzündungsgeschehen in mehreren Organen festgestellt [162, 163]. Die klinische Relevanz, und die Mechanismen dieser Vorgänge sind jedoch weitgehend unbekannt. Jedenfalls können schwere Entzündungszustände wie eine Sepsis eine Beeinträchtigung der Immunabwehr bedingen, und damit sekundäre Infektionen begünstigen [164].

Experimentell führt eine bakterielle Pneumonie zu einer akuten Phase-Reaktion in der Leber, welche über die Sekretion von akute-Phase-Proteinen das Abtöten von Bakterien in der Lunge durch AM verbessert [165, 166]. Durch diese Kommunikation zwischen den zwei Organen entstand der Begriff „liver-lung axis“. Auch konnte gezeigt werden, dass in der Leber gebildetes Hepcidin während einer bakteriellen Lungenentzündung Eisen depletiert, und dadurch die Beseitigung von Bakterien verbessert [167]. Somit sind Makrophagen an der Kommunikation zwischen Organen beteiligt.

Unabhängig von der Lunge wurde gezeigt, dass LM, PM, und Milzmakrophagen zum Beseitigen von Bakterien aus der Blutstrombahn oder in benachbarten Organen beitragen [89, 168, 169].

Bei intubierten Patienten kommt es häufig zu Säureaspirationen, aber auch nosokomialen Infektionen allgemein. Basierend auf dieser klinischen Überlegung, gingen wir in der vorliegenden Arbeit der Frage nach, ob eine Entzündung der Lunge ausgelöst durch Säure, antimikrobielle Eigenschaften von Makrophagen in anderen Organen verändert. Hierfür isolierten wir Makrophagen aus der Leber, dem Peritoneum, sowie der Milz. Bei den LM handelt es sich überwiegend (80-90%) um KPC. Während PM und Milzmakrophagen keine Änderung der Phagozytose oder des intrazellulären Abtötens von *P. aeruginosa* oder *Klebsiella pneumoniae* (*K. pneumoniae*) aufwiesen, zeigten LM von Mäusen nach Säureaspiration eine verminderte Fähigkeit diese Bakterien abzutöten (Abb. 9) [170]. Normwertige Transaminasen, ein fehlender Unterschied in Zytokinen in der Leber, und auch eine

fehlende Entzündungsreaktion in der Histopathologie lassen darauf schließen, dass diese Einschränkung der antibakteriellen Eigenschaften nicht auf einen Leberschaden zurückzuführen ist. Ebenso untersuchten wir, ob sich die Zahl oder die Komposition der LM oder Monozyten veränderte, fanden hier jedoch, bis auf eine Verminderung von Monozyten in der Gruppe nach Säureaspiration, keine Unterschiede.

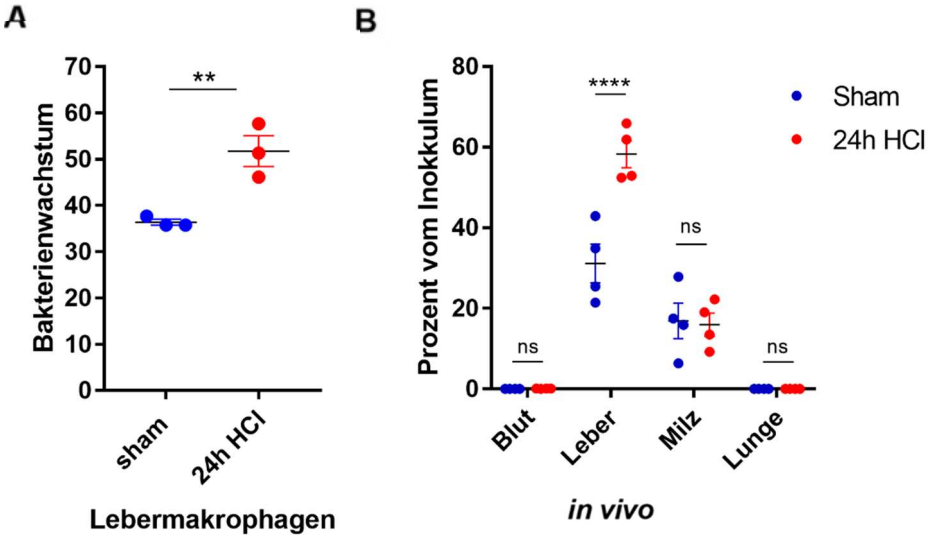

Abbildung 9: Pneumonitis verringert die Bakterienclearance in LM. Bakterielles Wachstum von intrazellulärem *P. aeruginosa ex vivo* in LM aus Kontrollmäusen, bzw. solchen die 24 Stunden vorher Säure intratracheal erhielten (**A**). Mäuse nach Säureaspiration (24h HCl) oder Kontrollen (Sham) erhielten 24 Stunden später *P. aeruginosa* i.v., 90 Minuten später wurde die Bakterienlast in verschiedenen Kompartimenten untersucht, für Blut 1ml (**B**). Daten sind als Mittelwert +/- Standardfehler gezeigt. **P < 0.01, **** P < 0.0001 versus Kontrolle.

Von allen F4/80 positiven LM waren 80-90% KPC. Deshalb, und bedingt durch unsere Isolationsmethode, schließen wir, dass vor allem KPC für den beobachteten Effekt verantwortlich sind. Transkriptionelle Analysen zeigten eine Änderung von metabolischen Genen, insbesondere von solchen, die an der oxidativen Phosphorylierung (OXPHOS) beteiligt sind. Mitochondriale Sauerstoffradikale entstehen entlang dieses metabolischen Zyklus. Tatsächlich fanden wir eine verminderte mROS-Produktion nach bakterieller Stimulation in LM nach Säureaspiration *ex vivo*.

KPC befinden sich in den Lebersinusoiden, und portales als auch systemisches Blut passiert diese Wächterzellen. Während Bakteriämien wurde u.a. mit *P. aeruginosa*, gezeigt, dass KPC zur Beseitigung der Bakterien beitragen [88]. Daher untersuchten wir, ob nach intravenöser Injektion von Bakterien nach einer Säureaspiration die Bakterienlast *in vivo* erhöht ist. Tatsächlich konnten wir in der Leber signifikant mehr

Bakterien nach Säureaspiration feststellen, wohingegen in der Milz bei relativ hoher Bakterienlast die Anzahl der Bakterien gleich war. Somit haben nach einer Säureaspiration KPC auch *in vivo* eine verminderte Fähigkeit *P. aeruginosa* abzutöten. Soweit es uns bekannt ist, ist die vorliegende Arbeit die erste, die verminderte antibakterielle Eigenschaften nach einem Lungenschaden in Makrophagen außerhalb der Lunge zeigt. Roquilly et al. untersuchten die Phagozytosefähigkeit von KM und PM 7 Tage nach *E. coli* Pneumonie, und fanden hier keine Unterschiede [54]. Das intrazelluläre Abtöten der Bakterien wurde jedoch nicht untersucht. Unsere Beobachtung, dass eine Lungenentzündung die antibakteriellen Eigenschaften von KPC *ex vivo* und *in vivo* vermindert, lässt vermuten, dass dadurch bakterielle Superinfektionen begünstigt werden.

Kommunikation zwischen verschiedenen Organen ist bei schweren Entzündungsvorgängen, wie zum Beispiel nach ARDS oder der Sepsis sicher von klinischer Relevanz. Die Mechanismen oder die funktionelle Bedeutung dieser Vorgänge ist bislang jedoch weitgehend unverstanden. So ist die Ursache der Niereninsuffizienz nach ARDS immer noch unbekannt [54]. Der Mechanismus unserer Beobachtung muss ebenso erst erforscht werden, aber die verminderte Fähigkeit von LM nach Säureaspiration, *P. aeruginosa* und *K. pneumoniae* abzutöten, könnte, zumindest teilweise, die erhöhte Anfälligkeit für nosokomiale Infektionen bei intubierten Patienten erklären. Unsere Arbeit legt nahe, dass organspezifischen Makrophagen als Wächterzellen in der Erkennung von Signalen oder auch in ihrer Filterfunktion (wie zum Beispiel von Milz- oder Nierenmakrophagen) eine wichtige Rolle in der Kommunikation zwischen Organen zukommt. Es wird interessant sein zu sehen, ob in anderen klinisch relevanten Modellen, zum Beispiel Nierenschaden nach ARDS, organspezifische Makrophagen ebenso eine Rolle spielen.

Zusammenfassend konnten wir in der vorliegenden Arbeit zeigen, dass LM in der Resolutionsphase einer Aspirationspneumonitis verminderte antibakterielle Eigenschaften aufweisen, und dies zu einer erhöhten Bakterienlast bei Pseudomonas-Bakteriämie in der Leber führt.

3. Zusammenfassung

Organspezifische Makrophagen sind eng mit ihrem Gewebe verbunden, vollziehen homöostatische Funktionen, und fungieren als Wächterzellen, die das Entzündungsgeschehen koordinieren oder zumindest beeinflussen. Zudem sind sie in der Beseitigung von Mikroben wichtig. Die Entdeckung, dass Makrophagen mittels PRRs wie den TLRs konservierte Strukturen von Pathogenen spezifisch erkennen können, und die der organspezifischen Ontogenese, haben Makrophagen vermehrt ins Rampenlicht der Forschung gerückt. Obwohl die meisten Makrophagen von embryonalen Zellen abstammen, stellen sie, bedingt durch organspezifische Anforderungen, komplett unterschiedliche Zellen dar. Diesen Erkenntnissen wird zunehmend, jedoch noch nicht in ausreichendem Maße, in der Forschung Rechnung getragen. Daraus und der Tatsache, dass während Entzündungsvorgängen eine Vielzahl von Stimuli (pro- als auch anti-inflammatorische) gleichzeitig vorliegen, ergibt sich die Notwendigkeit Makrophagen in ihrem jeweiligen Kontext des Gewebes und auch der Entzündung zu studieren. Nur so wird es möglich sein, zielgerichtete Therapien für Makrophagen am gewünschten Ort zu entwickeln. So schien vor 10-15 Jahren eine Immunmodulation von Makrophagen noch in weiter Ferne. Die Identifikation von weiteren Subpopulationen wie zum Beispiel synovialer Makrophagen [171], oder die Entdeckung, dass ein erhöhter Anteil von aus Monozyten stammenden kardialen Makrophagen mit einer schlechteren Prognose in der Herzinsuffizienz einhergehen [172], lassen die Hoffnung auf gezielte Therapieansätze wie hier beispielhaft bei rheumatoider Arthritis oder Herzinsuffizienz realistisch erscheinen.

Bakterielle Infektionen entstehen durch pathogene oder opportunistische Keime, wenn diese in ausreichender Menge aufgenommen werden, bzw. sich vermehren können. Dies kann – beispielhaft in der Lunge - durch hochpathogene Erreger wie zum Beispiel bei Inhalation von *Yersinia pestis*, der die Lungenpest auslöst, oder durch ein hohes Inokulum geschehen; aber auch sekundär nach Influenza-Pneumonie, oder nach Säureaspiration, wenn die lokale Immunität eingeschränkt ist, und nur eine Kolonisation mit dem Erreger ausreichend sein kann. Diese Einschränkung der lokalen Immunität auf Zellebene zu verstehen, eröffnet Möglichkeiten der Diagnostik aber auch gezielten Therapie, um zum Beispiel schwere Pneumonien oder ein ARDS beeinflussen zu können.

Während Entzündungen oder Infektionen können Organe fernab des Ursprungsorts betroffen sein. Wie die Kommunikation zwischen den Organen vonstatten geht, ist weitgehend unbekannt. Da Makrophagen eng mit ihrem „Heimatorgan“ verbunden sind, kommen sie als Sender oder auch Empfänger dieser Signale in Betracht. Da gezeigt wurde, dass Makrophagen mehrerer Gewebe (in der Leber, Milz, Niere und im Peritoneum) in der Kontrolle einer Bakteriämie eine Rolle spielen, ist anzunehmen, dass eine Veränderung ihres Aktivitätszustandes während oder auch nach schweren Entzündungen, wie zum Beispiel einer Sepsis oder eines ARDS, darüber entscheiden kann, ob geringe Mengen von Bakterien im Blut in Schach gehalten werden können, oder nicht.

In der vorliegenden Arbeit untersuchten wir antibakterielle Eigenschaften organspezifischer Makrophagen während Homöostase und Entzündungen bzw. Infektionen. So wurde gezeigt, dass eine Aspirationspneumonitis die Phagozytosefähigkeit von AM vermindert, und dadurch das Entstehen einer bakteriellen Superinfektion begünstigt (Kapitel 2.1). Eine, wie hier durch das Peptid $B\beta_{15\text{-}42}$, das alleine keinen Einfluss auf AM aufwies, bedingte verminderte Entzündung, konnte die antibakteriellen Eigenschaften der AM erhalten. Ursächlich für die verminderte Phagozytose könnte also eine Gegenregulation bei starker Entzündung sein. Welchen pathophysiologischen Zweck diese Aktivitätsänderung hat, muss erst gezeigt werden. Man kann spekulieren, dass dadurch Vorgänge die eine Entzündung auflösen im Gegenzug begünstigt werden. Die Aufklärung dieser Gegenmechanismen könnte mögliche therapeutische Angriffspunkte liefern.

Auch abseits der Lunge hat eine Säureaspiration Einfluss auf antibakterielle Eigenschaften von Makrophagen: so wiesen LM, aber nicht PM oder Milzmakrophagen nach einer Aspiration eine verminderte Fähigkeit auf, Bakterien abzutöten (Kapitel 2.5). Dies führt während einer Pseudomonas-Bakteriämie zu einer erhöhten Bakterienlast in der Leber, während andere Organe (Milz, Lunge, Blut) keine signifikanten Unterschiede zeigten. Da die Leber keine Entzündungszeichen aufwies, ist von einem direkten Einfluss auf LM auszugehen. Diese Daten zeigen, dass LM fernab des initialen Entzündungsgeschehen in ihren antibakteriellen Eigenschaften verändert werden, und dadurch die systemische Kontrolle der Pathogene beeinflusst wird.

Die Kinase PTEN spielt, als Gegenregulator von PI3K, eine wesentliche Rolle in der Regulation von Entzündungsvorgängen. In der vorliegenden Arbeit (Kapitel 2.2) wurde deren Rolle in AM während einer Pneumokokken-Pneumonie untersucht. PTEN Defizienz bewirkte in AM eine Verbesserung der antibakteriellen Eigenschaften (Phagozytose, Abtöten). Die Entzündungsantwort auf Pneumokokken war aber sowohl in AM, als auch während einer Pneumonie *in vivo* vermindert. In Summe führte der zellspezifische PTEN-knockout in myeloischen Zellen dadurch zu einem verbesserten Überleben in einer Pneumonie verursacht durch *S. pneumoniae*.

Makrophagen spielen in einer Infektion mit *M. tuberculosis* eine zentrale Rolle, da sie als Niche für die intrazellulären Erreger fungieren, und wichtig in der Kontrolle einer Infektion sind. Es zeigte sich, dass die Effluxpumpe BCRP-1 in Lungenmakrophagen während einer *M. tuberculosis* Infektion exprimiert ist, und durch IFN-γ hochreguliert wird. Dadurch wird die intrazelluläre Konzentration von INH, und das Abtöten der Bakterien vermindert. Ebenso ist PZA ein Substrat von BCRP-1, und Chloroquin, der als Inhibitor der Pumpe identifiziert werden konnte, verbesserte das Abtöten der Mykobakterien in Makrophagen. In Abwesenheit von Tuberkulostatika hatte eine Hemmung von BCRP-1 keinen Einfluss auf das Abtöten der Bakterien, oder die Sekretion von Zytokinen. Die vorliegende Arbeit wirft die spannende Frage der Rolle von BCRP-1 in Makrophagen in Abwesenheit von antibiotischen Substanzen in bakteriellen Infektionen auf, welche bislang völlig unklar ist.

Während bakteriellen Infektionen werden Sauerstoffradikale gebildet, die eine Oxidierung von Phospholipiden in Zellmembranen bedingen. Hier konnte gezeigt werden, dass während einer Peritonitis mit *E. coli* OxPL in Konzentrationen gebildet werden, die in PM die Phagozytose von Bakterien inhibieren (Kapitel 2.4). Mechanistisch induzierten OxPL eine Aktin-Polymerisation über das AKAP WAVE-1. Hemmung der AKAP-Bindung an PKA, oder der Knockout von WAVE-1 reversierten diesen Phänotyp nach Zugabe von OxPL *in vitro* und *in vivo*. Ohne Zugabe von OxPL konnten, trotz der Generierung von oxidierten Lipiden während der Infektion, keine signifikanten Effekte in Mäusen mit WAVE-1 defizienten PM festgestellt werden. Vielmehr fanden sich natürlich vorkommende Antikörper, die OxPL neutralisierten. Somit werden PM durch Antikörper vor negativen Auswirkungen der OxPL bei überschießender Entzündung geschützt.

Zusammenfassend zeigt die vorliegende Arbeit die Wichtigkeit von Makrophagen in der Kontrolle von Bakterien, und unterstreicht die Notwendigkeit ihre Funktion im jeweiligen Kontext des Gewebes und der spezifischen Infektion oder Entzündung zu studieren. Je detaillierter unser Wissen von organspezifischen Makrophagen in Homöostase aber auch während Entzündungen wird, um so eher wird es möglich sein, diese Erkenntnisse für die Klinik nutzbar zu machen.

Organspezifische Makrophagen haben während Entzündungen und Infektionen die duale Rolle die Homöostase im jeweiligen Gewebe wiederherzustellen, aber auch Bakterien in Schach zu halten. Je nach Bedarf wird sich der Makrophage der jeweiligen Situation im entzündeten Gewebe anpassen müssen. Dies kann auf Kosten der jeweils anderen Funktion gehen. Die Entschlüsselung der Mechanismen, die diese funktionellen Polarisierungen in Makrophagen im jeweiligen Organ oder auch, wie in Kapitel 2.5 gezeigt, in anderen Organen verursachen, könnte gezielte Therapien im Rahmen von Infektionen oder sterilen Entzündungen ermöglichen.

So untersucht unsere Forschungsgruppe derzeit, basierend auf den Ergebnissen der Arbeit, die in Kapitel 2.1 dargestellt wurde, die Polarisierung, und den Mechanismus der eingeschränkten antimikrobiellen Kapazität im Verlauf einer Aspirationspneumonitis (s. Abb. 2). Es zeigte sich, dass diese scheinbar nachteilige Aktivitätsänderung die Resolution der Entzündung verbessert. Aktuell untersuchen wir die Signalwege, die für diese funktionelle Polarisierung verantwortlich sind.

4. Abkürzungsverzeichnis

AKAP	A-kinase anchoring proteins
AM	alveoläre Makrophagen
ARDS	acute respiratory distress syndrome
BAL	broncho-alveoläre Lavage
BCRP-1	breast cancer resistance protein-1
CFU	colony forming unit (Kolonie-bildende Einheiten)
DAMP	danger-associated molecular pattern
E. coli	*Escherichia coli*
FACS	fluorescence-activated cell sorting (Durchflusszytometrie)
FITC	Fluorescein
GM-CSF	granulocyte-macrophage colony-stimulating factor
HIV	humanes Immundefizienz-Virus
IL	Interleukin (z.B. IL-6, IL-10 etc.)
IFN-γ	interferon-γ
INH	Isoniazid
KPC	Kupffer-Zellen (Kupffer cells)
KC	keratinocyte-derived chemokine
KM	Knochenmark-Makrophagen
KO	Knockout
P-gp	P-glycoprotein
LDL	low-density lipoprotein
LM	Lebermakrophagen
LPM	large peritoneal macrophage
LPS	Lipopolysaccharide
mROS	mitochondrial reactive oxygen species
M. tuberculosis	*Mycobacterium tuberculosis*
OXPHOS	oxidative Phosphorylierung
OxPL	oxidierte Phospholipide
P. aeruginosa	*P. aeruginosa*
PI3K	Phosphoinositid-3-Kinase

PKA	protein kinase A
PL	Peritoneale Lavage
PM	peritoneale Makrophagen
PRR	Pathogen recognition receptor
PZA	Pyrazinamid
PTEN	phosphatase and tensin homolog deleted on chromosome 10
ROS	reactive oxygen species
RPM	red pulp macrophages (Makrophagen der roten Pulpa)
S. pneumoniae	*Streptococcus pneumoniae* (Pneumokokken)
S. aureus	*Staphylococcus aureus*
SPM	small peritoneal macrophage
TGF-β	transforming growth factor- β
TLR	Toll-like Rezeptor
TNF-α	Tumor-necrosis factor-α
WT	Wildtyp

5. Referenzen

1. Tauber AI. Metchnikoff and the phagocytosis theory. Nat Rev Mol Cell Biol **2003**; 4(11): 897-901.
2. Boyle WJ, Simonet WS, Lacey DL. Osteoclast differentiation and activation. Nature **2003**; 423(6937): 337-42.
3. Stamatiades EG, Tremblay ME, Bohm M, et al. Immune Monitoring of Trans-endothelial Transport by Kidney-Resident Macrophages. Cell **2016**; 166(4): 991-1003.
4. Soares MP, Hamza I. Macrophages and Iron Metabolism. Immunity **2016**; 44(3): 492-504.
5. Hulsmans M, Clauss S, Xiao L, et al. Macrophages Facilitate Electrical Conduction in the Heart. Cell **2017**; 169(3): 510-22 e20.
6. Sugita J, Fujiu K, Nakayama Y, et al. Cardiac macrophages prevent sudden death during heart stress. Nat Commun **2021**; 12(1): 1910.
7. Trapnell BC, Carey BC, Uchida K, Suzuki T. Pulmonary alveolar proteinosis, a primary immunodeficiency of impaired GM-CSF stimulation of macrophages. Curr Opin Immunol **2009**; 21(5): 514-21.
8. van Furth R, Cohn ZA. The origin and kinetics of mononuclear phagocytes. J Exp Med **1968**; 128(3): 415-35.
9. Fogg DK, Sibon C, Miled C, et al. A clonogenic bone marrow progenitor specific for macrophages and dendritic cells. Science **2006**; 311(5757): 83-7.
10. Katz SI, Tamaki K, Sachs DH. Epidermal Langerhans cells are derived from cells originating in bone marrow. Nature **1979**; 282(5736): 324-6.
11. Schulz C, Gomez Perdiguero E, Chorro L, et al. A lineage of myeloid cells independent of Myb and hematopoietic stem cells. Science **2012**; 336(6077): 86-90.
12. Perdiguero EG, Geissmann F. The development and maintenance of resident macrophages. Nat Immunol **2016**; 17(1): 2-8.
13. Utz SG, See P, Mildenberger W, et al. Early Fate Defines Microglia and Non-parenchymal Brain Macrophage Development. Cell **2020**; 181(3): 557-73 e18.
14. De Schepper S, Verheijden S, Aguilera-Lizarraga J, et al. Self-Maintaining Gut Macrophages Are Essential for Intestinal Homeostasis. Cell **2018**; 175(2): 400-15 e13.
15. Guilliams M, Scott CL. Does niche competition determine the origin of tissue-resident macrophages? Nat Rev Immunol **2017**; 17(7): 451-60.
16. Ginhoux F, Guilliams M. Tissue-Resident Macrophage Ontogeny and Homeostasis. Immunity **2016**; 44(3): 439-49.
17. Lavin Y, Winter D, Blecher-Gonen R, et al. Tissue-resident macrophage enhancer landscapes are shaped by the local microenvironment. Cell **2014**; 159(6): 1312-26.
18. Gosselin D, Link VM, Romanoski CE, et al. Environment drives selection and function of enhancers controlling tissue-specific macrophage identities. Cell **2014**; 159(6): 1327-40.
19. Gibbings SL, Thomas SM, Atif SM, et al. Three Unique Interstitial Macrophages in the Murine Lung at Steady State. Am J Respir Cell Mol Biol **2017**; 57(1): 66-76.
20. Martinez FO, Sica A, Mantovani A, Locati M. Macrophage activation and polarization. Front Biosci **2008**; 13: 453-61.
21. Gordon S, Martinez FO. Alternative activation of macrophages: mechanism and functions. Immunity **2010**; 32(5): 593-604.
22. Piccolo V, Curina A, Genua M, et al. Opposing macrophage polarization programs show extensive epigenomic and transcriptional cross-talk. Nat Immunol **2017**; 18(5): 530-40.
23. Glass CK, Natoli G. Molecular control of activation and priming in macrophages. Nat Immunol **2016**; 17(1): 26-33.
24. Martinez FO, Gordon S. The M1 and M2 paradigm of macrophage activation: time for reassessment. F1000Prime Rep **2014**; 6: 13.
25. Van den Bossche J, O'Neill LA, Menon D. Macrophage Immunometabolism: Where Are We (Going)? Trends Immunol **2017**; 38(6): 395-406.

26. Underhill DM, Ozinsky A. Phagocytosis of microbes: complexity in action. Annu Rev Immunol **2002**; 20: 825-52.
27. Flannagan RS, Cosio G, Grinstein S. Antimicrobial mechanisms of phagocytes and bacterial evasion strategies. Nat Rev Microbiol **2009**; 7(5): 355-66.
28. Heyworth PG, Cross AR, Curnutte JT. Chronic granulomatous disease. Curr Opin Immunol **2003**; 15(5): 578-84.
29. Nathan C, Cunningham-Bussel A. Beyond oxidative stress: an immunologist's guide to reactive oxygen species. Nat Rev Immunol **2013**; 13(5): 349-61.
30. Mailloux RJ. Teaching the fundamentals of electron transfer reactions in mitochondria and the production and detection of reactive oxygen species. Redox Biol **2015**; 4: 381-98.
31. Preston JA, Bewley MA, Marriott HM, et al. Alveolar Macrophage Apoptosis-associated Bacterial Killing Helps Prevent Murine Pneumonia. Am J Respir Crit Care Med **2019**; 200(1): 84-97.
32. Hall CJ, Sanderson LE, Lawrence LM, et al. Blocking fatty acid-fueled mROS production within macrophages alleviates acute gouty inflammation. J Clin Invest **2018**; 128(5): 1752-71.
33. Collini PJ, Bewley MA, Mohasin M, et al. HIV gp120 in the Lungs of Antiretroviral Therapy-treated Individuals Impairs Alveolar Macrophage Responses to Pneumococci. Am J Respir Crit Care Med **2018**; 197(12): 1604-15.
34. Mahlapuu M, Hakansson J, Ringstad L, Bjorn C. Antimicrobial Peptides: An Emerging Category of Therapeutic Agents. Front Cell Infect Microbiol **2016**; 6: 194.
35. Pieters J. Mycobacterium tuberculosis and the macrophage: maintaining a balance. Cell Host Microbe **2008**; 3(6): 399-407.
36. Bustamante J, Boisson-Dupuis S, Abel L, Casanova JL. Mendelian susceptibility to mycobacterial disease: genetic, immunological, and clinical features of inborn errors of IFN-gamma immunity. Semin Immunol **2014**; 26(6): 454-70.
37. Kopf M, Schneider C, Nobs SP. The development and function of lung-resident macrophages and dendritic cells. Nat Immunol **2015**; 16(1): 36-44.
38. Hume PS, Gibbings SL, Jakubzick CV, et al. Localization of Macrophages in the Human Lung via Design-based Stereology. Am J Respir Crit Care Med **2020**; 201(10): 1209-17.
39. Gomez Perdiguero E, Klapproth K, Schulz C, et al. Tissue-resident macrophages originate from yolk-sac-derived erythro-myeloid progenitors. Nature **2015**; 518(7540): 547-51.
40. Hashimoto D, Chow A, Noizat C, et al. Tissue-resident macrophages self-maintain locally throughout adult life with minimal contribution from circulating monocytes. Immunity **2013**; 38(4): 792-804.
41. Guilliams M, De Kleer I, Henri S, et al. Alveolar macrophages develop from fetal monocytes that differentiate into long-lived cells in the first week of life via GM-CSF. J Exp Med **2013**; 210(10): 1977-92.
42. Yu X, Buttgereit A, Lelios I, et al. The Cytokine TGF-beta Promotes the Development and Homeostasis of Alveolar Macrophages. Immunity **2017**; 47(5): 903-12 e4.
43. Kaur M, Bell T, Salek-Ardakani S, Hussell T. Macrophage adaptation in airway inflammatory resolution. Eur Respir Rev **2015**; 24(137): 510-5.
44. Westphalen K, Gusarova GA, Islam MN, et al. Sessile alveolar macrophages communicate with alveolar epithelium to modulate immunity. Nature **2014**; 506(7489): 503-6.
45. Aggarwal NR, King LS, D'Alessio FR. Diverse macrophage populations mediate acute lung inflammation and resolution. Am J Physiol Lung Cell Mol Physiol **2014**; 306(8): L709-25.
46. Neupane AS, Willson M, Chojnacki AK, et al. Patrolling Alveolar Macrophages Conceal Bacteria from the Immune System to Maintain Homeostasis. Cell **2020**.
47. Herold S, Mayer K, Lohmeyer J. Acute lung injury: how macrophages orchestrate resolution of inflammation and tissue repair. Front Immunol **2011**; 2: 65.
48. Hussell T, Bell TJ. Alveolar macrophages: plasticity in a tissue-specific context. Nat Rev Immunol **2014**; 14(2): 81-93.

49. Medeiros AI, Serezani CH, Lee SP, Peters-Golden M. Efferocytosis impairs pulmonary macrophage and lung antibacterial function via PGE2/EP2 signaling. J Exp Med **2009**; 206(1): 61-8.
50. Sun K, Metzger DW. Inhibition of pulmonary antibacterial defense by interferon-gamma during recovery from influenza infection. Nat Med **2008**; 14(5): 558-64.
51. Sun K, Metzger DW. Influenza infection suppresses NADPH oxidase-dependent phagocytic bacterial clearance and enhances susceptibility to secondary methicillin-resistant Staphylococcus aureus infection. J Immunol **2014**; 192(7): 3301-7.
52. Didierlaurent A, Goulding J, Patel S, et al. Sustained desensitization to bacterial Toll-like receptor ligands after resolution of respiratory influenza infection. J Exp Med **2008**; 205(2): 323-9.
53. Roquilly A, McWilliam HEG, Jacqueline C, et al. Local Modulation of Antigen-Presenting Cell Development after Resolution of Pneumonia Induces Long-Term Susceptibility to Secondary Infections. Immunity **2017**; 47(1): 135-47 e5.
54. Roquilly A, Jacqueline C, Davieau M, et al. Alveolar macrophages are epigenetically altered after inflammation, leading to long-term lung immunoparalysis. Nat Immunol **2020**.
55. Aegerter H, Kulikauskaite J, Crotta S, et al. Influenza-induced monocyte-derived alveolar macrophages confer prolonged antibacterial protection. Nat Immunol **2020**; 21(2): 145-57.
56. Yao Y, Jeyanathan M, Haddadi S, et al. Induction of Autonomous Memory Alveolar Macrophages Requires T Cell Help and Is Critical to Trained Immunity. Cell **2018**; 175(6): 1634-50 e17.
57. Ghosn EE, Cassado AA, Govoni GR, et al. Two physically, functionally, and developmentally distinct peritoneal macrophage subsets. Proc Natl Acad Sci U S A **2010**; 107(6): 2568-73.
58. Cassado Ados A, de Albuquerque JA, Sardinha LR, et al. Cellular renewal and improvement of local cell effector activity in peritoneal cavity in response to infectious stimuli. PLoS One **2011**; 6(7): e22141.
59. Kim KW, Williams JW, Wang YT, et al. MHC II+ resident peritoneal and pleural macrophages rely on IRF4 for development from circulating monocytes. J Exp Med **2016**; 213(10): 1951-9.
60. Bain CC, Hawley CA, Garner H, et al. Long-lived self-renewing bone marrow-derived macrophages displace embryo-derived cells to inhabit adult serous cavities. Nat Commun **2016**; 7: ncomms11852.
61. Okabe Y, Medzhitov R. Tissue-specific signals control reversible program of localization and functional polarization of macrophages. Cell **2014**; 157(4): 832-44.
62. Davis LE, Kornfeld M, Daniels RS, Skehel JJ. Experimental influenza causes a non-permissive viral infection of brain, liver and muscle. J Neurovirol **2000**; 6(6): 529-36.
63. Rosas M, Davies LC, Giles PJ, et al. The transcription factor Gata6 links tissue macrophage phenotype and proliferative renewal. Science **2014**; 344(6184): 645-8.
64. Yona S, Kim KW, Wolf Y, et al. Fate mapping reveals origins and dynamics of monocytes and tissue macrophages under homeostasis. Immunity **2013**; 38(1): 79-91.
65. Cassado Ados A, D'Imperio Lima MR, Bortoluci KR. Revisiting mouse peritoneal macrophages: heterogeneity, development, and function. Front Immunol **2015**; 6: 225.
66. Baumgarth N. The double life of a B-1 cell: self-reactivity selects for protective effector functions. Nat Rev Immunol **2011**; 11(1): 34-46.
67. Ruiz-Alcaraz AJ, Carmona-Martinez V, Tristan-Manzano M, et al. Characterization of human peritoneal monocyte/macrophage subsets in homeostasis: Phenotype, GATA6, phagocytic/oxidative activities and cytokines expression. Sci Rep **2018**; 8(1): 12794.
68. Stengel S, Quickert S, Lutz P, et al. Peritoneal Level of CD206 Associates With Mortality and an Inflammatory Macrophage Phenotype in Patients With Decompensated Cirrhosis and Spontaneous Bacterial Peritonitis. Gastroenterology **2020**; 158(6): 1745-61.
69. Bastos KR, Alvarez JM, Marinho CR, Rizzo LV, Lima MR. Macrophages from IL-12p40-deficient mice have a bias toward the M2 activation profile. J Leukoc Biol **2002**; 71(2): 271-8.

70. Davies LC, Rice CM, Palmieri EM, Taylor PR, Kuhns DB, McVicar DW. Peritoneal tissue-resident macrophages are metabolically poised to engage microbes using tissue-niche fuels. Nat Commun **2017**; 8(1): 2074.
71. Wang J, Kubes P. A Reservoir of Mature Cavity Macrophages that Can Rapidly Invade Visceral Organs to Affect Tissue Repair. Cell **2016**; 165(3): 668-78.
72. Jorch SK, Surewaard BG, Hossain M, et al. Peritoneal GATA6+ macrophages function as a portal for Staphylococcus aureus dissemination. J Clin Invest **2019**; 129(11): 4643-56.
73. Jenne CN, Kubes P. Immune surveillance by the liver. Nat Immunol **2013**; 14(10): 996-1006.
74. Bleriot C, Ginhoux F. Understanding the Heterogeneity of Resident Liver Macrophages. Front Immunol **2019**; 10: 2694.
75. Mass E, Ballesteros I, Farlik M, et al. Specification of tissue-resident macrophages during organogenesis. Science **2016**; 353(6304).
76. Sierro F, Evrard M, Rizzetto S, et al. A Liver Capsular Network of Monocyte-Derived Macrophages Restricts Hepatic Dissemination of Intraperitoneal Bacteria by Neutrophil Recruitment. Immunity **2017**; 47(2): 374-88 e6.
77. MacParland SA, Liu JC, Ma XZ, et al. Single cell RNA sequencing of human liver reveals distinct intrahepatic macrophage populations. Nat Commun **2018**; 9(1): 4383.
78. Scott CL, Zheng F, De Baetselier P, et al. Bone marrow-derived monocytes give rise to self-renewing and fully differentiated Kupffer cells. Nat Commun **2016**; 7: 10321.
79. Sakai M, Troutman TD, Seidman JS, et al. Liver-Derived Signals Sequentially Reprogram Myeloid Enhancers to Initiate and Maintain Kupffer Cell Identity. Immunity **2019**; 51(4): 655-70 e8.
80. Willekens FL, Werre JM, Kruijt JK, et al. Liver Kupffer cells rapidly remove red blood cell-derived vesicles from the circulation by scavenger receptors. Blood **2005**; 105(5): 2141-5.
81. Theurl I, Hilgendorf I, Nairz M, et al. On-demand erythrocyte disposal and iron recycling requires transient macrophages in the liver. Nat Med **2016**; 22(8): 945-51.
82. Shi J, Gilbert GE, Kokubo Y, Ohashi T. Role of the liver in regulating numbers of circulating neutrophils. Blood **2001**; 98(4): 1226-30.
83. Rosso C, Kazankov K, Younes R, et al. Crosstalk between adipose tissue insulin resistance and liver macrophages in non-alcoholic fatty liver disease. J Hepatol **2019**; 71(5): 1012-21.
84. Lefere S, Tacke F. Macrophages in obesity and non-alcoholic fatty liver disease: Crosstalk with metabolism. JHEP Rep **2019**; 1(1): 30-43.
85. Tacke F, Zimmermann HW. Macrophage heterogeneity in liver injury and fibrosis. J Hepatol **2014**; 60(5): 1090-6.
86. Krenkel O, Tacke F. Liver macrophages in tissue homeostasis and disease. Nat Rev Immunol **2017**; 17(5): 306-21.
87. Broadley SP, Plaumann A, Coletti R, et al. Dual-Track Clearance of Circulating Bacteria Balances Rapid Restoration of Blood Sterility with Induction of Adaptive Immunity. Cell Host Microbe **2016**; 20(1): 36-48.
88. Zeng Z, Surewaard BG, Wong CH, Geoghegan JA, Jenne CN, Kubes P. CRIg Functions as a Macrophage Pattern Recognition Receptor to Directly Bind and Capture Blood-Borne Gram-Positive Bacteria. Cell Host Microbe **2016**; 20(1): 99-106.
89. Wong CH, Jenne CN, Petri B, Chrobok NL, Kubes P. Nucleation of platelets with blood-borne pathogens on Kupffer cells precedes other innate immunity and contributes to bacterial clearance. Nat Immunol **2013**; 14(8): 785-92.
90. Llorente C, Schnabl B. Fast-Track Clearance of Bacteria from the Liver. Cell Host Microbe **2016**; 20(1): 1-2.
91. Christou L, Pappas G, Falagas ME. Bacterial infection-related morbidity and mortality in cirrhosis. Am J Gastroenterol **2007**; 102(7): 1510-7.
92. World Health Organization. Global priority list of antibiotic-resistant bacteria to guide research, discovery, and development of new antibiotics. **2017**.

93. Iwasaki A, Foxman EF, Molony RD. Early local immune defences in the respiratory tract. Nat Rev Immunol **2017**; 17(1): 7-20.
94. Schyns J, Bai Q, Ruscitti C, et al. Non-classical tissue monocytes and two functionally distinct populations of interstitial macrophages populate the mouse lung. Nat Commun **2019**; 10(1): 3964.
95. Schyns J, Bureau F, Marichal T. Lung Interstitial Macrophages: Past, Present, and Future. J Immunol Res **2018**; 2018: 5160794.
96. Guilliams M, Lambrecht BN, Hammad H. Division of labor between lung dendritic cells and macrophages in the defense against pulmonary infections. Mucosal Immunol **2013**; 6(3): 464-73.
97. Wipf JE, Lipsky BA, Hirschmann JV, et al. Diagnosing pneumonia by physical examination: relevant or relic? Arch Intern Med **1999**; 159(10): 1082-7.
98. Gennis P, Gallagher J, Falvo C, Baker S, Than W. Clinical criteria for the detection of pneumonia in adults: guidelines for ordering chest roentgenograms in the emergency department. J Emerg Med **1989**; 7(3): 263-8.
99. Metlay JP, Kapoor WN, Fine MJ. Does this patient have community-acquired pneumonia? Diagnosing pneumonia by history and physical examination. JAMA **1997**; 278(17): 1440-5.
100. Mandell LA, Niederman MS. Aspiration Pneumonia. N Engl J Med **2019**; 380(7): 651-63.
101. Huxley EJ, Viroslav J, Gray WR, Pierce AK. Pharyngeal aspiration in normal adults and patients with depressed consciousness. Am J Med **1978**; 64(4): 564-8.
102. Metheny NA, Clouse RE, Chang YH, Stewart BJ, Oliver DA, Kollef MH. Tracheobronchial aspiration of gastric contents in critically ill tube-fed patients: frequency, outcomes, and risk factors. Crit Care Med **2006**; 34(4): 1007-15.
103. Raghavendran K, Nemzek J, Napolitano LM, Knight PR. Aspiration-induced lung injury. Crit Care Med **2011**; 39(4): 818-26.
104. Cook DJ, Walter SD, Cook RJ, et al. Incidence of and risk factors for ventilator-associated pneumonia in critically ill patients. Ann Intern Med **1998**; 129(6): 433-40.
105. Akca O, Koltka K, Uzel S, et al. Risk factors for early-onset, ventilator-associated pneumonia in critical care patients: selected multiresistant versus nonresistant bacteria. Anesthesiology **2000**; 93(3): 638-45.
106. Chastre J, Trouillet JL, Vuagnat A, et al. Nosocomial pneumonia in patients with acute respiratory distress syndrome. Am J Respir Crit Care Med **1998**; 157(4 Pt 1): 1165-72.
107. Markowicz P, Wolff M, Djedaini K, et al. Multicenter prospective study of ventilator-associated pneumonia during acute respiratory distress syndrome. Incidence, prognosis, and risk factors. ARDS Study Group. Am J Respir Crit Care Med **2000**; 161(6): 1942-8.
108. Hsu WT, Lai CC, Wang YH, et al. Risk of pneumonia in patients with gastroesophageal reflux disease: A population-based cohort study. PLoS One **2017**; 12(8): e0183808.
109. Gaude GS. Pulmonary manifestations of gastroesophageal reflux disease. Ann Thorac Med **2009**; 4(3): 115-23.
110. Matt U, Warszawska JM, Bauer M, et al. Bbeta(15-42) protects against acid-induced acute lung injury and secondary pseudomonas pneumonia in vivo. Am J Respir Crit Care Med **2009**; 180(12): 1208-17.
111. van Westerloo DJ, Knapp S, van't Veer C, et al. Aspiration pneumonitis primes the host for an exaggerated inflammatory response during pneumonia. Crit Care Med **2005**; 33(8): 1770-8.
112. Dragan V, Wei Y, Elligsen M, Kiss A, Walker SAN, Leis JA. Prophylactic Antimicrobial Therapy for Acute Aspiration Pneumonitis. Clin Infect Dis **2018**; 67(4): 513-8.
113. Wilcox CM, Dismukes WE. Spontaneous bacterial peritonitis. A review of pathogenesis, diagnosis, and treatment. Medicine (Baltimore) **1987**; 66(6): 447-56.
114. Pinheiro da Silva F, Aloulou M, Skurnik D, et al. CD16 promotes Escherichia coli sepsis through an FcR gamma inhibitory pathway that prevents phagocytosis and facilitates inflammation. Nat Med **2007**; 13(11): 1368-74.

115. Calandra T, Cohen J, International Sepsis Forum Definition of Infection in the ICUCC. The international sepsis forum consensus conference on definitions of infection in the intensive care unit. Crit Care Med **2005**; 33(7): 1538-48.
116. Runyon BA, Antillon MR, McHutchison JG. Diuresis increases ascitic fluid opsonic activity in patients who survive spontaneous bacterial peritonitis. J Hepatol **1992**; 14(2-3): 249-52.
117. Simberkoff MS, Moldover NH, Weiss G. Bactericidal and opsonic activity of cirrhotic ascites and nonascitic peritoneal fluid. J Lab Clin Med **1978**; 91(5): 831-9.
118. Boussif A, Rolas L, Weiss E, Bouriche H, Moreau R, Perianin A. Impaired intracellular signaling, myeloperoxidase release and bactericidal activity of neutrophils from patients with alcoholic cirrhosis. J Hepatol **2016**; 64(5): 1041-8.
119. Rimola A, Soto R, Bory F, Arroyo V, Piera C, Rodes J. Reticuloendothelial system phagocytic activity in cirrhosis and its relation to bacterial infections and prognosis. Hepatology **1984**; 4(1): 53-8.
120. O'Brien AJ, Fullerton JN, Massey KA, et al. Immunosuppression in acutely decompensated cirrhosis is mediated by prostaglandin E2. Nat Med **2014**; 20(5): 518-23.
121. Jones RN. Microbial etiologies of hospital-acquired bacterial pneumonia and ventilator-associated bacterial pneumonia. Clin Infect Dis **2010**; 51 Suppl 1: S81-7.
122. Lister PD, Wolter DJ, Hanson ND. Antibacterial-resistant Pseudomonas aeruginosa: clinical impact and complex regulation of chromosomally encoded resistance mechanisms. Clin Microbiol Rev **2009**; 22(4): 582-610.
123. Petzelbauer P, Zacharowski PA, Miyazaki Y, et al. The fibrin-derived peptide Bbeta15-42 protects the myocardium against ischemia-reperfusion injury. Nat Med **2005**; 11(3): 298-304.
124. Groger M, Pasteiner W, Ignatyev G, et al. Peptide Bbeta(15-42) preserves endothelial barrier function in shock. PLoS One **2009**; 4(4): e5391.
125. Stephens L, Ellson C, Hawkins P. Roles of PI3Ks in leukocyte chemotaxis and phagocytosis. Curr Opin Cell Biol **2002**; 14(2): 203-13.
126. Subramanian KK, Jia Y, Zhu D, et al. Tumor suppressor PTEN is a physiologic suppressor of chemoattractant-mediated neutrophil functions. Blood **2007**; 109(9): 4028-37.
127. Shi J, Hua L, Harmer D, Li P, Ren G. Cre Driver Mice Targeting Macrophages. Methods Mol Biol **2018**; 1784: 263-75.
128. Schabbauer G, Matt U, Gunzl P, et al. Myeloid PTEN promotes inflammation but impairs bactericidal activities during murine pneumococcal pneumonia. J Immunol **2010**; 185(1): 468-76.
129. Stark AK, Sriskantharajah S, Hessel EM, Okkenhaug K. PI3K inhibitors in inflammation, autoimmunity and cancer. Curr Opin Pharmacol **2015**; 23: 82-91.
130. Luyendyk JP, Schabbauer GA, Tencati M, Holscher T, Pawlinski R, Mackman N. Genetic analysis of the role of the PI3K-Akt pathway in lipopolysaccharide-induced cytokine and tissue factor gene expression in monocytes/macrophages. J Immunol **2008**; 180(6): 4218-26.
131. Martin M, Rehani K, Jope RS, Michalek SM. Toll-like receptor-mediated cytokine production is differentially regulated by glycogen synthase kinase 3. Nat Immunol **2005**; 6(8): 777-84.
132. Gunzl P, Bauer K, Hainzl E, et al. Anti-inflammatory properties of the PI3K pathway are mediated by IL-10/DUSP regulation. J Leukoc Biol **2010**; 88(6): 1259-69.
133. Huang Y, Wang H, Hao Y, et al. Myeloid PTEN promotes chemotherapy-induced NLRP3-inflammasome activation and antitumour immunity. Nat Cell Biol **2020**.
134. Riquelme SA, Hopkins BD, Wolfe AL, et al. Cystic Fibrosis Transmembrane Conductance Regulator Attaches Tumor Suppressor PTEN to the Membrane and Promotes Anti Pseudomonas aeruginosa Immunity. Immunity **2017**; 47(6): 1169-81 e7.
135. Sahin E, Haubenwallner S, Kuttke M, et al. Macrophage PTEN regulates expression and secretion of arginase I modulating innate and adaptive immune responses. J Immunol **2014**; 193(4): 1717-27.
136. Yue S, Rao J, Zhu J, et al. Myeloid PTEN deficiency protects livers from ischemia reperfusion injury by facilitating M2 macrophage differentiation. J Immunol **2014**; 192(11): 5343-53.

137. Li Y, Jia Y, Pichavant M, et al. Targeted deletion of tumor suppressor PTEN augments neutrophil function and enhances host defense in neutropenia-associated pneumonia. Blood **2009**; 113(20): 4930-41.
138. Organization WH. **2019**.
139. Rajaram MV, Ni B, Dodd CE, Schlesinger LS. Macrophage immunoregulatory pathways in tuberculosis. Semin Immunol **2014**; 26(6): 471-85.
140. Kerner G, Rosain J, Guerin A, et al. Inherited human IFN-gamma deficiency underlies mycobacterial disease. J Clin Invest **2020**; 130(6): 3158-71.
141. Adams KN, Takaki K, Connolly LE, et al. Drug tolerance in replicating mycobacteria mediated by a macrophage-induced efflux mechanism. Cell **2011**; 145(1): 39-53.
142. Adams KN, Verma AK, Gopalaswamy R, et al. Diverse Clinical Isolates of Mycobacterium tuberculosis Develop Macrophage-Induced Rifampin Tolerance. J Infect Dis **2019**; 219(10): 1554-8.
143. Dlugosz A, Janecka A. ABC Transporters in the Development of Multidrug Resistance in Cancer Therapy. Curr Pharm Des **2016**; 22(30): 4705-16.
144. Du D, Wang-Kan X, Neuberger A, et al. Multidrug efflux pumps: structure, function and regulation. Nat Rev Microbiol **2018**; 16(9): 523-39.
145. Matt U, Selchow P, Dal Molin M, et al. Chloroquine enhances the antimycobacterial activity of isoniazid and pyrazinamide by reversing inflammation-induced macrophage efflux. Int J Antimicrob Agents **2017**; 50(1): 55-62.
146. Bochkov V, Gesslbauer B, Mauerhofer C, Philippova M, Erne P, Oskolkova OV. Pleiotropic effects of oxidized phospholipids. Free Radic Biol Med **2017**; 111: 6-24.
147. Furnkranz A, Schober A, Bochkov VN, et al. Oxidized phospholipids trigger atherogenic inflammation in murine arteries. Arterioscler Thromb Vasc Biol **2005**; 25(3): 633-8.
148. Bochkov VN, Kadl A, Huber J, Gruber F, Binder BR, Leitinger N. Protective role of phospholipid oxidation products in endotoxin-induced tissue damage. Nature **2002**; 419(6902): 77-81.
149. Knapp S, Matt U, Leitinger N, van der Poll T. Oxidized phospholipids inhibit phagocytosis and impair outcome in gram-negative sepsis in vivo. J Immunol **2007**; 178(2): 993-1001.
150. Esseltine JL, Scott JD. AKAP signaling complexes: pointing towards the next generation of therapeutic targets? Trends Pharmacol Sci **2013**; 34(12): 648-55.
151. Matt U, Sharif O, Martins R, Knapp S. Accumulating evidence for a role of oxidized phospholipids in infectious diseases. Cell Mol Life Sci **2015**; 72(6): 1059-71.
152. Leibundgut G, Witztum JL, Tsimikas S. Oxidation-specific epitopes and immunological responses: Translational biotheranostic implications for atherosclerosis. Curr Opin Pharmacol **2013**; 13(2): 168-79.
153. O'Donnell VB, Aldrovandi M, Murphy RC, Kronke G. Enzymatically oxidized phospholipids assume center stage as essential regulators of innate immunity and cell death. Sci Signal **2019**; 12(574).
154. Bochkov VN. Inflammatory profile of oxidized phospholipids. Thromb Haemost **2007**; 97(3): 348-54.
155. Serbulea V, DeWeese D, Leitinger N. The effect of oxidized phospholipids on phenotypic polarization and function of macrophages. Free Radic Biol Med **2017**; 111: 156-68.
156. Kadl A, Meher AK, Sharma PR, et al. Identification of a novel macrophage phenotype that develops in response to atherogenic phospholipids via Nrf2. Circ Res **2010**; 107(6): 737-46.
157. Bisgaard LS, Mogensen CK, Rosendahl A, et al. Bone marrow-derived and peritoneal macrophages have different inflammatory response to oxLDL and M1/M2 marker expression - implications for atherosclerosis research. Sci Rep **2016**; 6: 35234.
158. Kadl A, Galkina E, Leitinger N. Induction of CCR2-dependent macrophage accumulation by oxidized phospholipids in the air-pouch model of inflammation. Arthritis Rheum **2009**; 60(5): 1362-71.
159. Di Gioia M, Spreafico R, Springstead JR, et al. Endogenous oxidized phospholipids reprogram cellular metabolism and boost hyperinflammation. Nat Immunol **2020**; 21(1): 42-53.

160. Imai Y, Parodo J, Kajikawa O, et al. Injurious mechanical ventilation and end-organ epithelial cell apoptosis and organ dysfunction in an experimental model of acute respiratory distress syndrome. JAMA **2003**; 289(16): 2104-12.
161. Quilez ME, Lopez-Aguilar J, Blanch L. Organ crosstalk during acute lung injury, acute respiratory distress syndrome, and mechanical ventilation. Curr Opin Crit Care **2012**; 18(1): 23-8.
162. Heuer JF, Sauter P, Pelosi P, et al. Effects of pulmonary acid aspiration on the lungs and extra-pulmonary organs: a randomized study in pigs. Crit Care **2012**; 16(2): R35.
163. Goldman G, Welbourn R, Klausner JM, et al. Leukocytes mediate acid aspiration-induced multiorgan edema. Surgery **1993**; 114(1): 13-20.
164. Hotchkiss RS, Monneret G, Payen D. Sepsis-induced immunosuppression: from cellular dysfunctions to immunotherapy. Nat Rev Immunol **2013**; 13(12): 862-74.
165. Hilliard KL, Allen E, Traber KE, et al. The Lung-Liver Axis: A Requirement for Maximal Innate Immunity and Hepatoprotection during Pneumonia. Am J Respir Cell Mol Biol **2015**; 53(3): 378-90.
166. Hilliard KL, Allen E, Traber KE, et al. Activation of Hepatic STAT3 Maintains Pulmonary Defense during Endotoxemia. Infect Immun **2015**; 83(10): 4015-27.
167. Michels KR, Zhang Z, Bettina AM, et al. Hepcidin-mediated iron sequestration protects against bacterial dissemination during pneumonia. JCI Insight **2017**; 2(6): e92002.
168. Deniset JF, Surewaard BG, Lee WY, Kubes P. Splenic Ly6G(high) mature and Ly6G(int) immature neutrophils contribute to eradication of S. pneumoniae. J Exp Med **2017**; 214(5): 1333-50.
169. Jones-Nelson O, Hilliard JJ, DiGiandomenico A, et al. The Neutrophilic Response to Pseudomonas Damages the Airway Barrier, Promoting Infection by Klebsiella pneumoniae. Am J Respir Cell Mol Biol **2018**; 59(6): 745-56.
170. Langelage M, Better J, Wetstein M, et al. Acid Aspiration Impairs Antibacterial Properties of Liver Macrophages. Am J Respir Cell Mol Biol **2021**; 64(5): 641-3.
171. Culemann S, Gruneboom A, Nicolas-Avila JA, et al. Locally renewing resident synovial macrophages provide a protective barrier for the joint. Nature **2019**; 572(7771): 670-5.
172. Bajpai G, Schneider C, Wong N, et al. The human heart contains distinct macrophage subsets with divergent origins and functions. Nat Med **2018**; 24(8): 1234-45.

6. Liste der Anhänge

Anlage A	Bβ15-42 protects against acid-induced acute lung injury and secondary Pseudomonas pneumonia *in vivo*. **Matt, U.**, Warszawska, J.M., Bauer, M., Dietl, W., Mesteri, I., Doninger, B., Haslinger, I., Schabbauer, G., Perkmann, T., Binder, C.J., Reingruber, S., Petzelbauer, P. und S. Knapp. American Journal of Respiratory and Critical Care Medicine, 2009, 180(12):1208-17
Anlage B	Myeloid PTEN promotes inflammation but impairs bactericidal activities during murine pneumococcal pneumonia. Schabbauer, G.*, **Matt, U.***, Günzl, P., Furtner, T., Hainzl, E., Mesteri, I., Doninger, B., Binder, B.R. und S. Knapp. Journal of Immunology, 2010, 185(1):468-76; * geteilte Autorenschaft.
Anlage C	Chloroquine enhances the antimycobacterial activity of isoniazid and pyrazinamide by reversing inflammation-induced macrophage efflux. **Matt, U.**, Selchow, P., Dal Molin, M., Strommer, S., Sharif, O., Schilcher, K., Andreoni, F., Stenzinger, A., Zinkernagel, A.S., Zeitlinger, M., Sander, P. und J. Nemeth. International Journal of Antimicrobial Agents, 2017, 50(1):55-62
Anlage D	WAVE1 mediates phospholipid-derived danger-associated molecular pattern (DAMP) suppression of phagocytosis. **Matt, U.***, Sharif, O.*, Martins, R., Furtner, T., Langeberg, L., Gawish, R., Elbau, I., Zivkovic, A., Lakovits, K., Stich, K., Oskolkova, O., Doninger, B., Perkmann, T., Schabbauer, G., Binder, C.J., Bochkov, V.N., Scott, J.D. und S. Knapp. Journal of Clinical Investigation, 2013, 123(7):3014–3024; * geteilte Autorenschaft
Anlage E	Acid aspiration impairs antibacterial properties of liver macrophages. Langelage, M., Better, J., Wetstein, M., Selvakumar, B., Malainou, C., Kimmig, L., Arneth, B., Köhler, K., Herden, C., Susanne Herold, S*. und **U. Matt***. American Journal of Respiratory Cell and Molecular Biology, 2021, 64(5):641-643 * geteilte Autorenschaft

7. Erklärung

Ich erkläre hiermit, dass die vorliegende kumulative Habilitationsschrift „Antibakterielle Eigenschaften von organspezifischen Makrophagen“ eigenständig und ohne fremde Hilfe von mir verfasst wurde.

Ich erkläre hiermit, keine anderen als die angegebenen Quellen verwendet zu haben, wobei wörtlich oder annähernd wörtlich aus anderen Arbeiten entnommene Stelle als solche genau erkenntlich gemacht worden sind.

Dr. med. univ. Ulrich Matt, PhD

8. Anhänge

$B\beta_{15–42}$ Protects against Acid-induced Acute Lung Injury and Secondary *Pseudomonas* Pneumonia *In Vivo*

Ulrich Matt[1,2], Joanna Maria Warszawska[1,2], Michael Bauer[3], Wolfgang Dietl[3], Ildiko Mesteri[4], Bianca Doninger[1,2], Isabella Haslinger[2], Gernot Schabbauer[5], Thomas Perkmann[6], Christoph J. Binder[1,6], Sonja Reingruber[7], Peter Petzelbauer[8], and Sylvia Knapp[1,2]

[1]Research Center for Molecular Medicine of the Austrian Academy of Sciences (CeMM), Vienna, Austria; [2]Department of Medicine I, Division of Infectious Diseases and Tropical Medicine, [3]Ludwig Boltzmann Cluster for Cardiovascular Research, Department of Biomedical Research, [4]Department of Pathology, [5]Institute of Vascular Biology and Thrombosis Research, Center for Biomolecular Medicine and Pharmacology, [6]Department of Medical and Chemical Laboratory Diagnostics, and [8]Department of Dermatology, Division of General Dermatology, Medical University Vienna, Vienna, Austria; and [7]Fibrex Medical Research and Development GmbH, Vienna, Austria

***Rationale*: Acute lung injury (ALI) is a serious condition in critically ill patients that predisposes to secondary bacterial pneumonia. Vascular leak is a hallmark in the pathogenesis of ALI. The fibrin-derived peptide $B\beta_{15–42}$ was shown to preserve endothelial barriers, thereby reducing vascular leak. The potential therapeutic role of $B\beta_{15–42}$ in ALI has not been addressed so far.**

***Objectives*: To investigate the therapeutic potential of $B\beta_{15–42}$ in ALI and secondary pneumonia induced by *Pseudomonas aeruginosa*.**

***Methods*: The effect of the fibrin-derived peptide $B\beta_{15–42}$ was studied in models of ALI, induced either by pulmonary administration of LPS or hydrochloric acid. Lung inflammation was analyzed by quantifying cell influx, cytokine levels, and oxidized lipids. Vascular leak was determined by Evans Blue extravasations and alveolar protein content. In subsequent two-hit studies, mice were infected with *P. aeruginosa* 24 hours after induction of aspiration pneumonitis and effects of $B\beta_{15–42}$ on inflammation, bacterial clearance, and survival were evaluated.**

***Measurements and Main Results*: After LPS or acid inhalation, proinflammatory cytokine levels, neutrophil influx, and vascular leak were found diminished in mice treated with $B\beta_{15–42}$. Acid aspiration impaired macrophage functions and rendered mice more susceptible to subsequent *P. aeruginosa* infection, whereas mice that received $B\beta_{15–42}$ during acid aspiration and were subsequently challenged with bacteria displayed reduced inflammation, enhanced bacterial clearance, and ultimately improved survival.**

***Conclusions*: The fibrin-derived peptide $B\beta_{15–42}$ exerted protective effects during ALI, resulting in diminished lung injury and preserved antibacterial properties of macrophages, which improved outcome during subsequent *P. aeruginosa* pneumonia.**

Keywords: acute lung injury; inflammation; pneumonia; *Pseudomonas aeruginosa*

Acute lung injury (ALI) is a serious condition defined as rapid-onset bilateral pulmonary infiltrates and hypoxemia of non-cardiac origin (1, 2). Acute respiratory distress syndrome is the most severe form of ALI. With a reported incidence of 79 per 100,000 and an in-hospital mortality of 40%, ALI represents a serious problem among intensive care unit (ICU) patients (3). ALI can develop as a result of direct injury to the lungs, such as during pneumonia, or aspiration of gastric contents, or occur in the course of systemic inflammation, such as during sepsis or after trauma (4). Despite these different etiologies, the pathological features observed in ALI share common findings like protein-rich edema and accumulation of neutrophils (4, 5).

To investigate the molecular mechanisms leading to ALI, a number of animal models have been established. Among them, LPS- and hydrochloric acid (HCl)-induced ALI are known to yield very reproducible results and are characterized by a rapid influx of polymorphonuclear leukocytes (PMNs) and release of proinflammatory cytokines. Although both models ultimately lead to the disruption of endothelial barriers, LPS seems to primarily target the endothelium, whereas HCl has been reported to initially damage epithelial cells (6). Acid aspiration is a widely used model of ALI in mice, as it ideally imitates the pathophysiologic events observed in humans (7–9) by mimicking the clinically relevant event of aspiration of gastric contents in patients with reduced consciousness, referred to as aspiration pneumonitis (10).

Secondary bacterial infection is a frequent and dreaded complication in critically ill patients suffering from ALI (10). *Pseudomonas aeruginosa* is one of the most common pathogens causing nosocomial pneumonia, particularly in ICUs, where intubation favors its colonization, and antibiotic therapy selects multiresistant strains (11). Experimentally it was shown that preceding acid aspiration primes for an exaggerated, and thereby harmful, inflammation to subsequent administration of LPS (12) or bacteria (13). In both reports, administration of LPS or bacteria after instillation of acid led to a dramatic increase in proinflammatory cytokines, such as IL-6, IL-1β, keratinocyte-

AT A GLANCE COMMENTARY

Scientific Knowledge on the Subject

Vascular leak and neutrophil migration are hallmarks of acute lung injury (ALI). Despite high mortality rates, specific therapies to prevent lung injury and inflammation are not available.

What This Study Adds to the Field

The fibrin-derived peptide $B\beta_{15–42}$ prevents vascular leak and protects mice from ALI and secondary *Pseudomonas aeruginosa* pneumonia *in vivo*.

(*Received in original form April 29, 2009; accepted in final form September 17, 2009*)

Supported by a grant from the Austrian Research Funding Society (FFG #811037, Bridge I).

Correspondence and requests for reprints should be addressed to Sylvia Knapp, M.D., Ph.D., Research Center for Molecular Medicine (CeMM) of the Austrian Academy of Sciences, and Department of Medicine I, Division of Infectious Diseases and Tropical Medicine, Medical University Vienna, Waehringer Guertel 18-20, 1090 Vienna, Austria. E-mail: sylvia.knapp@meduniwien.ac.at

This article has an online supplement, which is accessible from this issue's table of contents at www.atsjournals.org

Am J Respir Crit Care Med Vol 180. pp 1208–1217, 2009
Originally Published in Press as DOI: 10.1164/rccm.200904-0626OC on September 17, 2009
Internet address: www.atsjournals.org

derived chemokine (KC), or macrophage-inflammatory protein (MIP)-2 (13). van Westerloo and colleagues nicely demonstrated that clearance of *Klebsiella pneumoniae* was greatly impaired in mice suffering from preceding acid aspiration (13). In addition, others reported that acid aspiration enhanced bacterial adherence (14) and that gastric acid and particulate aspiration impaired pulmonary bacterial clearance (15). Hence, although ALI itself is considered a life-threatening condition, it furthermore predisposes to nosocomial pneumonia, thus underlining the urgent need for better treatment of ALI.

In 2005 a naturally occurring peptide derived from the N-terminus of the β-chain of fibrin, $B\beta_{15–42}$, was shown to protect from myocardial reperfusion injury in rats due to its capacity to prevent leukocyte migration (16). In a subsequently installed multicenter phase IIa clinical trial, these findings could be confirmed in patients suffering from acute myocardial infarction (17). $B\beta_{15–42}$ significantly reduced the size of necrotic zones in patients with acute myocardial infarction undergoing primary percutaneous coronary intervention (17). In another series of experiments, $B\beta_{15–42}$ was shown to be vasculoprotective in models of vascular leak, such as Dengue hemorrhagic shock or LPS shock (18). It improved survival and reduced vascular leak in a Fyn-dependent manner (18). The antiinflammatory and vasculoprotective features of the peptide prompted us to test its therapeutic potential in the lung.

Although our understanding of pathophysiological mechanisms underlying ALI has improved substantially over the last years, therapeutic advances are missing and treatment recommendations are limited to protective ventilation and supportive care (19). The high lethality and great clinical importance of ALI prompted us to explore the therapeutic potential of $B\beta_{15–42}$ during ALI and secondary bacterial pneumonia.

METHODS

Animals

Pathogen-free 9- to 11-week-old male C57BL/6 mice were purchased from Charles River (Sulzfeld, Germany). All experiments were approved by the local Ethics Committee of the Medical University Vienna and the Ministry of Sciences.

Induction of ALI and Pneumonia

ALI and pneumonia were induced as described previously (20). Briefly, mice were short-term anesthetized by inhalation of isoflurane (Abbott Laboratories, Vienna, Austria), and 50 μl of LPS (*Escherichia coli* O55:B5, 100 ng; Sigma, St. Louis, MO) or *P. aeruginosa* (PA103) at indicated amounts was instilled intranasally. For the induction of acid-induced lung injury mice were anesthetized using ketamine and xylazine and 50 μl of 0.1 N endotoxin-free HCl (Sigma) was injected intratracheally. For more detailed information see the online supplement.

Peptide Preparation and Administration

$B\beta_{15–42\text{-}NH_2}$ (GHRPLDKKREEAPSLRPAPPPISGGGYR-NH_2) was used as a proteolytically stable analog of $B\beta_{15–42}$; random peptide or saline was used as control. Peptides were produced by solid-phase peptide synthesis and purified with reverse-phase high-performance liquid chromatography using nucleosil 100-10C18 columns (Lonza, Brussels, Belgium, and piChem Forschungs- und Entwicklungs-GmbH, Graz, Austria) (16). Mice were treated with 4.8 mg/kg intraperitoneally at t = 0 and t = +1 hour after LPS or acid challenge, respectively. In all experiments lasting longer than 24 hours mice received a third dose at t = +6 hours.

Lung Sampling and Quantification of Colony-forming Units

Whole lungs were harvested and processed as described (21, 22); determination of lung cfu is described in the online supplement.

Determination of Vascular Permeability, Edema, and Histology

Vascular leak was determined using Evans Blue extravasations as described (23). Edema was quantified by determining total protein concentration in bronchoalveolar lavage fluid (BALF) using a protein assay kit (Pierce, Rockford, IL). For lung histology the left lobe was removed and processed as described earlier (21) and paraffin sections were stained with hematoxylin and eosin. The degree of inflammation was scored based on the size of the infiltrate, presence of edema, bronchitis, thrombi, endotheliitis, pleuritis, and perivascular infiltrates by a pathologist blinded for groups. Immunohistochemical staining of interleukin-1 receptor associated kinase (IRAK)-M was done as described (24). Further details are outlined in the online supplement.

BAL and Differential Cell Count

BAL was performed as described previously (21). Cells were enumerated using a hemocytometer and differential cell counts were performed on cytospin preparations stained with Giemsa. The BALF was stored at −70°C for determination of cytokines, protein content, and oxidized lipids.

Protein, Oxidized Phospholipids, and Myeloperoxidase Assays

Tumor necrosis factor (TNF)-α, IL-1β, IL-6, IL-10, KC, MIP-2, and myeloperoxidase (MPO) were quantified in BALF and lung homogenates using specific ELISAs (R&D Systems, Minneapolis, MN and HyCult, Uden, the Netherlands) according to the manufacturers' instructions. Oxidized lipids were measured as described (25). More detailed information is provided in the online supplement.

Phagocytosis Assay

Phagocytosis of heat-killed *P. aeruginosa* (PA103) was assessed in essence as described (26), and is further outlined in the online supplement.

Evaluation of mRNA Levels in Whole Lung Preparations

Semiquantitative mRNA analysis for IRAK-M transcripts in whole lung preparations was done as described (24) and is further outlined in the online supplement.

Statistics

Values are expressed as mean ± SEM. Data between two groups were analyzed using unpaired Student *t* test; for more than two groups one-way analysis of variance followed by Tukey multiple comparison test was used. Differences in cfu counts (nonparametric) were calculated using Mann-Whitney test (two groups) or Kruskal-Wallis test followed by Dunn multiple comparison test (more than two groups). Survival data were analyzed by Kaplan-Meier followed by log-rank test. Criteria for significance for all experiments were P less than 0.05.

RESULTS

$B\beta_{15–42\text{-}NH_2}$ Exerts Antiinflammatory Properties within the Lungs

We first analyzed the effects of $B\beta_{15–42\text{-}NH_2}$ during acute pulmonary inflammation and challenged mice with 100 ng LPS intranasally and administered 4.8 mg/kg of the peptide intraperitoneally immediately after LPS challenge and 1 hour later. Control animals received saline or control peptides, respectively. After 6 hours we enumerated cells in BALF where we found significantly reduced numbers of neutrophils in mice treated with the peptide (Figure 1A). In line with the decreased influx of PMNs we observed significantly reduced levels of proinflammatory cytokines and chemokines in BALF (Figure 1B) and lungs (Figure 1C) from $B\beta_{15–42\text{-}NH_2}$-treated mice. Although TNF-α levels were significantly diminished in the bronchoalveolar compartment, IL-10 concentrations were elevated in lungs of $B\beta_{15–42\text{-}NH_2}$-treated animals (Figure 1C).

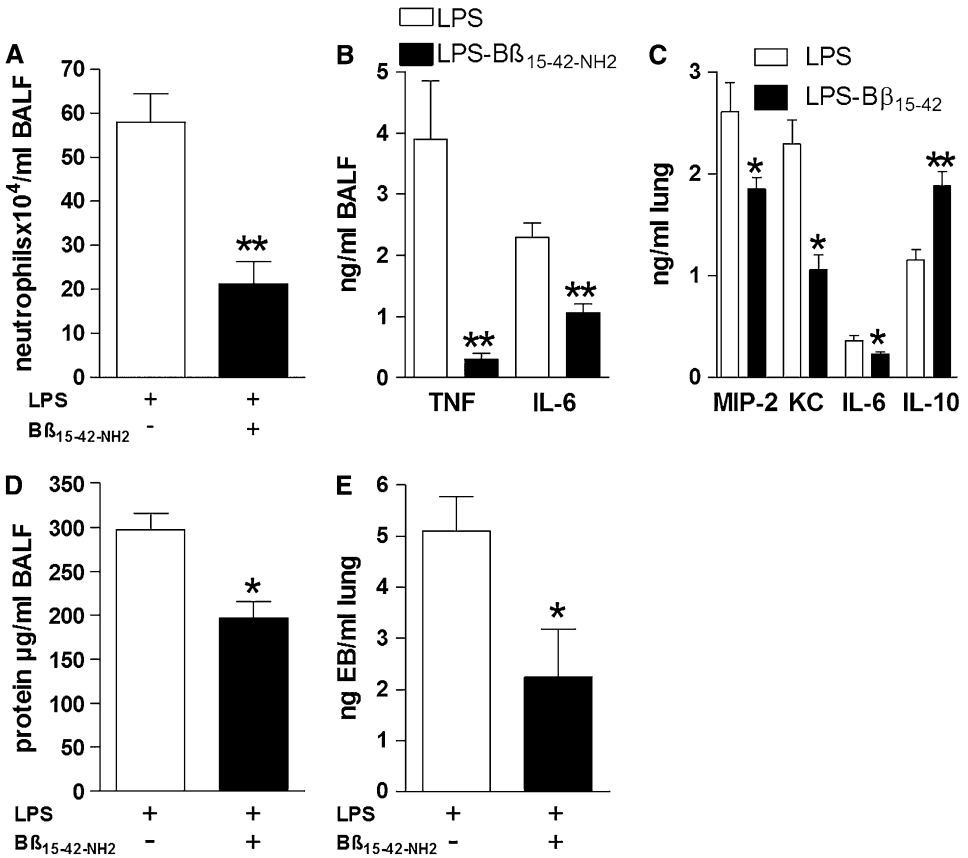

Figure 1. $B\beta_{15-42-NH_2}$ exerts antiinflammatory properties in the lung. Mice received 100 ng LPS intranasally and $B\beta_{15-42-NH_2}$ or carrier (NaCl), respectively, intraperitoneally at t = 0 and t = +1 hour. After 6 hours (*A*) polymorphonuclear leukocyte influx was assessed by cytospin preparations of bronchoalveolar lavage fluid (BALF), (*B*) cytokines were measured in BALF and (*C*) lung homogenates, and (*D*) total protein content in the BALF. (*E*) For measurement of Evans Blue extravasations mice received 10 µg LPS intranasally and $B\beta_{15-42-NH_2}$ or NaCl treatment, respectively, as described above. (*A–D*) n = 6 mice/group, (*E*) n = 4 mice/group. Depicted are representative data out of three independent experiments. Data are mean ± SEM; $^*P < 0.05$, $^{**}P < 0.01$.

Because vascular leak is considered a hallmark of ALI, we also measured total protein contents in BALF of LPS-challenged mice and detected lower protein amounts in $B\beta_{15-42-NH_2}$-treated animals (Figure 1D). Finally, we were able to confirm that $B\beta_{15-42-NH_2}$ treatment reduced vascular leak within the pulmonary compartment by illustrating diminished Evans Blue extravasations during LPS-induced ALI (Figure 1E). Hence, these data demonstrate that $B\beta_{15-42-NH_2}$ exerts potent antiinflammatory effects within the respiratory tract and attenuates vascular leak during ALI *in vivo*.

$B\beta_{15-42-NH_2}$ Dampens Acid-induced Lung Inflammation

Having established that $B\beta_{15-42-NH_2}$ reduces inflammation and improves vascular barrier function during LPS pneumonitis *in vivo*, we next aimed for a model in which these findings could be used for therapeutic purposes and decided to extend our studies to acid-induced ALI, which more closely reflects the situation seen in ICU patients. For this purpose we administered 50 µl of endotoxin-free 0.1 N HCl intratracheally, treated mice with $B\beta_{15-42-NH_2}$ or saline as described above, and evaluated mice every 2 hours up to 8 hours. As depicted in Figures 2A–2D, $B\beta_{15-42-NH_2}$ treatment resulted in a diminished PMN influx to the bronchoalveolar compartment, reduced levels of proinflammatory cytokines, and decreased total protein concentration in BALF. To investigate the inflammatory response and impact of $B\beta_{15-42-NH_2}$ in more detail we then focused on 6 hours after instillation of acid and revealed that treatment with the peptide markedly contained the increase of leukocytes (Figure 2E). A similar pattern was observed for levels of the proinflammatory cytokines in BALF and lung tissue (Figures 2F and 2G). In line with a previous report, which delineated IL-6 as a crucial mediator of acid-induced lung inflammation (25), we found IL-6 highly elevated on acid aspiration, whereas $B\beta_{15-42-NH_2}$ treatment resulted in diminished IL-6 levels (Figures 2F and 2G). IL-1β was significantly reduced in lungs of mice that received $B\beta_{15-42-NH_2}$ (Figure 2G), which is noteworthy as an earlier report discovered that IL-1R gene deficient mice exhibited an improved bacterial clearance during *P. aeruginosa* pneumonia (27). Similar to what we observed during LPS pneumonitis, $B\beta_{15-42-NH_2}$ treatment led to enhanced levels of the antiinflammatory cytokine IL-10; significantly higher IL-10 concentrations were discovered in BALF from the treatment group, and IL-10 levels obtained from lung homogenates were modestly elevated, although differences did not reach significance ($P = 0.055$) (Figures 2F and 2G). Furthermore, the inhibitory effects of $B\beta_{15-42-NH_2}$ on vascular leak during acid aspiration were confirmed by showing reduced total protein concentrations in BALF and diminished Evans Blue extravasations (Figures 2H and 2I). Because acid aspiration–associated generation of reactive oxygen species and subsequent oxidation of pulmonary phospholipids were shown recently to perpetuate ALI *in vivo* (25), we measured BALF levels of oxidized phospholipids using the well-described antibody E06 (28). In accordance with diminished pulmonary inflammation, we observed a tendency toward reduced levels of oxidative epitopes in $B\beta_{15-42-NH_2}$-treated animals (Figure 2J), although differences did not reach significance ($P = 0.07$). Together, $B\beta_{15-42-NH_2}$ was able to attenuate lung injury after acid aspiration *in vivo*.

Preceding Acid Aspiration Impairs Bacterial Clearance during *P. aeruginosa* Pneumonia

Arguing that preexisting acid-induced lung damage predisposes patients for subsequent bacterial pneumonia, we hypothesized that attenuation of acid-induced lung injury might improve outcome during secondary bacterial respiratory tract infection.

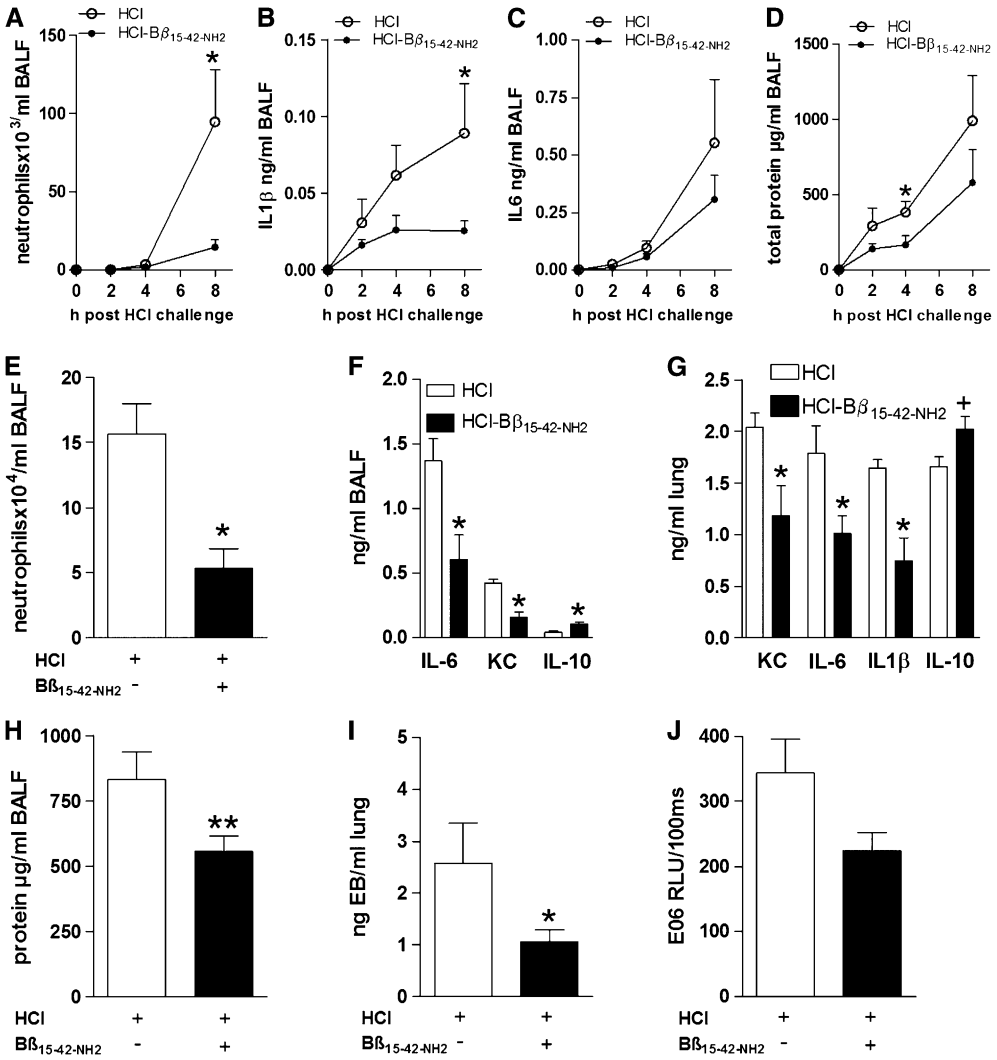

Figure 2. $B\beta_{15-42-NH_2}$ dampens acid-induced lung inflammation endotoxin-free 0.1 N HCl (50 µl) was instilled intratracheally in mice followed by intraperitoneal injection of $B\beta_{15-42-NH_2}$ or carrier (NaCl) at t = 0 and t = +1 hour. Time-course analysis for (*A*) polymorphonuclear leukocyte (PMN) influx, (*B*) IL-1β, (*C*) IL-6 levels, and (*D*) total protein concentration in bronchoalveolar lavage fluid (BALF) are depicted. (*E*) After 6 hours PMN influx in BALF was assessed on cytospin preparations, cytokines and chemokines were measured in (*F*) BALF and (*G*) lung homogenates. (*H*) Total protein content was measured in BALF. (*I*) Evans Blue extravasations were quantified in lung homogenates and (*J*) oxidation epitopes (E06) in BALF. (*A–I*) n = 6 to 8 mice/group; (*J*) pooled data of two experiments (n = 11–13 mice/group). Data shown are one out of two independent experiments and depicted as mean ± SEM; $*P < 0.05$, $**P < 0.01$.

To test this concept we first attempted to establish that acid aspiration would alter the course of secondary pneumonia induced by *P. aeruginosa*, the most frequently isolated pathogen in hospital-acquired pneumonia (29). For this purpose we induced acid aspiration or administered saline, respectively, and infected all mice intranasally with *P. aeruginosa* after 24 hours. This specific infection time point was chosen after we had determined that acid-induced lung inflammation gradually resolved by 24 hours. Mice were then killed 16 hours after secondary intranasal infection with *P. aeruginosa* and the inflammatory response and bacterial clearance were evaluated. As anticipated, preceding acid aspiration was associated with highly elevated lung levels of proinflammatory cytokines, such as KC, IL-6, IL-1β, or TNF-α, compared with control animals (Figure 3A). Neutrophil influx, which was assessed by measuring lung MPO concentrations, was significantly higher in mice that underwent acid aspiration before pneumonia as compared with saline-treated mice (Figure 3B). Furthermore, despite this exaggerated inflammatory response, bacterial clearance was greatly impaired, leading to almost 1000-fold increased bacterial

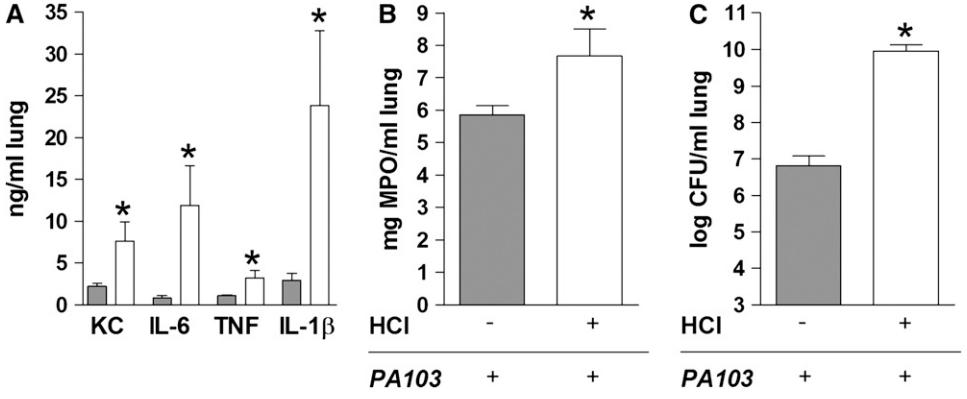

Figure 3. Acid aspiration impairs host response to *Pseudomonas aeruginosa* pneumonia. Mice received 50 µl of 0.1N HCl (HCl group, *open bars*) or sterile NaCl (sham group, *shaded bars*) and 24 hours later 1×10^4 cfu *P. aeruginosa* intranasally. (*A, B*) Mice were killed 16 hours after bacterial infection and lung cytokines, chemokines, and myeloperoxidase were evaluated. (*C*) Serial dilutions of lung homogenates were plated on blood agar plates to determine bacterial cfu. Data are from n = 8 mice/group and represent mean ± SEM. $*P < 0.05$.

TABLE 1. PULMONARY INFLAMMATION MARKERS 24 HOURS AFTER ACID ASPIRATION

Lung	Sham	HCl	HCl-B$\beta_{15-42\text{-}NH_2}$
MPO mg/ml	1.2 ± 0.08	1.5 ± 0.02*	1.1 ± 0.01
IL-6 ng/ml	0.28 ± 0.02	0.53 ± 0.13	0.31 ± 0.03
KC ng/ml	1.64 ± 0.06	2.7 ± 0.12*	1.24 ± 0.02
TNF ng/ml	0.23 ± 0.01	0.23 ± 0.02	0.21 ± 0.03
E06 RLU/100 ms	6108 ± 2085	15947 ± 4190	5453 ± 887

Definition of abbreviations: E06 = oxidation epitopes; KC = keratinocyte-derived chemokine; MPO = myeloperoxidase; TNF = tumor necrosis factor.

Mice underwent NaCl (sham) or acid aspiration (HCl) with subsequent B$\beta_{15-42\text{-}NH_2}$ treatment (HCl-B$\beta_{15-42\text{-}NH_2}$). Pulmonary inflammation markers were evaluated after 24 hours. Shown are mean ± SEM of n = 3 mice/group.

* $P < 0.05$ versus sham and HCl-B$\beta_{15-42\text{-}NH_2}$ group.

counts in lungs from mice of the acid-aspiration group, as compared with control animals (Figure 3C). Therefore, preceding acid aspiration impairs host defense mechanisms against secondary *P. aeruginosa* infection.

B$\beta_{15-42\text{-}NH_2}$ Diminishes the Unfavorable, Exaggerated Immune Response to *P. aeruginosa* after Acid Aspiration

We next tested our hypothesis that B$\beta_{15-42\text{-}NH_2}$ treatment would reduce acid-induced lung injury and thus attenuate detrimental effects on the host response to subsequent bacterial pneumonia. For this purpose we repeated previously described experiments, challenged mice with HCl or saline (sham group), respectively, and treated one group of mice that received HCl intratracheally with B$\beta_{15-42\text{-}NH_2}$ intraperitoneally at t = 0 hours, +1 hour, and +6 hours after intratracheal acid administration. Twenty four hours later we ensured gradual resolution of acid-induced lung inflammation and observed that inflammatory markers did not differ between the sham group and HCl-mice that received B$\beta_{15-42\text{-}NH_2}$ (Table 1).

Next we aimed to evaluate the effects of these differences on a second-hit pneumonia with *P. aeruginosa*. We therefore inoculated mice intranasally 24 hours after acid aspiration or sham surgery, respectively, with *P. aeruginosa* and evaluated the host inflammatory response 16 hours thereafter (i.e., 24 h acid aspiration + 16 h infection). On analysis of pulmonary cytokine and chemokine levels, we discovered that B$\beta_{15-42\text{-}NH_2}$ treatment of mice that received HCl resulted in almost identical lung concentrations of MPO, KC, IL-6, TNF-α, and IL-1β as those found in mice that received saline instead of HCl (Figures 4A–4C). Although acid aspiration followed by *P. aeruginosa* infection led to an enhanced inflammatory response, sham-treated mice (i.e., NaCl instead of HCl) and B$\beta_{15-42\text{-}NH_2}$-treated mice (i.e., HCl and B$\beta_{15-42\text{-}NH_2}$) displayed significantly reduced concentrations of proinflammatory mediators and MPO

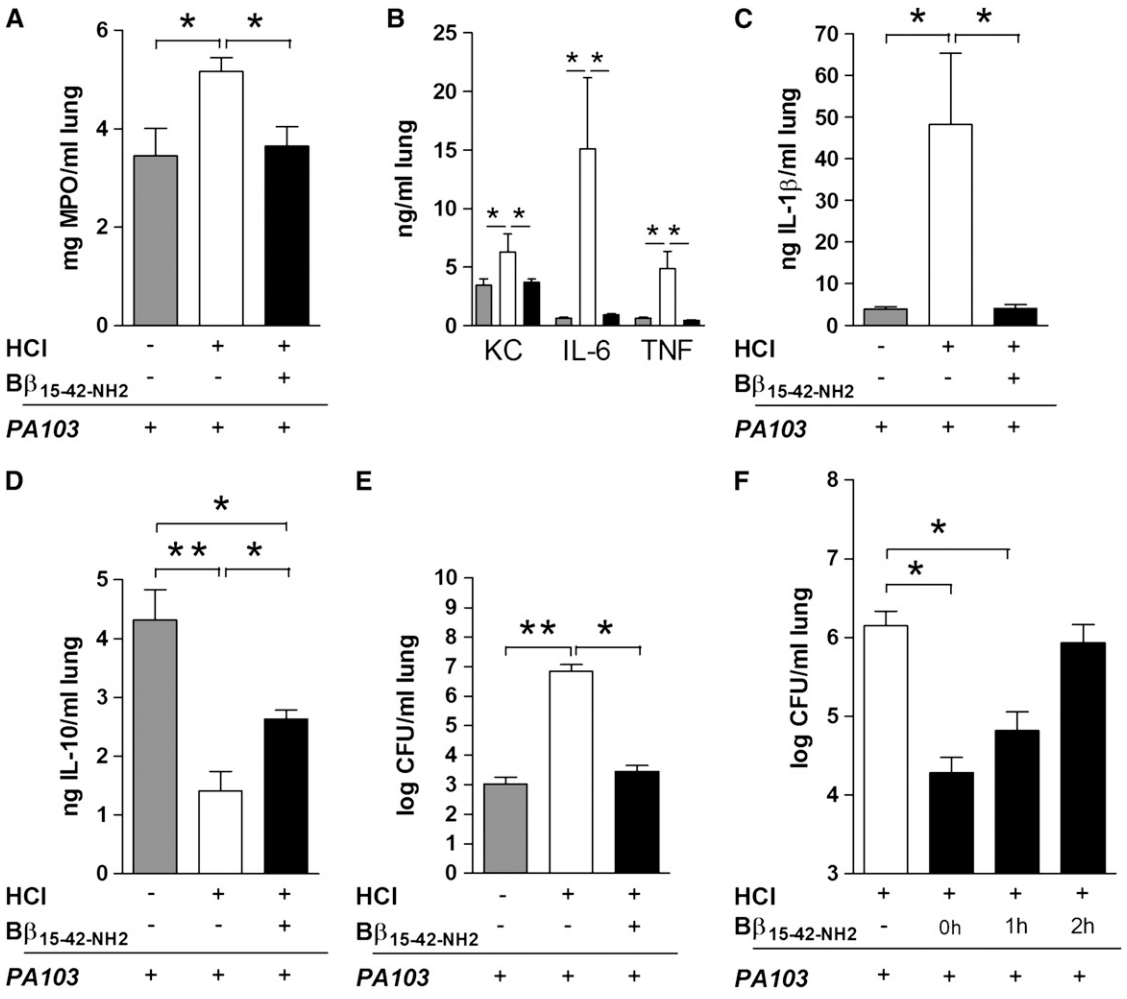

Figure 4. B$\beta_{15-42\text{-}NH_2}$ treatment of aspiration-induced acute lung injury dampens inflammation during secondary *Pseudomonas aeruginosa* pneumonia. Endotoxin-free 0.1 N HCl (50 μl) was instilled intratracheally in mice followed by intraperitoneal injection of B$\beta_{15-42\text{-}NH_2}$ (HCl-B$\beta_{15-42\text{-}NH_2}$) (*solid bars*) or sterile NaCl (HCl) (*open bars*) at t = 0, t = +1 hour, and t = +6 hours. Sham-treated (*shaded bars*) animals received sterile NaCl intratracheally and intraperitoneally (sham group). After 24 hours all three groups were infected with 1×10^4 cfu *P. aeruginosa* intranasally. (*A–D*) Sixteen hours after infection mice were killed and myeloperoxidase, cytokines, and chemokines in lung homogenates were evaluated. (*E*) Lung cfu were determined on blood agar plates. Depicted is one out of three independent experiments of n = 6 to 9 mice/group. In (*F*) mice were treated as described above with the exception that B$\beta_{15-42\text{-}NH_2}$ treatment was started at t = 0 hours, t = +1 hour, or t = +2 hours after acid aspiration (*solid bars*). Control mice (*open bars*) did not receive any B$\beta_{15-42\text{-}NH_2}$. All mice were infected with *P. aeruginosa* 24 hours after acid aspiration. (*A–F*) Data are mean ± SEM; *$P < 0.05$, **$P < 0.01$.

levels. In parallel, the antiinflammatory cytokine IL-10 showed the opposite feature, with lowest levels found in mice that underwent acid aspiration before infection (Figure 4D). When enumerating lung cfu we observed striking differences: $B\beta_{15–42\text{-}NH_2}$-treated mice that underwent acid aspiration showed an identical bacterial load as sham-treated control animals (NaCl aspiration), whereas in mice that underwent acid aspiration followed by bacterial infection approximately 4-log higher numbers of bacteria were recovered from lungs (Figure 4E). Likewise, systemic bacterial dissemination was found reduced in $B\beta_{15–42\text{-}NH_2}$-treated mice. Although 33% of blood cultures were positive in acid-aspiration mice, only 8% and 13% of control or $B\beta_{15–42\text{-}NH_2}$ treated mice, respectively, displayed systemic bacterial spread. To finally test if administration of $B\beta_{15–42\text{-}NH_2}$ after onset of lung injury still exerts therapeutic effects, we repeated the second-hit study and started peptide treatment at t = 0 hours, t = +1 hour, or t = +2 hours after acid aspiration. Identical to earlier experiments, all mice received additional doses of $B\beta_{15–42\text{-}NH_2}$ 1 hour and 6 hours after the first application and *P. aeruginosa* was administered 24 hours after acid aspiration. As depicted in Figure 4F, $B\beta_{15–42\text{-}NH_2}$ treatment 1 hour after the initial injury still exerted beneficial effects and resulted in significantly improved bacterial clearance.

In line with enhanced bacterial outgrowth and proinflammatory cytokine levels, mice of the acid aspiration and infection group exhibited significantly more pronounced signs of lung inflammation and injury as assessed by histopathological scoring of lung slides (Figure 5). Lungs from both control and $B\beta_{15–42\text{-}NH_2}$-treated mice showed only residual signs of inflammation. Therefore, improvement of lung barrier function during acid aspiration attenuated detrimental effects of subsequent *P. aeruginosa* challenge *in vivo*.

$B\beta_{15–42\text{-}NH_2}$ Treatment Reduces Mortality Due to Secondary *P. aeruginosa* Pneumonia

To ultimately verify the potential therapeutic benefit of $B\beta_{15–42\text{-}NH_2}$ treatment during acid-induced ALI followed by bacterial infection, we induced acid or NaCl aspiration in mice, treated one HCl group with $B\beta_{15–42\text{-}NH_2}$, followed by *P. aeruginosa* infection, and monitored survival over 4 days. To exclude any potential effect of $B\beta_{15–42\text{-}NH_2}$ on the course of bacterial infection itself, we included a second sham group that received $B\beta_{15–42\text{-}NH_2}$ together with NaCl aspiration (sham-treated $B\beta_{15–42\text{-}NH_2}$). Survival data clearly demonstrated the impact of preceding acid aspiration on secondary pneumonia, as well as the therapeutic role of $B\beta_{15–42\text{-}NH_2}$ herein. Although all mice undergoing acid aspiration succumbed to bacterial infection within 44 hours, 50% of control animals (i.e., NaCl aspiration) and 40% of $B\beta_{15–42\text{-}NH_2}$-treated acid aspiration mice survived secondary *P. aeruginosa* pneumonia (both control groups and HCl-$B\beta_{15–42\text{-}NH_2}$ mice $P < 0.05$ vs. HCl) (Figure 6). $B\beta_{15–42\text{-}NH_2}$ administration to sham-treated mice had no effect on the course of bacterial infection. Hence, $B\beta_{15–42\text{-}NH_2}$ treatment clearly improved the acid aspiration–induced impairment in host defense mechanisms and decreased death from secondary bacterial pneumonia.

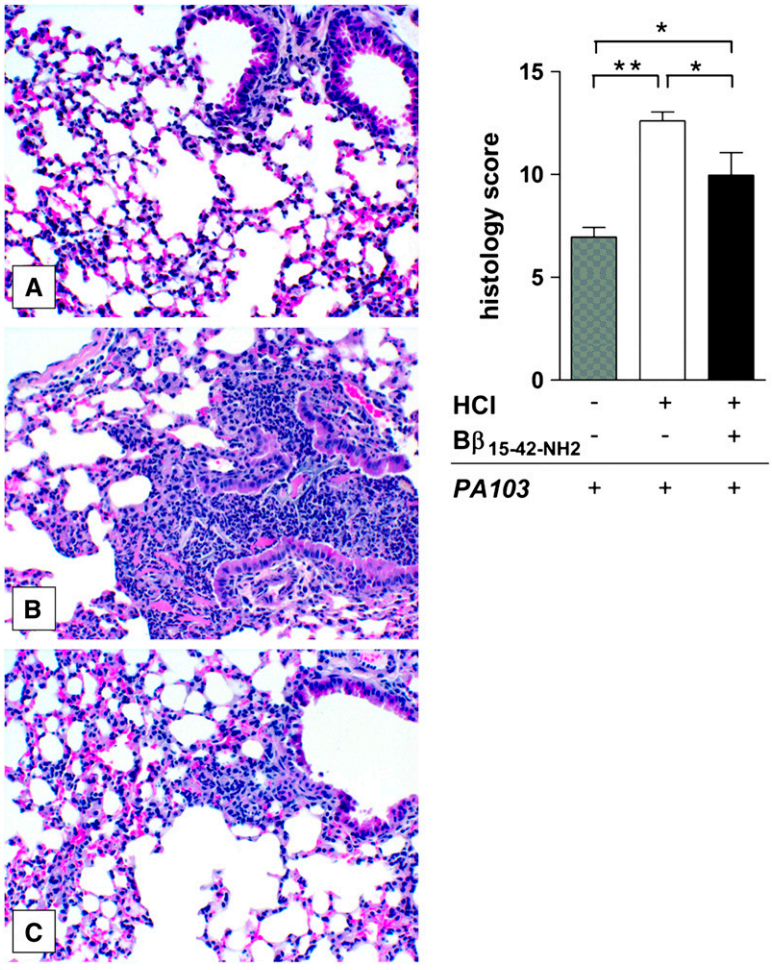

Figure 5. Less severe pulmonary infiltrates in $B\beta_{15–42\text{-}NH_2}$-treated mice. Endotoxin-free 0.1 N HCl (50 μl) was instilled intratracheally in mice followed by intraperitoneal injection of (*C*) $B\beta_{15–42\text{-}NH_2}$ (HCl-$B\beta_{15–42\text{-}NH_2}$) or (*B*) sterile NaCl (HCl) at t = 0, t = +1 hour, and t = +6 hours. (*A*) Control groups received sterile NaCl intratracheally and intraperitoneally. After 24 hours all three groups were infected with 1×10^4 cfu *Pseudomonas aeruginosa* intranasally. Lung sections stained with hematoxylin and eosin were scored as described in the METHODS section by a pathologist blinded for groups and are expressed as inflammation score. Representative slides are shown; magnification ×20. Depicted is one out of three independent experiments of n = 6 to 9 mice/group; data are mean ± SEM; $*P < 0.05$, $**P < 0.01$.

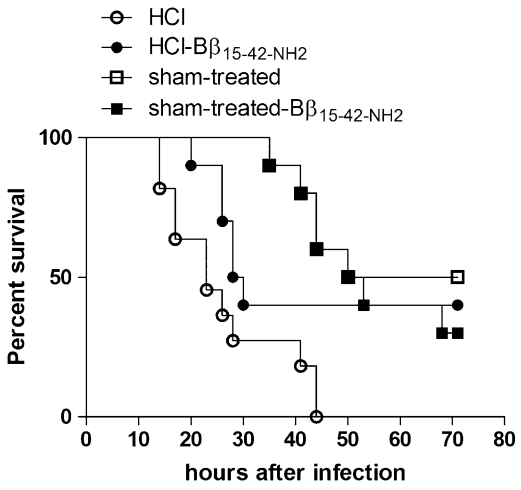

Figure 6. $B\beta_{15–42\text{-}NH_2}$ improves survival during secondary *P. aeruginosa* pneumonia. Endotoxin-free 0.1 N HCl (50 μl) was instilled intratracheally in mice followed by intraperitoneal injection of $B\beta_{15–42\text{-}NH_2}$ (HCl-$B\beta_{15–42\text{-}NH_2}$) or sterile NaCl (HCl) at t = 0, t = +1 hour, and t = +6 hours. Control groups received sterile NaCl intratracheally and intraperitoneally (sham-treated) or NaCl intratracheally and $B\beta_{15–42\text{-}NH_2}$ intraperitoneally (sham-treated-$B\beta_{15–42\text{-}NH_2}$). After 24 hours all four groups were intranasally infected with 1×10^4 cfu *P. aeruginosa*. Survival of n = 9 to 11 mice/group was monitored over 72 hours. Control and $B\beta_{15–42\text{-}NH_2}$-treated mice displayed an improved survival compared with the HCl-group ($P < 0.05$).

Preceding Acid Aspiration Impairs Antibacterial Properties of Alveolar Macrophages

In our efforts to understand how $B\beta_{15–42\text{-}NH_2}$ treatment improved bacterial clearance during secondary pneumonia despite decreased inflammation, we hypothesized that prevention of ALI might preserve antibacterial properties of phagocytes at the onset of infection. To test this idea we first investigated if acid aspiration *per se* impaired the phagocytic properties of macrophages and repeated acid aspiration studies to isolate primary alveolar macrophages 24 hours after mice received HCl alone or in combination with $B\beta_{15–42\text{-}NH_2}$ (i.e., at the time when we challenged mice with *P. aeruginosa* in earlier experiments). Isolated primary alveolar macrophages were then studied for their ability to phagocytose *P. aeruginosa ex vivo*. As shown in Figure 7A, preceding acid aspiration significantly impaired phagocytosis of bacteria by alveolar macrophages ($P < 0.001$ vs. sham-treated mice), whereas treatment with $B\beta_{15–42\text{-}NH_2}$ completely prevented this effect ($P < 0.001$ vs. HCl group). Hence, preceding acid aspiration itself led to impaired antimicrobial properties of alveolar macrophages and attenuation of pulmonary inflammation (as seen in $B\beta_{15–42\text{-}NH_2}$-treated animals) restored the phagocytic functions of alveolar macrophages. To understand how preceding lung injury interfered with bactericidal properties of phagocytes, we hypothesized that expression of negative regulators, which are required for resolution of inflammation, might concurrently affect the antimicrobial functions of macrophages. We therefore quantified expression levels of IRAK-M in lung homogenates 24 hours after induction of acid aspiration and indeed found significantly enhanced IRAK-M transcript levels in lungs from mice that received HCl, as compared with sham-treated or HCl-$B\beta_{15–42\text{-}NH_2}$ animals (Figure 7B). In addition, immunohistochemical studies on primary alveolar macrophages disclosed strongest IRAK-M protein expression in cells from HCl-treated mice as compared with HCl-$B\beta_{15–42\text{-}NH_2}$ animals (Figure 7C). Together, we demonstrated that preceding lung injury increased expression of negative regulators, such as IRAK-M, which was associated with impaired bactericidal properties of alveolar macrophages at the onset of bacterial infection (i.e., 24 h after HCl administration) and might thus explain worsened outcome during subsequent *Pseudomonas* pneumonia.

DISCUSSION

Vascular leak, neutrophil influx, and increase in cytokines at the site of injury are hallmarks of ALI in humans and animals (5, 6, 30). Although important progress has been made in understanding the pathogenesis of ALI over the last years, significant therapeutic implications are still missing. To fill this gap we decided to investigate the potential role of a peptide that has been shown earlier to prevent transmigration of neutrophils and vascular leak in models of myocardial reperfusion injury. This peptide is called $B\beta_{15–42,}$ consists of 28 amino acids, and is a natural plasmin digest of fibrin (16). For studies shown here we have used a proteolytically stable analog, $B\beta_{15–42\text{-}NH_2}$. We studied different models of ALI and show that treatment with $B\beta_{15–42\text{-}NH_2}$ diminished lung inflammation *in vivo*. Furthermore, we were able to illustrate that acid-induced ALI impaired antibacterial defense mechanisms and thus primed for an exaggerated inflammatory response to secondary bacterial infection by *P. aeruginosa* and that treatment with $B\beta_{15–42\text{-}NH_2}$ could attenuate the detrimental effects of preceding ALI *in vivo*. The net result was improved survival from secondary *P. aeruginosa* pneumonia. We suggest that reduced inflammation throughout the course of acid aspiration in animals treated with the peptide, and therefore accelerated regeneration from this injurious event (Table 1) with restored antimicrobial properties (Figure 7A), is responsible for the improved outcome in the second-hit model. To our knowledge, this is the first report that explicitly demonstrates a therapeutic strategy to improve outcome during secondary bacterial pneumonia by diminishing ALI *in vivo*.

Endothelial cells play a central role in the pathogenesis of ALI (31). The biological properties of $B\beta_{15–42}$ were first described in 2005, when antiinflammatory features of the peptide were identified (16). We have extended these studies and showed recently that $B\beta_{15–42}$ antagonizes stress-induced RhoA activation (18), which is an integral regulator of endothelial cell contraction by regulating levels of myosin light chain phosphorylation (32–34). Cell contraction and breaking of cell–cell contacts results in gap formation and leak (32, 35, 36). Earlier studies thoroughly investigated the role of myosin light chain kinase 210 (MLCK210), which is abundantly present in endothelial cells, during sepsis and LPS-induced ALI. Using MLCK210 gene-deficient mice or a small-molecule inhibitor approach, respectively, two reports demonstrated diminished lung injury in response to sepsis or LPS and mechanical ventilation *in vivo* (37, 38). Furthermore, genetic studies revealed single nucleotide polymorphisms of the MLCK210 gene to confer susceptibility to sepsis- and trauma-associated ALI in humans (39, 40). These findings are in line with the proposed mode of action of $B\beta_{15–42}$, namely inhibiting RhoA activation with subsequently reduced myosin light chain phosphorylation (18). The functional importance of this finding was conclusively confirmed by showing reduced vascular leak in LPS-challenged mice that have received $B\beta_{15–42}$. We hereby extended these findings and focused on the potential therapeutic role of $B\beta_{15–42}$ during ALI *in vivo*. Using two distinct mouse models of ALI enabled us to show that early treatment with $B\beta_{15–42}$ efficiently preserved the endothelial barrier and diminished pulmonary inflammation after LPS or hydrochloric acid administration.

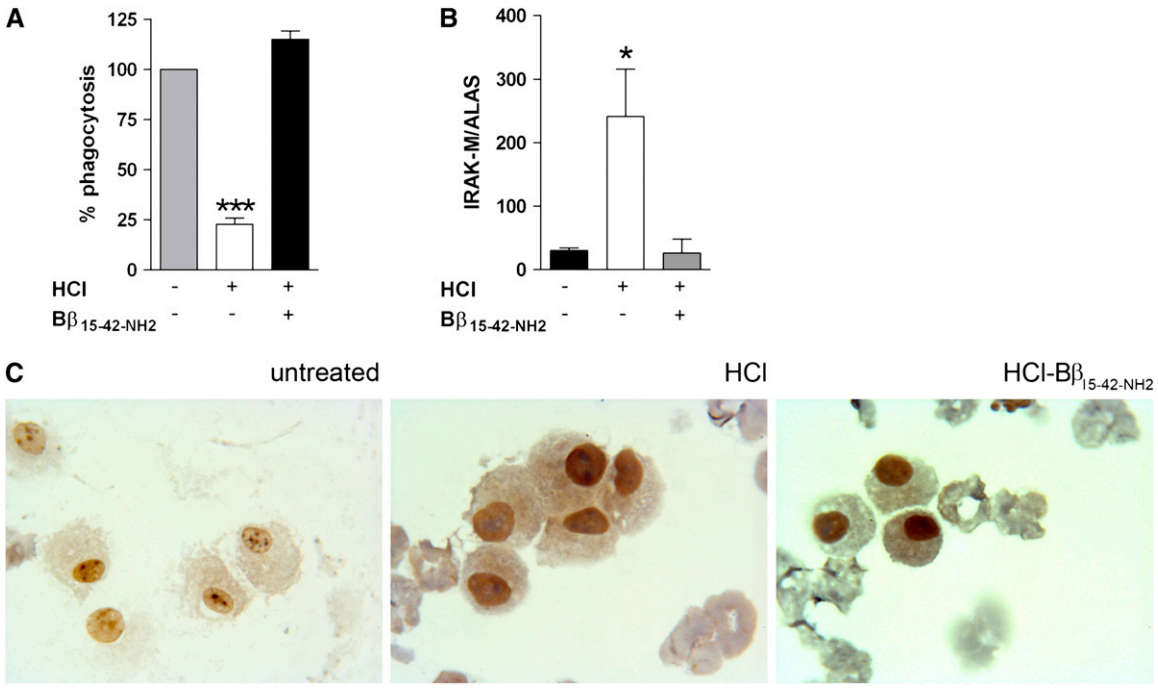

Figure 7. Acid-induced inflammation impairs bacterial phagocytosis by alveolar macrophages. Endotoxin-free 0.1 N HCl (50 μl) was instilled intratracheally in mice followed by intraperitoneal injection of $B\beta_{15–42\text{-}NH_2}$ (HCl-$B\beta_{15–42\text{-}NH_2}$) or sterile NaCl (HCl) at t = 0, t = +1 hour, and t = +6 hours. Control groups received sterile NaCl intratracheally and intraperitoneally (sham-treated). (*A*) After 24 hours alveolar macrophages were harvested, and uptake of fluorescein isothiocyanate–labeled *P. aeruginosa* was assessed by fluorescence-activated cell sorter; (n = 7 mice/group). (*B*) Lungs were harvested after 24 hours to conduct reverse transcriptase–polymerase chain reaction on interleukin-1 receptor associated kinase (IRAK)-M; (n = 3 mice/group). (*C*) Representative slides from immunohistochemical staining of IRAK-M on alveolar macrophages 24 hours after acid aspiration. Values are expressed as mean ± SEM; *$P < 0.05$, ***$P < 0.001$.

Aspiration of acid represents a clinically relevant and useful tool to study ALI (6), as aspiration of gastric contents is a major cause of ALI and is associated with high mortality rates (27, 41). Adding to the poor prognosis, patients with ALI who require mechanical ventilation are at increased risk for secondary bacterial infection (42). The chemical injury by HCl is believed to directly damage airway epithelia, which in turn triggers an inflammatory response followed by edema formation and influx of neutrophils (5, 43–47). Experimentally it has been shown that prior lung injury caused by acid aspiration or during sepsis primes for fatal secondary pneumonia (13, 48). van Westerloo and colleagues observed acid-induced enhanced inflammation to result in worsened outcome during secondary *Klebsiella* pneumonia. In line with these findings, we also observed a tremendously enhanced inflammatory response and impaired bacterial clearance in a model of secondary bacterial pneumonia induced by *P. aeruginosa* after acid aspiration. We moreover disclosed that acid aspiration resulted in impaired bacterial clearance, which was associated with enhanced pulmonary expression of the negative regulator IRAK-M (Figures 7B and 7C). IRAK-M is an inhibitor of TLR-signaling and is involved in the resolution of inflammation (49). Deng and colleagues demonstrated the crucial role of IRAK-M in bacterial clearance of *P. aeruginosa* earlier using a model of sublethal cecal ligation puncture followed by secondary bacterial pneumonia (48). We hereby confirmed and extended these observations by demonstrating that $B\beta_{15–42\text{-}NH_2}$ treatment was able to reduce lung injury, diminish IRAK-M expression, and thus restore antimicrobial properties of alveolar macrophages.

Time-course studies revealed the immediate leakage of proteins into the alveolar compartment and therefore suggest an early involvement of endothelial cells. In parallel, beneficial effects of $B\beta_{15–42\text{-}NH_2}$ were discernable 2 hours after induction of lung injury and ultimately resulted in less pronounced inflammation and thus accelerated resolution. It therefore seems likely that increased IL-10 levels 6 hours after acid aspiration already reflected the early resolution phase, because increased phagocytosis by macrophages of spent cells is associated with release of IL-10 (50). This concept was further confirmed by reduced IRAK-M transcript levels in $B\beta_{15–42\text{-}NH_2}$-treated animals after 24 hours. Hence, $B\beta_{15–42\text{-}NH_2}$-associated attenuation of lung injury expedited resolution and recovery.

To our current knowledge, VE-cadherin is the only transmembrane ligand of $B\beta_{15–42}$. VE-cadherin is expressed on endothelial cells and is of integral importance in regulating endothelial barrier function and inflammation (51). The reduced cytokine levels seen after treatment with $B\beta_{15–42}$ could be a secondary effect of vascular integrity *in vivo*, as incubation of $B\beta_{15–42}$ with LPS-stimulated monocytes, alveolar macrophages, or endothelial cells *in vitro* did not result in an altered release of proinflammatory cytokines (data not shown). Moreover, we could clearly illustrate that $B\beta_{15–42}$ administration to sham-treated mice did not affect host defense mechanisms against *P. aeruginosa in vivo*. Of interest is the observation that even mice that were treated 1 hour after acid aspiration showed improved bacterial clearance in a second-hit model (Figure 4F). Apart from endothelial cells, alveolar epithelial cells importantly contribute to the integrity of the alveolar barrier and are crucially involved in formation and clearance of ALI (52). Although it is tempting to speculate that $B\beta_{15–42}$ also acts on epithelial cells, we currently have no data that would imply a role for $B\beta_{15–42}$ in specifically affecting the epithelial barrier function.

In conclusion, we hereby established tissue-protective properties of $B\beta_{15–42}$ within the pulmonary compartment by in-

vestigating two distinct models of ALI. Our data furthermore indicate that mitigation of ALI can restore antimicrobial properties of alveolar macrophages and thus improve outcome during secondary bacterial pneumonia. Together these results as well as recently published data on the tolerability and efficacy of $B\beta_{15-42}$ in patients undergoing coronary intervention (17) suggest that $B\beta_{15-42}$ might be an attractive therapy to abate harmful consequences of ALI.

Conflict of Interest Statement: U.M. does not have a financial relationship with a commercial entity that has an interest in the subject of this manuscript. J.M.W. does not have a financial relationship with a commercial entity that has an interest in the subject of this manuscript. M.B. does not have a financial relationship with a commercial entity that has an interest in the subject of this manuscript. W.D. does not have a financial relationship with a commercial entity that has an interest in the subject of this manuscript. I.M. does not have a financial relationship with a commercial entity that has an interest in the subject of this manuscript. B.D. does not have a financial relationship with a commercial entity that has an interest in the subject of this manuscript. I.H. does not have a financial relationship with a commercial entity that has an interest in the subject of this manuscript. G.S. does not have a financial relationship with a commercial entity that has an interest in the subject of this manuscript. T.P. does not have a financial relationship with a commercial entity that has an interest in the subject of this manuscript. C.J.B. does not have a financial relationship with a commercial entity that has an interest in the subject of this manuscript. S.R. is the founder and a share holder of Fibrex Medical Inc. Patents include Use of peptides derived from the a α or b β chain of human fibrinogen for the treatment of shock, publication info: BRPI0506148-2006-10-24; Peptides and/or proteins and use thereof for the production of a therapeutic and/or prophylactic medicament, publication info: U.S. patent application 2004019259, DK 1341819T-2006-10-16; Pharmazeutische Zubereitung zur Behandlung von Schock, publication info: AT414097B-2006-09-15; Peptide and/or proteins and their use for manufacture of a therapeutic and/or preventive medicament, publication info: AT329614T-2006-07-15; Pharmaceutical preparation for the treatment of hemorrhagic shock and the sequels thereof A2067/2005; Methods of screening for compounds having antiinflammatory activity, which also prevent vascular leak and edema formation and use thereof, US 11/860, 488/2007. P.P. is the founder and a share holder of Fibrex Medical Inc. Patents include Use of peptides derived from the a α or b β chain of human fibrinogen for the treatment of shock, publication info: BRPI0506148-2006-0-24; Peptides and/or proteins and use thereof for the production of a therapeutic and/or prophylactic medicament, publication info: U.S. patent application 2004019259, DK 1341819T-2006-10-16; Pharmazeutische Zubereitung zur Behandlung von Schock, publication info: AT414097B-2006-09-15; Peptide and/or proteins and their use for manufacture of a therapeutic and/or preventive medicament, publication info: AT329614T-2006-07-15; Pharmaceutical preparation for the treatment of hemorrhagic shock and the sequels thereof A2067/2005; Methods of screening for compounds having antiinflammatory activity, which also prevent vascular leak and edema formation and use thereof US 11/860, 488/2007. S.K. does not have a financial relationship with a commercial entity that has an interest in the subject of this manuscript

Acknowledgment: The authors thank Peter Haslinger for graphical assistance.

References

1. Herridge MS, Angus DC. Acute lung injury–affecting many lives. *N Engl J Med* 2005;353:1736–1738.
2. Bernard GR, Artigas A, Brigham KL, Carlet J, Falke K, Hudson L, Lamy M, Legall JR, Morris A, Spragg R. The American-European Consensus Conference on ARDS. Definitions, mechanisms, relevant outcomes, and clinical trial coordination. *Am J Respir Crit Care Med* 1994;149:818–824.
3. Rubenfeld GD, Caldwell E, Peabody E, Weaver J, Martin DP, Neff M, Stern EJ, Hudson LD. Incidence and outcomes of acute lung injury. *N Engl J Med* 2005;353:1685–1693.
4. Ware LB, Matthay MA. The acute respiratory distress syndrome. *N Engl J Med* 2000;342:1334–1349.
5. Matthay MA, Zimmerman GA. Acute lung injury and the acute respiratory distress syndrome: four decades of inquiry into pathogenesis and rational management. *Am J Respir Cell Mol Biol* 2005;33:319–327.
6. Matute-Bello G, Frevert CW, Martin TR. Animal models of acute lung injury. *Am J Physiol Lung Cell Mol Physiol* 2008;295:L379–L399.
7. Imai Y, Parodo J, Kajikawa O, de Perrot M, Fischer S, Edwards V, Cutz E, Liu M, Keshavjee S, Martin TR, *et al.* Injurious mechanical ventilation and end-organ epithelial cell apoptosis and organ dysfunction in an experimental model of acute respiratory distress syndrome. *JAMA* 2003;289:2104–2112.
8. Imai Y, Kuba K, Rao S, Huan Y, Guo F, Guan B, Yang P, Sarao R, Wada T, Leong-Poi H, *et al.* Angiotensin-converting enzyme 2 protects from severe acute lung failure. *Nature* 2005;436:112–116.
9. Nagase T, Uozumi N, Ishii S, Kume K, Izumi T, Ouchi Y, Shimizu T. Acute lung injury by sepsis and acid aspiration: a key role for cytosolic phospholipase A2. *Nat Immunol* 2000;1:42–46.
10. Marik PE. Aspiration pneumonitis and aspiration pneumonia. *N Engl J Med* 2001;344:665–671.
11. Sadikot RT, Blackwell TS, Christman JW, Prince AS. Pathogen-host interactions in Pseudomonas aeruginosa pneumonia. *Am J Respir Crit Care Med* 2005;171:1209–1223.
12. Yamada H, Miyazaki H, Kikuchi T, Fujimoto J, Kudoh I. Acid instillation enhances the inflammatory response to subsequent lipopolysaccharide challenge in rats. *Am J Respir Crit Care Med* 2000;162:1366–1371.
13. van Westerloo DJ, Knapp S, van't Veer C, Buurman WA, de Vos AF, Florquin S, van der Poll T. Aspiration pneumonitis primes the host for an exaggerated inflammatory response during pneumonia. *Crit Care Med* 2005;33:1770–1778.
14. Mitsushima H, Oishi K, Nagao T, Ichinose A, Senba M, Iwasaki T, Nagatake T. Acid aspiration induces bacterial pneumonia by enhanced bacterial adherence in mice. *Microb Pathog* 2002;33:203–210.
15. Rotta AT, Shiley KT, Davidson BA, Helinski JD, Russo TA, Knight PR. Gastric acid and particulate aspiration injury inhibits pulmonary bacterial clearance. *Crit Care Med* 2004;32:747–754.
16. Petzelbauer P, Zacharowski PA, Miyazaki Y, Friedl P, Wickenhauser G, Castellino FJ, Groger M, Wolff K, Zacharowski K. The fibrin-derived peptide Bbeta15–42 protects the myocardium against ischemia-reperfusion injury. *Nat Med* 2005;11:298–304.
17. Atar D, Petzelbauer P, Schwitter J, Huber K, Rensing B, Kasprzak JD, Butter C, Grip L, Hansen PR, Suselbeck T, *et al.* Effect of intravenous FX06 as an adjunct to primary percutaneous coronary intervention for acute ST-segment elevation myocardial infarction results of the F.I.R.E. (Efficacy of FX06 in the Prevention of Myocardial Reperfusion Injury) trial. *J Am Coll Cardiol* 2009;53:720–729.
18. Gröger M, Pasteiner W, Ignatyev G, Matt U, Knapp S, Atrasheuskaya A, Bukin E, Friedl P, Zinkl D, Hofer-Warbinek R, *et al.* Peptide Bb15–42 preserves endothelial barrier function in shock. *PLoS One* 2009;4:e5391.
19. McIntyre RC Jr, Pulido EJ, Bensard DD, Shames BD, Abraham E. Thirty years of clinical trials in acute respiratory distress syndrome. *Crit Care Med* 2000;28:3314–3331.
20. Knapp S, Wieland CW, Florquin S, Pantophlet R, Dijkshoorn L, Tshimbalanga N, Akira S, van der Poll T. Differential roles of CD14 and toll-like receptors 4 and 2 in murine Acinetobacter pneumonia. *Am J Respir Crit Care Med* 2006;173:122–129.
21. Knapp S, Wieland CW, van 't Veer C, Takeuchi O, Akira S, Florquin S, van der Poll T. Toll-like receptor 2 plays a role in the early inflammatory response to murine pneumococcal pneumonia but does not contribute to antibacterial defense. *J Immunol* 2004;172:3132–3138.
22. Knapp S, Leemans JC, Florquin S, Branger J, Maris NA, Pater J, van Rooijen N, van der Poll T. Alveolar macrophages have a protective antiinflammatory role during murine pneumococcal pneumonia. *Am J Respir Crit Care Med* 2003;167:171–179.
23. Wangle F, Patel M, Razavi HM, Weicker S, Joseph MG, McCormack DG, Mehta S. Role of inducible nitric oxide synthase in pulmonary microvascular protein leak in murine sepsis. *Am J Respir Crit Care Med* 2002;165:1634–1639.
24. Lagler H, Sharif O, Haslinger I, Matt U, Stich K, Furtner T, Doninger B, Schmid K, Gattringer R, de Vos AF, *et al.* TREM-1 activation alters the dynamics of pulmonary IRAK-M expression in vivo and improves host defense during pneumococcal pneumonia. *J Immunol* 2009;183:2027–2036.
25. Imai Y, Kuba K, Neely GG, Yaghubian-Malhami R, Perkmann T, van Loo G, Ermolaeva M, Veldhuizen R, Leung YH, Wang H, *et al.* Identification of oxidative stress and toll-like receptor 4 signaling as a key pathway of acute lung injury. *Cell* 2008;133:235–249.
26. Knapp S, Matt U, Leitinger N, van der Poll T. Oxidized phospholipids inhibit phagocytosis and impair outcome in gram-negative sepsis in vivo. *J Immunol* 2007;178:993–1001.
27. Schultz MJ, Rijneveld AW, Florquin S, Edwards CK, Dinarello CA, van der Poll T. Role of interleukin-1 in the pulmonary immune response during Pseudomonas aeruginosa pneumonia. *Am J Physiol Lung Cell Mol Physiol* 2002;282:L285–L290.
28. Friedman P, Horkko S, Steinberg D, Witztum JL, Dennis EA. Correlation of antiphospholipid antibody recognition with the structure of

synthetic oxidized phospholipids. Importance of Schiff base formation and aldol condensation. *J Biol Chem* 2002;277:7010–7020.
29. Hoffken G, Niederman MS. Nosocomial pneumonia: the importance of a de-escalating strategy for antibiotic treatment of pneumonia in the ICU. *Chest* 2002;122:2183–2196.
30. Park WY, Goodman RB, Steinberg KP, Ruzinski JT, Radella F II, Park DR, Pugin J, Skerrett SJ, Hudson LD, Martin TR. Cytokine balance in the lungs of patients with acute respiratory distress syndrome. *Am J Respir Crit Care Med* 2001;164:1896–1903.
31. Maniatis NA, Orfanos SE. The endothelium in acute lung injury/acute respiratory distress syndrome. *Curr Opin Crit Care* 2008;14:22–30.
32. Garcia JG, Davis HW, Patterson CE. Regulation of endothelial cell gap formation and barrier dysfunction: role of myosin light chain phosphorylation. *J Cell Physiol* 1995;163:510–522.
33. Minshall RD, Malik AB. Transport across the endothelium: regulation of endothelial permeability. *Handb Exp Pharmacol* 2006;107–144.
34. van Nieuw Amerongen GP, Beckers CM, Achekar ID, Zeeman S, Musters RJ, van Hinsbergh VW. Involvement of Rho kinase in endothelial barrier maintenance. *Arterioscler Thromb Vasc Biol* 2007;27: 2332–2339.
35. Konstantoulaki M, Kouklis P, Malik AB. Protein kinase C modifications of VE-cadherin, p120, and beta-catenin contribute to endothelial barrier dysregulation induced by thrombin. *Am J Physiol Lung Cell Mol Physiol* 2003;285:L434–L442.
36. Wojciak-Stothard B, Potempa S, Eichholtz T, Ridley AJ. Rho and Rac but not Cdc42 regulate endothelial cell permeability. *J Cell Sci* 2001; 114:1343–1355.
37. Rossi JL, Velentza AV, Steinhorn DM, Watterson DM, Wainwright MS. MLCK210 gene knockout or kinase inhibition preserves lung function following endotoxin-induced lung injury in mice. *Am J Physiol Lung Cell Mol Physiol* 2007;292:L1327–L1334.
38. Wainwright MS, Rossi J, Schavocky J, Crawford S, Steinhorn D, Velentza AV, Zasadzki M, Shirinsky V, Jia Y, Haiech J, *et al.* Protein kinase involved in lung injury susceptibility: evidence from enzyme isoform genetic knockout and in vivo inhibitor treatment. *Proc Natl Acad Sci USA* 2003;100:6233–6238.
39. Gao L, Grant A, Halder I, Brower R, Sevransky J, Maloney JP, Moss M, Shanholtz C, Yates CR, Meduri GU, *et al.* Novel polymorphisms in the myosin light chain kinase gene confer risk for acute lung injury. *Am J Respir Cell Mol Biol* 2006;34:487–495.
40. Christie JD, Ma SF, Aplenc R, Li M, Lanken PN, Shah CV, Fuchs B, Albelda SM, Flores C, Garcia JG. Variation in the myosin light chain kinase gene is associated with development of acute lung injury after major trauma. *Crit Care Med* 2008;36:2794–2800.
41. Doyle RL, Szaflarski N, Modin GW, Wiener-Kronish JP, Matthay MA. Identification of patients with acute lung injury. Predictors of mortality. *Am J Respir Crit Care Med* 1995;152:1818–1824.
42. Chastre J, Fagon J-Y. Ventilator-associated pneumonia. *Am J Respir Crit Care Med* 2002;165:867–903.
43. Kennedy TP, Johnson KJ, Kunkel RG, Ward PA, Knight PR, Finch JS. Acute acid aspiration lung injury in the rat: biphasic pathogenesis. *Anesth Analg* 1989;69:87–92.
44. Holter JF, Weiland JE, Pacht ER, Gadek JE, Davis WB. Protein permeability in the adult respiratory distress syndrome. Loss of size selectivity of the alveolar epithelium. *J Clin Invest* 1986;78:1513–1522.
45. Weiland JE, Davis WB, Holter JF, Mohammed JR, Dorinsky PM, Gadek JE. Lung neutrophils in the adult respiratory distress syndrome. Clinical and pathophysiologic significance. *Am Rev Respir Dis* 1986;133:218–225.
46. Abraham E. Neutrophils and acute lung injury. *Crit Care Med* 2003; 31(4 suppl)S195–S199.
47. Zarbock A, Singbartl K, Ley K. Complete reversal of acid-induced acute lung injury by blocking of platelet-neutrophil aggregation. *J Clin Invest* 2006;116:3211–3219.
48. Deng JC, Cheng G, Newstead MW, Zeng X, Kobayashi K, Flavell RA, Standiford TJ. Sepsis-induced suppression of lung innate immunity is mediated by IRAK-M. *J Clin Invest* 2006;116:2532–2542.
49. Kobayashi K, Hernandez LD, Galan JE, Janeway CA Jr, Medzhitov R, Flavell RA. IRAK-M is a negative regulator of toll-like receptor signaling. *Cell* 2002;110:191–202.
50. Voll RE, Herrmann M, Roth EA, Stach C, Kalden JR, Girkontaite I. Immunosuppressive effects of apoptotic cells. *Nature* 1997;390: 350–351.
51. Vestweber D. VE-cadherin: the major endothelial adhesion molecule controlling cellular junctions and blood vessel formation. *Arterioscler Thromb Vasc Biol* 2008;28:223–232.
52. Gropper MA, Wiener-Kronish J. The epithelium in acute lung injury/ acute respiratory distress syndrome. *Curr Opin Crit Care* 2008;14: 11–15.

Myeloid PTEN Promotes Inflammation but Impairs Bactericidal Activities during Murine Pneumococcal Pneumonia

Gernot Schabbauer,*[,1] Ulrich Matt,[†,1] Philipp Günzl,* Joanna Warszawska,[†,‡] Tanja Furtner,[†,‡] Eva Hainzl,* Immanuel Elbau,[†,‡] Ildiko Mesteri,[§] Bianca Doninger,[†] Bernd R. Binder,* and Sylvia Knapp[†,‡]

Phosphatidylinositol 3-kinase has been described as an essential signaling component involved in the chemotactic cell influx that is required to eliminate pathogens. At the same time, PI3K was reported to modulate the immune response, thus limiting the magnitude of acute inflammation. The precise role of the PI3K pathway and its endogenous antagonist phosphatase and tensin homolog deleted on chromosome 10 (PTEN) during clinically relevant bacterial infections is still poorly understood. Utilizing mice lacking myeloid cell-specific PTEN, we studied the impact of PTEN on the immune response to *Streptococcus pneumoniae*. Survival analysis disclosed that PTEN-deficient mice displayed less severe signs of disease and prolonged survival. The inflammatory response to *S. pneumoniae* was greatly reduced in macrophages in vitro and in vivo. Unexpectedly, neutrophil influx to the lungs was significantly impaired in animals lacking myeloid-cell PTEN, whereas the additional observation of improved phagocytosis by alveolar macrophages lacking PTEN ultimately resulted in unaltered lung CFUs following bacterial infection. Together, the absence of myeloid cell-associated PTEN and consecutively enhanced PI3K activity dampened pulmonary inflammation, reduced neutrophil influx, and augmented phagocytic properties of macrophages, which ultimately resulted in decreased tissue injury and improved survival during murine pneumococcal pneumonia. ***The Journal of Immunology*****, 2010, 185: 468–476.**

Infectious diseases are a major burden for our society, with respiratory tract infections being a leading cause of morbidity and mortality worldwide. *Streptococcus pneumoniae* is the most frequent causative pathogen of community acquired pneumonia, affecting >500,000 people in the United States annually (1, 2). The worldwide increase in antibiotic resistance among *S. pneumoniae* strains underlines the urgent need for a better understanding of molecular mechanisms associated with pneumococcal pneumonia (3).

The phosphatase and tensin homolog deleted on chromosome 10 (PTEN) is a well-described tumor suppressor gene and multifunctional phosphatase that antagonizes PI3K's enzymatic activity by dephosphorylating phosphatidylinositol (3,5)-trisphosphate to generate phosphatidylinositol (4,5)-biphosphate. PI3K's enzymatic activity is warranted by two distinct subclasses, namely class Ia (p110α, β, δ) and class Ib (p110γ) (4). PTEN efficiently limits PI3K activity and downstream Akt signaling. PI3K/PTEN has been shown to play a prominent role in a variety of cellular mechanisms, such as survival, migration, and proliferation (5). However, little is known about the biological role of PTEN in inflammation and in particular during infectious diseases. The PI3K/Akt signaling axis is crucial for site-directed migration and diapedesis of immune effector cells, such as neutrophils and monocytes, to the site of inflammation and infection (6–10). In contrast to the conception that PI3K mediates proinflammatory signals, several studies indicate that the PI3K/PTEN pathway modulates the inflammatory response to bacterial cell wall components (11–15). Making use of a combination of pharmacologic and genetic means, we and others could previously show that the PI3K pathway provides beneficial anti-inflammatory properties in mouse models of endotoxemia and sepsis. These observations have been further supported by Martin et al. (16), who intriguingly demonstrated that TLR-induced PI3K/Akt activation phosphorylated, and thereby inactivated, downstream glycogen synthase kinase (GSK) 3β, which in turn resulted in diminished NF-κB–driven proinflammatory gene expression in monocytic cells.

The precise function of PI3K signaling during infections with viable bacteria is less well understood. Maus et al. (17) published a report that investigated the contribution of the γ-catalytic subunit of PI3K (p110γ) during pneumococcal pneumonia. They hereby demonstrated that p110γ, which is generally thought to be responsible for the G-protein coupled receptor-induced chemotactic response of neutrophils and monocytes, was not required for neutrophil influx

*Department of Vascular Biology and Thrombosis Research, Center for Biomolecular Medicine and Pharmacology, [‡]Division of Infectious Diseases and Tropical Medicine, Department of Medicine I, and [§]Institute for Clinical Pathology, Medical University of Vienna, Wien; and [†]Research Center for Molecular Medicine, Austrian Academy of Sciences, Vienna, Austria

[1]G.S. and U.M. contributed equally to this work.

Received for publication July 9, 2009. Accepted for publication April 22, 2010.

This work was supported in part by Grant FWF P19850-B12 from the Austrian Science Fund (to G.S.).

Address correspondence and reprint requests to Dr. Gernot Schabbauer, Department of Vascular Biology and Thrombosis Research, Center for Biomolecular Medicine and Pharmacology, Medical University of Vienna, Schwarzspanierstrasse 17, 1090 Wien, Austria, or Dr. Sylvia Knapp, Center for Molecular Medicine of the Austrian Academy of Sciences, Division of Infectious Diseases and Tropical Medicine, Department of Medicine I, Medical University of Vienna, Waehringer Guertel 18-20, 1090 Vienna, Austria. E-mail addresses: gernot.schabbauer@meduniwien.ac.at or sylvia.knapp@meduniwien.ac.at

Abbreviations used in this paper: AM, alveolar macrophage; BAL, bronchoalveolar lavage; BALF, bronchoalveolar lavage fluid; BMDM, bone marrow-derived macrophage; GSK, glycogen synthase kinase; iNOS, inducible NO synthase; KC, keratinocyte-derived chemokine; LysM, lysozyme M; MPO, myeloperoxidase; PTEN, phosphatase and tensin homolog deleted on chromosome 10.

www.jimmunol.org/cgi/doi/10.4049/jimmunol.0902221

following pulmonary inoculation of pneumolysin or whole bacteria in vivo (17). However, p110γ-deficient mice displayed an impaired bacterial clearance and delayed recruitment of exudate macrophages (17).

Still, the role of myeloid cell-associated PTEN upon infection with clinically relevant pathogens in healthy mice, such as community-acquired pneumonia by *S. pneumoniae*, is incompletely understood. The increasing number of patients and clinical trials applying drugs targeting the PI3K/PTEN pathway highlights the urgent need for better comprehension of PI3K/PTEN signaling during clinically relevant infections (18). To elucidate the contribution of myeloid cell-associated PI3K/PTEN during *S. pneumoniae* infection, we therefore made use of a conditional knockout strategy to specifically eliminate PTEN expression in myeloid cells (we hereafter refer to these mice as $PTEN^{MC\text{-}KO}$ animals and $PTEN^{MC\text{-}Wt}$ littermate controls, respectively). Pneumococcal pneumonia was then induced in $PTEN^{MC\text{-}KO}$ mice, which displayed enhanced PI3K activity, and littermate $PTEN^{MC\text{-}Wt}$ controls, after which the inflammatory response was investigated.

Materials and Methods

Mice

Floxed PTEN mice were kindly provided by T.W. Mak (Cancer Institute at Princess Margaret Hospital, University Health Network, Toronto, Ontario, Canada) (19); lysozyme M (LysM) Cre recombinase transgenic mice were a kind gift from R. Johnson (University of California San Diego, La Jolla, CA) (20). PI3Kγ (p110γ) mice were obtained from J.M. Penninger (Institute of Molecular Biotechnology of Austrian Academy of Sciences, Vienna, Austria) (9). Intercrossed mice were backcrossed to a C57BL/6J background for at least eight generations. Littermate-controlled experiments were performed using 8–12-wk-old male mice. For genotyping, murine tissue was lysed in PCR-lysis buffer, and direct PCR was performed using GoTaq DNA Polymerase (Promega, Madison, WI). All animal studies were approved and comply with institutional guidelines (BMWF-66.009/0103-C/GT/2007).

Harvest of primary cells

Thioglycollate-elicited peritoneal macrophages were isolated from $PTEN^{MC\text{-}KO}$ and $PTEN^{MC\text{-}Wt}$ controls as described previously (21). Alveolar macrophages were isolated by bilateral bronchoalveolar lavage (BAL) as described elsewhere (22, 23). Bone marrow was isolated from femurs and tibias of healthy $PTEN^{MC\text{-}KO}$ and $PTEN^{MC\text{-}Wt}$ mice. Bone marrow cells were incubated with conditioned media from L929 cells (20% in RPMI 1640) for 10 d to allow differentiation and maturation of macrophages.

Western blotting

Macrophage cell lysates were separated by SDS-PAGE, blotted to membrane (Immobilon PVDF Transfer Membrane, Millipore, Bedford, MA), probed with rabbit primary Abs against PTEN, protein kinase B, phospho-protein kinase B (Ser473), phospho-GSK3β (Ser9) (Cell Signaling Technology, Beverly, MA), and β-actin (Sigma-Aldrich, St. Louis, MO). For detection, a goat anti-rabbit secondary Ab conjugated with HRP (Amersham Biosciences, Piscataway, NJ) was used.

Inducible NO synthase induction and NO generation assay

RNA from cell culture was extracted using Qiagen's RNEasy kit (Qiagen, Valencia, CA), and real-time PCR was conducted according to the LightCycler FastStart DNA MasterPLUS SYBR Green I system using the Roche Light cycler II sequence detector (Roche Diagnostic Systems, Somerville, NJ). Cycling conditions were set at 1 cycle at 95°C for 10 min, 50 cycles at 95°C for 5 s, 68°C for 5 s, and 72°C for 10 s. To confirm specificity of the reaction products, the melting profile of each sample was analyzed using the LightCycler Software 3.5 (Roche Diagnostic Systems). Mouse gene-specific primer sequences for inducible NO synthase (iNOS) were: 5′-ACC TCA CTG TGG CCT TGG TC-3′ (forward) and 5′-GGG TCC TCA GGG AGC TGG AA-3′ (reverse). NO release was measured by the generation of nitrite (Sigma-Aldrich) in supernatants of $PTEN^{MC\text{-}KO}$ and $PTEN^{MC\text{-}Wt}$ littermate control macrophages incubated with heat-killed *S. pneumonia* (ATCC 6303) for 24 h. Assays were performed according to the manufacturer's protocol (24).

Phagocytosis and killing assays

Primary alveolar macrophages (AMs) were incubated with FITC-labeled heat-killed *S. pneumoniae* (ATCC 6303) at a multiplicity of infection of 100 for 30 min at 37°C. After washing steps, lysosomes were stained with Lysotracker red and nuclei with DAPI (Invitrogen, Carlsbad, CA), followed by visualization using confocal laser scanning microscopy (LSM 510, Zeiss, Oberkochen, Germany). The ratio of engulfed bacteria (as determined by overlay of green bacteria and red lysosomes) were quantified by an independent researcher from 300–400 counted cells per well and are expressed as percentage of cells that contain bacteria. In addition, an FACS-based phagocytosis assay was performed exactly as described earlier (25). In brief, primary AMs were allowed to adhere overnight before being incubated with FITC-labeled *S. pneumoniae* at 37°C or 4°C, respectively. Uptake of bacteria was quantified by FACS, and the phagocytosis index was calculated as follows: (mean fluorescence × % positive cells at 37°C) − (mean fluorescence × % positive cells at 4°C). Bacterial killing was performed as described (25). In brief, AMs were isolated, plated at a density of 2×10^5 cells/well, and allowed to adhere. *S. pneumoniae* were added at a multiplicity of infection of 100, and plates were placed at 37°C for 10 min. Each well was then washed five times with ice-cold PBS to remove extracellular bacteria. To determine bacterial uptake after 10 min, triplicate of wells were lysed with sterile H_2O and designated as $t = 0$. Prewarmed SF-RPMI 1640 was added to remaining wells, and plates were

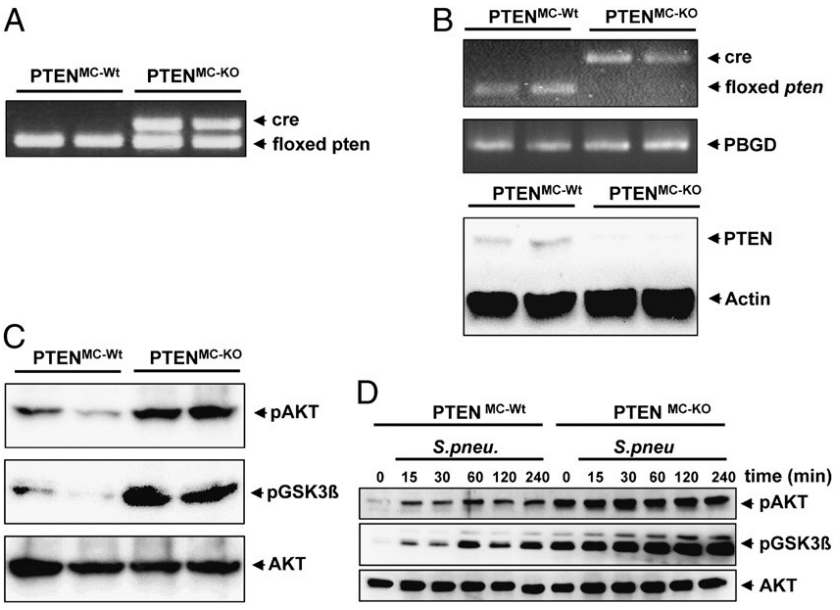

FIGURE 1. PTEN deficiency in myeloid cells. *A*, Genomic DNA PCR analysis of *pten* and *cre* alleles was performed on tissue from fl/fl *pten*, LysM Cre-positive, or -negative mice. *B*, Excision of the *pten* allele was detected by PCR analysis of macrophage genomic DNA; *pbgd* was used as internal control. PTEN deficiency of peritoneal macrophages was analyzed by Western blotting using a PTEN-specific Ab. Cell lysates derived from two mice per genotype are shown. *C*, Constitutive PI3K/PTEN-dependent signaling was determined in resting macrophages derived from two mice per genotype using phospho-Akt and phospho-GSK3β Abs. Total Akt was used as loading control. *D*, Time course analysis of PI3K/PTEN-dependent signaling in *S. pneumoniae*-stimulated macrophages. Phosphorylation of Akt and GSK3β was determined by Western blotting. Total Akt was used as loading control.

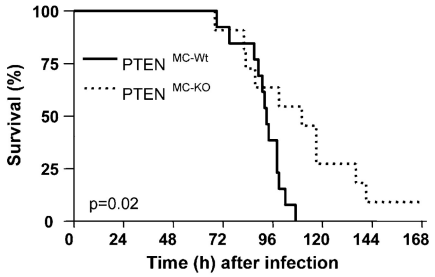

FIGURE 2. Improved survival of pneumococci infected PTEN$^{MC\text{-}KO}$ mice. PTEN$^{MC\text{-}KO}$ and PTEN$^{MC\text{-}Wt}$ littermate controls were infected intranasally with *S. pneumoniae* (4×10^5 CFU) and monitored over 7 d (n = 11–13 per group). Statistical analysis was performed by log-rank test; the p value is depicted in the graph.

placed at 37°C for 10, 30, 60, or 90 min, after which cells were again washed five times with ice-cold PBS and lysed as described above. Cell lysates were plated in serial-fold dilutions on blood agar plates, and bacterial counts were enumerated after 16 h. Bacterial killing was expressed as the percentage of killed bacteria in relation to $t = 0$ (percent killing = 100 − [(number of CFUs at time x/number of CFUs at time 0) × 100]).

Pneumonia experiments

Pneumococcal pneumonia was induced as described previously (26–28). Briefly, *S. pneumoniae* serotype 3 was obtained from American Type Culture Collection (ATCC 6303, Rockville, MD) and grown to log-phase. Mice were short-term anesthetized with isoflurane (Forene, Abbott Laboratories, Abbott Part, IL) and 50 μl bacterial suspension (~5×10^4 CFUs) was inoculated intranasally. For survival analysis, infected mice were observed every 3 h. At indicated time points, mice were sacrificed; BAL was performed, and blood and lungs were collected and processed as described (27, 29). CFUs were determined from serial dilutions of lung homogenates, blood, and BAL fluid (BALF), plated on blood agar plates, and incubated at 37°C for 16 h before colonies were counted. Cytokines and chemokines were quantified in lung homogenates and BALF. TNF-α, IL-6, keratinocyte-derived chemokine (KC), MCP-1, and MIP-2 were measured using ELISAs (R&D Systems, Minneapolis, MN), as was myeloperoxidase (MPO) (HyCult Biotechnology, Uden, The Netherlands) and IL-10 (Bender Medsystems, Vienna, Austria). Detection limits were: 15 ng/ml for TNF-α; 16 pg/ml for IL-6; 12 pg/ml for KC; 4 pg/ml for MCP-1; 94 pg/ml for MIP-2; and 15 pg/ml for IL-10. Differential cell counts were determined using counting chambers and cytospin preparations stained with Giemsa.

Histology

Lungs were fixed in formalin and embedded in paraffin; 4-μm sections were stained in H&E and analyzed by a blinded pathologist. The lung was scored with respect to the following parameters: interstitial inflammation, edema, endothelitis, bronchitis, pleuritis, and thrombi formation. Each parameter was graded on a scale of 0–3 (0: absent; 1: mild; 2: moderate; and 3: severe). The total lung inflammation score was expressed as the sum of the scores for each parameter, the maximum being 18. Granulocyte immunostaining was performed on paraffin-embedded lungs as described (27). After Ag retrieval using pepsin, tissue sections were incubated with FITC rat anti-mouse Ly-6G (BD Biosciences, San Jose, CA) or corresponding isotype control IgG (Emfret Analytics, Würzburg, Germany), followed by rabbit anti-FITC Ab (Zymed, Invitrogen) in normal mouse serum. Finally, slides were incubated with polyclonal anti-rabbit-HRP Ab (Immunologic, Duiven, The Netherlands) and visualized using 3,3-diaminobenzidine-tetrahydrochloride (Vector Laboratories, Burlingame, CA). Counterstaining was done with hemalaun solution.

Statistical analysis

Data were analyzed with GraphPad Prism 4 software (GraphPad, San Diego, CA) using unpaired Student t test or one-way ANOVA followed by post hoc tests when appropriate. Bacterial killing data were calculated by two-way ANOVA. Survival data were analyzed by Kaplan-Meier followed by log-rank test. Criteria for significance for all experiments were $p < 0.05$.

Results

PTEN depletion is associated with enhanced PI3K activity in macrophages

To investigate the role of myeloid cell-derived PTEN during the inflammatory response to bacterial infections, we generated conditional *pten* knockout mice in which PTEN expression was controlled by *LysM*, a myeloid cell-specific promoter (20). Depending on the presence of LysM Cre recombinase, double-floxed (*pten*$^{flox/flox}$) mice are referred to as PTEN$^{MC\text{-}KO}$ or PTEN$^{MC\text{-}Wt}$ mice, respectively (Fig. 1*A*). Deletion of PTEN was confirmed in primary macrophages (Fig. 1*B*), and resulting downstream effects of constitutively active PI3K were reflected by greatly elevated baseline levels of phospho-Akt and phospho-GSK3β in PTEN$^{MC\text{-}KO}$ macrophages (Fig. 1*C*). These findings also indicate that alternative

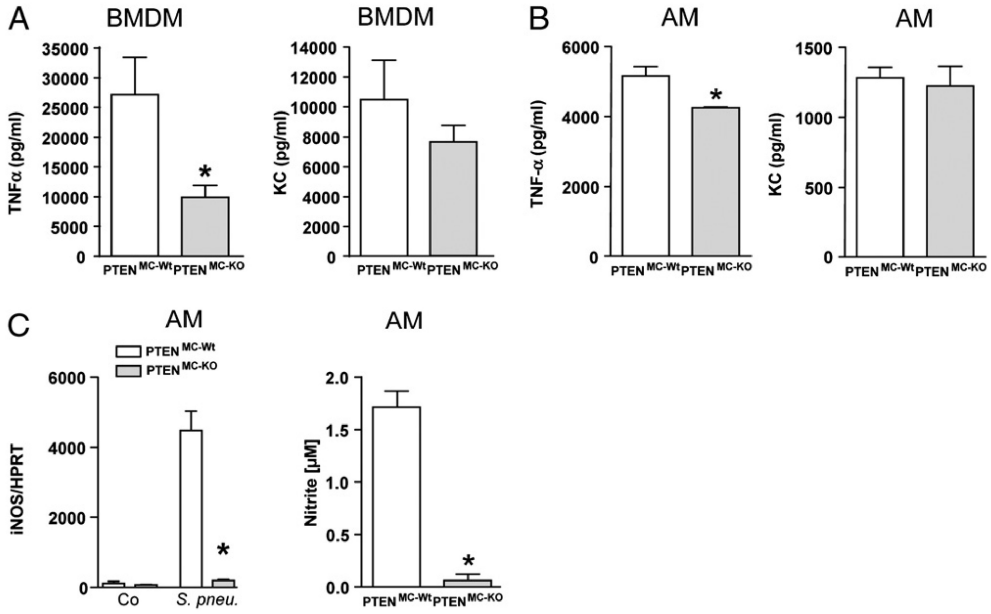

FIGURE 3. Role of PTEN in inflammation in vitro. BMDMs (*A*) and AMs (*B*, *C*) were stimulated with *S. pneumoniae* (10^7 CFU/ml) for 6 h, and TNF-α and KC release was measured in supernatants (*A*, *B*). *C*, iNOS expression was assessed by RT-PCR, and NO release was quantified in supernatants (t = 16 h). Data are representative of two independent experiments and show mean ± SEM of n = 3/genotype for BMDM and n = 4/genotype for AM. *$p < 0.05$ versus PTEN$^{MC\text{-}Wt}$.

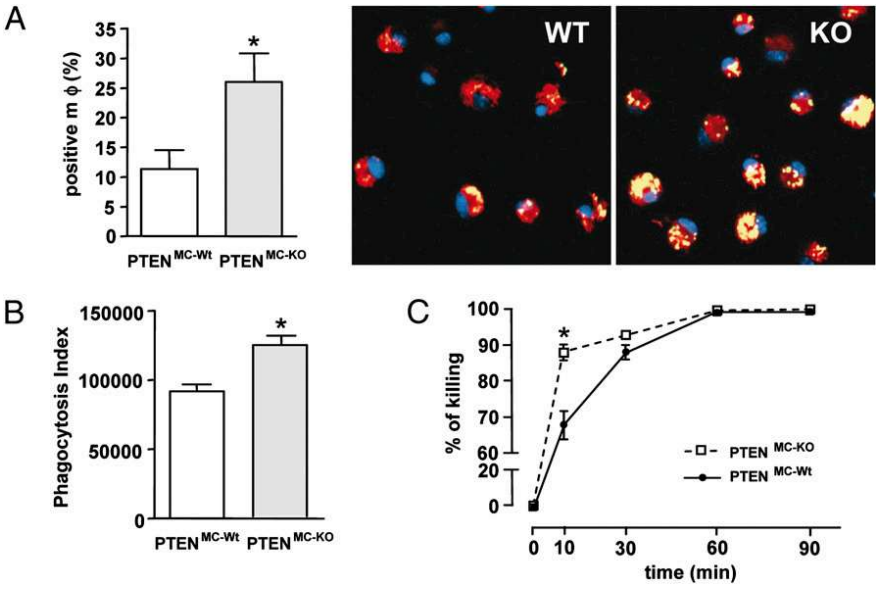

FIGURE 4. Role of PTEN in bacterial uptake and killing by AMs. AMs from PTEN$^{MC\text{-}KO}$ and PTEN$^{MC\text{-}Wt}$ littermate control mice were incubated with FITC-labeled *S. pneumoniae* for 30 min, and uptake of bacteria was quantified by microscopy (*A*) or FACS (*B*) as described in the *Materials and Methods*. *A*, The percentage of macrophages that contained bacteria and representative confocal microscopy images of AM (n = 3 per genotype) are depicted: PTEN$^{MC\text{-}Wt}$ (*left panel*) and PTEN$^{MC\text{-}KO}$ (*right panel*). Original magnification ×100. Nuclei are stained with DAPI (blue); ingested bacteria (green) are defined by colocalization with lysosomes (red) and appear yellow. *B*, Phagocytosis of bacteria was analyzed by FACS. *C*, Time-dependent bacterial killing by AM was analyzed as described in the *Materials and Methods* section. Data are presented as mean ± SEM. $*p < 0.05$ versus PTEN$^{MC\text{-}Wt}$.

lipid phosphatases, such as SHIP1 and SHIP2, which are known to influence phosphatidylinositol (3,4,5)-triphosphate plasma membrane content (30), do not sufficiently limit PI3K activity in macrophages or compensate for the loss of PTEN.

To characterize PTEN-associated properties of macrophages during bacterial infection, we next examined kinase phosphorylation downstream of PI3K in PTEN$^{MC\text{-}Wt}$ and PTEN$^{MC\text{-}KO}$ macrophages upon stimulation with *S. pneumoniae*. Bacterial challenge led to Akt and GSK3β phosphorylation in PTEN$^{MC\text{-}Wt}$ cells with highest levels 60 min postactivation (Fig. 1*D*). Although Akt phosphorylation only modestly increased over baseline levels upon *S. pneumoniae* stimulation in PTEN-deficient macrophages, GSK3β phosphorylation was found markedly enhanced in these cells (Fig. 1*D*). These data illustrate that the innate immune response to *S. pneumoniae* involves downstream PI3K pathway activation.

Improved survival of PTEN$^{MC\text{-}KO}$ mice infected with S. pneumoniae

To test whether PTEN deficiency in myeloid cells might impact the outcome of pneumococcal pneumonia in vivo, we infected PTEN$^{MC\text{-}KO}$ and PTEN$^{MC\text{-}Wt}$ mice with 5×10^4 CFU *S. pneumoniae* and monitored survival over 7 d. Already 2 d postinfection, we found PTEN$^{MC\text{-}KO}$ mice to show less severe signs of disease, which was quantified using a clinical severity score (data not shown). PTEN$^{MC\text{-}Wt}$ animals rapidly displayed signs of serious infection, and all mice succumbed within 107 h postinduction of pneumonia,

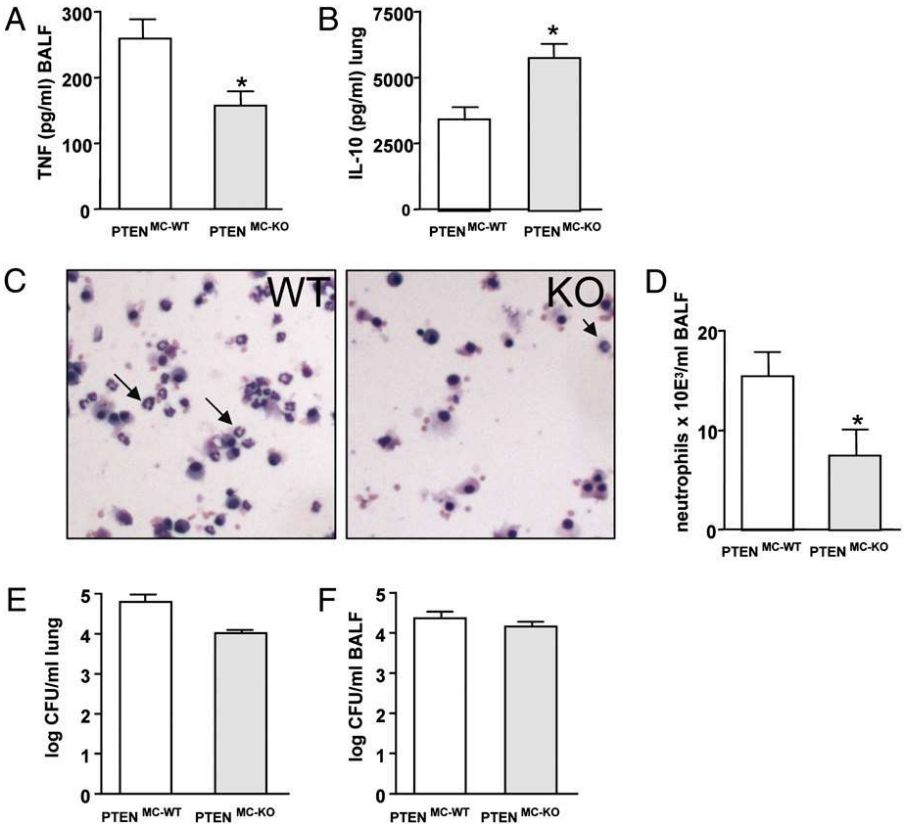

FIGURE 5. Role of PTEN early post-induction of pneumonia (6 h). PTEN$^{MC\text{-}KO}$ and PTEN$^{MC\text{-}Wt}$ mice were infected intranasally with *S. pneumoniae* (4×10^5 CFU); BALF and lungs were harvested 6 h postinfection. TNF-α levels in BALF (*A*) and lung IL-10 concentrations (*B*) were determined by ELISA. Representative BALF cytospins stained with Giemsa are depicted in *C* (neutrophils are indicated by arrows; original magnification ×20). Enumeration of neutrophils in BALF (*D*). Bacterial CFU counts were determined in lung homogenates (*E*) and BALF (*F*). Data are presented as mean ± SEM of n = 6–7 mice/group. $*p < 0.05$.

Table I. *BALF cytokine and chemokine levels (pg/ml) in PTEN$^{MC\text{-}KO}$ and PTEN$^{MC\text{-}Wt}$ mice 48 h post* S. pneumoniae *infection*

BALF	PTEN$^{MC\text{-}Wt}$	PTEN$^{MC\text{-}KO}$
TNF-α	1566 ± 586	206 ± 60*
IL-6	379 ± 191	104 ± 15
KC	162 ± 41	85 ± 18*
MCP-1	929 ± 393	229 ± 128*

Data are presented as mean ± SEM of n = 9–10 mice/group.
*$p < 0.05$.

at a time when >50% of PTEN$^{MC\text{-}KO}$ animals were still alive (Fig. 2). Together, myeloid-cell specific PTEN deficiency was associated with less severe signs of disease and significantly improved survival during pneumococcal pneumonia in vivo.

PTEN enhanced the inflammatory response and attenuated bactericidal properties in vitro

In our effort to elucidate the detrimental role of PTEN during pneumococcal pneumonia, we investigated PTEN's contribution to basic functional properties of myeloid cells, such as cytokine secretion or bacterial phagocytosis and killing. Upon stimulation of bone marrow-derived macrophages (BMDMs) and primary AMs from PTEN$^{MC\text{-}KO}$ and PTEN$^{MC\text{-}Wt}$ mice with *S. pneumoniae*, we observed a significantly reduced TNF-α release by PTEN$^{MC\text{-}KO}$ macrophages compared with PTEN$^{MC\text{-}Wt}$ cells, whereas KC levels did not differ significantly (Fig. 3*A*, 3*B*). To study effector molecules importantly associated with bactericidal mechanisms, we next investigated the pathogen-induced expression of iNOS in AMs and BMDMs. Surprisingly, we hereby discovered that PTEN$^{MC\text{-}KO}$ BMDMs stimulated with *S. pneumoniae* expressed significantly higher iNOS levels 8 h postinduction (data not shown), whereas iNOS expression was diminished in PTEN-deficient AMs (Fig. 3*C*). We furthermore confirmed that decreased iNOS expression correlated with suppressed NO production by quantifying nitrite in supernatants of AMs (Fig. 3*C*).

We then isolated primary AMs from PTEN$^{MC\text{-}Wt}$ and PTEN$^{MC\text{-}KO}$ mice and explored their ability to phagocytose *S. pneumoniae* using confocal microscopy as well as an FACS-based phagocytosis assay. By quantifying the proportion of macrophages that contained intracellular bacteria, we discovered a significantly increased uptake of *S. pneumoniae* by PTEN$^{MC\text{-}KO}$ cells ($p < 0.05$ versus wild-type cells) (Fig. 4*A*, 4*B*). Furthermore, performing a killing assay enabled us to demonstrate enhanced bacterial killing by AMs from PTEN$^{MC\text{-}KO}$ mice (Fig. 4*C*).

Hence, these data illustrate that PTEN activity strongly impacted functional properties attributed to macrophages. Although constitutively active PI3K signaling counteracted the proinflammatory TNF-α and iNOS response, it augmented the phagocytic and bactericidal properties of primary AMs upon challenge with *S. pneumoniae* in vitro.

Anti-inflammatory phenotype and reduced neutrophil influx early during pneumococcal pneumonia in PTEN$^{MC\text{-}KO}$ mice

To discern the in vivo impact of myeloid-cell associated PTEN on inflammation during bacterial infection, we then asked how above described findings would translate into the immediate host response during bacterial pneumonia in vivo. For this purpose, we infected PTEN$^{MC\text{-}KO}$ and PTEN$^{MC\text{-}Wt}$ mice with *S. pneumoniae* and studied the early inflammatory response after 6 h. In line with in vitro data depicted in Fig. 3, PTEN$^{MC\text{-}KO}$ animals exhibited a diminished proinflammatory cytokine response, illustrated by significantly lower TNF-α concentrations in BALF of these mice ($p < 0.01$ versus PTEN$^{MC\text{-}Wt}$ mice) (Fig. 5*A*). At the same time, the anti-inflammatory cytokine IL-10 was found significantly increased in lungs of PTEN$^{MC\text{-}KO}$ mice as compared with wild-type animals (Fig. 5*B*), indicating that the constitutive activation of myeloid cell-derived PI3K pathways dampened the inflammatory response in vivo.

Host defense against respiratory tract infections critically depends on the effective influx of neutrophils. Because PI3K activation has been repeatedly shown to promote neutrophil chemotaxis (10), and in light of a recent publication that highlighted the role of myeloid PTEN as a suppressor of neutrophil migration (31), we expected PTEN$^{MC\text{-}KO}$ mice to exhibit an enhanced recruitment of neutrophils to the alveolar compartment. When enumerating the number of cells attracted to the alveolar compartment 6 h postinduction of pneumococcal pneumonia, we surprisingly found a significantly impaired influx of neutrophils in the absence of PTEN (Fig. 5*C*, 5*D*). Despite this reduced neutrophil attraction and diminished TNF-α response, bacterial outgrowth in lungs and BALF of PTEN$^{MC\text{-}KO}$ mice was not affected at this early time point (Fig. 5*E*, 5*F*). Together, PTEN deficiency dampened the early inflammatory response during bacterial pneumonia.

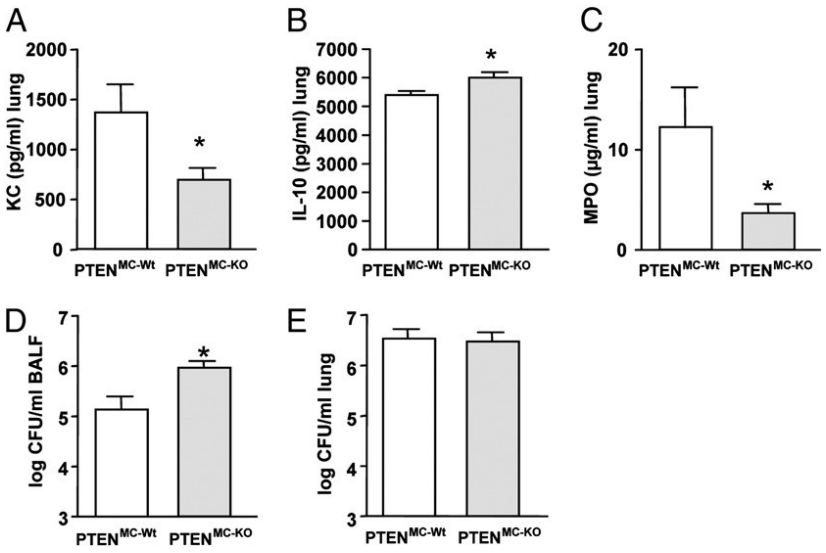

FIGURE 6. Role of PTEN 48 h postinduction of pneumococcal pneumonia. PTEN$^{MC\text{-}KO}$ and littermate PTEN$^{MC\text{-}Wt}$ mice were infected intranasally with 4 × 10^5 CFU *S. pneumoniae* and sacrificed after 48 h (n = 7–9/group). KC (*A*), IL-10 (*B*), and MPO (*C*) concentrations were determined in lung homogenates by ELISA. Bacterial CFUs were enumerated by plating serial dilutions of BALF (*D*) and lung homogenates (*E*). Data are presented as mean ± SEM. *$p < 0.05$.

Table II. *BALF cellular composition in PTEN$^{MC\text{-}KO}$ and PTEN$^{MC\text{-}Wt}$ mice 48 h post* S. pneumoniae *infection*

BALF	PTEN$^{MC\text{-}Wt}$	PTEN$^{MC\text{-}KO}$
Total cells × 10^4/ml	11.0 ± 4.6	12.8 ± 7.7
Neutrophils (%)	61.3 ± 5.9	47.7 ± 10.5*
Monocytes/macrophages (%)	38.2 ± 5.8	52.8 ± 10.6*

Data are presented as mean ± SEM of n = 9–10 mice/group.
*$p < 0.05$.

PTEN$^{MC\text{-}KO}$ mice exhibit a diminished inflammatory response and modestly enhanced bacterial burden 48 h postinduction of pneumonia

Having established PTEN's proinflammatory contribution to the induction-phase of *S. pneumoniae* infection in vivo, we then explored PTEN's impact over the course of pneumococcal pneumonia and investigated mice 48 h postinfection. At this later time point, we continued to observe reduced levels of proinflammatory mediators in BALF and lungs of mice lacking PTEN. As depicted in Table I, BALF concentrations of TNF-α, KC, and MCP-1 were significantly decreased, whereas IL-6 showed a modest but nonsignificant reduction in PTEN$^{MC\text{-}KO}$ versus PTEN$^{MC\text{-}Wt}$ mice. In contrast to the alveolar compartment, TNF-α and IL-6 levels did not differ in lung homogenates (data not shown), whereas KC concentrations were considerably decreased, and IL-10 levels significantly increased in lungs from PTEN$^{MC\text{-}KO}$ mice as compared with PTEN$^{MC\text{-}Wt}$ animals (Fig. 6*A*, 6*B*). In line with this diminished chemokine release, PTEN$^{MC\text{-}KO}$ animals displayed an impaired ability to attract neutrophils to the site of infection, as illustrated by a significantly decreased proportion of neutrophils in BALF (Table II) as well as reduced MPO levels in lungs from PTEN$^{MC\text{-}KO}$ mice (Fig. 6*C*) 48 h postinfection. The reduction in proinflammatory mediators and neutrophil influx was accompanied by modestly increased bacterial counts in the alveolar compartment of PTEN$^{MC\text{-}KO}$ mice 48 h postinfection with *S. pneumoniae* (Fig. 6*D*), whereas CFU counts in lung homogenates did not differ between the mouse strains (Fig. 6*E*).

Because PI3K activation has been repeatedly shown to promote migration of neutrophils (7, 8, 21, 32), the continual observation of impaired pulmonary neutrophil recruitment in PTEN$^{MC\text{-}KO}$ mice was unanticipated (Figs. 5*C*, 5*D*, 6*C*). Based on a recent report that illustrated PTEN's suppressive function on neutrophil migration during *Escherichia coli* peritonitis and sterile peritoneal inflammation (31), we wondered whether these contradicting results were due to pathogen- or organ-specific differences that have never been investigated before. To answer this question, we injected *S. pneumoniae* i.p. in PTEN$^{MC\text{-}KO}$ mice and PTEN$^{MC\text{-}Wt}$ littermate controls and enumerated peritoneal neutrophil counts after 6 h. In contrast to the diminished alveolar neutrophil influx during pneumonia, we found an enhanced peritoneal recruitment of neutrophils in animals lacking myeloid cell-associated PTEN (Fig. 7*A*). These findings indicate that organ-specific differences could explain our observation of diminished neutrophil migration in PTEN$^{MC\text{-}KO}$ mice suffering from pneumococcal pneumonia in vivo and argue against a fundamental cellular defect of PTEN-deficient neutrophils. To understand organ-specific differences in more detail, we additionally studied the inflammatory cytokine and chemokine response of primary peritoneal macrophages upon *S. pneumoniae* stimulation in vitro. Comparable to our observations from BMDMs and AMs (Fig. 3), we discovered reduced TNF-α secretion by peritoneal PTEN$^{MC\text{-}KO}$ macrophages (Fig. 7*B*). However, in strong contrast to BMDMs or AMs, peritoneal macrophages that lacked PTEN released significantly more KC than PTEN$^{MC\text{-}Wt}$ cells (Fig. 7*C*). This enhanced chemokine release by PTEN$^{MC\text{-}KO}$ peritoneal macrophages provides a potential explanation for the augmented PMN influx into the peritoneal cavity of PTEN$^{MC\text{-}KO}$ animals.

Constitutively active PI3K does not impact clearance of S. pneumoniae *65 h postinfection*

In an attempt to identify the contributing factors that ultimately led to improved outcome of PTEN$^{MC\text{-}KO}$ mice suffering from pneumococcal pneumonia, we repeated the pneumonia study and sacrificed mice after 65 h (i.e., right before animals started to succumb to infection). We hereby observed significantly decreased IL-6 levels and modestly reduced TNF-α and KC concentrations in BALF of PTEN$^{MC\text{-}KO}$ (Table III). In line with above-described findings at 6 h and 48 h postinfection, we continued to detect significantly higher IL-10 levels in lung homogenates of mice lacking myeloid PTEN (Fig. 8*A*). When analyzing the cellular composition in BALF, we found a predominance of monocytes/macrophages in PTEN$^{MC\text{-}KO}$ mice, whereas neutrophil numbers exceeded monocytes/macrophages in PTEN$^{MC\text{-}Wt}$ littermates (Fig. 8*B*, 8*C*). In accordance, histological evaluation of lung slides disclosed significantly more pronounced signs of inflammation in PTEN$^{MC\text{-}Wt}$ mice than PTEN$^{MC\text{-}KO}$ animals (Fig. 8*F*, 8*G*). However, when enumerating bacterial counts in BALF and lungs, we did not discover any differences between wild-type and PTEN-deficient mice 65 h postinfection (Fig. 8*D*, 8*E*). Furthermore, blood cultures did not reveal any differences between groups (data not shown).

Hence, these data indicate that the continuous activation of PI3K, as seen in PTEN$^{MC\text{-}KO}$ mice, beneficially modulated the inflammatory response to *S. pneumoniae*, thus allowing for accelerated resolution of pneumonia without impairing bacterial clearance in vivo.

Discussion

The role of PI3K pathways in the inflammatory response is a controversial matter, as published reports suggested either proinflammatory or anti-inflammatory properties (15, 33, 34). We and

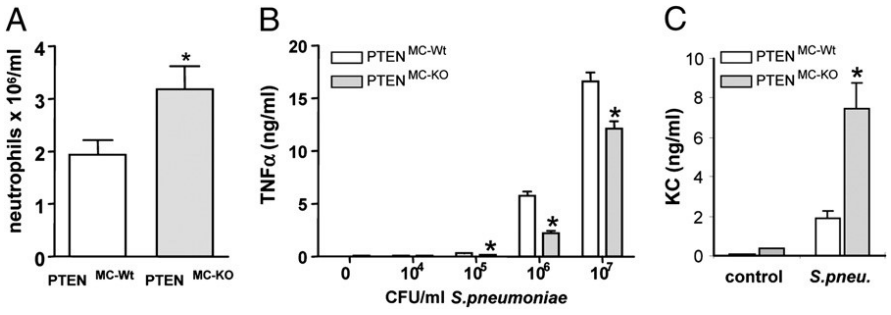

FIGURE 7. Immunomodulatory properties of PTEN during peritoneal inflammation. PTEN$^{MC\text{-}KO}$ and PTEN$^{MC\text{-}Wt}$ littermates were infected i.p. with *S. pneumoniae* (4×10^5 CFU). Peritoneal lavage was performed after 6 h and neutrophils (*A*) were enumerated (n = 6–7 mice/group). Dose-dependent (10^3/ml to 10^7/ml; heat-killed *S. pneumoniae*) TNF-α release (*B*) and KC secretion (*C*) in response to 10^7/ml *S. pneumoniae* was determined in supernatants of PTEN$^{MC\text{-}KO}$ and PTEN$^{MC\text{-}Wt}$ macrophages after 12 h (n = 9 per genotype). Data are presented as mean ± SEM. *$p < 0.05$.

Table III. *BALF cytokine and chemokine levels (pg/ml) in PTEN$^{MC\text{-}KO}$ and PTEN$^{MC\text{-}Wt}$ mice 65 h post* S. pneumoniae *infection*

BALF	PTEN$^{MC\text{-}Wt}$	PTEN$^{MC\text{-}KO}$
TNF-α	201 ± 63	107 ± 35
IL-6	547 ± 115	199 ± 59*
KC	259 ± 114	119 ± 49

Data are presented as mean ± SEM of n = 7–8 mice/group.
*$p < 0.05$.

others demonstrated earlier that PI3K activation exerts protective immunomodulatory effects in murine models of endotoxemia, sepsis, and viral infection (16, 35–37). These findings have been partly attributed to PI3K's ability to modulate the transcriptional activity of NF-κB and to efficiently limit proinflammatory signaling cascades induced via MAPK pathways (11, 34). Given that PTEN is a key regulator of PI3K activity, we hypothesized that PTEN might act as a critical modulator of the inflammatory response during bacterial infection. To investigate this idea in a clinically relevant model, we studied the role of PTEN during *S. pneumoniae* pneumonia in vivo and discovered that myeloid cell-specific PTEN deficiency exerted beneficial effects. PTEN deficiency was associated with diminished TNF-α and increased IL-10 responses, enhanced macrophage phagocytosis, reduced neutrophil migration to lungs, and, ultimately, improved survival.

Modulation of PI3K activity by cell type-specific *pten* gene ablation disclosed a markedly reduced TNF-α response by various primary macrophage subsets that were stimulated with *S. pneumoniae*. These findings correlated with earlier observations by us and other investigators who showed that LPS-challenged PTEN-deficient macrophages displayed a profoundly reduced TNF-α release and diminished activation of MAPKs (15, 38). We concurrently discovered the enhanced phosphorylation of GSK3β in PTEN-deficient macrophages. GSK3β is a constitutively active serine/threonine kinase and downstream target of PI3K that can be inactivated through phosphorylation by Akt (39). The biological significance of GSK3β during inflammation was discovered by Martin et al. (16), who revealed that GSK3β inhibition led to a diminished inflammatory response toward various TLR agonists, which was illustrated by reduced TNF-α and enhanced IL-10 releases. In striking agreement with this report, we hereby observed decreased levels of proinflammatory cytokines, such as TNF-α and elevated concentrations of the anti-inflammatory cytokine IL-10 in lungs of *S. pneumoniae*-infected PTEN$^{MC\text{-}KO}$ animals. Therefore, enhanced phosphorylation and consecutive inactivation of GSK3β activity in macrophages of PTEN$^{MC\text{-}KO}$ animals might explain our in vivo findings of a dampened inflammatory response in these mice.

The most unanticipated finding of our studies was the diminished pulmonary neutrophil influx in PTEN$^{MC\text{-}KO}$ mice suffering from pneumococcal pneumonia. Importantly, this observation was not related to constitutively reduced neutrophil numbers in

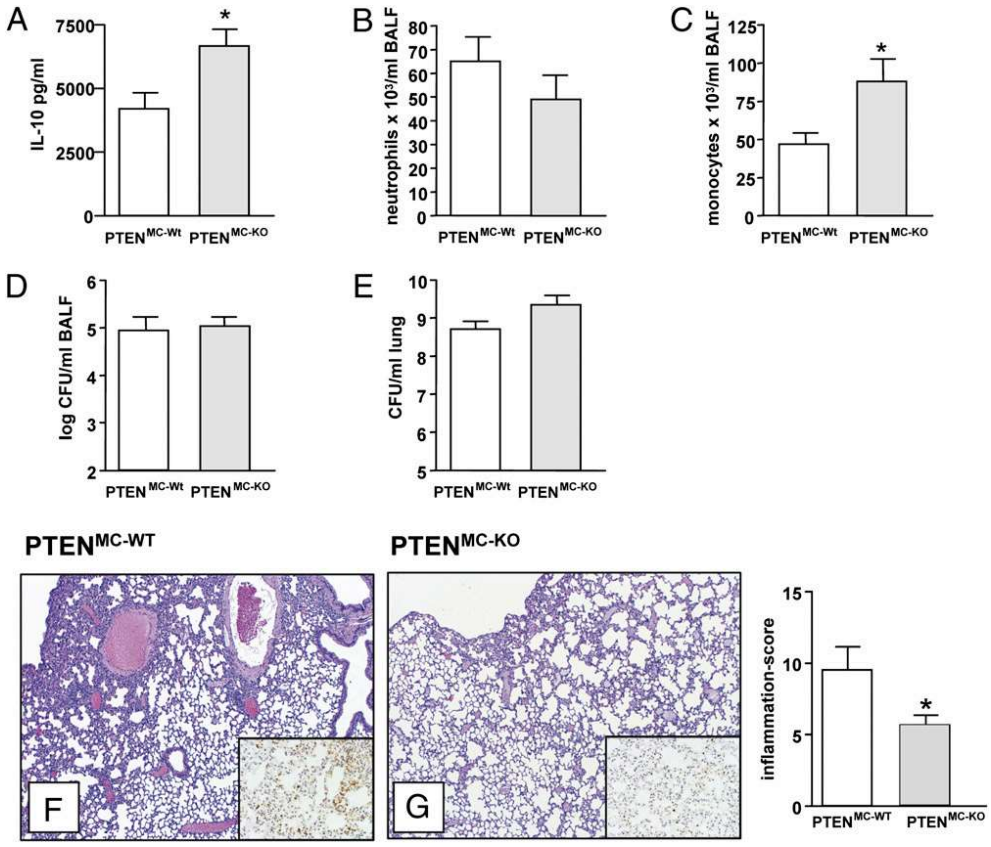

FIGURE 8. Unaltered bacterial counts despite reduced inflammation in PTEN$^{MC\text{-}KO}$ mice 65 h postinfection. PTEN$^{MC\text{-}KO}$ and PTEN$^{MC\text{-}Wt}$ littermates were infected with 4×10^5 CFU *S. pneumoniae* and sacrificed after 65 h. *A*, Whole lung IL-10 concentrations were determined by ELISA. Neutrophil (*B*) and monocyte/macrophage (*C*) influx into the bronchoalveolar compartment was determined on cytospins. Bacterial CFUs in BALF (*D*) and lungs (*E*) were quantified by plating serial dilutions on blood agar plates. *F* and *G*, Representative lung histology images of PTEN$^{MC\text{-}Wt}$ and PTEN$^{MC\text{-}KO}$ mice 65 h postinfection. Lung sections stained with H&E were scored (as described in the *Materials and Methods* section) by a trained pathologist blinded for groups and are expressed as inflammation score. The insets are representative pictures of immunostaining for neutrophils, confirming reduced influx in PTEN$^{MC\text{-}KO}$ mice. *F* and *G*, H&E, original magnification ×4; inset, Ly6-staining, original magnification ×20. Data are presented as mean ± SEM of n = 7–8 mice/group. *$p < 0.05$.

this specific mouse strain, because we previously showed that blood neutrophil numbers were even higher in healthy PTEN$^{MC\text{-}KO}$ animals as compared with wild-type mice (15). In support of the general notion of PI3K being a key player in cell migration (6–8, 10, 19), the migratory capacity of PTEN-deficient neutrophils was found enhanced in earlier reports (31). Furthermore, increased neutrophil recruitment was observed in PTEN$^{MC\text{-}KO}$ animals using models of thioglycollate or *E. coli*-induced peritonitis in vivo (31). Although we were able to confirm these data, as we also observed enhanced peritoneal neutrophil influx following thioglycollate administration in PTEN$^{MC\text{-}KO}$ mice (data not shown), we consistently observed reduced alveolar neutrophil migration during pneumococcal pneumonia in PTEN$^{MC\text{-}KO}$ animals. To exclude the possibility of pathogen-specific differences, we challenged mice i.p. with *S. pneumoniae* and observed enhanced peritoneal neutrophil recruitment in PTEN$^{MC\text{-}KO}$ mice (Fig. 7*A*). Because neutrophil attraction to sites of infection critically depends on the effective release of chemokines, such as KC (40, 41), we investigated if organ-specific differences in neutrophil migration in PTEN$^{MC\text{-}KO}$ animals were a consequence of altered chemokine release by resident macrophages. Indeed, when measuring KC concentrations in supernatants of alveolar and peritoneal macrophages that were stimulated with *S. pneumoniae* in vitro, we discovered an enhanced KC release by peritoneal but not alveolar PTEN$^{MC\text{-}KO}$ macrophages. Beside macrophages, respiratory epithelial cells are a major source of KC within the lungs in vivo, and release of this chemokine is largely triggered by macrophage-derived proinflammatory cytokines, such as TNF-α (42). The fact that we identified reduced KC levels in lung-homogenates from infected PTEN$^{MC\text{-}KO}$ mice in vivo (Table I) might therefore result from the attenuated macrophage-associated (e.g., TNF-α–mediated) activation of airway epithelial cells in vivo, ultimately resulting in reduced neutrophil recruitment. In contrast to our observations, Li et al. (43) disclosed increased pulmonary KC concentrations and enhanced neutrophil migration in PTEN-deficient mice suffering from *E. coli* pneumonia. It therefore seems that PTEN differentially regulates the attraction of neutrophils depending on either the affected organ and/or the inducing agent.

Unlike neutrophils, cells of monocytic origin (infiltrating monocytes/macrophages) were recruited in increased numbers to lungs of healthy and *S. pneumoniae*-infected PTEN$^{MC\text{-}KO}$ mice (data not shown) (Table I). This result is in agreement with a report by Maus et al. (17), who showed that monocyte/macrophage recruitment in pneumoccocal pneumonia critically depended on proper p110γ signal transduction. We recently demonstrated that AMs crucially contribute to host defense during murine pneumococcal pneumonia, as they exert an important role in the resolution of pneumococcal pneumonia by virtue of their capacity to eliminate apoptotic neutrophils (29). This idea is strengthened by data obtained in p110γ-deficient mice in which the recruitment of monocytes/macrophages was found to be impaired (17 and data not shown). PI3Kγ-KO mice showed substantial lung infiltrates and tissue injury during pneumococcal pneumonia (data not shown), whereas PTEN$^{MC\text{-}KO}$ mice that embraced significantly increased numbers of (alveolar) macrophages showed less severe signs of tissue damage (Fig. 8). We in addition discovered an increased phagocytic and killing potential of AMs in the absence of PTEN. The enhanced phagocytic properties of PTEN-deficient macrophages might have compensated for the reduced number of infiltrating neutrophils. However, the precise role of neutrophils during pneumococcal pneumonia has been challenged recently by a report showing unaltered bacterial clearance and improved survival in neutrophil-depleted animals that were infected with *S. pneumoniae* (44). It seems that enhanced neutrophil numbers prolong inflammation and ultimately fuel tissue damage, thus resulting in worsened outcome. It is therefore tempting to hypothesize that lower neutrophil counts and simultaneously increased numbers of macrophages in PTEN$^{MC\text{-}KO}$ animals improved bacterial clearance and augmented the resolution of inflammation, thus contributing to diminished tissue damage and favorable outcome in these animals.

In conclusion, our findings demonstrate that enhanced PI3K activity in PTEN-deficient mice resulted in an improved outcome during pneumococcal pneumonia. These findings implicate a crucial role for PTEN in the homeostasis of pro- and anti-inflammatory mechanisms evoked during a relevant bacterial infection. Thus, interfering with PI3K signaling might have tremendous implications on the course of pneumococcal pneumonia: although blockade of PTEN might be beneficial, reduced PI3K activity might prove detrimental.

Acknowledgments

We thank L. Erhart and R. Raim for excellent technical assistance.

Disclosures

The authors have no financial conflicts of interest.

References

1. National Immunization Program. 2007. *Epidemiology and Prevention of Vaccine-Preventable Diseases.* Centers for Disease Control and Prevention and U.S. Department of Health and Human Services, Atlanta, GA.
2. Ortqvist, A., J. Hedlund, and M. Kalin. 2005. *Streptococcus pneumoniae*: epidemiology, risk factors, and clinical features. *Semin. Respir. Crit. Care Med.* 26: 563–574.
3. Appelbaum, P. C. 2002. Resistance among *Streptococcus pneumoniae*: Implications for drug selection. *Clin. Infect. Dis.* 34: 1613–1620.
4. Tamguney, T., and D. Stokoe. 2007. New insights into PTEN. *J. Cell Sci.* 120: 4071–4079.
5. Cantley, L. C. 2002. The phosphoinositide 3-kinase pathway. *Science* 296: 1655–1657.
6. Curnock, A. P., M. K. Logan, and S. G. Ward. 2002. Chemokine signalling: pivoting around multiple phosphoinositide 3-kinases. *Immunology* 105: 125–136.
7. Hirsch, E., V. L. Katanaev, C. Garlanda, O. Azzolino, L. Pirola, L. Silengo, S. Sozzani, A. Mantovani, F. Altruda, and M. P. Wymann. 2000. Central role for G protein-coupled phosphoinositide 3-kinase gamma in inflammation. *Science* 287: 1049–1053.
8. Li, Z., H. Jiang, W. Xie, Z. Zhang, A. V. Smrcka, and D. Wu. 2000. Roles of PLC-beta2 and -beta3 and PI3Kgamma in chemoattractant-mediated signal transduction. *Science* 287: 1046–1049.
9. Sasaki, T., J. Irie-Sasaki, R. G. Jones, A. J. Oliveira-dos-Santos, W. L. Stanford, B. Bolon, A. Wakeham, A. Itie, D. Bouchard, I. Kozieradzki, et al. 2000. Function of PI3Kgamma in thymocyte development, T cell activation, and neutrophil migration. *Science* 287: 1040–1046.
10. Stephens, L., C. Ellson, and P. Hawkins. 2002. Roles of PI3Ks in leukocyte chemotaxis and phagocytosis. *Curr. Opin. Cell Biol.* 14: 203–213.
11. Fukao, T., and S. Koyasu. 2003. PI3K and negative regulation of TLR signaling. *Trends Immunol.* 24: 358–363.
12. Ruse, M., and U. G. Knaus. 2006. New players in TLR-mediated innate immunity: PI3K and small Rho GTPases. *Immunol. Res.* 34: 33–48.
13. Guha, M., and N. Mackman. 2002. The phosphatidylinositol 3-kinase-Akt pathway limits lipopolysaccharide activation of signaling pathways and expression of inflammatory mediators in human monocytic cells. *J. Biol. Chem.* 277: 32124–32132.
14. Günzl, P., and G. Schabbauer. 2008. Recent advances in the genetic analysis of PTEN and PI3K innate immune properties. *Immunobiology* 213: 759–765.
15. Luyendyk, J. P., G. A. Schabbauer, M. Tencati, T. Holscher, R. Pawlinski, and N. Mackman. 2008. Genetic analysis of the role of the PI3K-Akt pathway in lipopolysaccharide-induced cytokine and tissue factor gene expression in monocytes/macrophages. *J. Immunol.* 180: 4218–4226.
16. Martin, M., K. Rehani, R. S. Jope, and S. M. Michalek. 2005. Toll-like receptor-mediated cytokine production is differentially regulated by glycogen synthase kinase 3. *Nat. Immunol.* 6: 777–784.
17. Maus, U. A., M. Backi, C. Winter, M. Srivastava, M. K. Schwarz, T. Rückle, J. C. Paton, D. Briles, M. Mack, T. Welte, et al. 2007. Importance of phosphoinositide 3-kinase gamma in the host defense against pneumococcal infection. *Am. J. Respir. Crit. Care Med.* 175: 958–966.
18. Marone, R., V. Cmiljanovic, B. Giese, and M. P. Wymann. 2008. Targeting phosphoinositide 3-kinase: moving towards therapy. *Biochim. Biophys. Acta* 1784: 159–185.
19. Suzuki, A., M. T. Yamaguchi, T. Ohteki, T. Sasaki, T. Kaisho, Y. Kimura, R. Yoshida, A. Wakeham, T. Higuchi, M. Fukumoto, et al. 2001. T cell-specific loss of Pten leads to defects in central and peripheral tolerance. *Immunity* 14: 523–534.

20. Peyssonnaux, C., V. Datta, T. Cramer, A. Doedens, E. A. Theodorakis, R. L. Gallo, N. Hurtado-Ziola, V. Nizet, and R. S. Johnson. 2005. HIF-1alpha expression regulates the bactericidal capacity of phagocytes. *J. Clin. Invest.* 115: 1806–1815.
21. Davies, J. Q., and S. Gordon. 2005. Isolation and culture of murine macrophages. *Methods Mol. Biol.* 290: 91–103.
22. Knapp, S., S. Florquin, D. T. Golenbock, and T. van der Poll. 2006. Pulmonary lipopolysaccharide (LPS)-binding protein inhibits the LPS-induced lung inflammation in vivo. *J. Immunol.* 176: 3189–3195.
23. Lagler, H., O. Sharif, I. Haslinger, U. Matt, K. Stich, T. Furtner, B. Doninger, K. Schmid, R. Gattringer, A. F. de Vos, and S. Knapp. 2009. TREM-1 activation alters the dynamics of pulmonary IRAK-M expression in vivo and improves host defense during pneumococcal pneumonia. *J. Immunol.* 183: 2027–2036.
24. LeBel, C. P., H. Ischiropoulos, and S. C. Bondy. 1992. Evaluation of the probe 2′,7′-dichlorofluorescin as an indicator of reactive oxygen species formation and oxidative stress. *Chem. Res. Toxicol.* 5: 227–231.
25. Knapp, S., U. Matt, N. Leitinger, and T. van der Poll. 2007. Oxidized phospholipids inhibit phagocytosis and impair outcome in gram-negative sepsis in vivo. *J. Immunol.* 178: 993–1001.
26. Knapp, S., L. Hareng, A. W. Rijneveld, P. Bresser, J. S. van der Zee, S. Florquin, T. Hartung, and T. van der Poll. 2004. Activation of neutrophils and inhibition of the proinflammatory cytokine response by endogenous granulocyte colony-stimulating factor in murine pneumococcal pneumonia. *J. Infect. Dis.* 189: 1506–1515.
27. Knapp, S., C. W. Wieland, C. van 't Veer, O. Takeuchi, S. Akira, S. Florquin, and T. van der Poll. 2004. Toll-like receptor 2 plays a role in the early inflammatory response to murine pneumococcal pneumonia but does not contribute to antibacterial defense. *J. Immunol.* 172: 3132–3138.
28. Knapp, S., J. C. Leemans, S. Florquin, J. Branger, N. A. Maris, J. Pater, N. van Rooijen, and T. van der Poll. 2003. Alveolar macrophages have a protective antiinflammatory role during murine pneumococcal pneumonia. *Am. J. Respir. Crit. Care Med.* 167: 171–179.
29. Dessing, M. C., S. Knapp, S. Florquin, A. F. de Vos, and T. van der Poll. 2007. CD14 facilitates invasive respiratory tract infection by *Streptococcus pneumoniae*. *Am. J. Respir. Crit. Care Med.* 175: 604–611.
30. Sly, L. M., V. Ho, F. Antignano, J. Ruschmann, M. Hamilton, V. Lam, M. J. Rauh, and G. Krystal. 2007. The role of SHIP in macrophages. *Front. Biosci.* 12: 2836–2848.
31. Subramanian, K. K., Y. Jia, D. Zhu, B. T. Simms, H. Jo, H. Hattori, J. You, J. P. Mizgerd, and H. R. Luo. 2007. Tumor suppressor PTEN is a physiologic suppressor of chemoattractant-mediated neutrophil functions. *Blood* 109: 4028–4037.
32. Liu, L., K. D. Puri, J. M. Penninger, and P. Kubes. 2007. Leukocyte PI3Kgamma and PI3Kdelta have temporally distinct roles for leukocyte recruitment in vivo. *Blood* 110: 1191–1198.
33. Strassheim, D., J. Y. Kim, J. S. Park, S. Mitra, and E. Abraham. 2005. Involvement of SHIP in TLR2-induced neutrophil activation and acute lung injury. *J. Immunol.* 174: 8064–8071.
34. Hazeki, K., K. Nigorikawa, and O. Hazeki. 2007. Role of phosphoinositide 3-kinase in innate immunity. *Biol. Pharm. Bull.* 30: 1617–1623.
35. Williams, D. L., C. Li, T. Ha, T. Ozment-Skelton, J. H. Kalbfleisch, J. Preiszner, L. Brooks, K. Breuel, and J. B. Schweitzer. 2004. Modulation of the phosphoinositide 3-kinase pathway alters innate resistance to polymicrobial sepsis. *J. Immunol.* 172: 449–456.
36. Schabbauer, G., M. Tencati, B. Pedersen, R. Pawlinski, and N. Mackman. 2004. PI3K-Akt pathway suppresses coagulation and inflammation in endotoxemic mice. *Arterioscler. Thromb. Vasc. Biol.* 24: 1963–1969.
37. Schabbauer, G., J. Luyendyk, K. Crozat, Z. Jiang, N. Mackman, S. Bahram, and P. Georgel. 2008. TLR4/CD14-mediated PI3K activation is an essential component of interferon-dependent VSV resistance in macrophages. *Mol. Immunol.* 45: 2790–2796.
38. Cao, X., G. Wei, H. Fang, J. Guo, M. Weinstein, C. B. Marsh, M. C. Ostrowski, and S. Tridandapani. 2004. The inositol 3-phosphatase PTEN negatively regulates Fc gamma receptor signaling, but supports Toll-like receptor 4 signaling in murine peritoneal macrophages. *J. Immunol.* 172: 4851–4857.
39. Doble, B. W., and J. R. Woodgett. 2003. GSK-3: tricks of the trade for a multitasking kinase. *J. Cell Sci.* 116: 1175–1186.
40. Fillion, I., N. Ouellet, M. Simard, Y. Bergeron, S. Sato, and M. G. Bergeron. 2001. Role of chemokines and formyl peptides in pneumococcal pneumonia-induced monocyte/macrophage recruitment. *J. Immunol.* 166: 7353–7361.
41. Frevert, C. W., S. Huang, H. Danaee, J. D. Paulauskis, and L. Kobzik. 1995. Functional characterization of the rat chemokine KC and its importance in neutrophil recruitment in a rat model of pulmonary inflammation. *J. Immunol.* 154: 335–344.
42. Jones, M. R., B. T. Simms, M. M. Lupa, M. S. Kogan, and J. P. Mizgerd. 2005. Lung NF-kappaB activation and neutrophil recruitment require IL-1 and TNF receptor signaling during pneumococcal pneumonia. *J. Immunol.* 175: 7530–7535.
43. Li, Y., Y. Jia, M. Pichavant, F. Loison, B. Sarraj, A. Kasorn, J. You, B. E. Robson, D. T. Umetsu, J. P. Mizgerd, et al. 2009. Targeted deletion of tumor suppressor PTEN augments neutrophil function and enhances host defense in neutropenia-associated pneumonia. *Blood* 113: 4930–4941.
44. Marks, M., T. Burns, M. Abadi, B. Seyoum, J. Thornton, E. Tuomanen, and L. A. Pirofski. 2007. Influence of neutropenia on the course of serotype 8 pneumococcal pneumonia in mice. *Infect. Immun.* 75: 1586–1597.

International Journal of Antimicrobial Agents 50 (2017) 55–62

Contents lists available at ScienceDirect

International Journal of Antimicrobial Agents

journal homepage: www.elsevier.com/locate/ijantimicag

Chloroquine enhances the antimycobacterial activity of isoniazid and pyrazinamide by reversing inflammation-induced macrophage efflux

U. Matt [a,1], P. Selchow [b], M. Dal Molin [b], S. Strommer [c], O. Sharif [d], K. Schilcher [a], F. Andreoni [a], A. Stenzinger [e], A.S. Zinkernagel [a], M. Zeitlinger [c], P. Sander [b], J. Nemeth [a,*]

[a] Division of Infectious Diseases and Hospital Epidemiology, University Hospital Zurich, University of Zurich, Zurich, Switzerland
[b] Institute of Medical Microbiology, University of Zurich, Zurich, Switzerland
[c] Department of Clinical Pharmacology, Medical University of Vienna, Vienna, Austria
[d] Laboratory of Infection Biology, Department of Medicine 1, Medical University Vienna, CeMM Research Center for Molecular Medicine of the Austrian Academy of Science, Vienna, Austria
[e] Institute of Pathology, University Hospital Heidelberg, Heidelberg, Germany

ARTICLE INFO

Article history:
Received 22 September 2016
Accepted 19 February 2017

Keywords:
Mycobacterium tuberculosis
Chloroquine
BCRP-1

ABSTRACT

Mycobacterium tuberculosis (MTB) is notorious for persisting within host macrophages. Efflux pumps decrease intracellular drug levels, thus fostering persistence of MTB during therapy. Isoniazid (INH) and pyrazinamide (PZA) are substrates of the efflux pump breast cancer resistance protein-1 (BCRP-1), which is inhibited by chloroquine (CQ). In this study, BCRP-1 was found to be expressed on macrophages of human origin and on foamy giant cells at the site of MTB infection. In the current in vitro study, interferon-gamma (IFNγ) increased the expression of BCRP-1 in macrophages derived from the human monocytic leukaemia cell line THP-1. Using a BCRP-1-specific fluorescent dye and radioactively labelled INH, it was demonstrated that efflux from macrophages increased upon activation with IFNγ. CQ was able to inhibit active efflux and augmented the intracellular concentrations both of INH and the dye. In agreement, CQ and specific inhibition of BCRP-1 increased the antimycobacterial activity of INH against intracellular MTB. Although PZA behaved differently, CQ had comparable advantageous effects on the intracellular pharmacokinetics and activity of PZA. The adjunctive effects of CQ on intracellular killing of MTB were measurable at concentrations achievable in humans at approved therapeutic doses. Therefore, CQ, a widely used and worldwide available drug, may potentiate the efficacy of standard MTB therapy against bacteria in the intracellular compartment.

1. Introduction

With an estimated 1.5 million deaths from tuberculosis (TB) in 2013, it remains among the most important causes of death due to an infectious agent [1]. The duration of standard short-course treatment for susceptible TB with the combination of four antituberculous drugs, comprising isoniazid (INH), pyrazinamide (PZA), rifampicin and ethambutol, lasts ≥6 months. Unfortunately, exposure to antibiotics for 6 months results in considerable hurdles, including significant adverse drug events, poor patient adherence, high treatment costs and insecure access to drugs with logistic bottlenecks. In part, these shortcomings of standard TB treatment contributed to the development of multidrug-resistant TB [2]. Therefore, shortening TB therapy has become a research priority. Disappointingly, recent attempts to shorten the duration of treatment were not successful [3,4]. The difficulties encountered include mycobacterial factors, the host response and pharmacological compartmentalisation [5–7].

It is well described that *Mycobacterium tuberculosis* (MTB) survives intracellularly in macrophages by manipulating their defence system, thereby contributing to bacterial persistence [8]. Likewise, the intracellular localisation increases the complexity of pharmacodynamics by separating the bacterial population into two different subpopulations, i.e. extracellular and intracellular MTB [7]. Indeed, there is convincing evidence from animal models and observations in humans that macrophages provide an intracellular niche where MTB survives treatment [8–10].

Efflux pumps are localised on the plasma membrane and on endosomal membranes of macrophages. They are necessary to clear potentially toxic xenobiotics from the cell [11–13]. In the context of MTB infection, efflux pumps are thought to reduce the intracellular concentration of antibiotics, thus inadvertently providing an

* Corresponding author. Center for Infectious Disease Research, 307 Westlake Ave N #500, Seattle, WA 98109, USA. Fax: +1 (206) 256-7229.
E-mail address: johannes.nemeth@cidresearch.org (J. Nemeth).
[1] Present address: Department of Internal Medicine VI, Infectious Diseases, Immunology, Rheumatology, Pneumology, Medical University of Innsbruck, Innsbruck, Austria.

http://dx.doi.org/10.1016/j.ijantimicag.2017.02.022
0924-8579/

environment with reduced drug concentrations where bacteria can survive during antimicrobial treatment [8,9,14]. To deepen our understanding of active transport of anti-TB drugs, the interaction of anti-TB drugs with efflux pumps such as breast cancer resistance protein-1 (BCRP-1, ABCG2) is interesting. INH and PZA are predicted to be substrates for BCRP-1 based on their physical and chemical properties [15] and were proven to be substrates in a plasma membrane model (Anna Seelig, pers. comm.). Chloroquine (CQ) is a highly efficient inhibitor of BCRP-1 [16,17].

In this study, the interaction of two first-line anti-TB drugs (INH and PZA) with their specific efflux pump BCRP-1 was investigated. In particular, we hypothesised that CQ could increase the intracellular drug concentration and enhance the anti-TB activity of INH and PZA via inhibition of BCRP-1.

2. Materials and methods

2.1. Cells and flow cytometry

THP-1 cells (human monocytic leukaemia cell line) were cultured and differentiated to macrophages as previously described [18]. Cells were labelled with biotin-conjugated anti-BCRP-1 antibody (Abcam, Cambridge, UK) or an isotype control antibody provided by the manufacturer in 1% bovine serum albumin/phosphate-buffered saline (BSA/PBS) (Sigma-Aldrich, St Louis, MO) for 30 min at 4 °C. After washing, cells were incubated with streptavidin-conjugated phycoerythrin (Abcam) at 4 °C. Finally, cells were washed three times and were analysed with a CyAn™ ADP flow cytometer (Beckman Coulter, Munich, Germany).

2.2. Tissue samples and immunohistochemistry

Five formalin-fixed paraffin-embedded samples of lymph node TB were retrieved from the archives of the Department of Pathology of University Hospital Heidelberg (Heidelberg, Germany) and were transferred to the tissue bank of the National Center for Tumor Diseases (Heidelberg, Germany). Tissue samples were used in accordance with the regulations of the tissue bank and following approval of the Ethics Committee of Heidelberg University. Infection with mycobacteria was confirmed by microscopy (Ziehl–Neelsen staining) and subsequent PCR restriction enzyme analysis of the *hsp65* gene.

Anti-BRCP-1 (Abcam; clone BXP-21, dilution 1:200) was used for immunohistochemistry. For the detection of bound primary antibody, a DAKO Real Detection Multilink System (Agilent Technologies, Santa Clara, CA) with goat anti-mouse, anti-rabbit and anti-sheep antibodies was used. After antigen retrieval (citrate buffer, pH 6 in a steam pot), sections were blocked for endogenous avidin/biotin activity (Linaris, Dossenheim, Germany). Subsequently, sections were incubated for 30 min at room temperature with the primary antibody, were washed and were incubated with the respective secondary antibodies for 20 min at room temperature. Sections were then incubated with horseradish peroxidase for 12 min at room temperature and were counterstained with haematoxylin. Immunohistochemical staining was evaluated by a pathologist.

2.3. Dye efflux measurements

Following differentiation, cells were incubated with interferon-gamma (IFNγ) (BioLegend, San Diego, CA) at a concentration of 50 ng/mL. Subsequently, cells were washed with PBS and were incubated with 16.5 μM Hoechst 33342 fluorescent dye (Life Technologies, Carlsbad, CA) for 30 min. After washing in PBS, cells were re-incubated in dye-free medium for 30 min in the absence or presence of the BCRP-1 inhibitor YHO-13177 (Calbiochem, San Diego, CA)) or CQ (Sigma-Aldrich) at 1 μM. After 30 min, supernatants were removed and the extracellular dye was measured by spectrofluorometry (excitation 350 nm/emission 461 nm) using the default settings of SoftMax® Pro v.5 software (Molecular Devices, Sunnyvale, CA).

2.4. Accumulation of [^{14}C]-labelled drugs

Changes in intracellular concentrations of INH and PZA in the presence of different concentrations of BCRP-1 inhibitor or CQ were determined using [^{14}C]-PZA and [^{14}C]-INH purchased from ANAWA Trading SA (Zurich, Switzerland) [19]. Differentiated and activated THP-1 macrophages were incubated for 60 min with [^{14}C]-INH and unlabelled INH or with [^{14}C]-PZA and unlabelled PZA to achieve the following final radioactivity concentrations: for INH, 0.01 μCi/mL and 0.05 μCi/mL with a mass concentration of 1 mg/L; and for PZA, 0.05 μCi/mL with a mass concentration of 30 mg/L.

Following incubation, cells were washed twice with ice-cold NaCl 0.9% and were then re-suspended in liquid scintillation cocktail (Ultima Gold™ solution; PerkinElmer, Waltham MA). Radioactivity was measured in a liquid scintillation counter (WALLAC 1410; PerkinElmer Wallac Inc., Turku, Finland). Experiments were performed in triplicate.

2.5. Bacterial strains and growth conditions

Mycobacterium tuberculosis H37Rv #1424, a derivative of *M. tuberculosis* H37Rv carrying a non-restrictive *rpsL* mutation (RpsL, 42 Lys→Arg) conferring streptomycin resistance [20], was grown on Middlebrook 7H10 agar or in Middlebrook 7H9 liquid broth (BD Difco, Sparks, MD) supplemented with oleic acid–albumin–dextrose–catalase (OADC) (BD BBL, Sparks, MD). Middlebrook 7H9 liquid broth was supplemented with Tween 80 (0.05% v/v) to avoid clumping. For expression of green fluorescent protein (GFP) in *M. tuberculosis* H37Rv #1424, the vector pOLYG-Pr-GFP was transformed by electroporation (see Supplementary methods). Transformants were selected and propagated in the presence of hygromycin B (25 μg/mL) (Invitrogen, Carlsbad, CA).

2.6. Drug susceptibility testing of Mycobacterium tuberculosis

Two-fold microdilution chequerboard plates were produced with the robotic platform Freedom EVO 100 (Tecan, Männedorf, Switzerland) in 384-well plates containing 20 μL of the combinations INH/CQ (concentrations, INH 0.004–1.6 μg/mL; CQ 0.08–40 μg/mL) and INH/BCRP-1 inhibitor (concentration, BCRP-1 inhibitor 0.008–4 μM) as well as PZA/CQ (concentration, PZA 0.1–480 μg/ml) and PZA/BCRP-1 inhibitor.

Mycobacterium tuberculosis H37Rv #1424 harbouring the pOLYG-Pr-GFP vector was grown in a roller bottle at 37 °C. When mid-exponential phase was reached, the bacterial suspension was diluted to an optical density at 600 nm of 0.040 ± 0.005 in Middlebrook 7H9 broth. Then, 20 μL of this bacterial suspension was added to the 384-well microdilution chequerboard plates. Subsequently, GFP intensity was measured on a Bio-Tek Synergy™ HT microplate reader (Bio-Tek Instruments, Winooski, VT) with filter sets of 485 ± 20 nm excitation and 528 ± 20 nm emission to determine the initial fluorescence intensity. After 10 days of incubation at 37 °C, fluorescence intensity was measured to determine growth.

2.7. Intracellular growth experiments

Differentiated THP-1 macrophages were grown in 24-well plates (TPP, Trasadingen, Switzerland) at 7×10^5 cells per well and 2 mL of RPMI 1640 (Gibco, Life Technologies, Paisley, UK) per well supplemented with 10% foetal bovine serum (Gibco, Life Technologies). Bacterial suspensions were prepared using cultures grown to

mid-exponential phase in Middlebrook 7H9 broth in roller bottles at 2 rpm [21]. Macrophages were infected at 37 °C in 5% CO_2 at a multiplicity of infection (MOI) of 1 bacterium per cell in triplicate. At 2 h after infection, extracellular bacteria were removed by washing each well three times with RPMI [20]. Then, 24 h after infection, macrophages were activated using 5 ng/mL human IFNγ (BioLegend). The IFNγ concentration was maintained throughout the remaining time of the experiment. Two days after infection, drugs were added and were also maintained throughout the remaining time of the experiment. The number of viable intracellular bacteria was determined at Day 2 (before adding drugs) and at Day 5 (3 days after adding drugs) by lysing adherent cells with ice-cold water and 0.04% sodium dodecyl sulphate (SDS) (AppliChem, Darmstadt, Germany). Lysates were plated in serial dilutions on Middlebrook 7H10 OADC and the number of CFU was counted after 3 weeks of incubation at 37 °C.

2.8. Statistical analysis

Data are presented as the mean ± standard error of the mean. Student's *t*-test was used for comparison of two groups. For more than two groups, Dunnett's multiple comparisons test was used comparing treatment with the control group using GraphPad Prism (GraphPad Software Inc., La Jolla, CA). *P*-values of <0.05 were considered significant.

3. Results

3.1. Expression of BCRP-1 in macrophages during Mycobacterium tuberculosis infection

BCRP-1 is expressed in a wide variety of tissues and confers resistance to chemotherapy in haematopoietic stem cells [22]. Expression of BCRP-1 in human macrophages [11] and in THP-1 monocytes [23] has also been reported. To further investigate a potential role of BCRP-1 in this context, the human monocytic cell line THP-1 was used to test expression of BCRP-1. As assessed by flow cytometry, BCRP-1 was constitutively expressed at the cell surface of THP-1 macrophages (Fig. 1A) and human macrophages derived from peripheral monocytes (data not shown). Next, we aimed to assess whether BCRP-1 is expressed during MTB infection. Therefore, human lymph nodes with lymphatic MTB infection were stained using immunohistochemistry. BCRP-1 was abundantly expressed in foamy giant cells at the site of infection, both on the membrane as well as in the perinuclear region (Fig. 1B).

3.2. IFNγ increases BCRP-1 expression and activity

Infection with MTB manifests both with local and systemic inflammation. Since the pro-inflammatory cytokine IFNγ plays a prominent role in MTB infection [24,25], we hypothesised that inflammation induced by IFNγ might trigger expression of BCRP-1, potentially influencing intracellular drug levels at the site of infection. Following stimulation of THP-1 macrophages with IFNγ, increased BCRP-1 expression over time was observed on the cell surface (Fig. 2A). Also, enhanced expression of BCRP-1 within the cell was confirmed by confocal microscopy (Fig. 2B). We next assessed whether this increase translates into enhanced functional activity of BCRP-1 using the fluorescent dye Hoechst 33342. Hoechst 33342 is a known substrate of BCRP-1 [26]. Incubation of THP-1 macrophages with IFNγ increased extracellular levels of Hoechst 33342 compared with the supernatant of untreated cells (Fig. 2C). Thus, increased expression of BCRP-1 translated into increased function of the efflux pump. Previously, it was demonstrated that quinines in general, and CQ in particular, inhibit the efflux pump BCRP-1 [16]. Both CQ and the BCRP-1 inhibitor YHO-13177 blocked the efflux of Hoechst 33342-loaded macrophages stimulated with IFNγ (Fig. 2D) [27]. Interestingly, whilst CQ inhibited efflux in a dose-dependent manner, the BCRP-1 inhibitor did not, suggesting that BCRP-1 inhibition was saturated at 1 μM and remained specific (data not shown), in line with the published properties of YHO-13177 [28]. Of note, CQ decreases the fluorescence of Hoechst 33342 if incubated simultaneously without any cells (data not shown), thus we cannot preclude a bias on the fluorescence signal in this experiment. In contrast, YHO-13177 had no interference in the same settings.

3.3. IFNγ decreases and chloroquine increases intracellular levels of isoniazid and pyrazinamide in THP-1 macrophages

As a next step, the potential influence of IFNγ on the pharmacokinetics of the BCRP-1 substrates INH and PZA was studied. To assess intracellular drug levels, radioactively labelled INH and PZA were used [19]. In line with the results obtained with the Hoechst 33342 dye to assess BCRP-1 activity, THP-1 macrophages previously stimulated with IFNγ had lower intracellular levels of INH (Fig. 3A). In contrast, levels of PZA remained unaffected (Fig. 3D). Addition of CQ increased the intracellular concentrations both of INH and of PZA (Fig. 3B,E).

CQ treatment of IFNγ-stimulated cells resulted in higher intracellular levels of INH and a trend towards higher levels of PZA compared with unstimulated cells (Supplementary Fig. S1). The

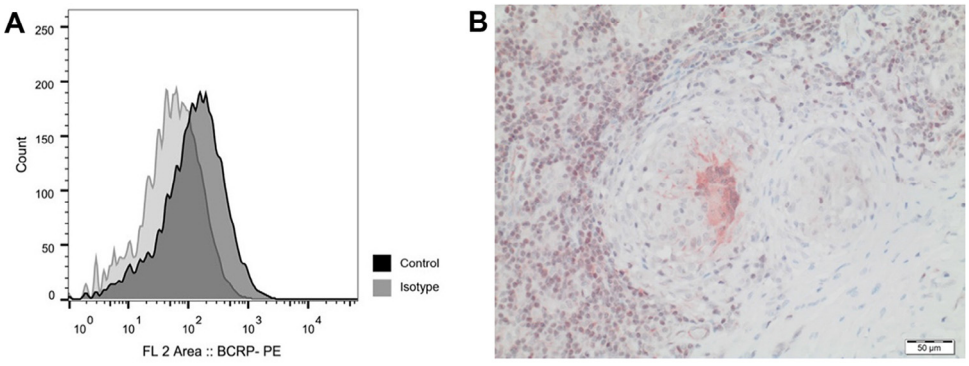

Fig. 1. BCRP-1 is expressed on human macrophages and during *Mycobacterium tuberculosis* infection. (A) Human THP-1 macrophages were stained with an antibody for BCRP-1 (control) or isotype as indicated in Section 2.1 and were assessed by flow cytometry. (B) An infected lymph node of a patient with *M. tuberculosis* infection (mycobacteria detectable upon Ziehl–Neelsen staining) was incubated with an anti-BCRP-1 antibody for immunohistochemistry.

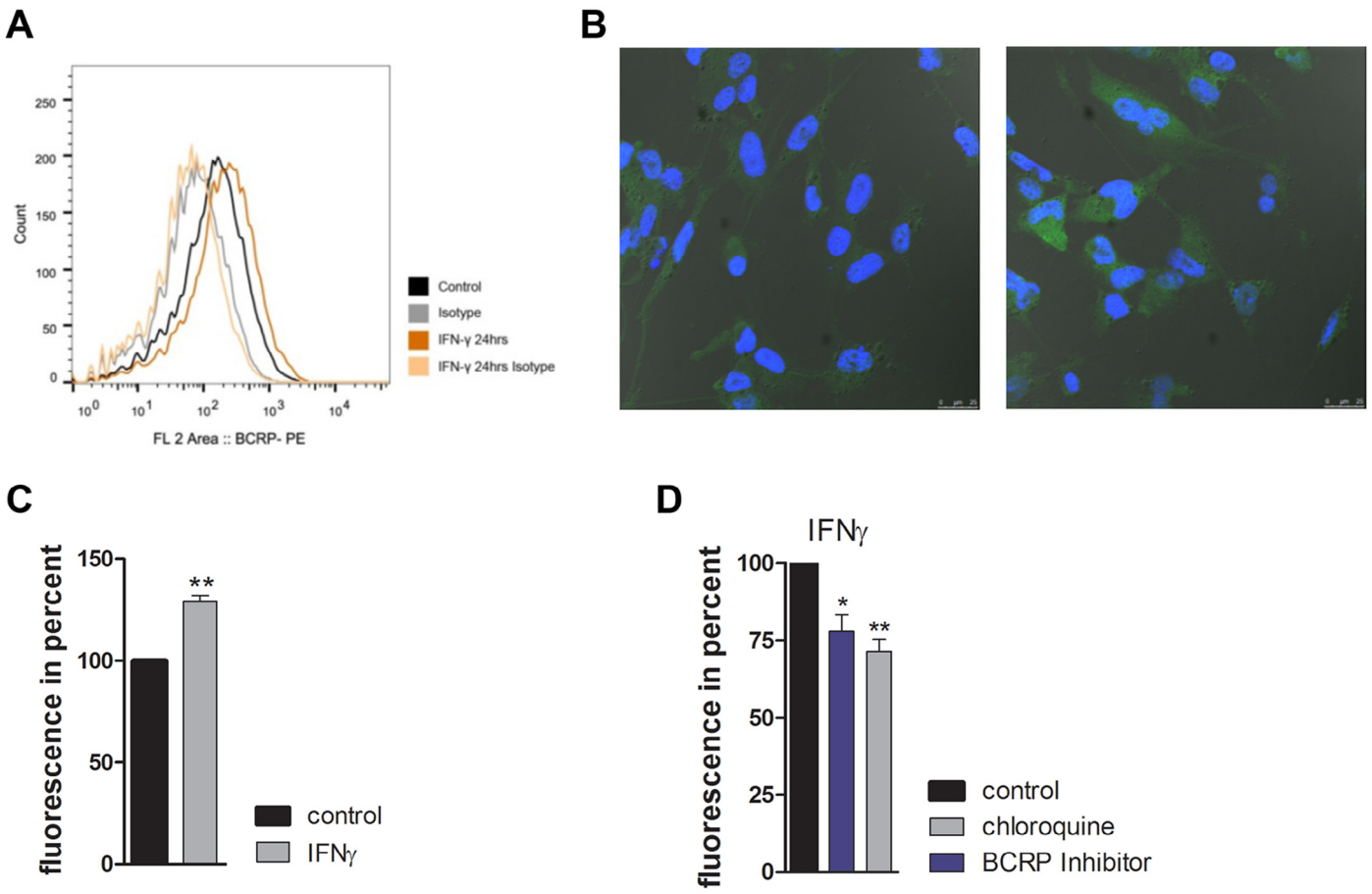

Fig. 2. Interferon-gamma (IFNγ) stimulation increases BCRP-1 expression and function. (A) THP-1 macrophages were stimulated with IFNγ at 50 ng/mL overnight and were subsequently stained with anti-BCRP-1 antibodies and analysed by flow cytometry. (B) Cells were either left untreated (left) or were stimulated with IFNγ (50 ng/mL) overnight (right) and were then fixed, permeabilised and stained with a monoclonal anti-BCRP-1 (green) and DAPI for the nucleus (blue); additionally differential interference contrast microscopy was used. (C,D) THP-1 macrophages were incubated with 16.5 μM Hoechst 33342 for 30 min. Subsequently, cells were washed and were incubated in dye-free medium for 30 min in the absence (C) or presence (D) of chloroquine or BCRP-1 inhibitor YHO-13177, after which supernatants were removed and extracellular dye was measured by spectrofluorometry. Experiments were performed in triplicate; shown is one representative of three independent experiments. (C,D) Data are represented as the mean ± standard error of the mean. * $P < 0.05$; ** $P < 0.01$ versus controls.

BCRP-1 inhibitor did not significantly increase intracellular INH and PZA levels (Fig. 3C,F), but a trend towards increased levels of INH was observed (Fig. 3C).

3.4. Inhibition of BCRP-1 potentiates the antimycobacterial effect of isoniazid

Next, the potential functional consequence of increased INH levels was assessed. To exclude possible direct effects of either the BCRP-1 inhibitor or CQ alone or combined with INH and PZA, MTB was exposed to the compounds or the respective combinations. As depicted in Fig. 4A, neither the BCRP-1 inhibitor nor CQ, alone or in combination with tuberculostatic drugs (Fig. 4B), affected the extracellular growth of MTB. Next, THP-1 macrophages were infected with MTB and the number of CFU was determined 5 days after infection. The IFNγ dose was reduced for the in vitro infection study since it requires a longer incubation compared with the short-term pharmacokinetic assays. Compared with untreated controls, INH significantly reduced the number of CFUs. CQ alone reduced the outgrowth of MTB, whereas BCRP-1 inhibitor alone did not affect survival of intracellular bacteria (Fig. 5A).

Addition of CQ or BCRP-1 inhibitor to INH resulted in a significant reduction of viable mycobacteria (Fig. 5B). Thus, reduction of BCRP-1 activity potentiated the antimycobacterial effect of INH. Incubation with PZA resulted in a significant reduction of intracellular bacteria. CQ also potentiated the effect of PZA. In contrast, the additional inhibition of BCRP-1 with the inhibitor YHO-13177 did not alter intracellular survival of mycobacteria compared with PZA alone (Fig. 5C).

4. Discussion

In this study, we found that CQ increased both the concentration and the activity of INH and PZA within macrophages.

Efflux pumps have been investigated with regard to the pharmacokinetics and pharmacodynamics of antituberculous drugs within macrophages, with a strong focus on P-glycoprotein (P-gp) and rifampicin [9]. Also, the induction of efflux pumps by IFNγ has been demonstrated for P-gp [27]. However, to the best of our knowledge, BCRP-1 has not yet been described in macrophages or foamy giant cells in the context of MTB infection. Furthermore, BCRP-1 expression and function appears to be inducible by IFNγ, which is significantly increased at the site of MTB infection [24,25]. The role of BCRP-1 in TB is interesting considering the observation that MTB is able to survive 6 months of daily directly observed therapy (DOT) in mesenchymal stem cells [10], which were

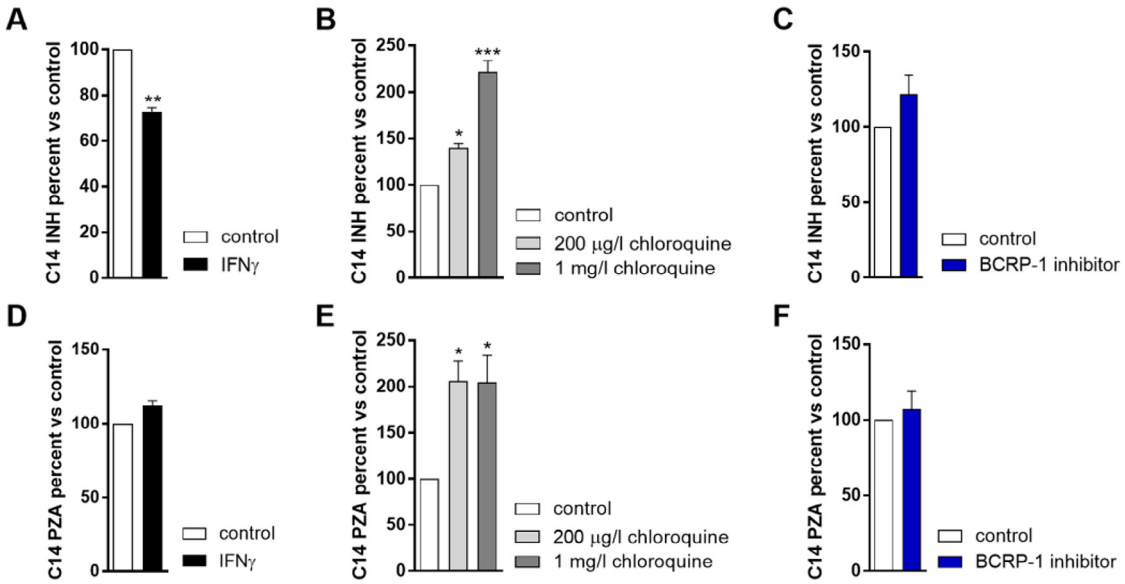

Fig. 3. Effect of chloroquine (CQ) and BCRP-1 inhibitor YHO-13177 on intracellular levels of isoniazid (INH) and pyrazinamide (PZA). THP-1 macrophages were stimulated with interferon-gamma (IFNγ) at 50 ng/mL overnight. Subsequently, radioactively labelled drugs with [^{14}C] INH and unlabelled INH or [^{14}C]-PZA and unlabelled PZA were added for 30 min, were washed off and intracellular radioactivity was assessed by liquid scintillation. For INH, concentrations of (A) 0.05 µCi/mL or (B,C) 0.01 µCi/mL were used; for PZA, 0.05 µCi/mL was used. In (A) and (D), IFNγ at 50 ng/mL intracellular drug levels of stimulated macrophages versus a control (=unstimulated macrophages) are shown. For the other experiments, cells were washed after incubation with radioactively labelled drugs and were subsequently incubated with either chloroquine at the concentrations indicated (B,E) or with BCRP-1 inhibitor at 1 µM (C,F) for another 30 min before intracellular radioactivity was assessed. Percent is relative to the untreated control. Shown is one of three representative experiments, except for (C) and (F) where data from two experiments were pooled. Data are presented as the mean percentage ± standard error of the mean with respect to the control. * $P < 0.05$; ** $P < 0.01$ versus controls.

previously shown to express BCRP-1 [22]. Moreover, we were able to directly link inflammation and changing intracellular pharmacokinetics: the finding that IFNγ stimulation decreased intracellular levels of INH suggests that the ongoing inflammation at the site of infection may substantially reduce the potency of INH therapy in active TB.

Generally, the notion that inflammation may indeed change intracellular pharmacokinetics and affect treatment outcomes of intracellular pathogens is per se not well described in the literature and, in our view, is an important observation reaching beyond the focus of INH and TB.

CQ showed a clear dose dependency, suggesting that it is also able to block other pumps than BCRP-1. Indeed, CQ has been reported to block different efflux pumps at high concentrations, including P-gp [16,29]. Furthermore, this finding proposes that Hoechst 33342 is not entirely specific for BCRP-1. Indeed, polyspecificity has been discussed previously for different efflux pumps and dyes, including Hoechst 33342 [30,31]. CQ may interfere with the fluorescence read-out of Hoechst 33342; therefore, we cannot exclude some interference in this experiment (Fig. 2). However, a significant increase in radioactively labelled INH and PZA was detected in the presence of CQ. Since the radioactivity assay does not suffer from potential interference, our conclusions about active efflux and intracellular retention remain unchanged. Moreover, when unstimulated macrophages were compared with IFNγ-treated cells, less Hoechst 33342 was observed in the supernatant of stimulated cells (Fig. 2C), corroborating the hypothesis of an inducible and active efflux.

The investigations of INH and PZA revealed different pharmacokinetics and pharmacodynamics. As predicted from the Hoechst model, INH efflux was inducible by inflammation. Furthermore, a clear dose-dependent intracellular increase after treatment with CQ was detectable. Whilst we were unable to confirm an increase of INH after specific BCRP-1 blockade at the whole cell level (Fig. 3C), a clear synergistic effect of specific BCRP-1 blockade with INH on intracellular MTB growth was detectable (Fig. 5B). The discrepancy between net cellular accumulation within the whole cell despite inhibition of specific efflux pumps has been described previously and has been attributed to changes of drug concentrations within subcellular compartments [32]. The direction of efflux is dependent on the localisation of the pump within the cell. ATP transporters in the plasma membrane deliver into the extracellular space. In contrast, pumps in membranes of intracellular vesicles deliver their substrate into the lumen of the given vesicle. The same is true for BCRP-1: BCRP-1 is located on the plasma membrane and pumps xenobiotics from the intracellular compartment into the extracellular space, whereas pumps located in the membranes of intracellular compartments pump the substrate into the respective compartment. It has been demonstrated that BCRP-1-containing vesicles colocalise with lysosomes.

These vesicles then pump xenobiotics accumulating in lysosomes into the lumen of these vesicles, thereby detoxifying the lysosome. Therefore, changes in drug concentration within the cell may account for the observed adjunctive effects of INH and BCRP-1 blockade [32,33].

In contrast to INH, PZA efflux was not induced by inflammation, and treatment with CQ did not show a dose dependency in terms of intracellular retention of PZA (Fig. 3E). Likewise, BCRP-1 blockade using YHO-13177 did not show any effect either on the retention of radioactive PZA (Fig. 3F) or on intracellular growth (Fig. 5C). This is an obvious discrepancy with the results from the membrane model, which suggest that PZA is a substrate of BCRP-1. With the data at hand we do not have an explanation for this observation. However, it is tempting to speculate that upon inhibition of BCRP-1, other efflux pumps 'take over' and transport the xenobiotic out of the cell. As mentioned above, both pumps and inhibitors are known to be polyspecific and most efflux pumps have a variety of substrates at different concentrations [30,31]. We therefore hypothesise that PZA is subject to efflux by a pump that is not clearly inducible by IFNγ (Supplementary Fig. S1) and impaired by

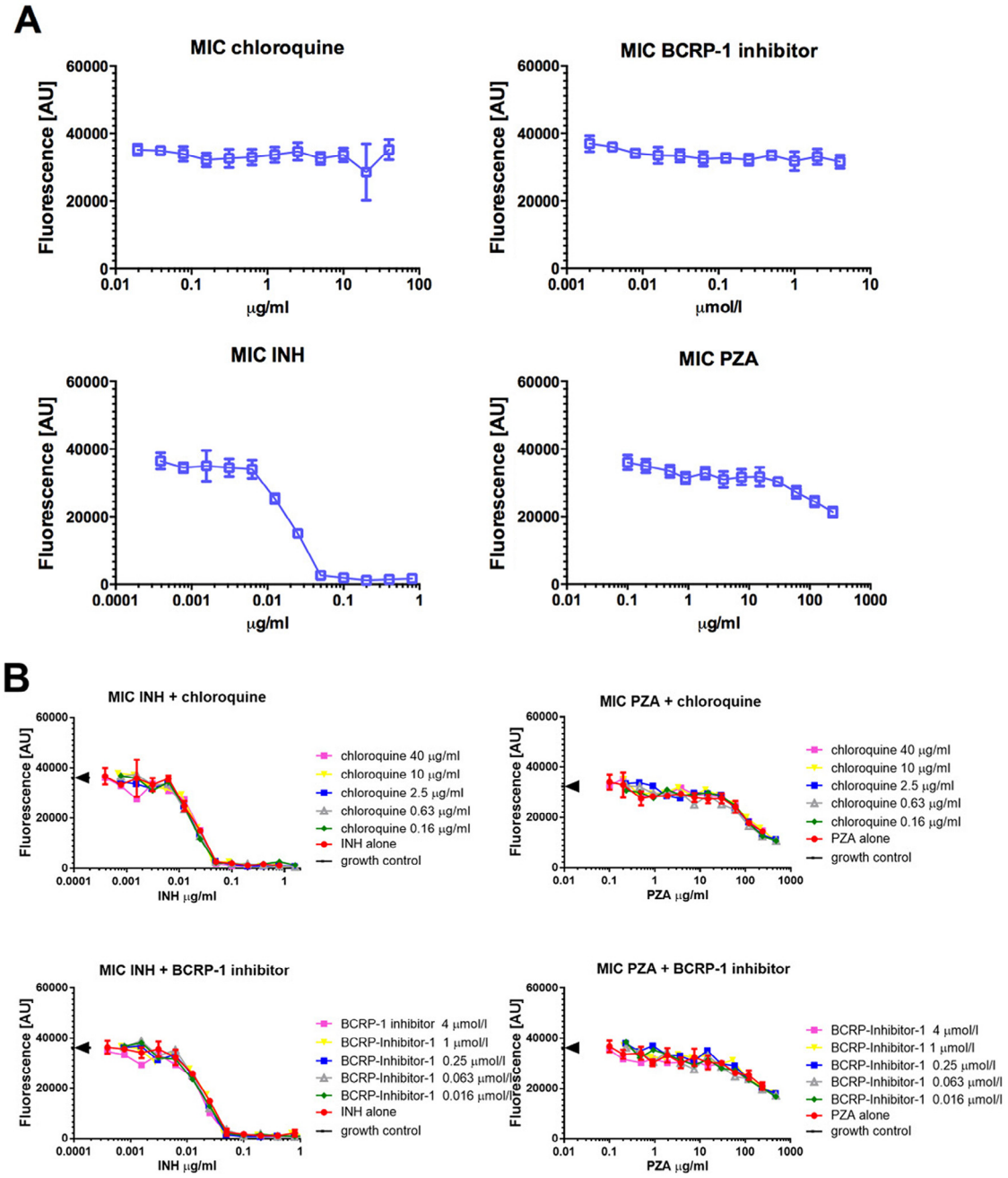

Fig. 4. Drug susceptibility testing of *Mycobacterium tuberculosis*. Dose–response curves of (A) the four single drugs and (B) chequerboard microdilutions of the two drugs isoniazid (INH) and pyrazinamide (PZA) in combination with chloroquine and BCRP-1 inhibitor, respectively. Plotted is the concentration versus the fluorescence intensity (correlated with growth). The arrow at the *y*-axis in (B) indicates the mean of the solvent control. Shown is one of three representative experiments as the mean ± standard error of the mean.

CQ at lower concentrations than the efflux pump(s) for INH. The actual mechanism notwithstanding, CQ was able to double the intracellular concentration of PZA and increase anti-MTB activity of PZA significantly.

The synergistic activity of CQ and PZA is somewhat counterintuitive, since PZA requires a low pH to be active [34]. Conversely, CQ increases the pH in the phagolysosome. Indeed, Crowle and May noted this contradiction already 20 years ago [35]. However, CQ doubled the concentration of intracellular PZA, which may well override the pH dependency of the drug. The fact that CQ per se is active against intracellular living MTB has been described previously and has been attributed to different mechanisms, such as iron depletion and inhibition of phagosome–lysosome fusion [35–38]. We hereby demonstrate that CQ has an additional effect when administered with INH and PZA, i.e. a significant elevation of intracellular drug levels.

In conclusion, we uncovered a relevant role for BCRP-1 in the pharmacokinetics and pharmacodynamics of macrophages on a cellular level, which may play a role during active TB. Furthermore, the intracellular activity of INH and PZA can significantly be increased if active efflux is inhibited, which is, at least for INH, in part due to BCRP-1. Importantly, these results show that CQ, a cheap and very well known drug with few side effects, has synergistic effects for treatment of the intracellular compartment population of MTB

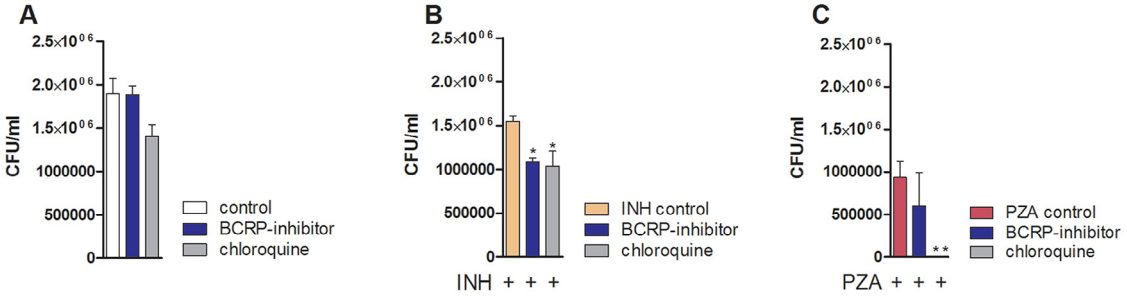

Fig. 5. Inhibition of BCRP-1 potentiates the antimycobacterial effects of isoniazid (INH). THP-1 macrophages were infected at a multiplicity of infection (MOI) of 1 *M. tuberculosis*. Interferon-gamma (IFNγ) at 5 ng/mL was added 1 day after infection and drugs were added 2 days after infection [chloroquine at 10 μg/mL, BCRP-inhibitor at 1 μM, INH at 0.05 μg/mL and pyrazinamide (PZA) at 30 μg/mL]. After 2 days of infection (before adding drugs) and after 5 days of infection (3 days of drug treatment), THP-1 cells were lysed and the lysates were plated in serial dilutions. (A) shows control, BCRP-1 inhibitor and chloroquine, (B) the same conditions with co-incubation of INH and (C) with co-incubation of PZA. Shown is one of three independent experiments as the mean ± standard error of the mean and expressed as difference in number of CFU at Day 5 minus number of CFU at Day 2. * $P < 0.05$; ** $P < 0.01$ compared with the control.

mediated via efflux inhibition. The effects in terms of synergistic killing are observable at concentrations easily achievable in humans (10–200 μg/L) [39]. Thus, we suggest that CQ should be tested in a clinical setting for the adjuvant treatment of MTB infection to potentially increase the activity of standard TB therapy against the intracellular compartment population of MTB. CQ might also be able to shorten the treatment of latent TB infection with INH increasing the antimycobacterial action of INH owing to improving killing of intracellular MTB. This includes mesenchymal and hematopoietic stem cells, which have been recently discovered to serve as a compartment for latent TB [40].

Acknowledgments

Rainer Weber, Nicolas Müller, Stefan Kuster, Lucas Böck, Anna Seelig, Stefan Winkler and Dominique Braun are acknowledged for support and discussions. Imaging was performed with equipment maintained by the Center for Microscopy and Image Analysis, University of Zurich (Zurich, Switzerland).

Funding: The authors are grateful for generous financial support by the Swiss Foundation for Excellence and Talent (Basel, Switzerland) and the Herzog Egli Stiftung (Zurich, Switzerland). UM was supported by the University of Zurich (protected time grant). Work in the laboratory of P. Sander is supported by the Swiss National Foundation [#31003A_153349], and funding to AZ by the Swiss National Foundation [project grant #310030_146295].

Competing interests: None declared.

Ethical approval: Tissue samples were used in accordance with the regulations of the tissue bank of the National Center for Tumor Diseases (Heidelberg, Germany) and following approval of the Ethics Committee of Heidelberg University (Heidelberg, Germany) [project #1610].

Appendix. Supplementary data

Supplementary data associated with this article can be found, in the online version, at doi:10.1016/j.ijantimicag.2017.02.022.

References

[1] World Health Organization. Global tuberculosis report 2014. Geneva, Switzerland: WHO; 2014. Available from: http://apps.who.int/iris/bitstream/10665/137094/1/9789241564809_eng.pdf. [Accessed 2 May 2017].
[2] Zumla A, Raviglione M, Hafner R, von Reyn CF. Tuberculosis. N Engl J Med 2013;368:745–55.
[3] Merle CS, Fielding K, Sow OB, Gninafon M, Lo MB, Mthiyane T, et al. OFLOTUB/Gatifloxacin for Tuberculosis Project. A four-month gatifloxacin-containing regimen for treating tuberculosis. N Engl J Med 2014;371:1588–98.
[4] Gillespie SH, Crook AM, McHugh TD, Mendel CM, Meredith SK, Murray SR, et al. REMoxTB Consortium. Four-month moxifloxacin-based regimens for drug-sensitive tuberculosis. N Engl J Med 2014;371:1577–87.
[5] Gomez JE, McKinney JD. *M. tuberculosis* persistence, latency, and drug tolerance. Tuberculosis (Edinb) 2004;84:29–44.
[6] Behr MA, Waters WR. Is tuberculosis a lymphatic disease with a pulmonary portal? Lancet Infect Dis 2014;14:250–5.
[7] Dartois V. The path of anti-tuberculosis drugs: from blood to lesions to mycobacterial cells. Nat Rev Microbiol 2014;12:159–67.
[8] Adams KN, Takaki K, Connolly LE, Wiedenhoft H, Winglee K, Humbert O, et al. Drug tolerance in replicating mycobacteria mediated by a macrophage-induced efflux mechanism. Cell 2011;145:39–53.
[9] Hartkoorn RC, Chandler B, Owen A, Ward SA, Bertel Squire S, Back DJ, et al. Differential drug susceptibility of intracellular and extracellular tuberculosis, and the impact of P-glycoprotein. Tuberculosis (Edinb) 2007;87:248–55.
[10] Das B, Kashino SS, Pulu I, Kalita D, Swami V, Yeger H, et al. CD271+ bone marrow mesenchymal stem cells may provide a niche for dormant *Mycobacterium tuberculosis*. Sci Transl Med 2013;5:170ra113.
[11] Moreau A, Le Vee M, Jouan E, Parmentier Y, Fardel O. Drug transporter expression in human macrophages. Fundam Clin Pharmacol 2011;25:743–52.
[12] Horsey AJ, Cox MH, Sarwat S, Kerr ID. The multidrug transporter ABCG2: still more questions than answers. Biochem Soc Trans 2016;44:824–30.
[13] Chen Z, Shi T, Zhang L, Zhu P, Deng M, Huang C, et al. Mammalian drug efflux transporters of the ATP binding cassette (ABC) family in multidrug resistance: a review of the past decade. Cancer Lett 2016;370:153–64.
[14] Gupta S, Tyagi S, Almeida DV, Maiga MC, Ammerman NC, Bishai WR. Acceleration of tuberculosis treatment by adjunctive therapy with verapamil as an efflux inhibitor. Am J Respir Crit Care Med 2013;188:600–7.
[15] Egido E, Muller R, Li-Blatter X, Merino G, Seelig A. Predicting activators and inhibitors of the breast cancer resistance protein (ABCG2) and P-glycoprotein (ABCB1) based on mechanistic considerations. Mol Pharm 2015;12:4026–37.
[16] Rijpma SR, van den Heuvel JJ, van der Velden M, Sauerwein RW, Russel FG, Koenderink JB. Atovaquone and quinine anti-malarials inhibit ATP binding cassette transporter activity. Malaria J 2014;13:359.
[17] Hayeshi R, Masimirembwa C, Mukanganyama S, Ungell AL. The potential inhibitory effect of antiparasitic drugs and natural products on P-glycoprotein mediated efflux. Eur J Pharm Sci 2006;29:70–81.
[18] Furnkranz U, Nagl M, Gottardi W, Matt U, Aspock H, Walochnik J. N-Chlorotaurine shows high in vitro activity against promastigotes and amastigotes of *Leishmania* species. J Med Microbiol 2009;58:1298–302.
[19] Leitner I, Nemeth J, Feurstein T, Abrahim A, Matzneller P, Lagler H, et al. The third-generation P-glycoprotein inhibitor tariquidar may overcome bacterial multidrug resistance by increasing intracellular drug concentration. J Antimicrob Chemother 2011;66:834–9.
[20] Raynaud C, Papavinasasundaram KG, Speight RA, Springer B, Sander P, Bottger EC, et al. The functions of OmpATb, a pore-forming protein of *Mycobacterium tuberculosis*. Mol Microbiol 2002;46:191–201.
[21] Master SS, Rampini SK, Davis AS, Keller C, Ehlers S, Springer B, et al. *Mycobacterium tuberculosis* prevents inflammasome activation. Cell Host Microbe 2008;3:224–32.
[22] Zhou S, Schuetz JD, Bunting KD, Colapietro AM, Sampath J, Morris JJ, et al. The ABC transporter Bcrp1/ABCG2 is expressed in a wide variety of stem cells and is a molecular determinant of the side-population phenotype. Nat Med 2001;7:1028–34.
[23] Nagai S, Takenaka K, Nachagari D, Rose C, Domoney K, Sun D, et al. Deoxycytidine kinase modulates the impact of the ABC transporter ABCG2 on clofarabine cytotoxicity. Cancer Res 2011;71:1781–91.
[24] Nemeth J, Rumetshofer R, Winkler HM, Burghuber OC, Muller C, Winkler S. Active tuberculosis is characterized by an antigen specific and strictly localized expansion of effector T cells at the site of infection. Eur J Immunol 2012;42:2844–50.

[25] Nemeth J, Winkler HM, Zwick RH, Rumetshofer R, Schenk P, Burghuber OC, et al. Recruitment of *Mycobacterium tuberculosis* specific $CD4^+$ T cells to the site of infection for diagnosis of active tuberculosis. J Intern Med 2009;265:163–8.
[26] Scharenberg CW, Harkey MA, Torok-Storb B. The ABCG2 transporter is an efficient Hoechst 33342 efflux pump and is preferentially expressed by immature human hematopoietic progenitors. Blood 2002;99:507–12.
[27] Puddu P, Fais S, Luciani F, Gherardi G, Dupuis ML, Romagnoli G, et al. Interferon-gamma up-regulates expression and activity of P-glycoprotein in human peripheral blood monocyte-derived macrophages. Lab Invest 1999;79:1299–309.
[28] Yamazaki R, Nishiyama Y, Furuta T, Hatano H, Igarashi Y, Asakawa N, et al. Novel acrylonitrile derivatives, YHO-13177 and YHO-13351, reverse BCRP/ABCG2-mediated drug resistance in vitro and in vivo. Mol Cancer Ther 2011;10:1252–63.
[29] Vezmar M, Georges E. Reversal of MRP-mediated doxorubicin resistance with quinoline-based drugs. Biochem Pharmacol 2000;59:1245–52.
[30] Shapiro AB, Corder AB, Ling V. P-glycoprotein-mediated Hoechst 33342 transport out of the lipid bilayer. Eur J Biochem 1997;250:115–21.
[31] Martinez L, Arnaud O, Henin E, Tao H, Chaptal V, Doshi R, et al. Understanding polyspecificity within the substrate-binding cavity of the human multidrug resistance P-glycoprotein. FEBS J 2014;281:673–82.
[32] Rajagopal A, Simon SM. Subcellular localization and activity of multidrug resistance proteins. Mol Biol Cell 2003;14:3389–99.
[33] Rajagopal A, Pant AC, Simon SM, Chen Y. In vivo analysis of human multidrug resistance protein 1 (MRP1) activity using transient expression of fluorescently tagged MRP1. Cancer Res 2002;62:391–6.
[34] McDermott W, Tompsett R. Activation of pyrazinamide and nicotinamide in acidic environments in vitro. Am Rev Tuberc 1954;70:748–54.
[35] Crowle AJ, May MH. Inhibition of tubercle bacilli in cultured human macrophages by chloroquine used alone and in combination with streptomycin, isoniazid, pyrazinamide, and two metabolites of vitamin D3. Antimicrob Agents Chemother 1990;34:2217–22.
[36] Hart PD. Evidence that killing of *Mycobacterium tuberculosis* by chloroquine-treated culture macrophages is cell-mediated and not direct. J Med Microbiol 1982;15:iv.
[37] Hart PD, Young MR, Gordon AH, Sullivan KH. Inhibition of phagosome–lysosome fusion in macrophages by certain mycobacteria can be explained by inhibition of lysosomal movements observed after phagocytosis. J Exp Med 1987;166:933–46.
[38] Boelaert JR, Appelberg R, Gomes MS, Blasi E, Mazzolla R, Grosset J, et al. Experimental results on chloroquine and AIDS-related opportunistic infections. J Acquir Immune Defic Syndr 2001;26:300–1.
[39] Documed AG. Schweizer Kompendium. Basel, Switzerland [Accessed 2016].
[40] Tornack J, Reece ST, Bauer WM, Vogelzang A, Bandermann S, Zedler U, et al. Human and mouse hematopoietic stem cells are a depot for dormant *Mycobacterium tuberculosis*. PLoS ONE 2017;12:e0169119.

WAVE1 mediates suppression of phagocytosis by phospholipid-derived DAMPs

Ulrich Matt,[1,2] Omar Sharif,[1,2] Rui Martins,[1,2] Tanja Furtner,[1,2] Lorene Langeberg,[3] Riem Gawish,[1,2] Immanuel Elbau,[1,2] Ana Zivkovic,[1,2] Karin Lakovits,[2] Olga Oskolkova,[4] Bianca Doninger,[1,2] Andreas Vychytil,[5] Thomas Perkmann,[6] Gernot Schabbauer,[4] Christoph J. Binder,[1,6] Valery N. Bochkov,[4] John D. Scott,[3] and Sylvia Knapp[1,2]

[1]Research Center for Molecular Medicine (CeMM) of the Austrian Academy of Sciences, Vienna, Austria. [2]Department of Medicine I, Laboratory of Infection Biology, Medical University Vienna, Vienna, Austria. [3]Howard Hughes Medical Institute, Department of Pharmacology, University of Washington School of Medicine, Seattle, Washington, USA. [4]Institute of Vascular Biology and Thrombosis Research, Center for Biomolecular Medicine and Pharmacology, [5]Department of Medicine III, Division of Nephrology and Dialysis, and [6]Department of Medical and Chemical Laboratory Diagnostics, Medical University Vienna, Vienna, Austria.

Clearance of invading pathogens is essential to preventing overwhelming inflammation and sepsis that are symptomatic of bacterial peritonitis. Macrophages participate in this innate immune response by engulfing and digesting pathogens, a process called phagocytosis. Oxidized phospholipids (OxPL) are danger-associated molecular patterns (DAMPs) generated in response to infection that can prevent the phagocytic clearance of bacteria. We investigated the mechanism underlying OxPL action in macrophages. Exposure to OxPL induced alterations in actin polymerization, resulting in spreading of peritoneal macrophages and diminished uptake of *E. coli*. Pharmacological and cell-based studies showed that an anchored pool of PKA mediates the effects of OxPL. Gene silencing approaches identified the A-kinase anchoring protein (AKAP) WAVE1 as an effector of OxPL action in vitro. Chimeric *Wave1*$^{-/-}$ mice survived significantly longer after infection with *E. coli* and OxPL treatment in vivo. Moreover, we found that endogenously generated OxPL in human peritoneal dialysis fluid from end-stage renal failure patients inhibited phagocytosis via WAVE1. Collectively, these data uncover an unanticipated role for WAVE1 as a critical modulator of the innate immune response to severe bacterial infections.

Introduction

Invasion of bacteria into the peritoneal cavity leads to the immediate initiation of an inflammatory response. Integral to this response are oxygen radicals that are primarily generated to kill microbes. However, these agents also damage host structures through the peroxidation of membrane phospholipids (1). Oxidized phospholipids (OxPL) are endogenous modulators of the inflammatory response that were recently classified as a new entity of danger-associated molecular patterns (DAMPs) (2). As such, previous reports documented a role for these DAMPs in various inflammatory conditions such as atherosclerosis (3, 4) lung inflammation (5–8), or inflammatory brain lesions (9, 10). The precise contribution of OxPL to these diseases is not fully understood, with some reports postulating a proinflammatory role (7), while others describe antiinflammatory properties (11). The impact of OxPL on the course of infectious diseases was unknown until we discovered that administration of OxPL impaired survival during *E. coli* peritonitis by inhibiting phagocytosis of bacteria (12). More recently, OxPL were found involved in the host defense against *Mycobacterium leprae* in humans, which further underscores the critical crosstalk between innate immunity and lipid metabolism (13).

Phagocytosis of pathogens is a major defense mechanism provided by macrophages and neutrophils. Local control of bacterial replication is a prerequisite to preventing systemic spread and sepsis (14–16). Mechanistically, phagocytosis is a complex process employing a plethora of receptors and pathways that culminates in the modulation of the actin cytoskeleton (17). Here, we investigated the mechanism of action underlying the detrimental effects of OxPL during *E. coli* peritonitis. We found that OxPL induce alterations in actin polymerization, which resulted in spreading of peritoneal macrophages and concomitantly diminished uptake of *E. coli*. Biochemical and gene silencing studies revealed that an anchored pool of PKA mediated these effects. The specificity of PKA activity was provided by the Wiskott-Aldrich syndrome protein (WASP) family verprolin-homologous protein 1 (WAVE1), a protein that controls actin polymerization via the Arp2/3 complex (18). In contrast to all other WASP family members, WAVE1 is predominantly known as an A-kinase anchoring protein (AKAP) that contributes to the specificity of PKA by tethering it to Arp2/3 (19). Only recently, WAVE1 was found expressed in bone marrow–derived macrophages, but its function there remained unknown (20).

Results

OxPL as generated during E. coli peritonitis inhibit phagocytosis and induce a cell spread in peritoneal macrophages. We have shown that administration of OxPL impaired survival during *E. coli* peritonitis by inhibiting phagocytosis of the bacteria (12). Further investigation of this phenomenon has uncovered a role for endogenously produced OxPL as biologically relevant modulators of *E. coli* infections during peritonitis. Levels of OxPL in the peritoneal lavage fluid (PLF) were significantly increased after infection with *E. coli* when compared with samples from healthy mice, as

Authorship note: Ulrich Matt and Omar Sharif contributed equally to this work.
Conflict of interest: The authors have declared that no conflict of interest exists.
Citation for this article: *J Clin Invest.* 2013;123(7):3014–3024. doi:10.1172/JCI60681.

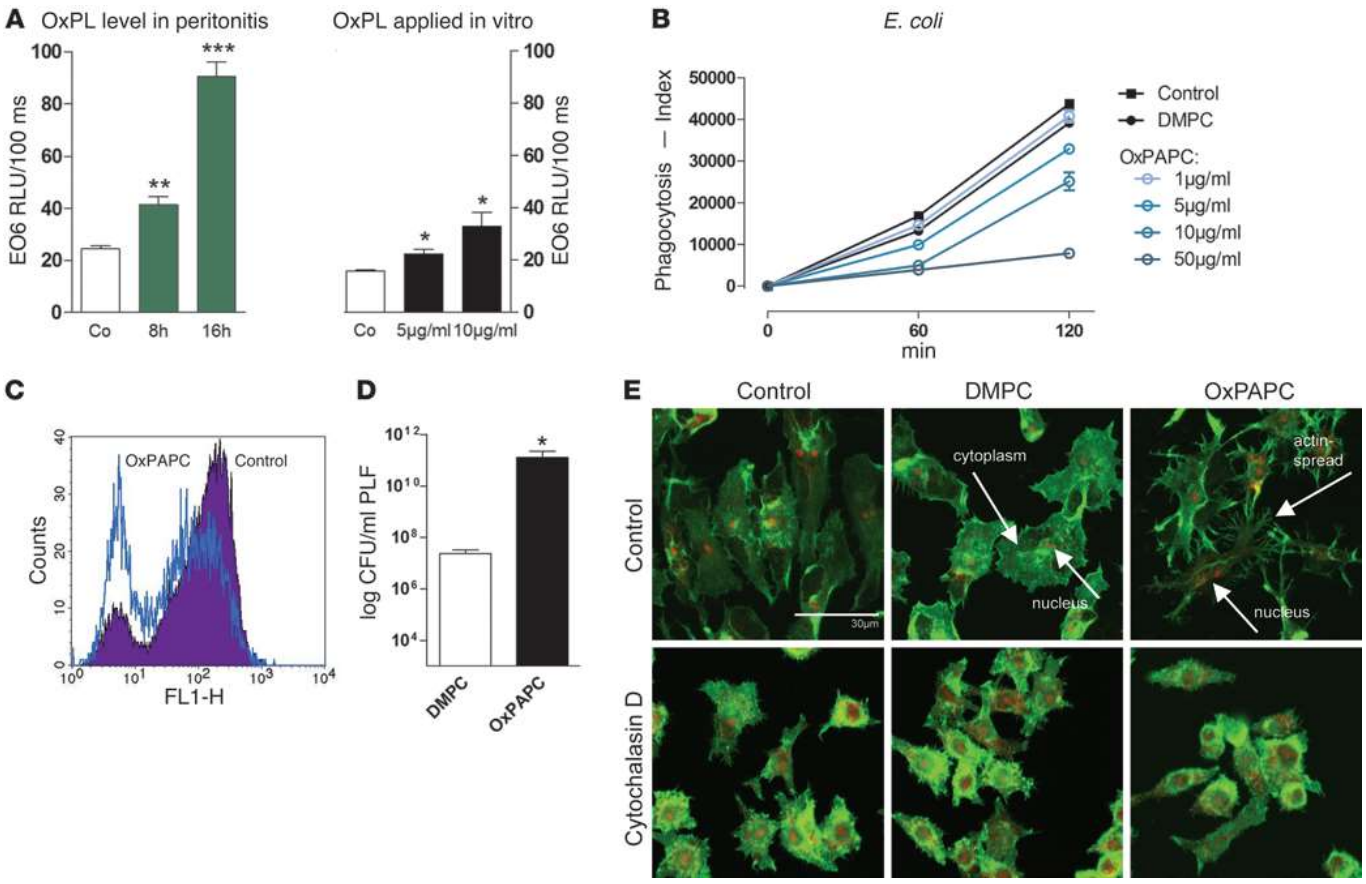

Figure 1

Oxidation of lipids occurs in *E. coli* peritonitis in vivo and leads to an actin-dependent change in cell shape in vitro. (**A**) Endogenous levels of oxidized phosphatidylcholine were measured in PLF of mice infected with *E. coli* after 8 or 16 hours, respectively, compared with supernatants of RAW 264.7 cells after adding 5 or 10 μg/ml of OxPAPC, respectively. Co, control. (**B**) RAW 267.4 cells were incubated with indicated doses of OxPAPC or DMPC for 15 minutes, and phagocytosis of *E. coli* was assessed after 60 and 120 minutes (triplicates, representative of 3 independent experiments). (**C**) FACS histogram showing uptake of FITC-labeled *E. coli* by resident peritoneal macrophages pretreated with 10 μg/ml of OxPAPC or DMPC after 60 minutes. (**D**) Mice (n = 8/group) were infected with 10^4 CFU *E. coli* i.p. and treated with 2.5 mg/kg DMPC or OxPAPC i.p. Peritoneal CFU counts were enumerated 10 hours after infection. Data (**A**–**D**) are presented as mean ± SEM; $^*P < 0.05$; $^{**}P < 0.01$ versus controls. $^{***}P < 0.001$. (**E**) RAW 264.7 cells were incubated with carrier, DMPC, or OxPAPC (10 μg/ml; 30 minutes) alone or following incubation with 2 μM cytochalasin D (30 minutes). Cells were subsequently stained for F-actin using phalloidin (green) and PI for nuclei (red). Scale bar: 30 μm.

measured with a monoclonal antibody that recognizes the phosphocholine headgroup of OxPL (Figure 1A and ref. 21). Quantification of OxPL generated during *E. coli* peritonitis in vivo as compared with OxPL levels in cell supernatants following exogenous administration of OxPL in vitro demonstrated comparable amounts (Figure 1A). More detailed analyses demonstrated that these equivalent amounts of OxPL (Figure 1A) reduced the uptake of bacteria by peritoneal macrophages in a dose-dependent manner (Figure 1, B and C). Consequently, administration of OxPL led to enhanced bacterial loads in the peritoneal cavity (Figure 1D). Control experiments confirmed that delivery of native phospholipids did not have this effect (Figure 1D).

The changes in cell shape associated with phagocytosis require the active remodeling of actin (22). Delivery of OxPL also affects actin polymerization (23). Further support for this notion was provided by fluorescent imaging of RAW 264.7 macrophages showing that treatment with OxPL induced cell spreading, which is a hallmark of actin reorganization (Figure 1E). This phenomenon was not observed in control experiments in which RAW 264.7 macrophages were treated with unoxidized phospholipids or cytochalasin D, a chemical inhibitor of actin polymerization (Figure 1E). Quantification of cell perimeter and area using CellProfiler cell image analysis software confirmed that OxPL treatment induced spreading of cells (Supplemental Figure 1; supplemental material available online with this article; doi:10.1172/JCI60681DS1). Related studies have suggested that this proceeds through a pathway where CD36 is a receptor for OxPL (24, 25). More detailed analyses attempted to assess the contribution of the CD36 scavenger receptor in mediating these OxPL effects. Interestingly, we could not discern a role for CD36 in OxPL-mediated cell spreading when experiments were performed in CD36 mutant oblivious ($CD36^{obl}$) peritoneal macrophages, which harbor a nonfunctional scavenger receptor (Supplemental Figure 2A). Further analyses in these cells demonstrated that although the absence of functional CD36 affected phagocytosis of *E. coli* when compared with WT macrophages, this process is still suppressed in the presence of OxPL (Supplemental Figure 2B). A number of other receptors have been described to be important in OxPL-

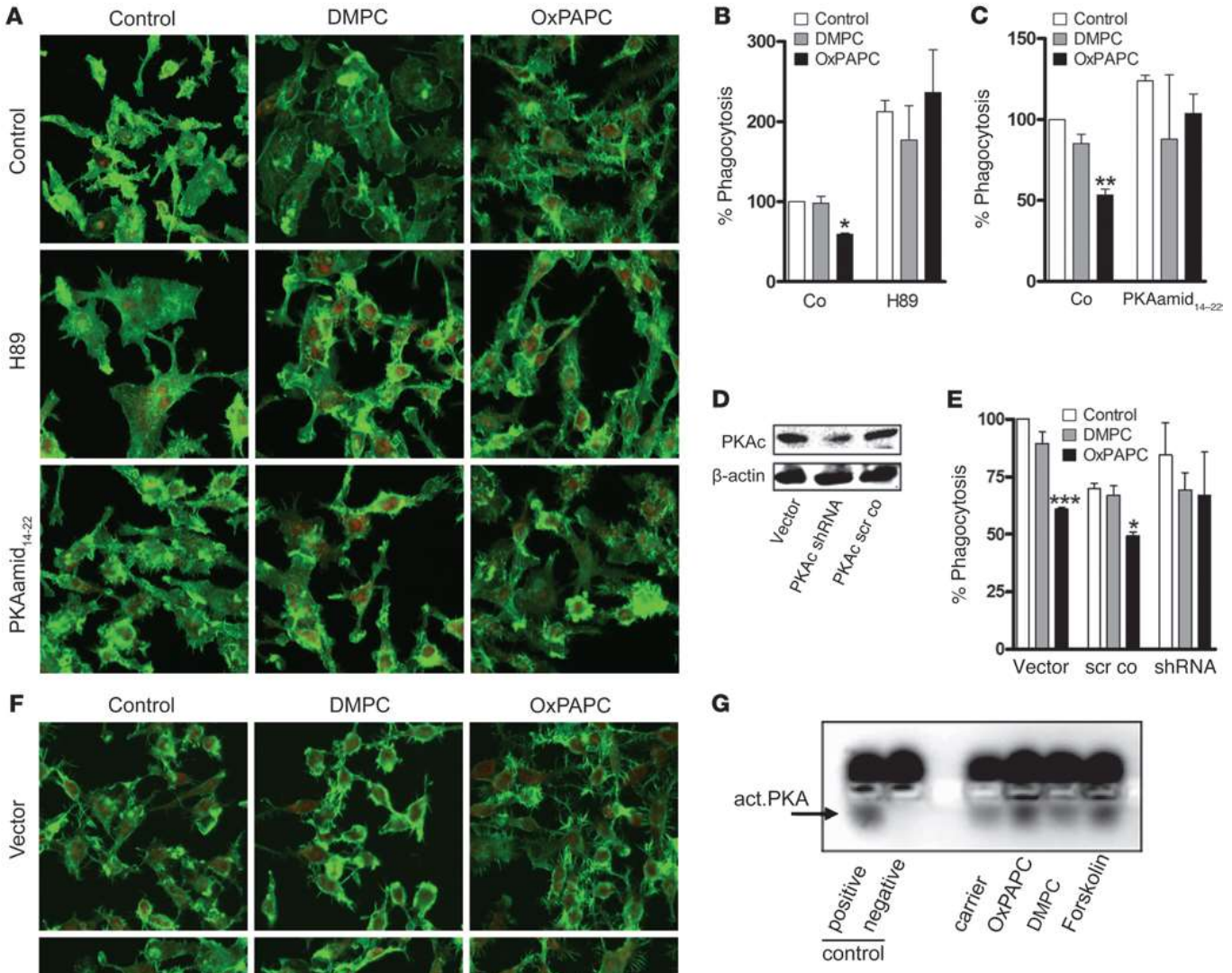

Figure 2

PKA activation mediates OxPAPC-associated cell spread and inhibition of phagocytosis. (**A**–**C**) RAW 264.7 cells were treated with carrier, DMPC, or OxPAPC (10 μg/ml, 30 minutes in **A**; 5 μg/m, 15 minutes in **B** and **C**) alone or following preincubation with H89 (10 μM) or PKA amide$_{14–22}$ (20 μM) (30 minutes). (**A**) Cells were subsequently stained for F-actin (phalloidin; green) and PI (red). (**B** and **C**) Uptake of FITC-labeled *E. coli* was evaluated after 60 minutes and is expressed relative to carrier. (**D**) RAW 264.7 cells were transfected with shRNA to the α-isoform of PKAc, and silencing was verified by Western blot. (**E** and **F**) Control (vector or scrambled control) and shRNA-transfected cells were preincubated with carrier, DMPC, or OxPAPC (5 μg/ml, 15 minutes in **E**; 10 μg/ml, 30 minutes in **F**). (**E**) Phagocytosis of FITC-labeled *E. coli* was examined after 60 minutes and is expressed relative to carrier. (**F**) Cells were stained with phalloidin–Alexa Fluor 488 (green) and PI (red). Representative images of 3 independent experiments are shown. (**G**) RAW 264.7 cells were incubated with DMPC or OxPAPC at 10 μg/ml, forskolin (100 μM), or carrier for 15 minutes. PKA activity was measured as described in Methods. Arrow indicates activated PKA (lower band); "positive" and "negative" indicate assay control. Data are mean ± SEM of triplicates and representative of 3 independent experiments; $^{*}P < 0.05$; $^{**}P < 0.01$; $^{***}P < 0.001$ versus corresponding carrier. Original magnification, ×800.

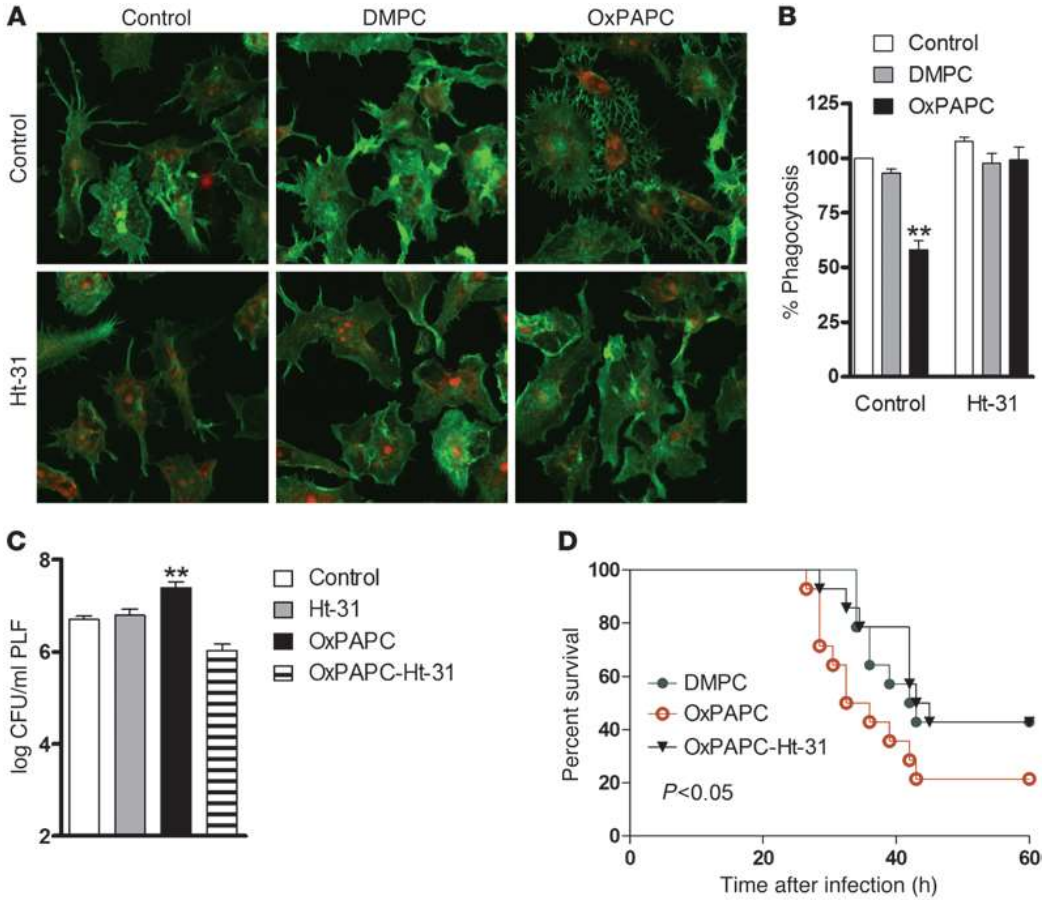

Figure 3

OxPL-induced inhibition of phagocytosis requires anchoring of PKA in vivo and in vitro. (**A**) RAW 264.7 cells were incubated with carrier, DMPC, or OxPAPC (10 μg/ml) alone or after treatment with 100 μM Ht-31 (30 minutes) and stained with phalloidin (green) and PI (red). Original magnification, ×800. (**B**) RAW 264.7 cells were treated with carrier or phospholipids (5 μg/ml; 15 minutes) alone or after preincubation with Ht-31 (100 μM) for 30 minutes. Phagocytosis of FITC-labeled *E. coli* was analyzed using FACS after 60 minutes. Uptake is expressed relative to carrier. $^{**}P < 0.01$. Data show mean ± SEM of triplicates and are representative of 3 independent experiments. (**C**) Mice received carrier or 2.5 mg/kg OxPAPC i.p. and/or 100 μM of Ht-31 immediately before infection with 10^4 CFU *E. coli*. At 10 hours after infection, PLF was harvested and bacterial CFUs enumerated. Data are mean ± SEM of 2 independent experiments from $n = 7–9$ mice/group; $^{**}P < 0.01$ versus carrier. (**D**) Mice received 2.5 mg/kg DMPC or OxPAPC i.p. followed by i.p. injection of vehicle or Ht-31 (OxPAPC–Ht-31), after which they were infected with 10^4 CFU *E. coli*. Survival was monitored every 2 hours; $n = 12$ mice/group. *P* values indicate differences between OxPAPC versus DMPC or OxPAPC versus OxPAPC-Ht-31, respectively.

mediated effects, such as the platelet-activating factor receptor (PAFR) and the prostaglandin E2 (EP2) receptor (26, 27). However, chemical inhibition of these receptors was neither able to abrogate OxPL-mediated spreading nor the inhibition of phagocytosis, suggesting that in our cell type and system, neither CD36 (Supplemental Figure 2) nor PAFR or EP2 receptor plays any role (data not shown). To exclude the possibility of toxic effects exerted by OxPL, we performed phagocytosis experiments in which phospholipids were removed after preincubation, but prior to addition of bacteria. These experiments showed that the inhibitory effects of OxPL were fully reversible over time (Supplemental Figure 3). Consistent with previous observations, this reversal was slow, suggesting that OxPL could affect cell-associated factors, including lipid raft or caveolae organization as described (28–30). Collectively, our data argue against toxic effects or competition for receptors shared between *E. coli* and OxPL. Rather, they imply that downstream signaling events account for OxPL-mediated effects on phagocytosis and cell spreading.

Cell spreading via specific PKA activation by OxPL inhibits phagocytosis. Next, we focused on assessing the relative contributions of phosphoinositide and cAMP-dependent signaling pathways in the control of OxPL-mediated phagocytosis and cell spreading. Activation of PI3K and the concomitant mobilization of Rho family small GTPases have been implicated in actin-remodeling events in macrophages (17, 23, 31). However, treatment with pharmacological agents that target PI3K (wortmannin at 50 nM and LY294002 at 10 μM) and Rho GTPases (Rho kinase inhibitor Y27632 at 10 μM and clostridium toxin B at 100 ng/ml, which inactivates Rho, Rac, and Cdc42) had no effect on OxPL action in macrophages (Supplemental Figure 4 and data not shown). Mobilization of cAMP-responsive events is known to suppress receptor-mediated phagocytosis in macrophages (32). Accordingly, pretreatment with pharmacological inhibitors of PKA, including H89 and PKA amide$_{14–22}$ (33, 34), abolished OxPL-induced actin spread (Figure 2A) and completely abrogated the inhibition of phagocytosis (Figure 2, B and C). However, H89 did increase baseline phagocytosis

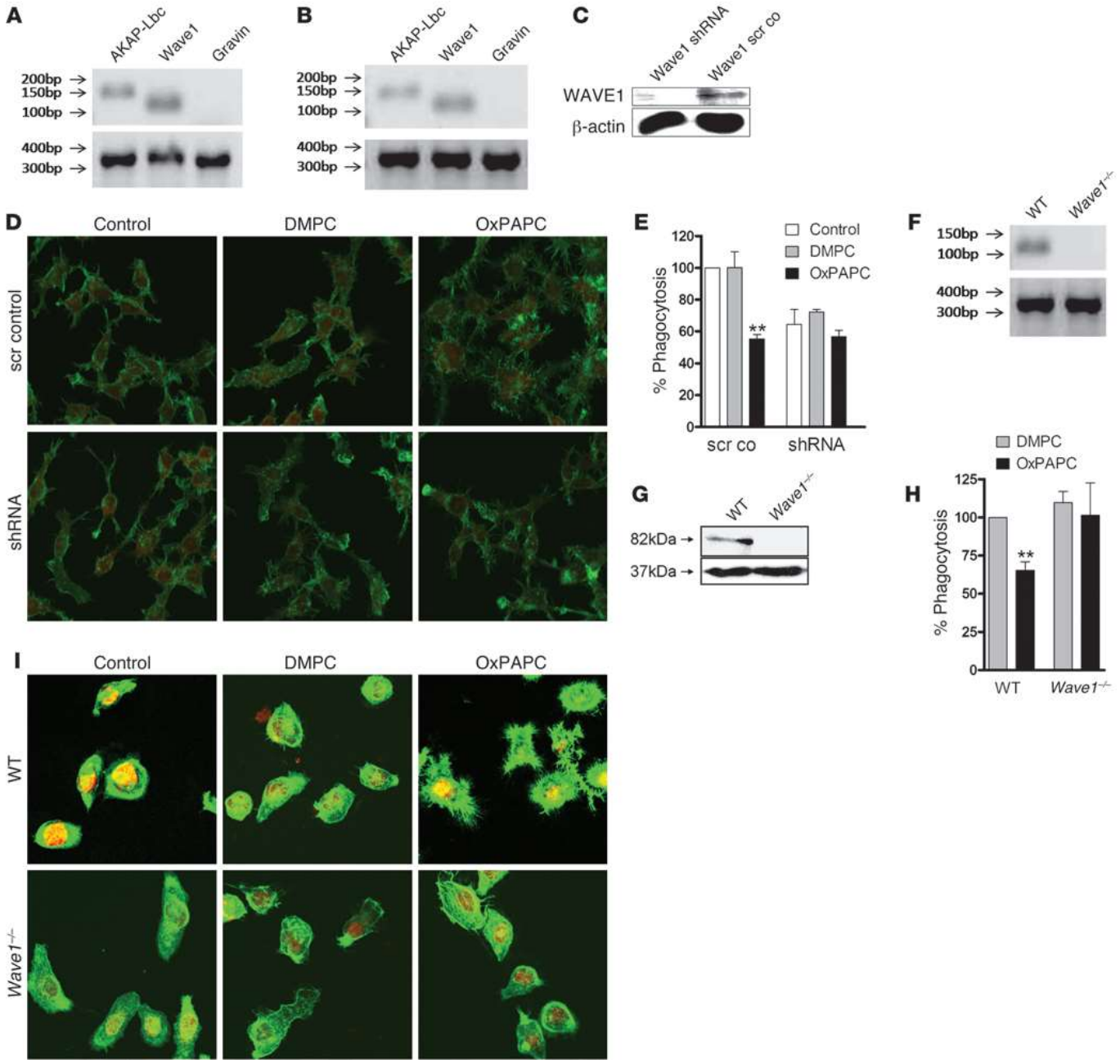

Figure 4

The AKAP WAVE1 mediates OxPL inhibition of phagocytosis in peritoneal macrophages. *AKAP-Lbc* (150 bp), *Wave1* (116 bp), and *Gravin* (136 bp) mRNA expression in (**A**) RAW 264.7 or (**B**) primary peritoneal macrophages; GAPDH (372 bp). (**C**) Western blot verifying silencing of *Wave1* (82 kD) in RAW 264.7 cells; β-actin control (37 kD). (**D**) Scrambled control and shRNA (targeting *Wave1*) cells incubated with carrier, DMPC, or OxPAPC (10 μg/ml) and stained with phalloidin (green) and PI for nuclei (red). Original magnification, ×800. (**E**) Phagocytosis of *E. coli* (60 minutes) assayed in scrambled control and shRNA-*Wave1* cells preincubated with carrier, DMPC, or OxPAPC (5 μg/ml). Data depicted are mean ± SEM of triplicates, **P* < 0.05 versus corresponding carrier/DMPC. (**F**) mRNA expression and (**G**) Western blot for *Wave1* in WT and *Wave1*$^{-/-}$ primary peritoneal macrophages (WAVE1 82 kD; β-actin 39 kD). (**H**) Primary peritoneal macrophages of WT and *Wave1*$^{-/-}$ mice incubated with carrier, DMPC, or OxPAPC (10 μg/ml) and stained with phalloidin (green) and PI (red). (**I**) Phagocytosis of FITC-labeled *E. coli* (60 minutes) by WT and *Wave1*$^{-/-}$ peritoneal macrophages analyzed after prior incubation with DMPC or OxPAPC (5 μg/ml). Data are mean ± SEM of triplicates of 2 independent experiments; ***P* < 0.01 versus corresponding DMPC.

of the dimyristoyl-phosphatodyl-choline (DMPC) control. This nonspecific effect was lower for PKA amide$_{14-22}$, a more specific inhibitor of PKA than H89, which binds to the catalytic subunit of PKA in the nanomolar range (refs. 35–37 and Figure 2, B versus C). More definitive results were obtained with gene silencing of the α-isoform of the catalytic subunit of PKA using shRNA, which successfully reversed OxPL-associated inhibition of phagocytosis and reduced OxPL-induced spreading (Figure 2, D–F). These find-

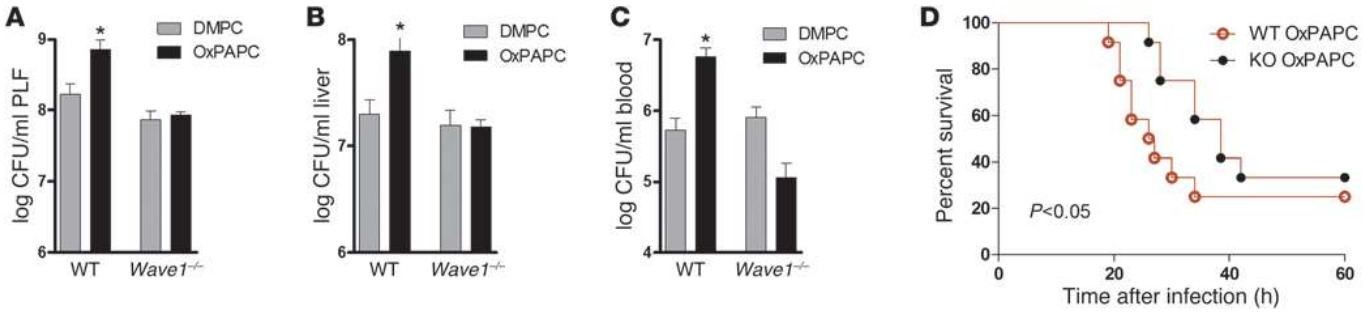

Figure 5

Chimeric *Wave1*-KO mice are rendered unresponsive to OxPL. (**A–D**) WT mice reconstituted with WT or *Wave1*$^{-/-}$ bone marrow were treated with DMPC or OxPAPC (2.5 mg/kg) i.p. and infected with 10^{4-5} CFU *E. coli* i.p. (**A**) Peritoneal, (**B**) liver, and (**C**) blood CFU counts were enumerated 10 hours after infection, and (**D**) survival was monitored every 2 hours. Data are from n = 9–12 mice/group and are presented as mean ± SEM; *P < 0.05 versus corresponding DMPC control.

ings led us to hypothesize that OxPL itself activates PKA. Indeed, incubation with OxPL but not native phospholipids (DMPC) increased PKA activity (Figure 2G). Of note, we observed that forskolin that activates PKA via cAMP was not able to mimic the antiphagocytic effects of OxPL (Supplemental Figure 5), strongly suggesting that although PKA's catalytic activity was necessary for OxPL-mediated effects and that OxPL can induce PKA phosphorylation, the localization of PKA is essential for OxPL-mediated effects. Taken together, these results allow us to demonstrate that OxPL activates PKA, which in turn propagates cellular events associated with actin spread and inhibition of phagocytosis.

AKAP inhibition prevents detrimental effects of OxPAPC in vitro and in vivo. It is widely acknowledged that PKA phosphorylation events control a plethora of processes and that the specificity of this kinase in different cellular compartments is directed through interaction with AKAPs (38, 39). To investigate whether PKA-AKAP interaction is required for OxPL-induced effects, we exploited a cell-permeable AKAP-inhibitory peptide (stearated Ht-31) that blocks association of the regulatory subunit RII of PKA with AKAPs (40). Preincubating macrophages with Ht-31 abrogated the change in cell shape caused by OxPL (Figure 3A) and concomitantly prevented OxPL-associated inhibition of phagocytosis (Figure 3B). Notably, administration of Ht-31 together with OxPL at the onset of *E. coli* peritonitis in mice prevented the increase in bacterial loads caused by OxPL in vivo (Figure 3C). Survival analysis corroborated these findings, as disruption of PKA anchoring with Ht-31 peptide was able to reverse the detrimental effects of OxPL during *E. coli* peritonitis in vivo (Figure 3D). These data strongly suggest that AKAP interactions contribute to OxPL-induced PKA activation, resulting in diminished phagocytosis of bacteria.

WAVE1 mediates antiphagocytic properties of OxPL in vitro. Among the 50 AKAPs discovered thus far, only Gravin, AKAP-Lbc, and WAVE1 are thought to interface with the actin cytoskeleton (38). However, only AKAP-Lbc and WAVE1 are expressed in RAW 264.7 cells and primary peritoneal macrophages (Figure 4, A and B, and Supplemental Figure 6). shRNA-mediated gene-silencing techniques revealed that knockdown of WAVE1 suppressed OxPL-associated actin spread and inhibition of phagocytosis (Figure 4, C–E). In contrast, gene silencing of AKAP-Lbc had no effect (data not shown). Given that WAVE1 shRNA also resulted in a decrease in baseline phagocytosis (Figure 4E), more definitive support for this concept was provided when similar experiments were performed in primary peritoneal macrophages isolated from *Wave1*$^{-/-}$ mice (Figure 4, F–H, and ref. 41). *Wave1*$^{-/-}$ macrophages exhibited neither cell spreading nor impaired bacterial uptake upon OxPL treatment (Figure 4, H and I). These results imply that a pool of PKA associated with WAVE1 modulates cell spreading and inhibition of phagocytosis in macrophages.

Knock out of Wave1 prevents detrimental effects of OxPL in E. coli peritonitis. We then evaluated the role of WAVE1 during *E. coli* peritonitis in vivo. To exclude the potential influence of the altered size of *Wave1*$^{-/-}$ mice (41), we generated chimeric mice on a C57BL/6 background. For this we administered bone marrow of *Wave1*$^{-/-}$ or WT littermates to lethally irradiated C57BL/6 mice and ensured complete reconstitution with *Wave1*$^{-/-}$ donor peritoneal macrophages after 9 weeks (Supplemental Figure 7 and ref. 42). Following i.p. injection of either DMPC or OxPL, we infected mice with *E. coli* i.p. and examined their ability to contain bacterial dissemination. OxPL treatment led to enhanced bacterial outgrowth in mice that received WT bone marrow (Figure 5, A–C). In contrast, chimeric mice with *Wave1*$^{-/-}$ peritoneal macrophages appeared resistant to the effects of OxPL (Figure 5, A–C). The CFU count in PLF, liver, and blood was similar to the values measured in control mice that received unoxidized lipids. Moreover, *Wave1*$^{-/-}$ macrophages seemed resistant to the OxPL-associated impairment of survival during *E. coli* peritonitis (Figure 5D). Collectively, these data confirm that WAVE1 mediates the inhibition of phagocytosis caused by OxPL in vitro and in vivo.

Endogenously generated OxPL inhibit phagocytosis in a WAVE1-dependent manner. To finally study the potential clinical implication, we investigated the direct impact of endogenously generated OxPL on bacterial phagocytosis. We searched for conditions of chronic inflammation with access to body fluids. We chose to collect peritoneal dialysis fluid (PDF) from patients with renal failure, as we anticipated this to contain enhanced levels of OxPL due to impaired antioxidant defense mechanisms, increased oxidative stress (43–45), and the risk for recurrent bacterial peritonitis and sepsis (46, 47), symptomatic for this group of patients. Therefore we studied PDF for the presence and activity of OxPL. OxPL could be detected in PDF from peritoneal dialysis patients (Figure 6A). Incubation of primary murine peritoneal macrophages with human PDF per se did not influence bacterial phagocytosis. However, upon removal of antibodies via protein G beads or heat inactivation (data not shown), human PDF particularly inhibited phagocytosis (Figure 6B and Supplemental Figure 8A), suggesting that contaminating proteins and antibodies compensated for the

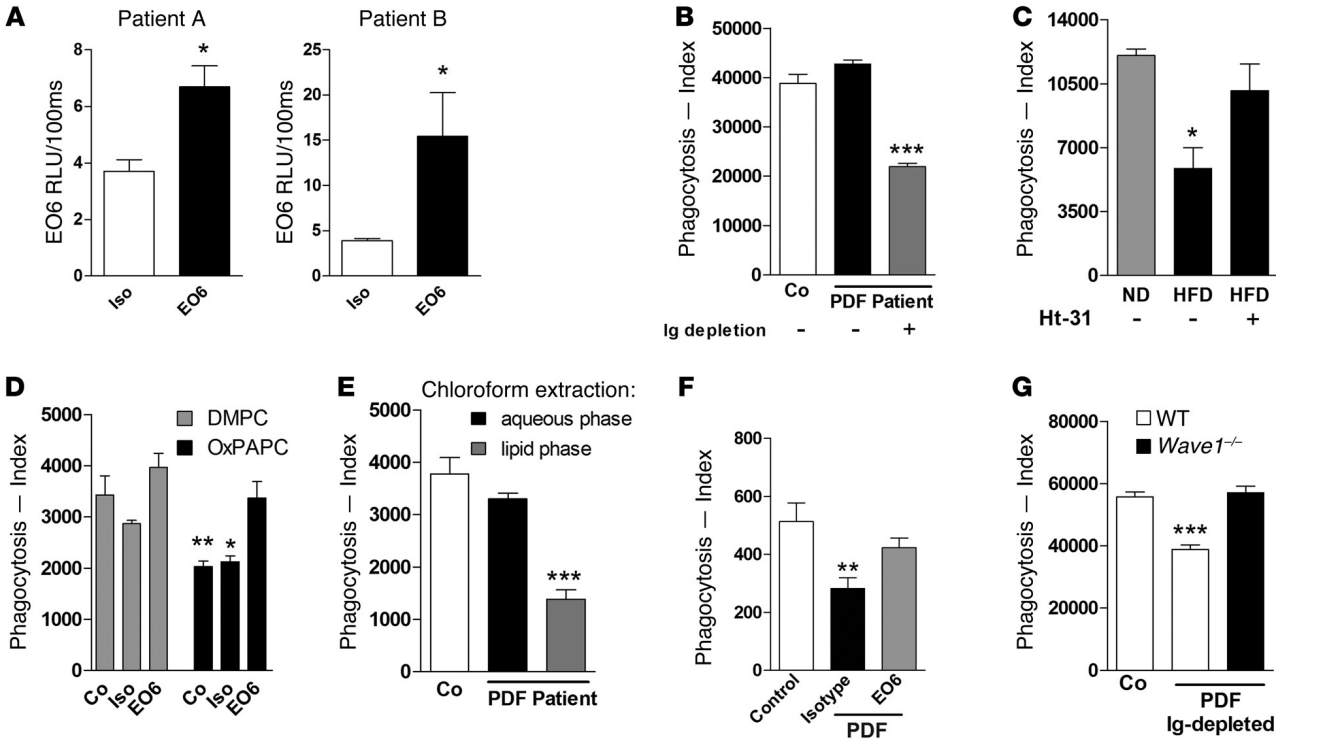

Figure 6

OxPL in human PDF inhibit phagocytosis in the presence of WAVE1. (**A**) Levels of oxidized phosphocholine were measured using the EO6 mAb or an isotype control in PDF from 2 patients undergoing peritoneal dialysis. (**B**) Murine primary peritoneal macrophages were incubated for 15 minutes with PDF of 1 representative patient (patient A), and phagocytosis of *E. coli* after 60 minutes was assessed by FACS. Ig depletion was done with protein G beads. (**C**) PLF from *Ldlr*$^{-/-}$*Rag*$^{-/-}$ mice on normal diet (ND) or high-fat diet (HFD) was placed on primary peritoneal macrophages in the presence or absence of Ht-31 (100 μM) and phagocytosis of *E. coli* after 60 minutes. (**D**) RAW 264.7 macrophages were either preincubated with EO6 antibody or isotype control (1 μg/ml) for 1 hour, then with OxPL or DMPC (5 μg/ml) for 15 minutes. Phagocytosis of *E. coli* was assessed after 60 minutes by FACS. Control assays were done in RPMI. (**E**) PDF of patient A was subjected to chloroform extraction, and the resultant water or lipid fraction was added to RAW 264.7 cells 15 minutes prior to addition of *E. coli*. Phagocytosis was assayed after 60 minutes by FACS. Control assays were done in RPMI. (**F**) RAW 264.7 macrophages were incubated for 15 minutes with IgG-depleted PDF that had been pretreated with either EO6 or isotype control antibody (10 μg/ml) for 1 hour, and phagocytosis of *E. coli* after 60 minutes was assessed by FACS. (**G**) WT and *Wave1*$^{-/-}$ primary peritoneal macrophages were incubated with Ig-depleted PDF from patient A, and phagocytosis of *E. coli* was determined was analyzed. Data are mean ± SEM of at least duplicate experiments; **P* < 0.05; ***P* < 0.01; ****P* < 0.001 versus corresponding control.

inhibitory effects of OxPL. Further confirmation that antibodies masked the antiphagocytic effects of OxPL was obtained by showing that PLF from *Ldlr/Rag*-DKO mice that contained elevated OxPL levels upon a high-fat diet (data not shown) but lacked antibodies due to the absence of B cells inhibited bacterial phagocytosis (Figure 6C). This inhibitory effect of PLF was abolished in the presence of H89 (not shown) or Ht-31 (Figure 6C). *Ldlr/Rag*-DKO mice not only lack IgG but also IgM. EO6 is a prototypic natural IgM antibody that specifically recognizes the phosphocholine head group of OxPL and was shown earlier to neutralize OxPL-mediated effects (21, 48, 49). We show here that EO6 was also able to reverse the OxPL-mediated inhibition of phagocytosis (Figure 6D). Strengthening the biological role of lipids such as OxPL in human PDF, we discovered that only the lipid phase of chloroform-extracted PDF potently inhibited phagocytosis (Figure 6E), whereas lipid removal from Ig-depleted PDF with charcoal reversed the inhibitory effect (data not shown). In line with Figure 6D, neutralization of OxPL by treatment with EO6 antibodies reversed the inhibitory effect on phagocytosis by Ig-depleted human PDF (Figure 6F). Last but not least, inhibition of phagocytosis by Ig-depleted human PDF was reversed in the absence of WAVE1 (Figure 6G and Supplemental Figure 8B). In concert, these data illustrate that WAVE1 mediates inhibition of phagocytosis by endogenously generated OxPL that can be detected in clinical specimens such as PDF.

Discussion

In this study, we investigated the mechanism by which OxPL affect phagocytosis during *E. coli* peritonitis. We have discovered what we believe is a previously unrecognized role of the cytoskeletal-associated AKAP WAVE1 in macrophages.

WAVE1 belongs to the WASP family, which controls actin polymerization via the Arp2/3 complex (18). In contrast with other WASP family members, WAVE1 also functions to anchor PKA and the Abl tyrosine kinase at sites of actin reorganization (19). So far, the majority of WAVE1 action has been studied in the brain. *Wave1*$^{-/-}$ mice exhibit altered synaptic transmission, depleted neuronal migration, behavioral deficits, and reduced viability (41, 50). These electrophysiological and behavioral deficits have been traced back to abnormalities in dynamic actin polymerization and dendritic spine morphology (51). We have now uncovered an unanticipated role for WAVE1 and PKA in innate immunity. Three lines of evidence

support this claim: (a) inhibition of PKA and disruption of PKA anchoring suppress OxPL-induced cell spreading and phagocytosis (Figures 2 and 3); (b) WAVE1 was recently found to be expressed in bone marrow–derived macrophages (20); and (c) gene silencing of WAVE1 or ablation of this *AKAP* gene in peritoneal macrophages protect against OxPL challenge in situ and in vivo (Figures 4–6).

We were able to corroborate previously described findings by making use of biological samples that contained endogenously enhanced levels of OxPL. Elevated levels of OxPL present in PDF from patients with renal failure undergoing peritoneal dialysis or in PLF from *Ldlr/Rag*-DKO mice on a high-fat diet diminished bacterial phagocytosis. In either case, disruption of PKA anchorage by administration of Ht-31 or WAVE1 deficiency proved sufficient to restore phagocytosis (Figure 6 and Supplemental Figure 8).

Several clinical conditions, such as end-stage renal failure, cardiovascular disease, and type 2 diabetes, are characterized by chronic inflammation and an increased risk for severe bacterial infection (47, 52–54). The reason for this enhanced susceptibility to bacterial infections is not well understood (53). Recent reports emphasized the tremendously enhanced risk of death from sepsis and infections in patients with renal failure, with mortality from sepsis being 50 times higher in patients on dialysis as compared with the general population (47, 55). We hypothesized that in these patients, chronic inflammation and the resulting generation of oxidation products such as OxPL might importantly contribute to impaired host defense by inhibiting phagocytosis of bacteria. To address this idea we selected end-stage renal failure patients undergoing peritoneal dialysis, since oxidative modifications in PDF and altered phagocytosis in the peritoneal compartment were observed earlier (44, 45, 56, 57). Our investigations clearly enabled us to demonstrate a role for OxPL in inhibiting phagocytosis in these patients (Figure 6) and furthermore allowed us to demonstrate the importance of the AKAP WAVE1 herein. Of note, the presence of endogenous antibodies and possibly other serum components partly masked the effects of endogenous OxPL in PDF. The importance of antibodies and complement in facilitating phagocytosis is well established (17) and explains that IgG-depleted PDF (Figure 6, B and E) or PLF from antibody-deficient *Ldlr/Rag*-DKO (Figure 6C) mice unleashed the pronounced effect of OxPL on phagocytosis. In line with this, higher incidences of bacterial peritonitis were reported in children on peritoneal dialysis with reduced antibody levels (58).

While IgG directly augments phagocytosis via opsonization of bacteria, serum components such as C-reactive protein and natural antibodies are able to bind and specifically neutralize the biological effects of OxPL (37, 38). We confirm the neutralizing role of natural antibodies, since the natural IgM antibody EO6 that recognizes and blocks the phosphocholine residue of OxPL was sufficient to abolish the antiphagocytic effects of OxPL (Figure 6D) as well as Ig-depleted human PDF (Figure 6F). These data not only reveal that EO6 prevents the antiphagocytic effects of OxPL but furthermore provide some evidence as to the active component in oxidized 1-palmitoyl-2-arachidonoyl-sn-glycero-3-phosphorylcholine (OxPAPC), since the biological activities of POVPC, PEIPC, and PECPC, but not PGPC, have been shown earlier to be particularly neutralized by this antibody (59, 60).

During acute infections, host defense mechanisms are primarily aimed at establishing a highly phagocytic milieu, which might be the reason why we did not observe a more pronounced, although still significant, effect of OxPL in this murine sepsis model. Given the protective mechanisms outlined above, we deem it still remarkable that WAVE1 deficiency was sufficient to protect against the detrimental effects of these DAMPs. We also performed cecal ligation and puncture (CLP) experiments, but could not observe any effect of OxPL and therefore also not WAVE1 in this model (data not shown). This indirectly confirms that OxPL predominantly affect phagocytosis because phagocytosis of bacteria is not that essential after CLP due to abscess formations around the cecum with containment of bacteria (61). As such, it is known that the lack of antibodies is not associated with an altered outcome from CLP (62), whereas *Rag*-deficient mice with *E. coli* peritonitis suffer from impaired bacterial clearance and worsened survival (63).

Collectively, these findings not only underscore the advantages of PKA anchoring as a means to enhance the selectivity of cAMP-responsive events, but also unearth an additional role for the WAVE1 signaling complex. We are the first, to our knowledge, to describe the function of WAVE1 in macrophages and a role for WAVE1 in innate immunity. However, it is important to note that WAVE1 affected phagocytosis only in the presence of OxPL, thus indicating a requirement for oxidative stress as seen during serious inflammatory diseases or infections. Although the precise contribution of OxPL in the *E. coli* peritonitis model and in patients with renal failure discussed in this report is not yet fully understood, an important implication of this study is that diminished bacterial clearance is attenuated by interfering with a WAVE1-associated pool of PKA.

The lack of effective therapies to combat sepsis (64) and the enhanced risk for bacterial infections in patients with chronic inflammatory diseases makes it tempting to speculate that targeting OxPL's negative impact on bacterial phagocytosis by WAVE1 inhibitors might prove to be a promising future direction for therapeutic intervention.

Methods

Phospholipids. PAPC and DMPC were obtained from Sigma-Aldrich. DMPC was used as control lipid, as it lacks unsaturated fatty acids and thus cannot be oxidized. OxPAPC was generated by air oxidation (11) and the extent of oxidation confirmed by electrospray ionization–mass spectrometry (42). Only preparations showing a reproducible pattern of lipid oxidation products were used, and after testing for biological activity and exclusion of LPS contamination using the Limulus assay.

Phagocytosis assays. Phagocytosis assays were performed as described previously (12). Briefly, RAW 264.7 cells or primary resident peritoneal macrophages were plated at 0.5×10^6/ml in 12-well microtiter plates (Greiner) and allowed to adhere overnight. After washing steps, RPMI was added to wells, and macrophages were incubated for 15 minutes with OxPAPC, DMPC (5 μg/ml, unless otherwise indicated), or saline (control). In selected experiments, cells were preincubated for 15 minutes with PDF from patients. Subsequently, FITC-labeled heat-killed *E. coli* (O18:K1) at a MOI of 100 was added for 1 hour at 37°C or 4°C, respectively. To remove adherent but not internalized bacteria, cells were treated with proteinase K at 50 μg/ml for 15 minutes at room temperature. Immediately thereafter, cells were placed on ice, washed, and analyzed using a FACScan (BD). The phagocytosis index of each sample was calculated as follows: (mean fluorescence × percentage of positive cells at 37°C) minus (mean fluorescence × percentage of positive cells at 4°C). Pretreatment with pharmacological inhibitors was performed as indicated.

Mice. Pathogen-free C57BL/6 mice were purchased from Charles River. $CD36^{obl}$ C57BL/6 mice were provided by Bruce Beutler via the Mutant Mouse Regional Resource Centers (MMRC) (65). *Wave1*$^{-/-}$ mice were gener-

ated as described (41) and backcrossed 10 times to a C57BL/6 background. *Ldlr*$^{-/-}$ were crossed with *Rag*$^{-/-}$ mice (Jackson), and backcrossed 10 times to a C57BL/6 background to generate *Ldlr*$^{-/-}$*Rag*$^{-/-}$ mice. Male *Ldlr*$^{-/-}$*Rag*$^{-/-}$ mice housed under specific pathogen–free conditions were fed on a regular chow diet for 8–10 weeks and then switched to an atherogenic diet containing 21% fat and 0.2% cholesterol (TD88137; Ssniff Spezialdiäten GmbH) for an additional 8–10 weeks.

Induction of peritonitis, enumeration of bacteria, and monitoring of survival. Peritonitis was induced by i.p. injection of 200 μl saline containing 10^4 to 10^5 CFUs *E. coli* 018:K1 that were harvested at mid-log phase (12). OxPAPC or DMPC (both at 2.5 mg/kg) were administered i.p. immediately before bacterial infection. 100 μM St-Ht-31 (Promega) was injected i.p. immediately before administering lipids and bacteria. In survival studies, 12 mice/group were inoculated with *E. coli*, and mortality was assessed every 2 hours. For quantification of bacteria, PLF and organs were harvested 10 hours after infection and processed for bacterial quantification as described (12).

Measurement of oxidized lipids. To prevent oxidation, all samples (human and mouse) were supplemented with butylated hydroxytoluene (0.01%) and diethylene triamine pentaacetic acid (DTPA) immediately after collection, purged with nitrogen, and stored in aliquots at –70°C. PLF and PDF samples were adjusted to 100 μg/ml protein concentration in PBS containing 0.27 mM EDTA and applied to 96-well MicroFluor microtiter plates (ThermoLabsystems) for overnight incubation at 4°C (7). Samples were then incubated with isotype control Ab or EO6 (provided by J. L. Witztum, UCSD, San Diego, California, USA) for 2 hours at room temperature, followed by a goat-anti-mouse IgM-AP–labeled secondary antibody (at 1:35,000; Sigma-Aldrich). For development, 25 μl of 33% LumiPhos Plus solution (Lumigen) were added and light emissions were measured as RLU on a WALLAC VIKTOR II luminometer (PerkinElmer).

Bone marrow transplantation. Recipient C57BL/6 bone marrow was ablated with a single dose of radiation (9 Gy) using a Cobalt 60 irradiator (MDS Nordion) followed by injection of 2×10^6 C57BL/6 or *Wave1*$^{-/-}$ bone marrow cells via the retroorbital sinus as described (66). To verify lethal irradiation, 1 mouse from each group (WT or *Wave1*$^{-/-}$ recipients) did not receive bone marrow and was followed over approximately 10 days, after which all of them succumbed. After 9 weeks, successful reconstitution of donor peritoneal macrophages was verified by checking for WAVE1 transcripts in freshly isolated peritoneal macrophages of $n = 3$ mice/group.

Confocal microscopy. Cytoskeletal staining was performed with Alexa Fluor 488–labeled phalloidin (Invitrogen). Blocking of unspecific background was done with PBS/1% BSA for 30 minutes. Propidium iodide (PI) (Sigma-Aldrich) in the presence of 0.1% Triton X-100 was used for nuclear staining. Cells were visualized using a LSM 510 Confocal Laserscanning microscope (Zeiss) with a 488 nm and 543 nm excitation line. Incubations with carrier, DMPC, or OxPAPC (10 μg/ml) were performed for 30 minutes; pretreatment with cytochalasin D, H89, PKA inhibitor amide$_{14–22}$ (Calbiochem), and Ht-31 (Promega) was performed as indicated. Slides were mounted in Fluoprep (BioMerieux). Images were generated with a Zeiss 40 Neofluor (×40/1,30 oil) objective at room temperature. LSM510 Basis Software Release 3.0 (Service Pack 3.2) was used as acquisition software. For automated cell shape analysis, confocal microscopy images were generated as described above and 4 randomly selected microscope field images were generated for each condition. The images were split into green and blue channels (Alexa Fluor 488–labeled phalloidin [Invitrogen] and DAPI [Sigma-Aldrich], respectively), and the CellProfiler cell image analysis software (http://www.cellprofiler.org) (67) was programmed to (a) load single images into the pipeline and identify primary objects (nuclei) using the Otsu Adaptative method with 2-class thresholding (threshold range 0.1–1), minimized weighted variance, and shape method to distinguish clumped objects; (b) identify secondary objects (cytoplasm), based on the previously identified primary objects (nuclei), using the propagation method with 2-class Otsu global thresholding (automatically calculated threshold range) and minimized weighted variance; and (c) generate tables containing cell counts, area, form factor, and perimeter measurements. Primary objects detected at the image border were excluded from the analysis.

PKA kinase assay. PKA kinase assay (PepTag; Promega) was performed according to the manufacturer's instructions. Briefly, RAW 264.7 cells were plated at a density of 1×10^7, treated as indicated, and then scratched off in PKA extraction buffer, homogenized using a 25-gauge needle, and centrifuged for 5 minutes at 20,000 *g*. Controls and sample reaction were prepared according to the manufacturer's instructions. After adjustment of protein contents, equal amounts were loaded on a 0.8% agarose gel, and chemiluminescence was recorded with a Bio-Rad UV-transilluminator.

Generation of PKAc and WAVE1 shRNA cell lines. PKAc and WAVE1 gene silencing was carried out by designing short hairpins using the siRNA target designer (Promega,) to nucleotide regions 930-948 (PKAc; GenBank NM_008854) and 219-237 (WAVE1; GenBank NM_031877). As a control, scrambled nucleotide sequences comprising the shRNA to each transcript were used (Supplemental Table 1). Nucleotides were annealed and ligated into the PstI site of the psiSTRIKE vector (Promega), and plasmids were transformed into competent DH5-α cells. Purified recombinant DNA (Promega Maxiprep kit) (2 μg) was transfected into 2×10^6 RAW 264.7 cells using the Amaxa Cell Line Kit V (Amaxa). Transfected cells were selected with 7 μg/ml puromycin and stable cell lines generated.

Western blotting. Macrophages were washed and lysed as described (68), and 25 μg of supernatant was separated by electrophoresis on a 10% SDS polyacrylamide gel. Following electrophoresis, the gels were transferred to PVDF membranes. Antibodies specific for PKAcα (Santa Cruz Biotechnology Inc.) and WAVE1 (Sigma-Aldrich) were used at a dilution of 1:1000 and β-actin antibody (Sigma-Aldrich) at 1:500. Immunoreactive proteins were detected by the enhanced chemiluminescent protocol (GE Healthcare).

Evaluation of mRNA expression in peritoneal macrophages. QIAGEN's RNEasy kit was used for RNA extraction, which included a DNase step, and cDNA was converted using the Superscript III first-strand synthesis system as described by the supplier (Invitrogen). RT-PCR was conducted according to the LightCycler FastStart DNA MasterPLUS SYBR Green I system using the Roche Light Cycler II sequence detector (Roche Applied Science). Sequences are listed in Supplemental Table 2.

Harvest and handling of PDF. In patients undergoing automated peritoneal dialysis, effluent samples were taken from a single long dwell performed with a conventional icodextrin-containing peritoneal dialysis solution (Extraneal; Baxter Healthcare). Dwell time was at least 14 hours. Informed consent was obtained from peritoneal dialysis patients before collection of effluent samples. PDF from these patients was depleted of IgG by repetitive incubation of 5 ml PDF with 300 μl protein G sepharose beads (GE Healthcare). Lipids were extracted by separating the PDF into 2 phases using chloroform/methanol, a method previously used to extract plasma lipids (www.cyberlipid.org/extract/extr0006.htm#6). Briefly, 3.75 ml of 0.5 M KH_2PO_4 was added to 2.5 ml of PDF, followed by 18.75 ml of chloroform and 6.25 ml of methanol. This mix was then vortexed for 2 minutes and centrifuged at 440 *g* for 5 minutes to separate the upper aqueous phase from the lower lipid phase.

Statistics. Data are presented as mean ± SEM. Comparisons between groups were assessed using either the Mann-Whitney *U* test or ANOVA followed by Bonferroni's multiple comparisons analysis, where appropriate. Survival data were analyzed by the Gehan-Breslow-Wilcoxon test using GraphPad Prism Software. $P < 0.05$ was considered significant.

Study approval. The local animal care committee of the Medical University of Vienna and Ministry of Sciences approved all animal experiments. Patients gave informed consent.

Acknowledgments

We are grateful to Harald Höger for excellent support in mouse breeding, Rita Böhs for animal care, and Edith Pfeiffer for assistance with irradiation. We thank Marion Gröger for technical advice and Julia Schatz for excellent graphical assistance. This work was supported by a grant from the Austrian Science Fund (FWF-P18232-B11 to S. Knapp and V.N. Bochkov). J.D. Scott was supported in part by NIH grant DK54441.

Received for publication December 26, 2012, and accepted in revised form May 2, 2013.

Address correspondence to: Sylvia Knapp, CeMM — Center for Molecular Medicine of the Austrian Academy of Sciences, and Department of Medicine I, Laboratory of Infection Biology, Medical University Vienna, Waehringer Guertel 18-20, 1090 Vienna, Austria. Phone: 43.1.40400.5139; Fax: 43.1.40400.5167; E-mail: sylvia.knapp@meduniwien.ac.at.

Ulrich Matt's present address is: Division of Infectious Diseases and Hospital Epidemiology, University Hospital Zurich, University of Zurich, Switzerland.

Tanja Furtner's present address is: Institute of Molecular Regenerative Medicine, Paracelsus Medical University, Salzburg, Austria.

1. Hampton MB, Kettle AJ, Winterbourn CC. Inside the neutrophil phagosome: oxidants, myeloperoxidase, and bacterial killing. *Blood*. 1998;92(9):3007–3017.
2. Miller YI, et al. Oxidation-specific epitopes are danger-associated molecular patterns recognized by pattern recognition receptors of innate immunity. *Circ Res*. 2011;108(2):235–248.
3. Binder CJ, et al. Innate and acquired immunity in atherogenesis. *Nat Med*. 2002;8(11):1218–1226.
4. Hansson GK, Libby P. The immune response in atherosclerosis: a double-edged sword. *Nat Rev Immunol*. 2006;6(7):508–519.
5. Yoshimi N, et al. Oxidized phosphatidylcholine in alveolar macrophages in idiopathic interstitial pneumonias. *Lung*. 2005;183(2):109–121.
6. Nakamura T, Henson PM, Murphy RC. Occurrence of oxidized metabolites of arachidonic acid esterified to phospholipids in murine lung tissue. *Anal Biochem*. 1998;262(1):23–32.
7. Imai Y, et al. Identification of oxidative stress and Toll-like receptor 4 signaling as a key pathway of acute lung injury. *Cell*. 2008;133(2):235–249.
8. Matt U, et al. Bbeta(15-42) protects against acid-induced acute lung injury and secondary pseudomonas pneumonia in vivo. *Am J Respir Crit Care Med*. 2009;180(12):1208–1217.
9. Newcombe J, Li H, Cuzner ML. Low density lipoprotein uptake by macrophages in multiple sclerosis plaques: implications for pathogenesis. *Neuropathol Appl Neurobiol*. 1994;20(2):152–162.
10. Dei R, et al. Lipid peroxidation and advanced glycation end products in the brain in normal aging and in Alzheimer's disease. *Acta Neuropathol*. 2002;104(2):113–122.
11. Bochkov VN, Kadl A, Huber J, Gruber F, Binder BR, Leitinger N. Protective role of phospholipid oxidation products in endotoxin-induced tissue damage. *Nature*. 2002;419(6902):77–81.
12. Knapp S, Matt U, Leitinger N, van der Poll T. Oxidized phospholipids inhibit phagocytosis and impair outcome in gram-negative sepsis in vivo. *J Immunol*. 2007;178(2):993–1001.
13. Cruz D, et al. Host-derived oxidized phospholipids and HDL regulate innate immunity in human leprosy. *J Clin Invest*. 2008;118(8):2917–2928.
14. Holzheimer RG, Muhrer KH, L'Allemand N, Schmidt T, Henneking K. Intraabdominal infections: classification, mortality, scoring and pathophysiology. *Infection*. 1991;19(6):447–452.
15. Wickel DJ, Cheadle WG, Mercer-Jones MA, Garrison RN. Poor outcome from peritonitis is caused by disease acuity and organ failure, not recurrent peritoneal infection. *Ann Surg*. 1997;225(6):744–753.
16. Pinheiro da Silva F, et al. CD16 promotes Escherichia coli sepsis through an FcR gamma inhibitory pathway that prevents phagocytosis and facilitates inflammation. *Nat Med*. 2007;13(11):1368–1374.
17. Underhill DM, Ozinsky A. Phagocytosis of microbes: complexity in action. *Annu Rev Immunol*. 2002;20:825–852.
18. Takenawa T, Suetsugu S. The WASP-WAVE protein network: connecting the membrane to the cytoskeleton. *Nat Rev Mol Cell Biol*. 2007;8(1):37–48.
19. Westphal RS, Soderling SH, Alto NM, Langeberg LK, Scott JD. Scar/WAVE-1, a Wiskott-Aldrich syndrome protein, assembles an actin-associated multi-kinase scaffold. *Embo J*. 2000;19(17):4589–4600.
20. Dinh H, Scholz GM, Hamilton JA. Regulation of WAVE1 expression in macrophages at multiple levels. *J Leukoc Biol*. 2008;84(6):1483–1491.
21. Friedman P, Horkko S, Steinberg D, Witztum JL, Dennis EA. Correlation of antiphospholipid antibody recognition with the structure of synthetic oxidized phospholipids. Importance of Schiff base formation and aldol condensation. *J Biol Chem*. 2002;277(9):7010–7020.
22. Kaksonen M, Toret CP, Drubin DG. Harnessing actin dynamics for clathrin-mediated endocytosis. *Nat Rev Mol Cell Biol*. 2006;7(6):404–414.
23. Miller YI, Worrall DS, Funk CD, Feramisco JR, Witztum JL. Actin polymerization in macrophages in response to oxidized LDL and apoptotic cells: role of 12/15-lipoxygenase and phosphoinositide 3-kinase. *Mol Biol Cell*. 2003;14(10):4196–4206.
24. Park YM, Febbraio M, Silverstein RL. CD36 modulates migration of mouse and human macrophages in response to oxidized LDL and may contribute to macrophage trapping in the arterial intima. *J Clin Invest*. 2009;119(1):136–145.
25. Boullier A, et al. The binding of oxidized low density lipoprotein to mouse CD36 is mediated in part by oxidized phospholipids that are associated with both the lipid and protein moieties of the lipoprotein. *J Biol Chem*. 2000;275(13):9163–9169.
26. Li R, et al. Identification of prostaglandin E2 receptor subtype 2 as a receptor activated by OxPAPC. *Circ Res*. 2006;98(5):642–650.
27. Birukova AA, Chatchavalvanich S, Oskolkova O, Bochkov VN, Birukov KG. Signaling pathways involved in OxPAPC-induced pulmonary endothelial barrier protection. *Microvasc Res*. 2007;73(3):173–181.
28. Walton KA, et al. Specific phospholipid oxidation products inhibit ligand activation of toll-like receptors 4 and 2. *Arterioscler Thromb Vasc Biol*. 2003;23(7):1197–1203.
29. Seyerl M, et al. Oxidized phospholipids induce anergy in human peripheral blood T cells. *Eur J Immunol*. 2008;38(3):778–787.
30. Levitan I, Gooch KJ. Lipid rafts in membrane-cytoskeleton interactions and control of cellular biomechanics: actions of oxLDL. *Antioxid Redox Signal*. 2007;9(9):1519–1534.
31. Birukov KG, et al. Epoxycyclopentenone-containing oxidized phospholipids restore endothelial barrier function via Cdc42 and Rac. *Circ Res*. 2004;95(9):892–901.
32. Bryn T, Mahic M, Enserink JM, Schwede F, Aandahl EM, Tasken K. The cyclic AMP-Epac1-Rap1 pathway is dissociated from regulation of effector functions in monocytes but acquires immunoregulatory function in mature macrophages. *J Immunol*. 2006;176(12):7361–7370.
33. Scott JD, Fischer EH, Demaille JG, Krebs EG. Identification of an inhibitory region of the heat-stable protein inhibitor of the cAMP-dependent protein kinase. *Proc Natl Acad Sci U S A*. 1985;82(13):4379–4383.
34. Scott JD, Glaccum MB, Fischer EH, Krebs EG. Primary-structure requirements for inhibition by the heat-stable inhibitor of the cAMP-dependent protein kinase. *Proc Natl Acad Sci U S A*. 1986;83(6):1613–1616.
35. Lochner A, Moolman JA. The many faces of H89: a review. *Cardiovasc Drug Rev*. 2006;24(3–4):261–274.
36. Cheng HC, et al. A potent synthetic peptide inhibitor of the cAMP-dependent protein kinase. *J Biol Chem*. 1986;261(3):989–992.
37. Kim C, Xuong NH, Taylor SS. Crystal structure of a complex between the catalytic and regulatory (RIalpha) subunits of PKA. *Science*. 2005;307(5710):690–696.
38. Tasken K, Aandahl EM. Localized effects of cAMP mediated by distinct routes of protein kinase A. *Physiol Rev*. 2004;84(1):137–167.
39. Scott JD, Pawson T. Cell signaling in space and time: where proteins come together and when they're apart. *Science*. 2009;326(5957):1220–1224.
40. Carr DW, Hausken ZE, Fraser ID, Stofko-Hahn RE, Scott JD. Association of the type II cAMP-dependent protein kinase with a human thyroid RII-anchoring protein. Cloning and characterization of the RII-binding domain. *J Biol Chem*. 1992;267(19):13376–13382.
41. Soderling SH, et al. Loss of WAVE-1 causes sensorimotor retardation and reduced learning and memory in mice. *Proc Natl Acad Sci U S A*. 2003;100(4):1723–1728.
42. Murch AR, Grounds MD, Papadimitriou JM. Improved chimaeric mouse model confirms that resident peritoneal macrophages are derived solely from bone marrow precursors. *J Pathol*. 1984;144(2):81–87.
43. Krediet RT, Balafa O. Cardiovascular risk in the peritoneal dialysis patient. *Nat Rev Nephrol*. 2010;6(8):451–460.

44. Himmelfarb J, Hakim RM. Oxidative stress in uremia. *Curr Opin Nephrol Hypertens*. 2003;12(6):593–598.
45. Oberg BP, et al. Increased prevalence of oxidant stress and inflammation in patients with moderate to severe chronic kidney disease. *Kidney Int*. 2004;65(3):1009–1016.
46. Troidle L, Finkelstein F. Treatment and outcome of CPD-associated peritonitis. *Ann Clin Microbiol Antimicrob*. 2006;5:6.
47. Sarnak MJ, Jaber BL. Mortality caused by sepsis in patients with end-stage renal disease compared with the general population. *Kidney Int*. 2000;58(4):1758–1764.
48. Palinski W, et al. Cloning of monoclonal autoantibodies to epitopes of oxidized lipoproteins from apolipoprotein E-deficient mice. Demonstration of epitopes of oxidized low density lipoprotein in human plasma. *J Clin Invest*. 1996;98(3):800–814.
49. Chang MK, et al. Monoclonal antibodies against oxidized low-density lipoprotein bind to apoptotic cells and inhibit their phagocytosis by elicited macrophages: evidence that oxidation-specific epitopes mediate macrophage recognition. *Proc Natl Acad Sci U S A*. 1999;96(11):6353–6358.
50. Soderling SH, et al. A WAVE-1 and WRP signaling complex regulates spine density, synaptic plasticity, and memory. *J Neurosci*. 2007;27(2):355–365.
51. Kim Y, et al. Phosphorylation of WAVE1 regulates actin polymerization and dendritic spine morphology. *Nature*. 2006;442(7104):814–817.
52. Cameron JS. Host defences in continuous ambulatory peritoneal dialysis and the genesis of peritonitis. *Pediatr Nephrol*. 1995;9(5):647–662.
53. Kato S, et al. Aspects of immune dysfunction in end-stage renal disease. *Clin J Am Soc Nephrol*. 2008;3(5):1526–1533.
54. Muller LM, et al. Increased risk of common infections in patients with type 1 and type 2 diabetes mellitus. *Clin Infect Dis*. 2005;41(3):281–288.
55. Jager KJ, et al. Cardiovascular and non-cardiovascular mortality in dialysis patients: where is the link? *Kidney Int Sup*. 2011;1:21–23.
56. Latcha S, Hong S, Gibbons N, Kohn N, Mattana J. Relationship between dialysate oxidized protein and peritoneal membrane transport properties in patients on peritoneal dialysis. *Nephrol Dial Transplant*. 2008;23(10):3295–3301.
57. Posthuma N, ter Wee P, Donker AJ, Dekker HA, Oe PL, Verbrugh HA. Peritoneal defense using icodextrin or glucose for daytime dwell in CCPD patients. *Perit Dial Int*. 1999;19(4):334–342.
58. Poyrazoglu HM, Dusunsel R, Patiroglu T, Gunduz Z, Utas C, Gunes T. Humoral immunity and frequency of peritonitis in chronic peritoneal dialysis patients. *Pediatr Nephrol*. 2002;17(2):85–90.
59. Horkko S, et al. Monoclonal autoantibodies specific for oxidized phospholipids or oxidized phospholipid-protein adducts inhibit macrophage uptake of oxidized low-density lipoproteins. *J Clin Invest*. 1999;103(1):117–128.
60. Subbanagounder G, et al. Epoxyisoprostane and epoxycyclopentenone phospholipids regulate monocyte chemotactic protein-1 and interleukin-8 synthesis. Formation of these oxidized phospholipids in response to interleukin-1β. *J Biol Chem*. 2002;277(9):7271–7281.
61. Maier S, et al. Cecal ligation and puncture versus colon ascendens stent peritonitis: two distinct animal models for polymicrobial sepsis. *Shock*. 2004;21(6):505–511.
62. Bosmann M, Russkamp NF, Patel VR, Zetoune FS, Sarma JV, Ward PA. The outcome of polymicrobial sepsis is independent of T and B cells. *Shock*. 2011;36(4):396–401.
63. Reim D, Westenfelder K, Kaiser-Moore S, Schlautkotter S, Holzmann B, Weighardt H. Role of T cells for cytokine production and outcome in a model of acute septic peritonitis. *Shock*. 2009; 31(3):245–250.
64. Riedemann NC, Guo RF, Ward PA. The enigma of sepsis. *J Clin Invest*. 2003;112(4):460–467.
65. Hoebe K, et al. CD36 is a sensor of diacylglycerides. *Nature*. 2005;433(7025):523–527.
66. Pawlinski R, et al. Role of tissue factor and protease-activated receptors in a mouse model of endotoxemia. *Blood*. 2004;103(4):1342–1347.
67. Carpenter AE, et al. CellProfiler: image analysis software for identifying and quantifying cell phenotypes. *Genome Biol*. 2006;7(10):R100.
68. Lagler H, et al. TREM-1 activation alters the dynamics of pulmonary IRAK-M expression in vivo and improves host defense during pneumococcal pneumonia. *J Immunol*. 2009;183(3):2027–2036.

Acid Aspiration Impairs Antibacterial Properties of Liver Macrophages

To the Editor:

Lung injury and its more severe form, acute respiratory distress syndrome, can be caused by direct (i.e., pneumonia and acid aspiration) or indirect (i.e., sepsis and pancreatitis) lung insults. Thus, extrapulmonary organs can induce lung inflammation. Reversely, lung injury itself has been described to affect a plethora of other tissues, such as the liver, the spleen, or the gastrointestinal tract (1). Mechanistically, interorgan communication between the lung and the liver has been characterized during bacterial pneumonia, and the term "liver–lung" axis was coined. In this model, pneumonia triggers the production of acute-phase proteins in the liver (2, 3). In return, acute-phase proteins activate airspace macrophages and promote bacterial clearance in the lung (4, 5). Thus, interorgan cross-talk involves activation of macrophages.

During bacteremia or infections in neighboring organs, liver, splenic, and peritoneal macrophages have been shown to contribute to clearance of pathogens (6–8). We speculated that the inflammatory response induced by lung injury might also affect antibacterial properties of macrophages in extrapulmonary tissues, potentially contributing to an increased susceptibility to secondary bacterial infections.

Using the model of acid-induced pneumonitis, we here investigated antibacterial properties of liver, peritoneal, and splenic macrophages after lung injury.

In our model, instillation of acid leads to a pneumonitis, peaking after 12 hours in terms of neutrophil accumulation, cytokine production, and edema formation (9). Twenty-four hours after acid instillation, cytokines and neutrophils are in decline, representing a state of resolution of inflammation (9), which coincides with an increased susceptibility to secondary bacterial infections in the lung (unpublished data). At this time point, we harvested splenic, liver, and peritoneal macrophages after acid aspiration and tested their capacity to kill intracellular *Pseudomonas aeruginosa* and *Klebsiella pneumonia*. Whereas peritoneal and splenic macrophages did not show an alteration of their antibacterial properties (Figures 1A and 1B), liver macrophages (LMs) exhibited a reduced killing capacity of *P. aeruginosa* (Figure 1C) and *K. pneumoniae* (Figure 1D), whereas phagocytic properties remained intact (data not shown). Next, we wanted to assess whether liver injury is responsible for the observed effect. Several cytokines tested in liver homogenates were not altered on the protein level (Figure E1 in the data supplement). Furthermore, histopathologic assessment of the liver did not show lesions in sham-treated animals and mice that underwent acid aspiration (Figure 1E). In line with this, liver function tests remained unchanged in the plasma of animals after acid aspiration compared with sham treatment (Figure 1F).

Supported by grants from the German Research Society (KFO 309, early career support).

Author Contributions: Conception and design: M.L., J.B., S.H., and U.M. Acquisition of the data: M.L., J.B., M.W., B.S., C.M., L.K., B.A., and K.K. Analysis and interpretation: M.L., J.B., M.W., L.K., C.H., S.H., and U.M. Drafting the manuscript: M.L., J.B., S.H., and U.M.

This letter has a data supplement, which is accessible from this issue's table of contents at www.atsjournals.org.

LMs consist of resident Kupffer cells (KCs), capsule macrophages and—during an inflammatory response—monocyte-derived macrophages (MDMs). Potentially, acid aspiration alters the composition of LMs and thereby antibacterial properties. To test this hypothesis, we stained liver single-cell suspensions taken from acid- or sham-treated mice 24 hours after the injury. Absolute numbers of KCs and capsule macrophages did not change 24 hours after induction of aspiration pneumonitis (Figures E2A and E2B). In line with the histopathologic assessment, neutrophil numbers were not elevated in acid-treated versus sham-treated mice (Figure E2C). In contrast, we found significantly lower numbers of MDMs in mice that underwent acid aspiration (Figure E2D). The significance of a reduction of MDMs after lung injury remains unclear, but most likely does not affect our observation; MDMs were gated as F4/80^{neg}, and the isolation of LMs for our *ex vivo* experiments is based on F4/80 beads. Of note, ~80–90% of F4/80-positive cells in the liver were KCs (Figure 1G). Thus, KCs account for the reduction of antimicrobial properties.

Transcriptional analysis of LMs after acid aspiration indicated alterations of genes involved in metabolism, particularly oxidative phosphorylation (data not shown). Mitochondrial reactive oxygen species (mROS) are produced along this metabolic cycle and are important contributors to an antibacterial response (10, 11). We therefore tested the capacity of LMs to mount mROS *ex vivo* and indeed found a profound impairment of mROS production in LMs isolated from animals after acid aspiration upon *P. aeruginosa* stimulation (Figure 1H).

KCs reside within liver sinusoids and are ideally positioned to remove pathogens from the circulation (7). To test the significance of our findings *in vivo*, we injected *P. aeruginosa* intravenously 24 hours after acid aspiration and assessed bacterial outgrowth in the liver, lung, spleen, and blood 90 minutes later. Strikingly, the bacterial load was significantly higher in liver homogenates of mice that underwent acid aspiration compared with sham-treated animals (Figure 1I). In contrast, we detected no significant difference in the other compartments (Figure 1I), albeit a trend toward a higher bacterial load in the blood and lung after acid aspiration at comparatively low levels.

In general, interorgan communication is poorly understood but most likely plays a key role in the outcome of severe infection or inflammation. Experimental acid aspiration has been shown to induce injury in a variety of organs such as the heart, kidney, and the liver (12, 13). This can lead to organ dysfunction but could also affect host defense against bacteria. Although some cross-talk may lead to antimicrobial synergy, this interplay may also dampen immune responses. During experimental bacteremia with different pathogens, including *P. aeruginosa*, sequestration of the bacteria in the liver was demonstrated (7, 14, 15). Previously, one study found that loss of KCs during sepsis due to *P. aeruginosa*–induced pneumonia impaired bacterial clearance (16). Recently, Roquilly and colleagues (17) could not detect a difference in the phagocytic capacity of splenic and bone marrow–derived macrophages to clear *Escherichia coli* 7 days after *E. coli* pneumonia, but bacterial killing was not assessed. Of note, uptake of bacteria by KCs does not necessarily mean that the pathogens are cleared; *Staphylococcus aureus* (18) and *Listeria monocytogenes* (19) were shown to proliferate within KCs. This might be a pathogen-specific phenomenon, but it implicates that reduced killing capacities might favor bacterial dissemination.

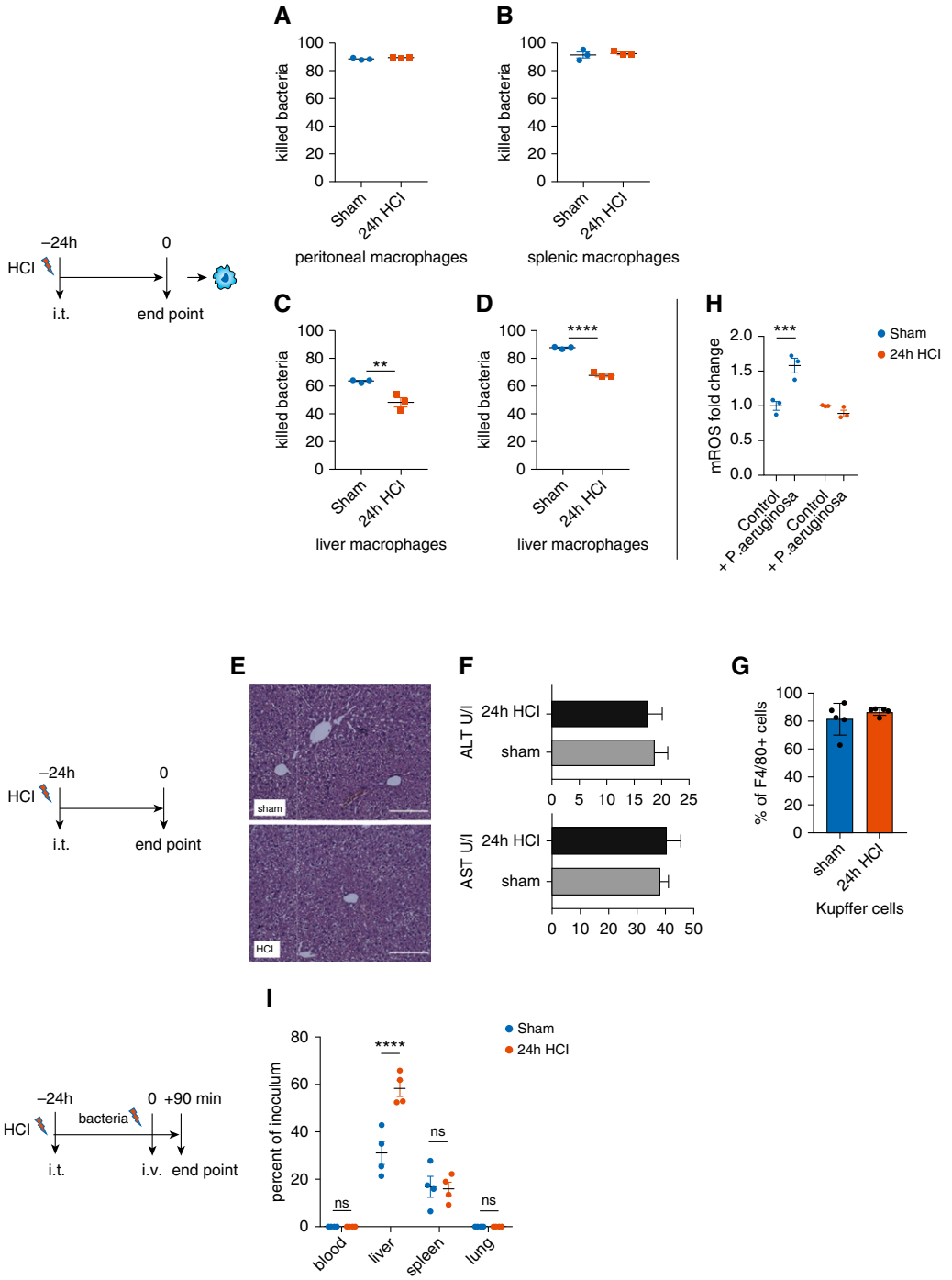

Figure 1. LM have reduced bacterial killing capacity of *Pseudomonas aeruginosa* and *Klebsiella pneumoniae* after acid aspiration in the absence of detectable liver injury. (*A–D*) Peritoneal macrophages (*A*), splenic macrophages (*B*), and liver macrophages (LMs) (*C* and *D*) were harvested 24 hours after acid aspiration, allowed to adhere for 3 hours, and subsequently infected with *P. aeruginosa* (*A–C*) or *K. pneumonia* (*D*). Bacterial killing was performed as described in the Methods section and expressed as killed bacteria relative to uptake. (*E*) Alanine aminotransferase (ALT) and aspartate transaminase (AST) in the blood 24 hours after acid aspiration or sham treatment; pooled data of three experiments; $n = 10–16$/group. (*F*) Representative liver histology stained with hematoxylin and eosin. Scale bars, 200 μm. (*G*) Percentage of Kupffer cells of all F4/80-positive cells in liver single-cell suspensions 24 hours after acid aspiration or sham treatment. (*H*) LMs were harvested 24 hours after acid aspiration, and mROS production was assessed using MitoSox after stimulation with heat-killed *P. aeruginosa*, expressed as fold change compared with the respective control. (*I*) C57BL/6 mice received 50 μl of NaCl (sham) or HCl intratracheally; 24 hours later, mice were intravenously injected with 1.5×10^9 cfu of *P. aeruginosa*, and subsequently the total bacterial load in whole organ homogenates was assessed. Shown is the percentage of bacterial load in every organ compared with the inoculum. For blood, the cfu contained in 1 ml was calculated. Bar and dot charts presented as the mean ± SEM and probability determined using *t* test for (*A–D* and *H*) and one-way ANOVA for (*I*) (**$P \leq 0.01$, ***$P < 0.001$, and ****$P < 0.0001$). cfu = colony-forming unit; *K. pneumonia* = *Klebsiella pneumoniae*; mROS = mitochondrial reactive oxygen species; ns = not significant; *P. aeruginosa* = *Pseudomonas aeruginosa*.

We hereby showed that LMs have, in the absence of any detectable hepatic inflammation or alteration of macrophage composition, an impaired capacity to kill *P. aeruginosa* and *K. pneumoniae* during resolution of acid pneumonitis, whereas peritoneal and splenic macrophages were not affected. Furthermore, we found a significant impairment of LMs to mount mROS after bacterial stimulation, which might account for the reduced clearance of bacteria in animals that underwent acid aspiration. Thus, the liver–lung axis not only affects antibacterial properties of alveolar macrophages but also LMs. Considering that KCs represented ~80–90% of all F4/80-positive cells, we conclude that our finding is largely attributable to KCs. We speculate that impaired bacterial clearance in LMs might contribute to increased susceptibility to bacterial infections after lung injury. ■

Author disclosures are available with the text of this letter at www.atsjournals.org.

Acknowledgment: The authors thank Florian Lück and Stefanie Jarmer for excellent technical assistance.

Martin Langelage*
Julian Better, M.D.*
Michael Wetstein
Justus-Liebig-University Giessen
Giessen, Germany

Balachandar Selvakumar, Ph.D.
Biomedicine Research Institute of Buenos Aires – CONICET-Partner Institute of the Max Planck Society (IBioBA-MPSP)
Buenos Aires, Argentina
and
Max Planck Institute for Heart and Lung Research
Bad Nauheim, Germany

Christina Malainou, M.D.
Justus-Liebig-University Giessen
Giessen, Germany

Lucas Kimmig, M.D.
Justus-Liebig-University Giessen
Giessen, Germany
and
University of Chicago Medicine
Chicago, Illinois

Borros Arneth, M.D.
Giessen University Hospital
Giessen, Germany

Kernt Köhler, Ph.D.
Christiane Herden, Ph.D.
Susanne Herold, M.D., Ph.D.‡§
Ulrich Matt, M.D., Ph.D.‡¶
Justus-Liebig-University Giessen
Giessen, Germany

*These authors contributed equally to this work.
‡Senior authors.
§S.H. is Deputy Editor of *AJRCMB*. Her participation complies with American Thoracic Society requirements for recusal from review and decisions for authored works.
¶Corresponding author (e-mail: ulrich.matt@innere.med.uni-giessen.de).

References

1. Quinton LJ, Walkey AJ, Mizgerd JP. Integrative physiology of pneumonia. *Physiol Rev* 2018;98:1417–1464.
2. Quinton LJ, Jones MR, Robson BE, Mizgerd JP. Mechanisms of the hepatic acute-phase response during bacterial pneumonia. *Infect Immun* 2009;77:2417–2426.
3. Quinton LJ, Blahna MT, Jones MR, Allen E, Ferrari JD, Hilliard KL, *et al*. Hepatocyte-specific mutation of both NF-κB RelA and STAT3 abrogates the acute phase response in mice. *J Clin Invest* 2012;122:1758–1763.
4. Hilliard KL, Allen E, Traber KE, Kim Y, Wasserman GA, Jones MR, *et al*. Activation of hepatic STAT3 maintains pulmonary defense during endotoxemia. *Infect Immun* 2015;83:4015–4027.
5. Hilliard KL, Allen E, Traber KE, Yamamoto K, Stauffer NM, Wasserman GA, *et al*. The lung-liver axis: a requirement for maximal innate immunity and hepatoprotection during pneumonia. *Am J Respir Cell Mol Biol* 2015;53:378–390.
6. Deniset JF, Surewaard BG, Lee WY, Kubes P. Splenic Ly6G^{high} mature and Ly6G^{int} immature neutrophils contribute to eradication of *S. pneumoniae*. *J Exp Med* 2017;214:1333–1350.
7. Wong CH, Jenne CN, Petri B, Chrobok NL, Kubes P. Nucleation of platelets with blood-borne pathogens on Kupffer cells precedes other innate immunity and contributes to bacterial clearance. *Nat Immunol* 2013;14:785–792.
8. Jorch SK, Surewaard BG, Hossain M, Peiseler M, Deppermann C, Deng J, *et al*. Peritoneal GATA6+ macrophages function as a portal for Staphylococcus aureus dissemination. *J Clin Invest* 2019;129:4643–4656.
9. Matt U, Warszawska JM, Bauer M, Dietl W, Mesteri I, Doninger B, *et al*. Bbeta(15-42) protects against acid-induced acute lung injury and secondary pseudomonas pneumonia *in vivo*. *Am J Respir Crit Care Med* 2009;180:1208–1217.
10. West AP, Brodsky IE, Rahner C, Woo DK, Erdjument-Bromage H, Tempst P, *et al*. TLR signalling augments macrophage bactericidal activity through mitochondrial ROS. *Nature* 2011;472:476–480.
11. Hall CJ, Sanderson LE, Lawrence LM, Pool B, van der Kroef M, Ashimbayeva E, *et al*. Blocking fatty acid-fueled mROS production within macrophages alleviates acute gouty inflammation. *J Clin Invest* 2018;128:1752–1771.
12. Heuer JF, Sauter P, Pelosi P, Herrmann P, Brück W, Perske C, *et al*. Effects of pulmonary acid aspiration on the lungs and extra-pulmonary organs: a randomized study in pigs. *Crit Care* 2012;16:R35.
13. Imai Y, Parodo J, Kajikawa O, de Perrot M, Fischer S, Edwards V, *et al*. Injurious mechanical ventilation and end-organ epithelial cell apoptosis and organ dysfunction in an experimental model of acute respiratory distress syndrome. *JAMA* 2003;289:2104–2112.
14. Kolaczkowska E, Jenne CN, Surewaard BG, Thanabalasuriar A, Lee WY, Sanz MJ, *et al*. Molecular mechanisms of NET formation and degradation revealed by intravital imaging in the liver vasculature. *Nat Commun* 2015;6:6673.
15. Zeng Z, Surewaard BG, Wong CH, Geoghegan JA, Jenne CN, Kubes P. CRIg functions as a macrophage pattern recognition receptor to directly bind and capture blood-borne gram-positive bacteria. *Cell Host Microbe* 2016;20:99–106.
16. Ashare A, Monick MM, Powers LS, Yarovinsky T, Hunninghake GW. Severe bacteremia results in a loss of hepatic bacterial clearance. *Am J Respir Crit Care Med* 2006;173:644–652.
17. Roquilly A, Jacqueline C, Davieau M, Mollé A, Sadek A, Fourgeux C, *et al*. Alveolar macrophages are epigenetically altered after inflammation, leading to long-term lung immunoparalysis. *Nat Immunol* 2020;21:636–648. [Published erratum appears in *Nat Immunol* 21:962.]
18. Surewaard BG, Deniset JF, Zemp FJ, Amrein M, Otto M, Conly J, *et al*. Identification and treatment of the Staphylococcus aureus reservoir *in vivo*. *J Exp Med* 2016;213:1141–1151.
19. Blériot C, Dupuis T, Jouvion G, Eberl G, Disson O, Lecuit M. Liver-resident macrophage necroptosis orchestrates type 1 microbicidal inflammation and type-2-mediated tissue repair during bacterial infection. *Immunity* 2015;42:145–158.

Danksagung

Zuerst möchte ich Susanne Herold meinen großen Dank aussprechen. Sie hat am Uniklinikum Gießen eine hervorragende Forschungsgruppe, -infrastruktur und ein Klima geschaffen, das eine profunde wissenschaftliche Auseinandersetzung zulässt, und auch fördert. Diese ausgezeichneten Rahmenbedingungen und auch ihre persönliche Unterstützung waren sehr fruchtbare Grundlagen für meine Arbeit.

Neben ihrer Forschungsaktivität ist ihr auch die klinische Infektiologie ein echtes Anliegen. Dieser Einsatz macht Mut und Hoffnung, dass unser Fach zum Wohle der Patientenbetreuung, auch über Gießen hinaus, den ihm gebührenden Stellenwert bekommt.

An dieser Stelle möchte ich auch Werner Seeger danken, der seit Jahrzehnten den Standort Gießen zu einem exzellenten Forschungsstandort mitausgebaut hat, und rastlos die Klinik umsichtig leitet.

Bedanken möchte ich mich herzlich bei allen die mir von Anfang an im Forschungsalltag stets kompetent geholfen haben, und für ein wirklich angenehmes Arbeitsklima sorgten: Barbara Sprenger, Christina Malainou, Christin Peteranderl, Corinna Bremer, Florian Flück, Irinia Kuznetsova, Ivonne Vazquez-Armendariz, Julia Kutsch, Larissa Hamman, Monika Heiner, Stefanie Jarmer.

Dem gesamten Team der Infektiologie möchte ich ein großes Danke sagen für die ausgesprochen kollegiale Aufnahme und die gute Zusammenarbeit: Janina Trauth, Melanie Westbrock, Thomas Discher, Ulla Albrecht, und Vera Kantelhardt.

Ein großes Danke auch an meine Schwerarbeiter Julian Better, Michael Wetstein, und Martin Langelage für ihren Einsatz und die spannende Zusammenarbeit.

Danke an Lucas Kimmig für den pneumologischen Input, und ihm und seiner Familie für die willkommene und sehr angenehme Abwechslung im Alltag.

Einen herzlichen Dank an meine Mutter Gertrud Matt und meine Schwiegereltern Elisabeth und Karl Schatz. Ohne ihre stetige Unterstützung wäre diese Arbeit sicher nicht möglich gewesen.

Meinem Freund und ausgezeichneten infektiologischen Praktiker Thomas Köck für die Aufmunterung und Motivation über all die Jahre.

Und schließlich an meine Frau Julia für die Stütze, Kritik und den Humor, die seit Beginn meines Medizinstudiums meinen beruflichen Werdegang begleiten.